2026

U.S. Department of Transportation Federal Highway Administration

NEBRASKA DEPARTMENT OF TRANSPORTATION

NEBRASKA TRANSPORTATION CENTER

Final Report SPR-FY24(034)

Ultra-High-Performance Concrete (UHPC) for Bridge Deck Overlay and Structural Deck Repair

Jiong Hu, Ph.D.
Professor
Department of Civil & Environmental Engineering
University of Nebraska-Lincoln

George Morcous, PE, Ph.D.
Professor
Durham School of Architectural Engineering & Construction
University of Nebraska-Lincoln

Akbota Aitbayeva, M.Sc.
Graduate Research Assistant
Department of Civil & Environmental Engineering
University of Nebraska-Lincoln

Mina Gerges, M.Sc.
Graduate Research Assistant
Durham School of Architectural Engineering & Construction
University of Nebraska-Lincoln

Nebraska Department of Transportation Research
Headquarters Address
1400 Nebraska Parkway
Lincoln, NE 68509
ndot.research@nebraska.gov
(402) 479-4697
https://dot.nebraska.gov/business-center/research/

Nebraska Transportation Center
262 Prem S. Paul Research Center at Whittier School
2200 Vine Street
Lincoln, NE 68583-0851
(402) 472-1932
http://ntc.unl.edu

This report was funded in part through grant from the U.S. Department of Transportation Federal Highway Administration. The views and opinions of the authors expressed herein do not necessarily state or reflect those of the U.S. Department of Transportation.

Ultra-High-Performance Concrete (UHPC) for Bridge Deck Overlay and Structural Deck Repair

Jiong Hu, Ph.D.
Professor
Department of Civil & Environmental Engineering
University of Nebraska-Lincoln

George Morcous, PE, Ph.D.
Professor
Durham School of Architectural Engineering & Construction
University of Nebraska-Lincoln

Akbota Aitbayeva, M.Sc.
Graduate Research Assistant
Department of Civil & Environmental Engineering
University of Nebraska-Lincoln

Mina Gerges, M.Sc.
Graduate Research Assistant
Durham School of Architectural Engineering & Construction
University of Nebraska-Lincoln

A Report on Research Sponsored by

Nebraska Department of Transportation (NDOT)

April 2026

Technical Report Documentation Page

1. Report No FY24(034)	2. Government Accession No.	3. Recipient's Catalog No.	
4. Title and Subtitle Ultra-High-Performance Concrete (UHPC) for Bridge Deck Overlay and Structural Deck Repair		5. Report Date April, 2026	
		6. Performing Organization Code	
7. Author/s Jiong Hu, George Morcous, Akbota Aitbayeva, and Mina Gerges		8. Performing Organization Report No.	
9. Performing Organization Name and Address University of Nebraska-Lincoln, Department of Civil Engineering Peter Kiewit Institute, Omaha, NE 68182-0178		10. Work Unit No. (TRAIS)	
		11. Contract or Grant No.	
12. Sponsoring Organization Name and Address Nebraska Department of Transportation 1400 Nebraska Parkway, PO Box 94759, Lincoln, NE 68509		13. Type of Report and Period Covered	
		14. Sponsoring Agency Code	
15. Supplementary Notes			

16. Abstract

Ultra-high-performance concrete (UHPC) is an advanced cementitious material known for its exceptional strength and durability, making it an ideal material for bridge deck overlays and repairs that address the common issue of premature deck deterioration. Conventional UHPC is typically flowable and self-leveling, which makes it unsuitable for deck surfaces with cross-slopes and/or sloped vertical profiles. Therefore, a highly thixotropic UHPC that responds well to vibration while remaining stable on sloped surfaces is needed for overlay applications. Mixtures with varying binder content, water-to-binder ratio, fiber content, and dosages of admixtures were developed and evaluated. Two of the most effective and economical mixtures were selected for full-scale mockup construction and testing.

Six full-scale sloped slabs were prepared using three surface preparation methods: surface retarder for fresh concrete, fine milling, and typical milling for hardened concrete to simulate field conditions for overlay applications. The structural performance of the composite slabs and the bond between UHPC overlays and concrete substrates were tested to evaluate the effectiveness of each surface preparation method. Flexural tests were conducted under both positive and negative bending, and the experimental results were compared with predictions according to the latest AASHTO UHPC Guide Specifications. The two UHPC mixtures developed in this study were further evaluated for their workability, mechanical, and durability properties. They showed excellent performance compared to the UHPC overlay mixes reported in the literature. The study also confirmed the constructability of the developed mixtures using traditional construction equipment. Recommended ranges for various workability indicators were proposed based on the performance of the UHPC mixtures included in the study and mockup evaluation. The three surface preparation methods investigated were sufficient to achieve an adequate bond between UHPC overlay and deck slab. Flexural test results of the slabs also demonstrated the significant contribution of UHPC to the flexural capacity of the deck slab in negative-moment regions and the adequacy of the developed prediction models.

17. Key Words UHPC overlay, Thixotropic UHPC, workability, mixture design, mock-up, flexural test, bonding	18. Distribution Statement		
19. Security Classification (of this report) Unclassified	20. Security Classification (of this page) Unclassified	21. No. of Pages 223	22. Price

Form DOT F 1700.7 (8-72) Reproduction of form and completed page is authorized.

Table of Contents

List of Figures

List of Tables

Acknowledgements

The authors would like to thank the Nebraska Department of Transportation (NDOT) for funding the research and providing the opportunity to continue studying ultra-high performance concrete. Special thanks to the Technical Advisory Committee members for their valuable input and assistance throughout the project. The author also wishes to thank the materials suppliers Ash Grove Cement Company, Central Plains Cement Company, GCP Applied Technologies, Lyman-Richey Corporation, and Chryso for generously donating materials for this research. Additionally, the author appreciates the help of students and laboratory technicians during the data collection process.

Disclaimer

The contents of this report reflect the views of the authors who are responsible for the facts and the accuracy of the data presented herein. The contents do not necessarily reflect the official views or policies of the Nebraska Department of Transportation, nor of the University of Nebraska-Lincoln. This report does not constitute a standard, specification, or regulation. Trade or manufacturers' names, which may appear in this report, are cited only because they are considered essential to the objectives of the report. The United States (U.S.) government and the State of Nebraska do not endorse products or manufacturers.

This material is based upon work supported by the Federal Highway Administration under FY24(034). Any opinions, findings, and conclusions or recommendations expressed in this publication are those of the author(s) and do not necessarily reflect the views of the Federal Highway Administration.

This report has been reviewed by the Nebraska Transportation Center for grammar and context, formatting, and 508 compliance.

Abstract

Ultra-high-performance concrete (UHPC) is an advanced cementitious material known for its exceptional strength and durability, making it an ideal material for bridge deck overlays and repairs that address the common issue of premature deck deterioration. Conventional UHPC is typically flowable and self-leveling, which makes it unsuitable for deck surfaces with cross-slopes and/or sloped vertical profiles. Therefore, a highly thixotropic UHPC that responds well to vibration while remaining stable on sloped surfaces is needed for overlay applications. Mixtures with varying binder content, water-to-binder ratio, fiber content, and dosages of admixtures were developed and evaluated. Two of the most effective and economical mixtures were selected for full-scale mockup construction and testing.

Six full-scale sloped slabs were prepared using three surface preparation methods: surface retarder for fresh concrete, fine milling, and typical milling for hardened concrete to simulate field conditions for overlay applications. The structural performance of the composite slabs and the bond between UHPC overlays and concrete substrates were tested to evaluate the effectiveness of each surface preparation method. Flexural tests were conducted under both positive and negative bending, and the experimental results were compared with predictions according to the latest AASHTO UHPC Guide Specifications. The two UHPC mixtures developed in this study were further evaluated for their workability, mechanical, and durability properties. They showed excellent performance compared to the UHPC overlay mixes reported in the literature. The study also confirmed the constructability of the developed mixtures using traditional construction equipment. Recommended ranges for various workability indicators were proposed based on the performance of the UHPC mixtures included in the study and mockup evaluation. The three surface preparation methods investigated were sufficient to achieve an adequate bond between UHPC overlay and deck slab. Flexural test results of the slabs also

demonstrated the significant contribution of UHPC to the flexural capacity of the deck slab in negative-moment regions and the adequacy of the developed prediction models.

Chapter 1 Introduction

1.1 Background

Ultra-high-performance concrete (UHPC) is a new type of concrete that significantly surpasses traditional concrete in mechanical and durability properties. Using UHPC greatly enhances the structural capacity and longevity of bridge components. In addition to bridge deck connection applications, the Federal Highway Administration (FHWA) Everyday Counts (EDC-6) program "UHPC for Bridge Preservation and Repair" highlights the benefits of UHPC for bridge repair and preservation, thanks to its superior mechanical and durability features. The nearly impervious nature of UHPC, along with its high initial and ultimate compressive and tensile strengths, makes it an excellent choice for overlay material and structural repair of deteriorating bridge decks. Because UHPC involves a high content of fine powders, a very low water-to-cement ratio, and a substantial amount of high-range water reducers (HRWR), its proportioning and batching differ greatly from those of conventional concrete. The research team has developed a non-proprietary mix using local materials through a recent NDOT project (SPR-P1(18) M072) titled "Feasibility Study of Development of Ultra-High-Performance Concrete (UHPC) for Highway Bridge Applications in Nebraska", with a unit cost of approximately $740 per cubic yard, about one-third of the cost of commercial proprietary products. However, this mix was designed for bridge connections and precast concrete construction, not for overlay use. While UHPC is generally expected to be self-consolidating with high flowability, overlay applications require a stiffer mixture to ensure slope stability, but one that still responds well to vibration (high thixotropy), enabling successful placement. Another challenge with UHPC overlays is its rapid loss of workability due to the high HRWR content. The workability cannot be maintained for long periods, leading to difficulties in transportation and placement of UHPC overlays. Due to these challenges, there are only a limited number of UHPC overlay projects

compared to bridge connections. As shown in Figure 1.1 and the FHWA UHPC Bridge Interactive Map, only 17 Bridge Deck Overlay (BDO) projects (4%) exist, while 312 connections between prefabricated elements (CPBE) projects (77%) have been implemented. Many recent design and construction documents have been developed by organizations such as AASHTO, FHWA, the American Concrete Institute (ACI) Technical Committee 239 (UHPC), the Precast/Prestressed Concrete Institute (PCI), and other state agencies. However, most of these documents focus on the structural design of UHPC components or the production and construction of precast and cast-in-place UHPC for bridges, which does not address the highly thixotropic UHPC used in bridge deck overlays. Therefore, there is a need for specific design and construction guidelines for UHPC in deck overlay and structural repair applications, particularly when non-proprietary mixes are employed.

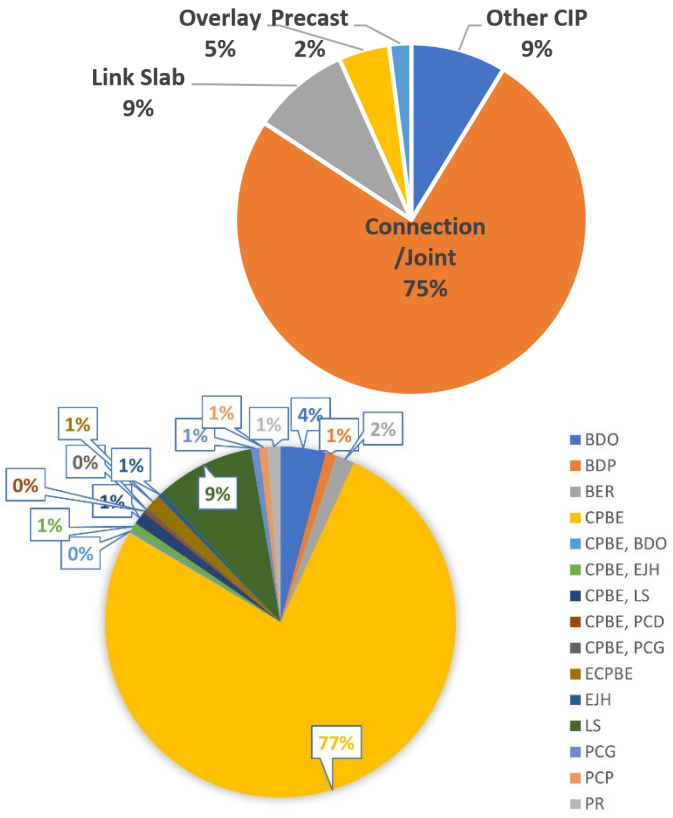

Figure 1.1 Documented UHPC projects based on FHWA UHPC Bridge Interactive Map (last accessed February 21, 2024)

1.2 Objectives

The main goal of this project is to develop a non-proprietary UHPC mixture specifically for bridge deck overlays and structural repairs in Nebraska, using local materials and focusing on cost-effectiveness. Additionally, the project seeks to verify the performance of the developed UHPC when applied to normal concrete (NC) slabs prepared with various commercially available surface preparation techniques.

The specific objectives are to:

- Design and optimize a thixotropic UHPC mixture suitable for overlay construction.
- Evaluate its fresh, mechanical, and durability properties using laboratory testing.

- Verify its constructability and performance using inclined full-scale mockup slabs.
- Assess flexural behavior and bond performance with normal concrete (NC) substrates.
- Develop a design methodology, verify its accuracy through experimental results, and perform a parametric study to investigate the effect of key material parameters on the flexural capacity of composite slabs.
- Provide practicing engineers with detailed calculation procedures for predicting the flexural capacity of the composite slabs in accordance with the AASHTO 2024 UHPC design specifications.
- Provide practical insights and recommendations to support future field implementation.

1.3 Report Organization

This report is structured as follows:

- **Chapter 1** introduces the motivation for the study, provides background on UHPC overlays, outlines the study objectives, and summarizes the overall structure of the report.
- **Chapter 2** presents a comprehensive literature review of UHPC overlay applications, mixture design, and testing practices adopted in recent research and field projects.
- **Chapter 3** details the experimental program, including materials, mixing procedures, and the test methods used for assessing fresh, mechanical, and durability properties.
- **Chapter 4** discusses the process of UHPC mixture development and evaluation, including constructability assessment and performance metrics.

- **Chapter 5** introduces a proposed analytical approach for calculating the flexural capacity of UHPC-overlaid slabs and presents a design example along with a parametric study.
- **Chapter 6** outlines the construction and testing of full-scale mockup specimens, including comparisons with analytical predictions and evaluation of bond performance.
- **Chapter 7** summarizes key findings and provides recommendations for implementation and future research.

Chapter 2 Literature Review

2.1 Introduction

This chapter provides a comprehensive overview of UHPC overlay, focusing on its current practices, mixture design, fresh and mechanical properties, and the exploration of new approaches and test methods. UHPC is increasingly valued for its superior performance in strength, durability, and long-term stability, making it an attractive choice for bridge deck overlays. However, the specific requirements for the fresh properties of UHPC overlay mixtures differ from those of conventional UHPC, requiring careful evaluation. Additionally, the mechanical testing for overlay applications will differ from that used in conventional UHPC applications. Therefore, this chapter will examine these aspects, drawing on the experiences of other field projects to identify and implement the best approaches. It synthesizes findings from various research reports, federal and state agency documents, journal articles, and conference publications to present a comprehensive understanding of current practices and advancements in UHPC overlay technology.

2.2 State-of-the-Practice of UHPC Overlay

This section provides an overview of various UHPC overlay projects conducted across different states in the U.S. from 2016 to 2025. These projects, carried out by state Departments of Transportation (DOTs) and other agencies, feature UHPC overlays with thicknesses ranging from 1.0 to 3.0 inches. The installation areas vary widely, with some projects covering extensive bridge surfaces up to 25,500 square feet. The data underscores the adoption of UHPC solutions for bridge preservation and repair, reflecting a growing trend to use this advanced material for its durability and cost-effectiveness in infrastructure maintenance.

Table 2.1 Summary of UHPC overlay projects in the United States (2016-2025).

	Source	Owner	Project name	Contractor	Year constructed	Overlay thickness (in.)	Approximate installation area (ft^2)
1	FHWA (2022)	Buchanan County (Iowa)	Mud Creek	N/A	2016	1.5	2850
2	FHWA (2022)	Delaware DOT	Blackbird Station	N/A	2017	1.5	3600
3	FHWA (2022)	Iowa DOT	Floyd River	UHPC Solutions Cramer & Associates Inc. Walo Iowa LLC as a sub	2018	1.0	17600
4	FHWA (2022)	Delaware DOT	State Road 1 Little Heaven	UHPC Solution	2019	3.0	9700
5	FHWA (2022)	New York State DOT	State Road 17B Hortonville	UHPC Solution	2019	1.5	8060
6	FHWA (2022)	New Jersey DOT	NJ-57	UHPC Solution	2020	1.5	800
7	FHWA (2022)	New Jersey DOT	I-280 WB	UHPC Solution	2020	1.5	13600
8	FHWA (2022)	New Jersey DOT	NJ-159 with	UHPC Solution	2020	2.75	7500
9	FHWA (2022)	New Jersey DOT	I-295 NB	UHPC Solution	2020	1.5	18900
10	UHPC Solution (n.d.)	New York State DOT	Bruckner Expressway over St. Ann's Avenue	UHPC Solution	2020	2.0	NM
11	Steelike (n.d.)	Kane County Division of Transportation (Illinois)	Granart Road Bridge	Steelike	2020	NM	2414
12	Steelike (n.d.)	Rhode Island Turnpike and Bridge Authority	Claiborne Pell Bridge	Steelike	2020	1.75	810
13	Tran-Set (2021)	New Mexico DOT	Bridge 7031	NM	2021	1.0	15350
14	DRBA (n.d.)	Delaware DOT	Memorial Bridge	UHPC Solution	2022	4.0	25500
15	Research Team Field Observation	Iowa DOT	IA 92 over Seven Mile Creek	NM	2023	1.25	NM
16	FHWA (2025)	Eastern Federal Lands Highway Division (EFLHD)	George Washington Memorial Parkway Bridges	NM	2025	NM	NM

NM: Not Mentioned

2.2.1 Surface Preparation of the Existing Concrete

Surface preparation is crucial for forming a strong bond between the new UHPC layer and the existing normal concrete (NC) bridge deck. According to the International Concrete Repair Institute (ICRI 310.2R), there are ten concrete surface profiles (CSP), as shown in Figure 2.1. Overlay applications can be achieved by attaining surface profiles from CSP-6 to CSP-10 or higher. Hydro-demolition and scarification (commonly called milling in the industry) can be used to reach the required surface roughness. Each method carries a relative risk of causing microcracking in the substrate concrete. Hydro-demolition and scarification are associated with low and moderate risks of microcracking, respectively. The quality of surface preparation can be evaluated using CSP Comparator Chips (ICRI 310.2R), as shown in Figure 2.2.

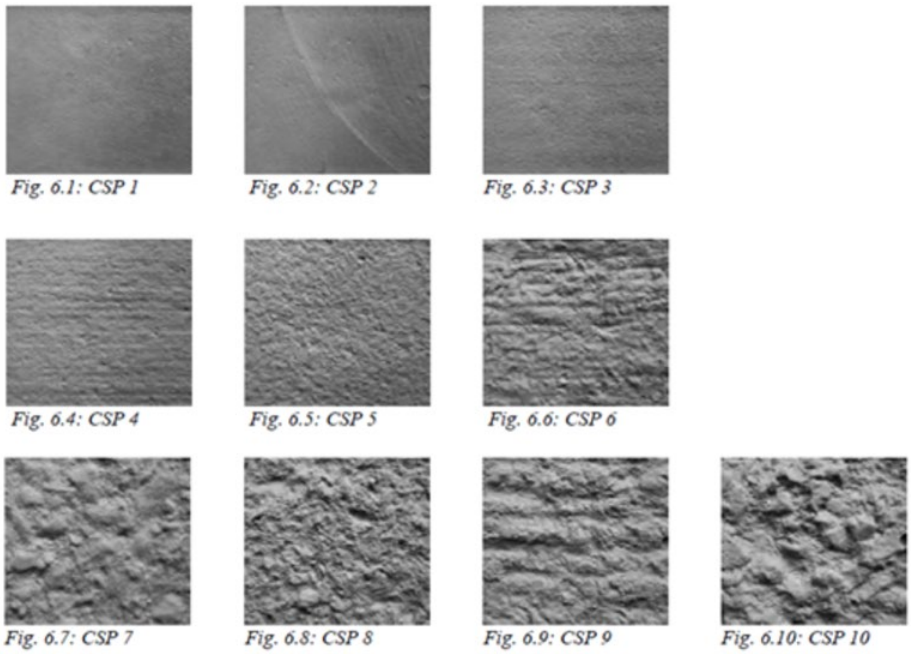

Figure 2.1 Concrete Surface Profiles (ICRI 310.2R, 2013).

Figure 2.2 CSP Comparator Chips (ICRI 310.2R 2013).

The concrete substrate should have a roughened surface with a minimum profile of 0.125 inches, measured as the average distance between the peaks and valleys, Haber et al. (2022a). When significant amounts of concrete need to be removed, such as for a partial-depth deck replacement, two removal techniques may be combined. For example, cold milling, which generally offers easier debris management, can be used for initial removal. Final removal and roughening can then be completed using hydro-demolition or shot blasting to ensure that no microfractures remain in the substrate, as shown in Figure 2.3. This approach could be especially beneficial when hydro-demolition is used to reduce the volume of wastewater that needs treatment and disposal. Laboratory studies have shown that UHPC can achieve interface bond strengths between 0.35 and 0.6 ksi when the substrate concrete is prepared with both macro- and micro-texture (i.e., exposed aggregate).

Figure 2.3 Deck surface prepared by hydro-demolition (Haber et al., 2022a).

Achieving the proper surface roughness and ensuring the surface is saturated surface dry (SSD) are crucial steps to improve the mechanical interlock and adhesion of the UHPC overlay. Table 2.2 summarizes surface preparation techniques for existing concrete prior to the placement of UHPC overlay are based on experiences from various projects. From 2016 to 2023, these projects employ techniques such as scarification, grinding, hydro-demolition, and ceramic bead blasting, with surface roughness thicknesses ranging from 1/8 to 1/2 inch. Ensuring the substrate is SSD before overlay placement is also noted, where applicable.

Table 2.2 Summary of surface preparation techniques for existing concrete.

	Source	Field Projects	Year	Technique	Surface roughness thickness (in.)	If SSD prior to placing an overlay
1	FHWA (2017)	Mud Creek	2016	Scarification	1/8	Yes
2	FHWA (2018)	Blackbird Station	2017	Roughened Surface	NM	NM
3	FHWA (2022)	Floyd River	2018	Hydro-demolition	NM	NM
4	UHPC Solution (2018)	State Road 1 Little Heaven	2019	Hydro-demolition	1/4	NM
5	FHWA (2022)	State Road 17B Hortonville	2019	Hydro-demolition	NM	NM
6	UHPC Solution (n.d.)	NJ-57	2020	Hydro-demolition	1/2	Yes
7	FHWA (2022)	I-280 WB	2020	Hydro-demolition	NM	NM
8	UHPC Solution (n.d.)	NJ-159	2020	Hydro-demolition	1/2	Yes
9	FHWA (2022)	I-295 NB	2020	Hydro-demolition	NM	NM
10	UHPC Solution (n.d.)	Bruckner Expressway over St. Ann's Avenue	2020	Scarification	NM	Yes
11	Steelike (n.d.)	Claiborne Pell Bridge	2020	Hydro-demolition	NM	NM
12	Tran-Set (2021)	Bridge 7032	2021	Ceramic bead blasted	1/4	Yes
13	DRBA (n.d.)	Delaware Memorial Bridge	2022	Hydro-demolition	NM	NM
14	Research Team Field Observation	IA 92 over Seven Mile Creek	2023	Hydro-demolition	NM	Yes

NM: Not Mentioned

2.2.2 Placing of UHPC Overlay

Table 2.3 provides an overview of mixer types and consolidation methods used in various field projects for UHPC overlays from 2016 to 2023. The projects use a range of mixer types, including high-shear pan mixers and standard front-loading ready-mix trucks. The consolidation methods reported in Table 2.3 can be grouped into four main categories: vibrating screed, vibrating truss screed, thin lift paver, and two-step consolidation. A vibrating screed is a screeding device that levels the fresh UHPC while applying vibration to mobilize the thixotropic mixture, improve consolidation, and help achieve the required thickness and surface profile. A

vibrating truss screed serves the same general purpose but uses a truss-type frame that spans a larger width, providing greater rigidity and more uniform strike-off and vibration across the deck surface. A thin lift paver is a mechanized paving system designed to place thin overlay layers in a continuous and controlled manner while maintaining elevation, width, and profile; in this report, the COMACO and Bid-Well equipment are treated as manufacturer-specific examples of this same method. Two-step consolidation refers to a process in which hand-operated concrete vibration is first used to assist local filling and consolidation, followed by a vibrating screed to complete strike-off, surface leveling, and overall profile control.

It is important to highlight the differences between vibratory screeds and Thin Lift UHPC pavers, which are often used for UHPC overlay consolidation. Vibratory screeds are generally suitable for small projects and situations where side access is limited by nearby traffic or narrow construction sites. However, vibratory screeds have limitations, such as being ineffective for thick overlays, uncontrolled vibration, and difficulty on steeper slopes. These issues can be addressed by using Thin Lift UHPC pavers, which are self-propelled. The Thin Lift UHPC paver offers advantages because it can manage UHPC thicknesses over 1.25 inches, ensures proper consolidation and surface uniformity with monitored vibration frequency, functions effectively on crowns and cross slopes up to 10%, speeds up installation time, and enables zero-clearance paving by positioning the legs where needed.

Table 2.3 Summary of mixer types and consolidation methods for UHPC overlay placement.

	Source	Field Projects	Year	Mixer type	Consolidation method
1	FHWA (2017)	Mud Creek	2016	High shear pan	Vibrating truss screed
2	FHWA (2018)	Blackbird Station	2017	NM	Vibrating screed
3	UHPC Solution (n.d.)	NJ-57	2020	NM	Vibrating screed
4	UHPC Solution (2022)	I-280 WB	2020	High shear mixers	Vibrating screed
5	UHPC Solution (n.d.)	NJ-159	2020	High shear mixers	Thin Lift Paver
6	UHPC Solution (n.d.)	Bruckner Expressway over St. Ann's Avenue	2020	High shear mixers	Vibrating screed
7	Steelike (n.d.)	Granart Road Bridge	2020	Standard front-loading ready-mix trucks	Vibration truss screed
8	Steelike (n.d.)	Claiborne Pell Bridge	2020	Standard front-loading ready-mix trucks	Vibration truss screed
9	Tran-Set (2021)	Bridge 7032	2021	High-energy, horizontal shaft mixers	Hand-operated concrete vibration, followed by vibration screed
10	DRBA (n.d.)	Delaware Memorial Bridge	2022	NM	Thin Lift Paver by COMACO Corp.
11	Research Team Field Observation	IA 92 over Seven Mile Creek	2023	Standard front-loading ready-mix trucks	Thin Lift Paver by Bid-well

NM: Not Mentioned

Construction joints in UHPC overlays are crucial when placement must be paused because of batching limitations, equipment reach, or site constraints. Current practice, as summarized by FHWA (2024), recommends placing these joints longitudinally and, when possible, away from wheel paths to reduce the risk of localized failure. Two common construction joint configurations have been adopted and shown in Figure 2.4. The first, derived from the Swiss SIA 2052 standard, incorporates a thicker UHPC section within the joint to ensure adequate consolidation and interlock. This approach allows the deeper portion of the first UHPC lift to bond effectively with the second casting, though some field reports note challenges in achieving full consolidation around reinforcement due to the material's thixotropic nature. A second, simplified joint geometry developed in Switzerland uses a butt joint between adjacent

UHPC casts, which facilitates easier fabrication while still maintaining a continuous UHPC layer across the joint. Both designs typically employ an exposed fiber surface finish at the UHPC-to-UHPC interface, achieved through the use of surface retarders, pressure washing, or sandblasting. Field experience has shown that the paste set retarder and pressure wash method provides a more uniform bond surface compared to sandblasting, which can be difficult to perform on hardened UHPC even after 24 hours. Overall, these joint details have demonstrated satisfactory performance with no significant cracking or bond deficiencies reported, provided that proper surface preparation and curing are maintained.

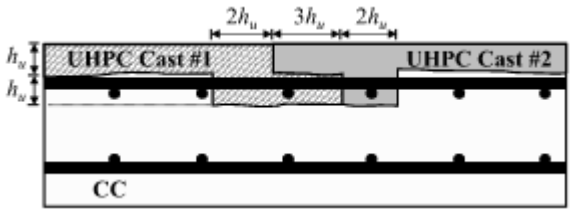

(a) proposed in SIA 2052

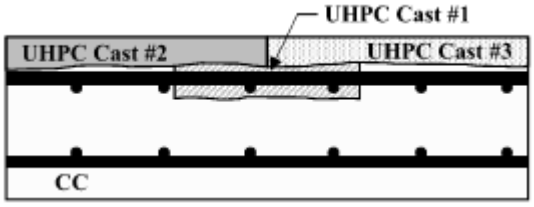

(b) emerging detail from Switzerland

Figure 2.4 Illustration. Examples of construction joint details (FHWA, 2024).

2.2.3 Finishing UHPC Overlay Surface

Table 2.4 summarizes various field projects involving UHPC overlays from 2016 to 2022, detailing the methods used for surface finishing and the minimum required compressive strength for each project. The projects employed a range of surface finishing techniques,

including grinding and grooving. Notably, some projects, such as those on NJ-57 and NJ-159, required specific compressive strengths (12 ksi) after two days of curing, while the Bruckner Expressway project required a higher strength (14 ksi). Other projects, such as Mud Creek, Granart Road Bridge, and Claiborne Pell Bridge, did not specify minimum strength requirements for surface finishing. The data indicates the variability in finishing requirements and methods across different UHPC overlay applications.

Table 2.4 Overview of surface finishing methods and compressive strength requirements for UHPC Overlay field projects.

	Source	**Field Projects**	**Year**	**Method**	**Minimum required com. strength for surface finishing**
1	FHWA (2017)	Mud Creek	2016	Grinding and grooving	NM
2	FHWA (2018)	Blackbird Station	2017	Diamond grinding	75% of the 28-day strength
3	UHPC Solution (2018)	State Road 1 Little Heaven	2019	Diamond grinding	NM
4	UHPC Solution (n.d.)	NJ-57	2020	Covered with 2.25" asphalt	After 2 days of curing: 12 ksi
5	UHPC Solution (n.d.)	NJ-159	2020	Diamond grinding and grooving	After 2 days of curing: 12 ksi
6	UHPC Solution (n.d.)	Bruckner Expressway over St. Ann's Avenue	2020	Diamond grinding and grooving	After 2 days of curing: 14 ksi
7	Steelike (n.d.)	Granart Road Bridge	2020	Grinding and grooving	NM
8	Steelike (n.d.)	Claiborne Pell Bridge	2020	Grinding	NM
9	DRBA (n.d.)	Delaware Memorial Bridge	2022	Diamond grinding and grooving	NM
10	Research Team Field Observation	IA 92 over Seven Mile Creek	2023	NM	After 3 days of curing: 11 ksi
11	NYSDOT	NM	2022	Diamond grinding (1/4")	After 2 days of curing: 12 ksi
12	NJDOT	NM	NM	Diamond grinding (1/4")	After 2 days of curing: 11 ksi

NM: Not Mentioned

2.2.4 Curing UHPC Overlay

Table 2.5 outlines the curing methods used in various UHPC overlay field projects from 2016 to 2021. Curing methods varied, including the use of curing compounds, plastic coverings,

and specialized techniques for specific conditions. Most projects utilized a curing compound combined with plastic sheeting for additional coverage. Notable exceptions include the State Road 1 Little Heaven project, which used tenting and hydronic heating due to low temperatures, and projects like the Granart Road Bridge and Claiborne Pell Bridge, which used white curing compounds without the need for plastic covers. This summary highlights the diversity of curing approaches to ensure optimal performance of UHPC overlays under different environmental conditions.

Table 2.5 Curing methods applied for UHPC overlay field projects.

No.	**Source**	**Field Projects**	**Year**	**Curing method**
1	FHWA (2017)	Mud Creek	2016	A water-based, wax-based concrete curing compound, wrapped by a thin plastic sheet
2	FHWA (2018)	Blackbird Station	2017	Curing compound and covered with polyethylene
3	UHPC Solution (2018)	State Road 1 Little Heaven	2019	Since the installation of the overlay was conducted at the low temperature of February, the freshly placed UHPC overlay was tented and heated. After one day, the tent was omitted, and hydronic heating hoses were utilized for three-day curing
4	UHPC Solution (n.d.)	NJ-57	2020	Curing compound and a plastic tarp for coverage
5	UHPC Solution (n.d.)	I-280 WB	2020	Curing compound, covered with a plastic tarp
6	UHPC Solution (n.d.)	NJ-159	2020	Curing compound, covered by a plastic tarp
7	UHPC Solution (n.d.)	Bruckner Expressway over St. Ann's Avenue	2020	Curing compound, covered by a plastic tarp
8	Steelike (n.d.)	Granart Road Bridge	2020	White curing compound, no need for a plastic sheet to be covered
9	Steelike (n.d.)	Claiborne Pell Bridge	2020	White curing compound in two coats without a plastic sheet to be covered
10	Tran-Set (2021)	Bridge 7032	2021	White curing compound and coverage with a plastic sheet

2.3 Mixture Design

After an extensive review of the literature, it is clear that the mixture design of self-consolidating UHPC closely resembles that of UHPC overlay, showing similar characteristics in terms of cementitious material content, fine aggregates, and water-to-binder ratio. Notably, the main difference between the two lies in fiber content and the amount of admixtures used. The amount of admixtures can be adjusted by achieving established mini-slump flow results. It is important to note that the admixture amounts in UHPC overlay mixtures differ from those in self-consolidating UHPC, mainly because the overlay requires high thixotropic and prolonged workability properties. Additionally, incorporating fibers into UHPC overlay significantly affects both its structural performance and rheology. Fibers increase viscosity, improve cohesiveness, and reduce segregation. Therefore, careful consideration of fiber content is crucial to optimize overall performance. State Departments of Transportation, such as Iowa DOT (2022), New York DOT (2021), and New Jersey DOT (2021), require steel fiber content in UHPC overlay applications to be approximately 3% to 3.25% by volume. Table 2.6 summarizes the incorporated fiber content amount by various implemented field projects in the USA.

Table 2.6 The incorporated fiber amount by different implemented field projects.

No.	**Owner**	**Project Name**	**Fiber Amount (%)**
1	Buchanan County (Iowa)	Mud Creek	3.25
2	Delaware DOT	Blackbird Station	3.25
3	Iowa DOT	Floyd River	3.25
4	Delaware DOT	State Road 1 Little Heaven	3.25
5	New York State DOT	State Road 17B Hortonville	3.25
6	New Jersey DOT	NJ-57	3.25
7	New Jersey DOT	I-280 WB	3.25
8	New Jersey DOT	NJ-159	3.25
9	New Jersey DOT	I-295 NB	3.25
10	New York State DOT	Bruckner Expressway over St. Ann's Avenue	3.25
11	Kane County Division of Transportation (Illinois)	Granart Road Bridge	3
12	New Mexico DOT	Bridge 7032	1.5
13	Delaware DOT	Memorial Bridge	3.25
14	Iowa DOT	IA 92 over Seven Mile Creek	3.25

2.4 Fresh Concrete Properties

Due to its limited flowability without external mechanical agitation, UHPC overlay material is typically referred to as thixotropic UHPC. Thixotropy, a characteristic of non-Newtonian fluids, involves time-dependent shear-thinning behavior, providing solid-like properties under static conditions while facilitating flow under agitation or shear (FHWA 2022). Predominantly used in the construction of bridge deck overlays, thixotropic UHPC addresses the unique construction requirements of bridge deck overlays (Holcim, 2023). This distinctive quality allows UHPC to be placed on sloped bridge surfaces, accommodating gradients of up to 10 percent while ensuring adherence to specified profiles (FHWA, 2022; Sritharan et al., 2018; FHWA, 2017; FHWA, 2018). Figure 2.5 presents the necessary workability characteristics of thixotropic UHPC with sample photographs from a bridge deck overlay project in September 2024 in Cass County, Iowa.

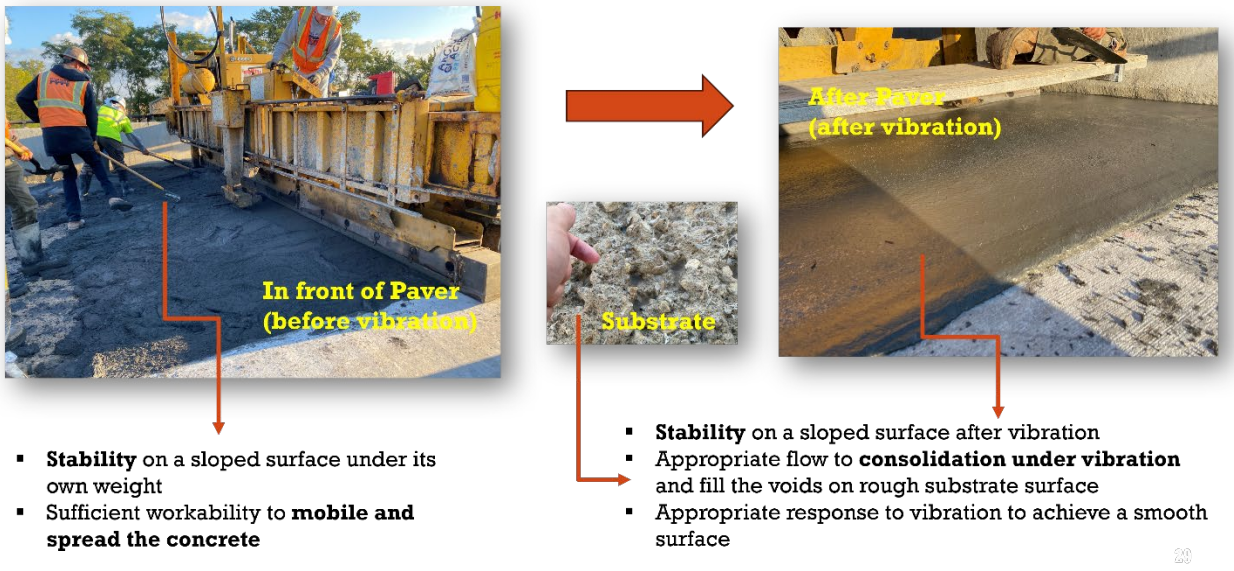

Figure 2.5 Thixotropic (overlay) UHPC workability characteristics.

Firstly, the thixotropic UHPC overlay must exhibit appropriate flow characteristics both before and after the paver. This ensures proper spread and mobility to adequately fill aggressive roughness caused by hydro-demolition, as illustrated in Figure 2.5. The standard static and dynamic flow tests are commonly used to assess the flowability of UHPC overlay before and after the paver. While self-consolidating (non-thixotropic), UHPC is generally evaluated only for static flow per ASTM 1856; understanding the behavior of UHPC overlay materials under movement and agitation requires dynamic flow testing. The kinetic energy imparted by the drops should induce UHPC dispersion, allowing assessment of whether the material exhibits excessive or insufficient flow. Multiple studies and agencies have reported typical dynamic flow ranges for UHPC overlay material as presented in Figure 2.6. FHWA and commercial Ductal® overlay UHPC indicated that the optimal dynamic flow is between 6 to 8 inches, while the IADOT and Harris et al. suggested a range of 8 to 10 inches. NJDOT established an efficient dynamic flow range of 7 to 10 inches. In fact, in their 2017 specifications, IADOT indicated an acceptable

dynamic flow range between 7 to 10 inches. However, in the 2022 specifications, this range was updated to 8 to 10 inches. The literature clearly shows that dynamic flow ranges can vary significantly. Therefore, it is essential to note that the acceptable dynamic flow range, typically between 6 and 10 inches, depends on factors such as bridge deck geometry, grade, and cross-slope. The values indicated by FHWA are for UHPC overlay materials that can be used on slopes up to 6 percent. In contrast, commercial Ductal® overlay UHPC reported that the same dynamic flow range can be used on slopes up to 15 percent. It is noted that the procedure for overlay dynamic flow testing was based on ASTM C1437; however, most of the literature states that only 20 drops were used. In their 2022 study, FHWA stated that the UHPC supplier can determine the number of drops within an acceptable spread range. Most literature does not specify the static flow ranges for UHPC overlays. However, commercial Ductal® overlay UHPC indicates that their UHPC overlay mixture usually has a static flow range of 4 to 6 inches.

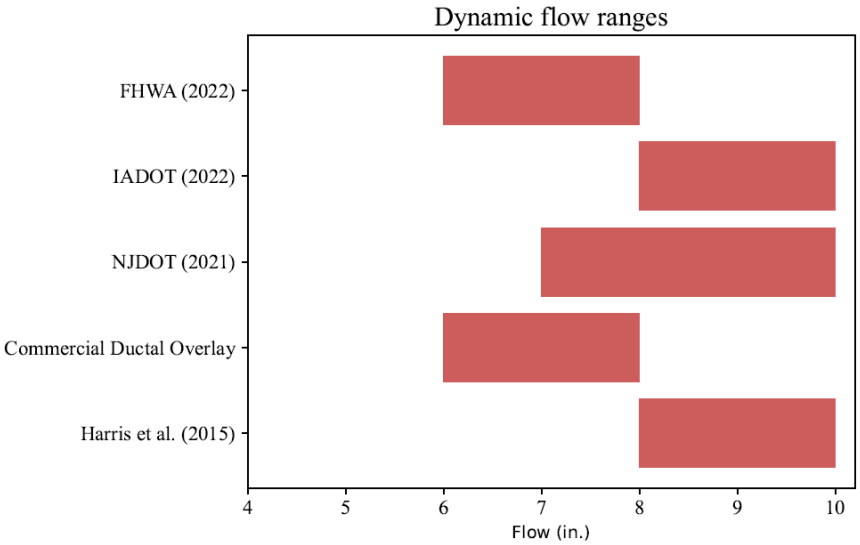

Figure 2.6 Dynamic flow ranges.

Since thixotropic UHPC for overlay requires external intervention, such as vibration, to shift from a stable workability to a flowable state, evaluating the material's performance under external energy to achieve a smooth surface and proper consolidation is crucial. This introduces the second unique workability characteristic of the thixotropic UHPC overlay: its response to vibration, as illustrated in Figure 2.5. Traditional slump or flow tests fail to accurately measure workability because they do not replicate field conditions where vibration energy is applied. The Vibrating Slope Apparatus (VSA) was developed by the Waterway Experiment Station (WES) of the US Army Corps of Engineers for the FHWA to qualify low-slump concrete used for paving (Bodenlos & Fowler, 2003). The VSA addresses this limitation by placing a concrete sample in a box chute, consolidating it, and then raising the chute to a specific angle (Bodenlos & Fowler, 2003). A vibrator evacuates the concrete, and the time taken for the concrete to move out of the chute under vibration is measured to quantify workability (Bodenlos & Fowler, 2003). Although the VSA does not directly assess the material's response to vibration, the sloped chute under vibration resembles the sloped construction of UHPC overlays. This brings up the third workability characteristic of the thixotropic UHPC overlay: its constructability on a sloped surface. Given the uneven nature of bridge decks, thixotropic UHPC must maintain its designated slope under vibration, as shown in Figure 2.7. While the VSA test does not examine mixtures for slope stability, vibrating under sloped conditions is beneficial. The Swiss Standard SIA 2052 for UHPFRC developed a similar method to validate a mixture's ability to maintain a desired slope. This involves using a platform to simulate the bridge deck's slope and adjust the UHPC overlay mixture accordingly (Figure 2.7). The objective is to formulate a mix that achieves optimal flowability for ease of placement while ensuring it retains the specified slope. However, it is essential to note that while the recommended slope test by SIA 2052 examines the

stability of a mixture under sloped conditions, it does not incorporate vibration to evaluate its effect on stability, thereby ignoring the relevance of paver-induced effects in field construction.

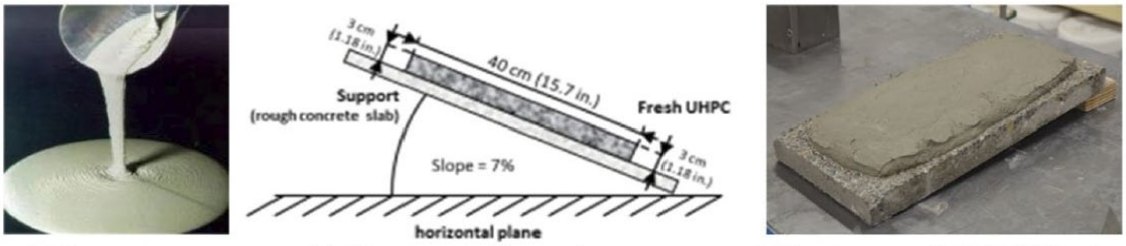

a) Flow test b) Slope test dimensions c) Slope test of a UHPC mix

Figure 2.7 Examining the rheological characteristics of UHPC overlay mixture (Sritharan et al., 2018).

In their 2018 research, Sritharan et al. used the above-mentioned technique to evaluate the quality of the UHPC overlay mix and enable practical testing by contractors. Two square slabs measuring 8 ft × 8 ft were cast, incorporating typical deck reinforcement details. Both slabs, each 7.75 inches thick, had different surface finishes – one with exposed aggregate and the other with a broom finish. Positioned at a 6° slope, the UHPC overlay mix was batched and applied to the slabs within the structural engineering laboratory at Iowa State University. This practical demonstration helped verify the suitability of the chosen UHPC overlay mix, confirming its workability and ability to maintain the specified slope on a textured surface. It is also important to highlight that, in addition to establishing acceptable flow ranges and testing slope stability, the UHPC overlay must not experience bleeding water or fiber instability.

2.5 Bond Between the NC and UHPC Overlay

The bond behavior between UHPC overlay and normal concrete (NC) bridge deck was investigated experimentally by Haber et al. (2018) and reported in FHWA-HRT-17-097. Tensile bond pull-off testing according to ASTM C1583 and Microstructural analysis (MSA) were

conducted to evaluate the bond behavior between UHPC overlay and the substrate NC. The 28-day compressive strength of normal concrete was 8 ksi, and the UHPC overlay material used in this study was procured from a commercial supplier with thixotropic properties specifically designed for overlays on sloped bridge decks. The UHPC was dosed with 3.25% fiber reinforcement by volume. Two surface preparation methods were used in this study: scarification and hydro-demolition. The concrete surface obtained by the scarification had a roughness corresponding to CSP-7 and the concrete surface obtained by hydro-demolition had a roughness that appeared higher than CSP-10, as shown in Figure 2.8. In the industry, scarification is commonly referred to as milling. Table 2.7 shows the results of tensile bond pull-off testing. The failure occurred at the interface between UHPC and NC in scarified specimens and in the substrate concrete in hydro-demolition specimens.

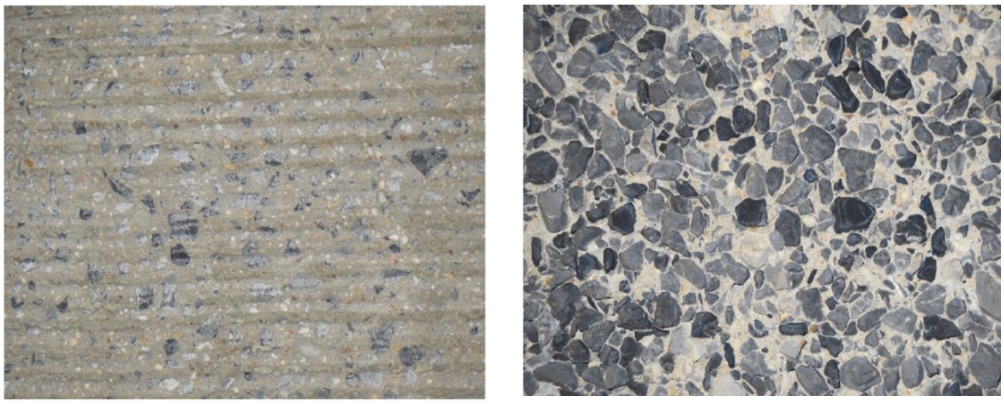

(a) scarification (b) hydro-demolition

Figure 2.8 Appearance of the concrete substrate (Haber et al., 2018).

Table 2.7 Results of tensile bond pull-off testing (Haber et al., 2018).

Technique of Surface Preparation	Average Peak Stress (ksi)	Failure Location
Milling (Scarification)	0.11	Interface
Hydro-Demolition	0.5	Substrate concrete

The Microstructural Analysis (MSA) was performed using backscattering image analysis. Generally, steel fibers were not present in the UHPC paste band that directly contacts the concrete substrate; therefore, the steel fibers did not directly contribute to or interfere with the paste's adhesion to the concrete substrate. On average, the thickness of this paste band, which lacks steel fibers, ranged from 0.4 mm to 2.4 mm. Concrete substrates prepared by scarification showed local damage in the form of microcracking in the exposed aggregate, as shown in Figure 2.9. This type of damage was not observed in substrates prepared with hydro-demolition. The hydro-demolition surface treatment results in increased macrotexture roughness, which improves mechanical interlock and reduces microcracking in the concrete, thereby boosting the tensile strength of the interface.

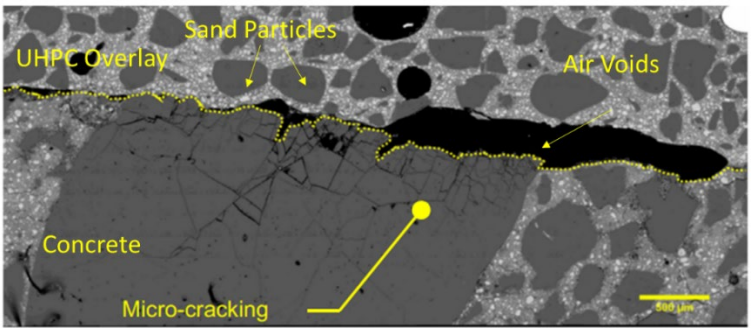

(a) Distressed aggregates in laboratory concrete substrate prepared using scarification

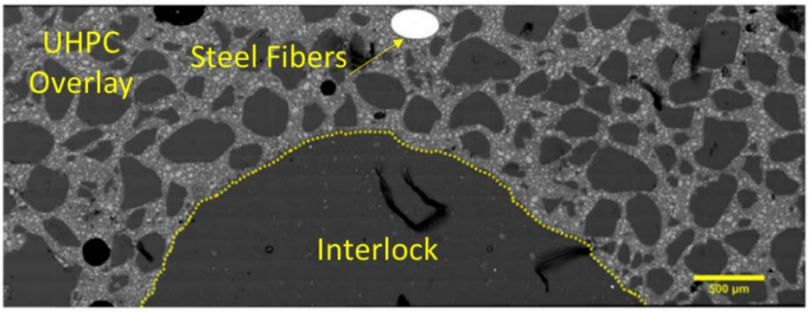

(b) Intact aggregate in laboratory concrete substrate prepared using hydro-demolition

Figure 2.9 Comparison of aggregate surface conditions in concrete substrates (Haber et al., 2018).

In addition to laboratory experimental work, Haber et al. (2018) also conducted a field study on the Laporte Road Bridge to assess the bond between the UHPC overlay and the substrate concrete deck. The same UHPC was used in both laboratory and field studies. The overlay thickness was 1.5 in. Prior to installing the overlay, the deck surface was scarified with a truck-mounted diamond grinder to remove the poor-quality concrete cover, as shown in Figure 2.10.

Figure 2.10 Deck surface after grinding (Haber et al., 2018).

Tensile bond pull-off testing according to ASTM C1583 was carried out at multiple locations. It can be observed that no failure occurred in the UHPC or at the interface between the substrate concrete and UHPC. Failures only occurred in the substrate concrete and the disc adhesive, as illustrated in Figure 2.11.

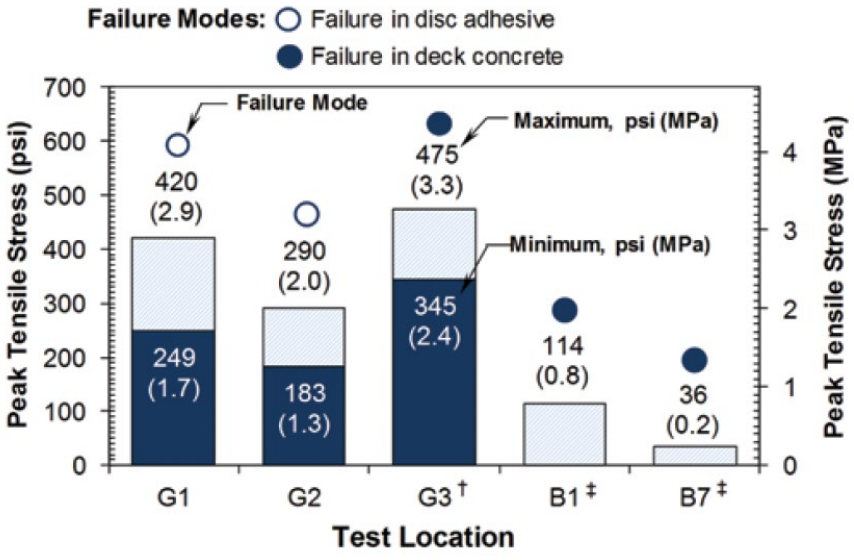

Figure 2.11 Peak stresses recorded from direct tension bond testing (Haber et al., 2018).

Wibowo et al. (2018) conducted a project using UHPC for a bridge deck overlay in Iowa. Mud Creek Bridge, built in the mid-1960s in Buchanan County, Iowa, was selected for the UHPC overlay demonstration. A special UHPC mix, known commercially as Ductal® NaG3 TX, was developed by Lafarge Holcim to accommodate the crown of the overlay. The 28-day compressive strength of UHPC was 18 ksi, and its thickness was 1.5 inches. The deck surface was ground and grooved to expose the aggregate and achieve a target surface roughness of about 1/8 inch. A standard vibratory concrete screed was used to place the UHPC. The curing compound was sprayed on top of the UHPC overlay immediately afterward. Thermal image scanning was conducted to evaluate the delamination risk of the UHPC overlay. The thermal camera was mounted on top of a vehicle before it was driven over the bridge. Areas at risk of delamination are shown by darker regions, as shown in Figure 2.12. Most of these areas align with those identified by the chain drag method, which was also used to assess the bond between the NC and UHPC overlay. Tensile bond pull-off testing according to ASTM C1583 was conducted to evaluate the bond strength between the UHPC overlay and the normal concrete. The results showed that delamination occurred within the NC deck and not at the UHPC-NC interface, and the average bond strength was 0.11 ksi.

Figure 2.12 Infrared imaging results for Mud Creek Bridge deck (Wibowo et al., 2018).

To evaluate the bond between the NC and UHPC overlay, Aaleti et al. (2017) experimentally investigated the shear transfer mechanism across the interface between UHPC and normal concrete (NC). Slant shear tests conforming to ASTM C882 were performed to assess this transfer mechanism. Prismatic specimens made of normal concrete with various textures along the interface and UHPC were used. The composite section had dimensions of 4.5 × 6 inches in the cross-section and 24 inches in length, with an interface angle of 53.1 degrees from the horizontal axis, as shown in Figure 2.13 (a).

Figure 2.13 Test setup and instrumentation of large prism slant shear test (Aaleti et al., 2017).

The concrete mixes used in specimen construction were obtained from local ready-mix concrete suppliers or precast producers. The 5 ksi concrete specimens were built using a standard Iowa DOT bridge deck mix ordered from a local ready-mix plant. UHPC, supplied by Lafarge North America, was used for casting test specimens. The UHPC, branded as Ductal® JS1000, was mixed at the overhead batch plant mixer at the Coreslab Structures precast plant in Omaha, Nebraska. The strengths of the UHPC material were measured to be between 15 and 21 ksi at the time of testing. The joint interface surfaces were prepared using five different form liners with varying roughness, ranging from 1/8 inch to 1/4 inch. The texture depth of the UHPC-NC interface was measured before pouring the second half of the slant shear specimen using a caliper.

During the testing of specimens, it was observed that they failed prematurely before the interface experienced significant sliding due to the formation of splitting cracks in the normal concrete. These cracks initiated at the ends of the interface and propagated into the normal concrete, as shown in Figure 2.13 (b). To prevent such premature failures, specimens were

retrofitted with fiber-reinforced polymer (FRP) wrap as shown in Figure 2.13 (c). However, even after the FRP retrofit, the splitting of the NC took place prior to the sliding interface failure. The interface bond strength was calculated as the maximum load along the inclined plane divided by the interface contact area. Figure 2.14 shows the minimum interface bond resistance.

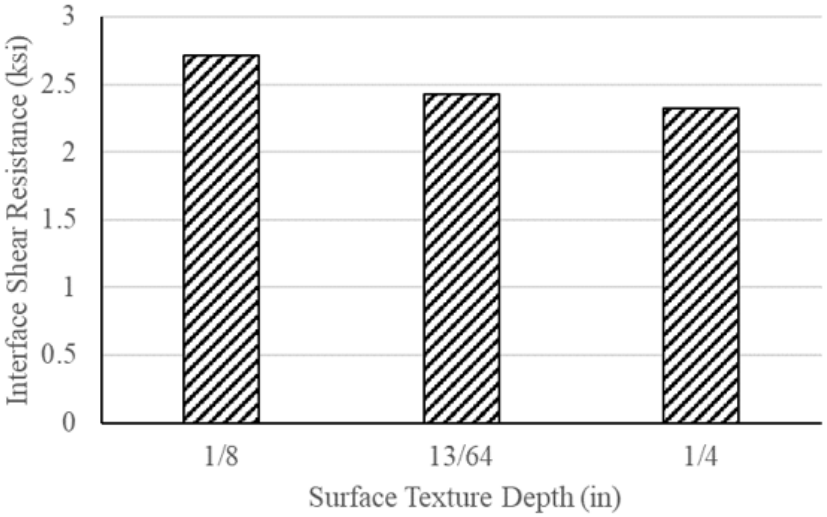

Figure 2.14 Interface shear resistance (Aaleti et al., 2017).

2.6 UHPC Overlay Acceptance Criteria and DOT Specifications

Table 2.8 presents various performance characteristics of UHPC overlay as specified by different Department of Transportation (DOT) guidelines and Holcim. Iowa, New York, and New Jersey are major states where UHPC overlay application projects are ongoing. Therefore, they have special provisions. According to the table, most criteria are similar among these states, but the compressive strength requirement for IADOT is notably lower than for NYSDOT and NJDOT. This difference can be attributed to the lack of requirement for high compressive strength in UHPC overlays due to their structural behavior and load distribution. Instead, tensile strength, bond strength, and durability requirements are more critical, as the overlay must

withstand tensile stresses without cracking. Other criteria, such as long-term shrinkage, chloride ion penetrability, and freeze-thaw resistance, are consistent across all states. Additionally, NJDOT includes specific tensile strength criteria that are listed in Table 2.9, highlighting its importance for overlay performance.

Table 2.8 Summary table with acceptance criteria from different agencies.

	Source	Flow (ASTM C1437 / ASTM C1856)	Compressive Strength at 28d (ksi)	Long-Term Shrinkage (ASTM C157/ AASHTO T160) (μ)	Chloride Ion Penetrability (AASHTO T277/ ASTM C1202) (coulombs)	Freeze-Thaw Resistance (%)	Scaling Resistance	Alkali-Silica Reaction
1	IADOT (2022)	Dynamic: 8”-10”	≥ 14	≤800 (at 28 days)	≤ 350	RDM>95	Y < 3	Innocuous
2	NYSDOT (2022)	N/A	≥18	≤766 (at 28 days)	≤ 250	RDM>96	Y < 3	Innocuous
3	NJDOT	Dynamic: 7”-10”	≥ 18	≤800 (at 28 days)	≤ 250	RDM>95	Y < 3	Innocuous
4	Commercial Ductal® Overlay	Static: 4”-6”; Dynamic: 6”-8”	≥ 18	≤500 (at 90 days)	≤ 100	RDM>98	N/A	N/A

Table 2.9 Tensile and bond performance acceptance criteria for UHPC overlays (NJDOT specifications).

	Source	Modulus of Elasticity (ASTM C1856)	Direct Tension 1st Cracking Strength (AASHTO T 397)	Direct Tension Post-Cracking Hardening Ratio (AASHTO T 397)	Direct tension bond strength (ASTM C1583, bonded to an exposed aggregate concrete surface)
1	NJDOT	≥ 6,500 ksi	f_{cr} ≥1000 psi	f_p/f_{cr} ≥ 1.25	100% failure in substrate concrete with concrete compressive strength ≥ 4ksi, or >400 psi

2.7 Flexural Testing of Bridge Deck with UHPC Overlay

UHPC-NC composite deck specimens with a texture depth varying from 1/20 in. to 1/5 in. were tested to evaluate the bond behavior between UHPC overlay and normal concrete by Aaleti et al. (2017). A deck slab between two adjacent girders was chosen for the experimental investigation, as shown in Figure 2.15. The specimens that had dimensions of 2 ft (width) × 8 ft (length) were fabricated at Iowa State University's structural laboratory. The reinforcement in the deck was designed according to AASHTO guide specifications (AASHTO 2010) and was the same reinforcement included in current Iowa DOT bridge decks.

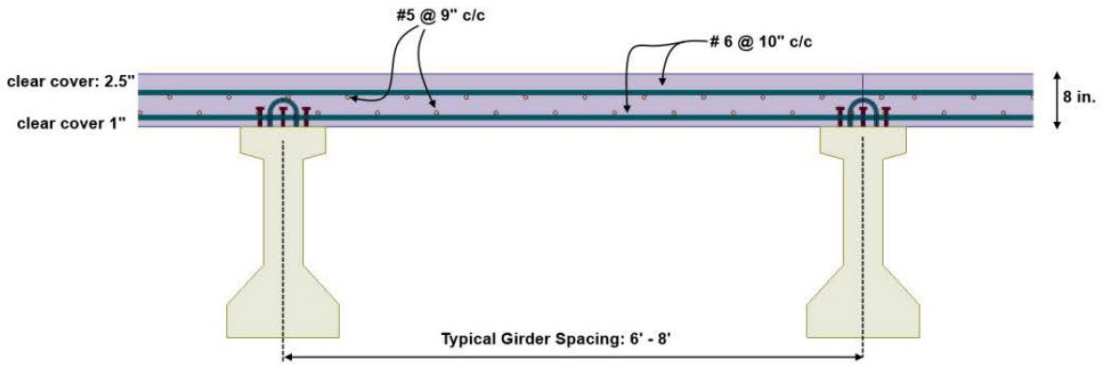

Figure 2.15 Details of a standard Iowa DOT bridge (Aaleti et al., 2017).

The interfaces on top of the slabs were created using form liners. The form liners were placed at the bottom of the deck panel formwork, and concrete was poured into the formwork. The UHPC overlay thickness was 1.5 inches. The measured compressive strengths of NC and UHPC at 28 days after casting were 4.55 ksi and 15.5 ksi, respectively.

During the curing period, one week after pouring the UHPC, delamination of the UHPC overlay was observed in a small section at the end of a composite specimen with the 1/20 in. texture. The delamination was caused by the high shrinkage of UHPC and the shallow interface texture depth.

The length of the delamination increased over time, reaching nearly 50% of the interface length at 28 days. As a result, this specimen was excluded from testing. No delamination was seen in any other specimens.

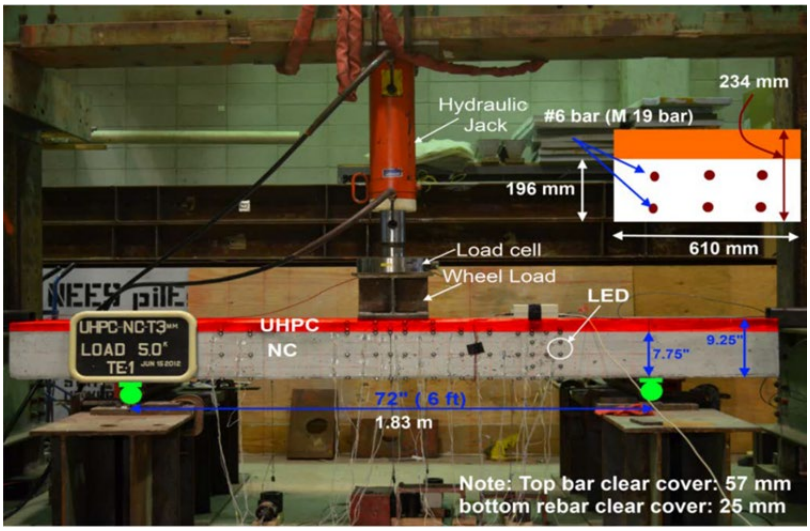

Figure 2.16 Test setup for the flexural testing of concrete deck specimens with UHPC overlay (Aaleti et al., 2017).

Figure 2.16 shows the test setup, the specimens were subjected to combined flexural and shear loading. The UHPC overlay was on the compression side. Figure 2.17 shows the load-displacement curve for the specimens. All specimens ultimately failed due to shear failure in the normal concrete part of the composite deck at a load around 70 kips, which is nearly 4.4 times the designed service-level wheel load. Slip along the UHPC-NC interface was monitored with a state-of-the-art 3D Optotrak system using LED targets. No slip was observed at the interface until shear failure was initiated in the specimens.

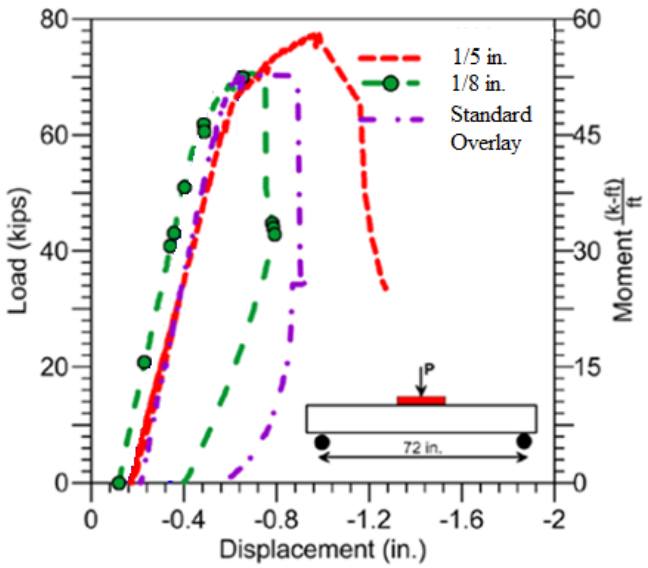

Figure 2.17 Load-displacement response of composite test specimens (Aaleti et al., 2017).

Wibowo et al. (2018) evaluated the benefits of using UHPC overlays through experimental testing. They cut three slab specimens from a larger concrete slab used in a project, which was designed to represent a typical concrete bridge deck in Iowa. Each specimen measured 2 ft by 8 ft with a thickness of 9 in. The plan dimensions matched those of specimens used in a previous study by Aaleti et al. (2013) to examine minimum interface roughness, although those slabs had a depth of 7.75 in. Two of these specimens were taken to the field, and their surfaces were manually grooved using a concrete diamond saw to simulate the required roughness, as shown in Figure 2.18. A 1.5-inch-thick UHPC layer was added to two specimens. Welded wire reinforcement at a 1.8% ratio was used in the UHPC layer.

Figure 2.18 Surface preparation on concrete deck used for slab specimens (Wibowo et al., 2018).

No heat treatment was applied to accelerate the strength gain of the UHPC, ensuring that the specimen preparation resembled real-world field conditions. The measured concrete strength of the slabs at 28 days was 6.6 ksi. The UHPC had a compressive strength of 17 ksi, and its assumed tensile strength was 1.3 ksi. All three deck specimens were tested to assess the performance of the UHPC overlay: a normal concrete deck without an overlay served as a benchmark case (no overlay [NO]), a normal concrete deck with a UHPC overlay on the compression side (OT), and a normal concrete deck with a UHPC overlay on the tension side (OB).

After the formation of flexural cracks, the normal concrete without overlay specimen (NO) failed in shear, with a large shear crack developing approximately 1 ft from the support toward the midspan, as expected, as shown in Figure 2.19 (a). For Specimen OT, a similar shear failure mode was observed, but it occurred at a higher load. The shear cracks did not penetrate

the UHPC layer; instead, they turned horizontally and began to separate the UHPC overlay from the NC specimen, as shown in Figure 2.19 (b). Similar observations were made by Aaleti (2017). For Specimen OB, a relatively brittle failure mode was observed, where a single flexural crack developed mainly in the UHPC layer at midspan and propagated upward before the specimen ultimately experienced flexural tension failure, with some of the concrete at the top being crushed, as shown in Figure 2.19 (c).

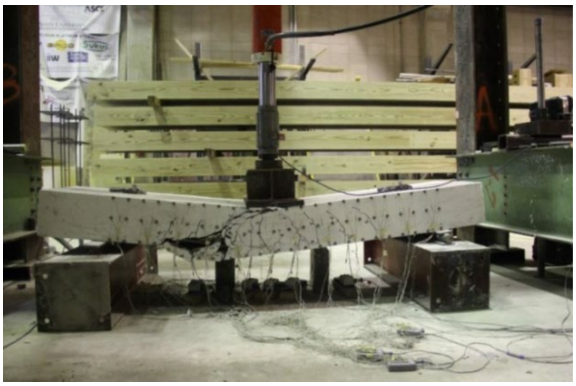

(a) NO (No overlay)

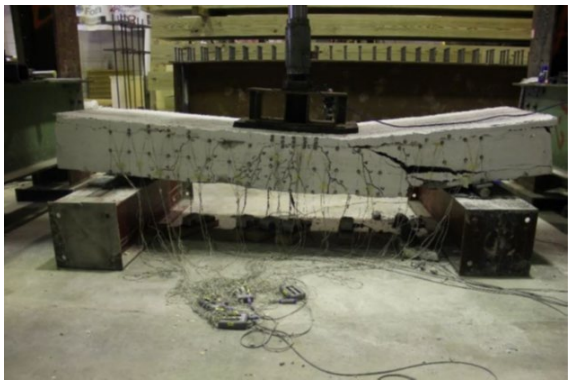

(b) OT (overlay in compression side)

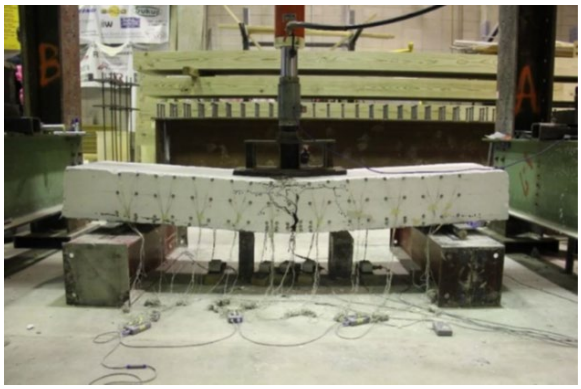

(c) OB (overlay in Tension side)

Figure 2.19 Slab specimens at failure (Wibowo et al., 2018).

This failure mode commonly occurs when tension reinforcement is insufficient to resist forces after flexural tension cracks develop in the UHPC. To enhance the negative moment capacity of the specimen with a UHPC overlay, additional rebar reinforcement within the overlay would be necessary. It is unclear whether increasing the amount of steel in the overlay would

negatively impact the bond between the UHPC and NC. The maximum applied loads for Specimens NO, OT, and OB are 48.22 kips, 61.58 kips, and 32.59 kips, respectively. The load versus displacement graphs for each case are shown in Figure 2.20.

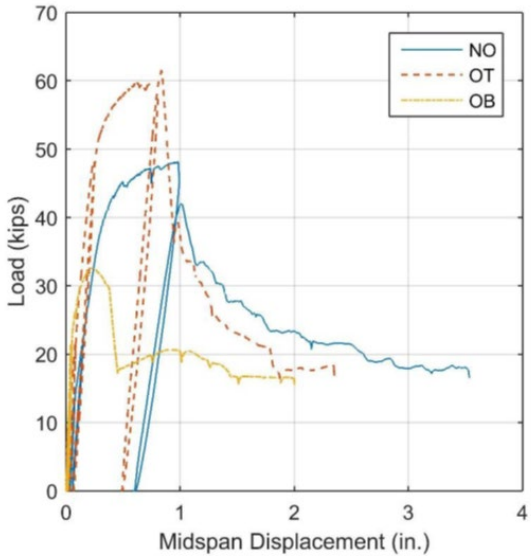

Figure 2.20 Load versus midspan displacement plots for all three specimens (Wibowo et al., 2018).

An experimental study was conducted by Starke et al. (2022) to examine the effects of changing UHPC thickness, the compressive strength of the NC bridge deck, and loading conditions. All specimens measured 21 inches wide, 93 inches long, with a 73-inch test span, and had the same reinforcement details. Three #5 Grade-60 bars were used in the bottom reinforcement layer, while two bars were placed in the top layer. #4 bars served as transverse steel. The bottom clear cover was 1 inch, and the center of the top reinforcement was located 0.31 inches below the UHPC layer. A surface retarder was used to simulate a hydro-demolished surface, promoting a strong bond between the NC slab and UHPC overlay. The study tested five specimens: one control slab of normal concrete (control), two slabs with different UHPC

thicknesses (O-PR1 and O-PR2), one composite section with weak substrate concrete (O-PW), and one composite section subjected to negative bending (UHPC in tension zone) (O-NR). Table 2.10 shows the midpoint dimensions of the specimens and the material properties on the testing day. All specimens were tested to failure in the Structures Lab at Michigan State University. The composite sections underwent 3-point bending tests, following the methodology used by Aaleti et al. (2017), with the load applied according to AASHTO-LRFD (2012). The test results indicated that the flexural capacity of specimens O-PR1 and O-PR2 was approximately 1.44 times higher than that of the control specimen. Specimen O-NR exhibited higher stiffness up to the cracking of the UHPC overlay. Afterward, it behaved similarly to the control specimen. Specimen O-PW showed a lower flexural capacity than O-PR1 and O-PR2 due to its smaller thickness.

Table 2.10 As-built dimensions and material properties (Starke et al., 2022).

Slab	**Layer**	**Thickness (in.)**	**Compressive strength (ksi)**	
			UHPC	**NC**
Control	Total	6.28	18.3	4.1
O-PR1	NC	4.96		
	UHPC	1.55		
	Total	6.51		
O-PR2	NC	4.82		
	UHPC	1.83		
	Total	6.64		
O-NR	NC	5.13		
	UHPC	1.55		
	Total	6.68		
O-PW	NC	4.5	17.6	2.7
	UHPC	1.23		
	Total	5.73		

2.8 Flexural Capacity Prediction Models

In addition to experimental work, an analytical study was also conducted by Starke et al. (2022) to predict the flexural capacity of the composite section according to ACI 318-19 and FHWA (Ocel, 2022). The Whitney stress block was used to model the NC and UHPC. However, it is recommended to use the compression model of UHPC according to AASHTO-UHPC (2024). The steel was modeled as elastic-perfectly plastic. Under negative bending moment (UHPC in tension zone), the ultimate moment capacity is calculated according to the mechanics proposed by FHWA (Ocel, 2022). The average measured moment capacity over the nominal predicted capacity reached a ratio of 1.25 for composite sections under positive bending moment. Meanwhile, the composite section under negative moment reached a ratio of 0.94.

An analytical study was conducted by Zhang et al. (2019) to predict the flexural capacity of a damaged reinforced concrete (RC) bridge deck strengthened with a UHPC layer. For a strengthened slab under negative bending moment at the ultimate state, the normal concrete in the compression zone of the RC layer approached its designed compression strength, and the internal steel in the compression zone also yielded (f_y). Additionally, the steel in both the UHPC and RC layers yielded (f_y). Since UHPC exhibits higher ductility in tension and can continue bearing the applied load after cracking, bilinear constitutive models in tension for UHPC assumed that the stress at the top of the reinforcement in the UHPC remained at its cracking strength, f_{ut}, until failure. Figure 2.21 shows the analytical model of the strengthened slab under negative ultimate moment based on the simple plastic theory of composite sections for calculation. The tension stress is evenly distributed along the height of UHPC. The calculation assumes that stress reaches the cracking strength f_{ut}. The value of the compression concrete depth x_n at the RC layer is obtained by the equilibrium of axial forces: $T_{uu} + T_{uus} + T_{ust} = C_{uc} + C_{usb}$, as simplified in **Error! Reference source not found.**. Then, the predicted flexural moment

capacity Mu- of the strengthened slab under negative bending moment is calculated by taking the moment of the forces about the neutral axis location, as given below and noted in (2.2.

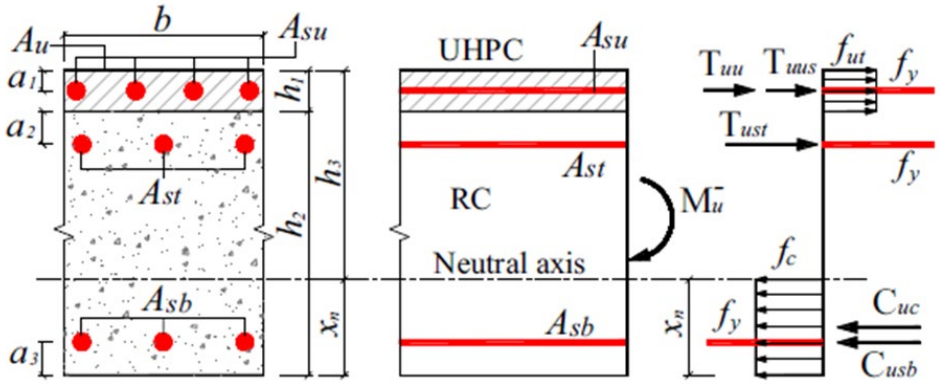

Figure 2.21 Analytical model of the strengthened slab under negative ultimate moment (Zhang et al, 2019)

$$x_n = \frac{A_u f_{ut} + f_y(A_{su} + A_{st} - A_{sb})}{f_c\, b} \tag{2.1}$$

$$M_u^- = f_{ut}\, b\, h_1(h_3 - \frac{h_1}{2}) + f_y\, A_{su}(h_3 - a_1) + f_y\, A_{st}(h_3 - h_1 - a_2) + f_y\, A_{sb}(x_n - a_3) + \frac{f_c\, b\, X_n^2}{2} \tag{2.2}$$

where T_{uu}, T_{uus}, and T_{ust} represent tensile resultant forces in UHPC, tensile resultant forces in steel in UHPC, and tensile resultant forces in steel in RC layer under the ultimate state, respectively. C_{usb} and C_{uc} represent compressive resultant forces in steel in the RC slab, and compressive resultant forces in the RC, respectively. f_y is the yield strength of steel, and f_c is the cube compressive strength of normal strength concrete.

Figure 2.22 shows an analytical model of the strengthened slab under positive ultimate moment at the ultimate state, where the entire section of the RC slab is in tension, the steel inside has yielded, and the NSC has cracked without contributing to flexure capacity. UHPC, with high

ductility, has a double-folded line constitutive model in tension. When calculating the flexure ultimate capacity of a strengthened slab under positive bending moment, as can be seen in Figure 2.22, UHPC in compression was assumed to reach the cube compression strength evenly. f_u and UHPC in tension evenly reached the cracking strength f_{ut}. Because the steel reinforcement in UHPC is located close to the plastic neutral axis, it does not contribute to the flexural ultimate capacity. The value of compression concrete depth x_0 in the UHPC layer is obtained by the equilibrium of axial forces: $T_{usb} + T_{ust} + T_{ub} = C_u$, as simplified in (2.3. Then, the predicted flexural moment capacity M_u+ of the strengthened slab under positive bending moment is calculated by taking the moment of forces about the neutral axis location at the UHPC layer as noted in (2.4.

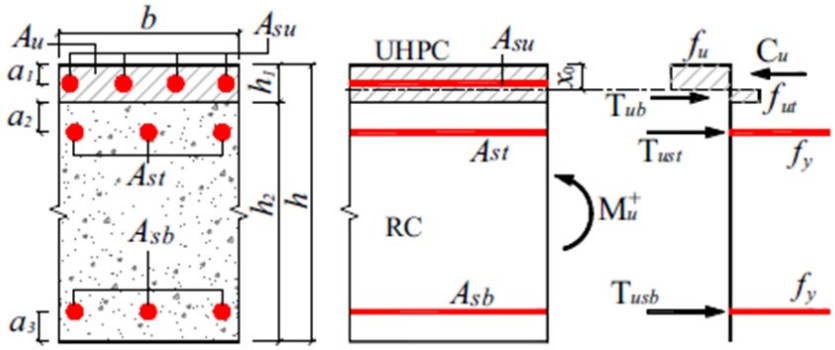

Figure 2.22 Analytical model of strengthened slab under positive ultimate moment (Zhang et al., 2019)

$$x_o = \frac{f_y A_{st} + f_y A_{sb} + f_{ut}\, b\, h_1}{b(f_{ut} + f_u)} \tag{2.3}$$

$$M_u^+ = \frac{f_u\, b\, X_o^2}{2} + \frac{f_{ut}\, b}{2}(h_1 - X_o)^2 + f_y A_{st}(h_1 + a_2 - X_o) + f_y A_{sb}(h - a_3 - X_o) \tag{2.4}$$

where f_u and f_{ut} represent the cube compressive strength of UHPC and cracking strength respectively; C_u represents compressive resultant forces in UHPC; and T_{ub}, T_{ust}, and T_{usb}

represent tensile resultant forces in UHPC and tensile resultant forces in steel at the top and bottom of the RC layer, respectively.

2.9 Lifecycle Cost Analysis of UHPC Overlay

The lifecycle cost analysis (LCCA) was conducted by a signature bridge owner to evaluate different overlay options for one of the bridges in Haber et al. (2022b). The study focused on the Delaware Memorial Bridge, which has a total surface area of 550,575 square feet. As clarified in Figure 2.23, three different overlay installation strategies were considered in this study. Installation strategy one (IS1) involved removing 1.75 inches of the existing normal concrete cover to within 0.4 inches of the top reinforcement. Installation strategy two involved removing 3.75 inches of normal concrete to a depth of 0.75 inches below the reinforcement. The removed cover in the first two strategies was replaced with overlay material. Meanwhile, strategy three involved removing 3.75 inches of normal concrete, similar to strategy two, but replacing it with 2.5 inches of overlay and 1.25 inches of asphalt. UHPC and latex-modified concrete (LMC) were utilized as overlay materials in this study.

As noted in Table 2.11, the construction costs, including materials, labor, hydro-demolition for bridge deck surface preparation, and traffic control, were estimated based on the experience in the projects with a 1.5 percent real discount rate.

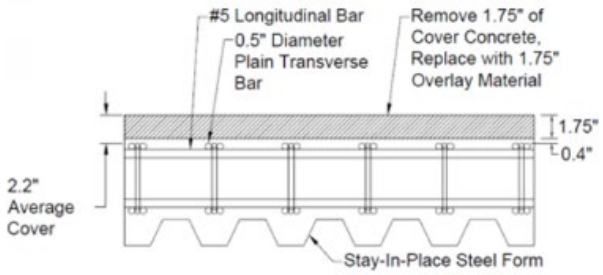

IS1: using a 1.75 in. overlay.

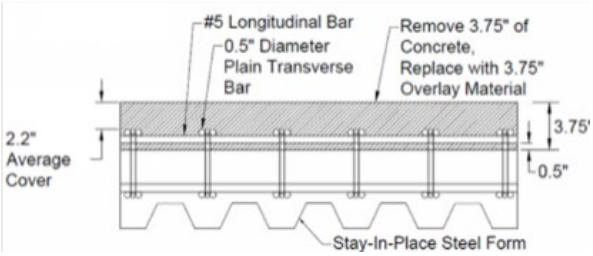

IS2: using a 3.75 in. overlay.

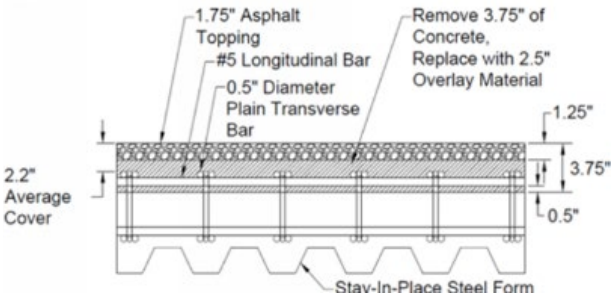

IS3: using a 2.5 in. overlay with 1.25 in. asphalt.

Figure 2.23 Illustration of the used strategies (Haber et al., 2022b)

Table 2.11 Estimated unit construction costs (Haber et al., 2022b).

Installation Strategy	**UHPC (Cost/ft^2)**	**LMC (Cost/ft^2)**
1	$55	$23
2	$127	$39
3	$109	Not considered for analysis

The analysis showed that although UHPC has a higher initial cost than other conventional overlays, it can offer long-term savings. Also, the cost of a UHPC overlay was much lower than that of a deck replacement, making up for a potentially shorter service life with a quicker installation. The results of the LCCA revealed that the UHPC overlay had the lowest 50-year lifecycle cost, making UHPC the most cost-effective choice, as illustrated in Figure 2.24.

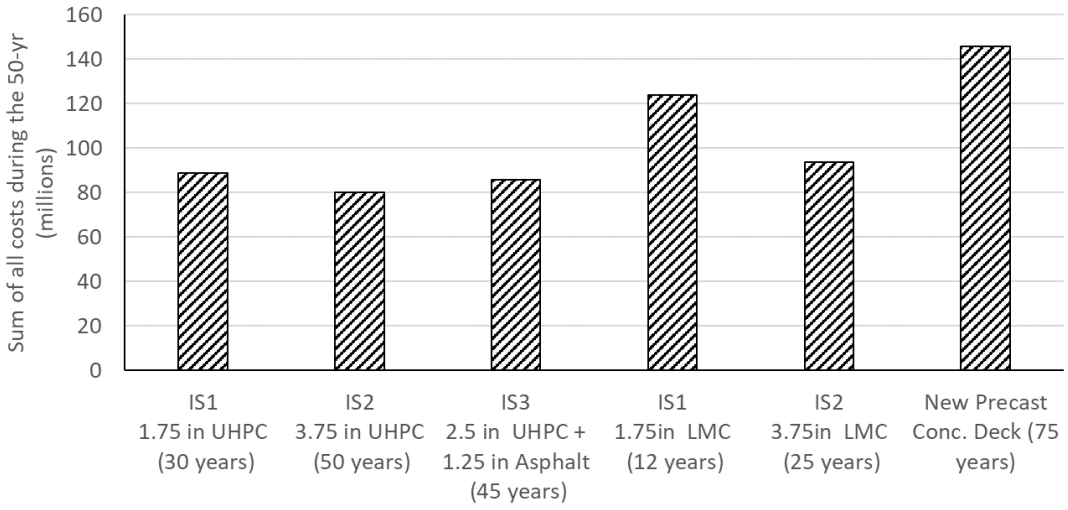

Figure 2.24 Lifecycle cost comparison for overlay methods and new precast concrete deck (Haber et al., 2022b)

2.10 Summary

This chapter presented the results of the literature review conducted for this research, summarizing all UHPC overlay projects completed to date and their construction methods. It discussed the mixture design of UHPC overlays, emphasizing differences from self-leveling traditional UHPC in terms of fiber content and rheological properties. The chapter also offered an overview of fiber amounts used by various agencies and field projects. Moreover, it detailed the fresh, mechanical, and durability properties of UHPC overlay materials, along with the relevant requirements set by state agencies. Additionally, it described common surface preparation techniques for NC bridge deck slabs and their bond strengths with UHPC overlays. The chapter included structural laboratory testing of NC slabs overlaid with UHPC and provided a summary of a life-cycle cost analysis of different overlay materials, highlighting the cost-effectiveness of UHPC overlays.

Chapter 3 Experimental Program

3.1 Introduction

This chapter offers a thorough overview of the materials, mixture design, mixing process, and test methods used in the production and assessment of UHPC overlay. Known for its exceptional mechanical properties and durability, UHPC overlay requires careful material selection and precise mixing procedures to achieve optimal performance. Unlike standard UHPC, UHPC overlays have unique properties tailored to their specific applications. Rigorous testing methods are crucial to ensure the quality and dependability of this overlay.

3.2 Materials and Mixture Design

In this study, all mixes used Type IL Portland cement that meets ASTM C150 standards, sand with a maximum particle size of 2 mm, ground-granulated blast-furnace slag following ASTM C989, densified silica fume, and micro straight steel fibers measuring 13.0 mm long and 0.2 mm in diameter as dry ingredients. The liquid parts included a water-reducing and retarding (WRT) admixture that complies with the Type S specifications in ASTM C494, along with a modified polycarboxylate-based high-range water-reducing (HRWR) admixture matching Type F standards. Tap water was used for mixing.

In this study, various UHPC overlay mixtures were prepared with different binder contents, w/b ratios, varying dosages of WRT and HRWR, and different amounts of incorporated fibers as outlined in Table 3.1. The mixtures were divided into seven groups, each distinguished by the amount of incorporated materials. Cast-in-place (CIP) UHPC is a recently developed NDOT non-proprietary UHPC mixture for precast and cast-in-place applications. Group B mixtures were adjusted with a higher amount of WRT than HRWR to achieve the desired workability while maintaining the same water-to-binder ratio (0.180) and fiber content (2%) as the reference mixture (CIP). Additionally, Group B has an increased binder content of 1900 pcy

(same as the CIP mixture). Meanwhile, Group C and D mixtures have a reduced binder content (1450 pcy), with Group C having an increased water-to-binder ratio (0.196). On the other hand, the mixtures for groups E, F, and G are identical to those for groups C, B, and D, respectively, except that the fiber content is adjusted to 3%. The amount of integrated HRWR and WRT were adapted from the reference mixture to reach thixotropic UHPC for overlay and structural repair applications.

The identification of each mixture relies on the following parameters: the percentage of fibers in the total volume, binder content, water-to-binder (w/b) ratio, and the amounts of HRWR and WRT admixtures in pounds per cubic yard (pcy). For each mixture ID, shortened IDs were used in the order of mixing for later reference in the report. The mass of the fine aggregate in Table 3.1 was measured in an air-dried state with about 0.2% moisture content, and minor differences in moisture level were equalized before batching. It is also important to note that when binder content was reduced, it was compensated for by increasing the sand amount.

Table 3.1 Mix design (pcy).

	Mixture ID	Mixture ID	Cement	Slag	Silica fume	Sand	Fiber	Water	HRWR	WRT	w/b	HRWR %	WRT (%)	Fib (%)
CIP	**CIP**	CIP-1900-0.180-H51-W21	1206	586	161	1597	265	302	50.8	20.7	0.180	2.60	1.06	2
B	**Mix 3**	F2%-1900-0.180-H21-W44	1206	586	161	1602	265	306	20.7	44.0	0.180	1.06	2.25	2
	Mix 4	F2%-1900-0.180-H10-W44	1206	586	161	1608	265	314	10.0	44.0	0.180	0.51	2.25	2
	Mix 5	F2%-1900-0.180-H0-W56	1206	586	161	1607	265	313	0	55.6	0.180	0	2.85	2
	Mix 6	F2%-1900-0.180-H0-W69	1206	586	161	1599	265	304	0	68.6	0.180	0	3.51	2
	Mix 12	F2%-1900-0.180-H4-W65	1206	586	161	1599	265	304	3.9	64.7	0.180	0.20	3.31	2
	Mix 13	F2%-1900-0.180-H4-W61	1206	586	161	1601	265	306	3.9	60.8	0.180	0.20	3.11	2
	Mix 16	F2%-1900-0.180-H4-W56	1206	586	161	1605	265	310	3.9	56.0	0.180	0.20	2.87	2
	Mix 18	F2%-1900-0.180-H0-W61	1206	586	161	1603	265	309	0	60.9	0.180	0	3.12	2
	Mix 28	F2%-1900-0.180-H3-W52	1206	586	161	1608	265	303	3.0	51.8	0.180	0.15	2.65	2
	Mix 29	F2%-1900-0.180-H3-W47	1206	586	161	1610	265	317	2.9	47.1	0.180	0.15	2.41	2
C	**Mix 7**	F2%-1450-0.196-H0-W52	895	435	120	2233	265	248	0	51.9	0.196	0	3.58	2
	Mix 8	F2%-1450-0.196-H3-W54	895	435	120	2230	265	245	2.6	53.6	0.196	0.18	3.70	2
	Mix 14	F2%-1450-0.196-H3-W52	895	435	120	2231	265	246	2.9	51.5	0.196	0.20	3.55	2
	Mix 15	F2%-1450-0.196-H3-W47	895	435	120	2234	265	249	2.9	47.1	0.196	0.20	3.25	2
	Mix 19	F2%-1450-0.196-H0-W49	895	435	120	2234	265	250	0	49.0	0.196	0	3.38	2
D	**Mix 9**	F2%-1450-0.180-H8-W54	895	435	120	2288	265	218	8.1	53.6	0.180	0.56	3.70	2
	Mix 11	F2%-1450-0.180-H8-W73	895	435	120	2275	265	205	8.1	72.5	0.180	0.56	5.00	2
	Mix 17	F2%-1450-0.180-H4-W54	895	435	120	2290	265	221	4.0	53.6	0.180	0.28	3.70	2
E	**Mix 20**	F3%-1450-0.196-H4-W59	895	435	120	2181	397	240	3.6	59.1	0.196	0.25	4.07	3
	Mix 24	F3%-1450-0.196-H3-W54	895	435	120	2186	397	245	2.6	53.6	0.196	0.18	3.70	3
	Mix 26	F3%-1450-0.196-H3-W47	895	435	120	2190	397	249	2.9	47.1	0.196	0.20	3.25	3
F	**Mix 21**	F3%-1900-0.180-H5-W62	1206	586	161	1555	397	305	5.0	62.0	0.180	0.26	3.17	3
	Mix 22	F3%-1900-0.180-H4-W58	1206	586	161	1558	397	308	3.9	58.2	0.180	0.20	2.98	3
	Mix 23	F3%-1900-0.180-H4-W56	1206	586	161	1560	397	310	3.9	56.0	0.180	0.20	2.87	3
	Mix 25	F3%-1900-0.180-H3-W54	1206	586	161	1562	397	312	2.6	53.7	0.180	0.13	2.75	3
	Mix 27	F3%-1900-0.180-H3-W47	1206	586	161	1566	397	316	2.9	47.2	0.180	0.15	2.42	3
G	**Mix 10**	F3%-1450-0.180-H10-W62	895	435	120	2236	397	210	10.3	62.2	0.180	0.71	4.29	3

3.3 Mixing Procedure

In this study, two different types of mixers were used, and their results were compared. For small batches, a 20-quart Vollrath benchtop mixer (0.5 HP) with three speed settings was used to mix 0.20 cubic feet (0.0045 m^3) of UHPC overlay. For larger batches, selected mixtures were prepared using a IMER 120 vertical shaft mixer (2 HP) with a batch size of 1 cubic feet (0.03 m^3) and an IMER 750 vertical shaft mixer (5 HP) with a batch size of approximately 4 cubic feet (0.11 m^3).Photos of the three different mixers used in the project are shown below in Figure 3.1.

Figure 3.1 Mixers used in UHPC batching (left to right: Vollrath benchtop mixer, IMER 120 mixer, and IMER 750 mixer)

The mixing procedure used in this study was based on the mixing procedure of recently developed NDOT non-proprietary UHPC with some minor adjustments (Mendonca et al. 2020). To achieve the desired consistency, UHPC was mixed in three main steps: first, mixing the dry ingredients; second, adding water and admixtures; and third, introducing steel fibers. It is important to note that mixing UHPC overlay in small batches requires adjusting the speed to

reach the desired consistency. Aside from this adjustment, the procedure is identical to that used for larger batches. Generally, the first step involved loading air-dried sand and silica fume into the mixer and stirring for five minutes, followed by adding cement and slag and mixing for another five minutes. Before adding water into the mixture (which begins the second step), 100% of the total WRT was premixed with 80% of the total water. This premixed solution was then added to the mixer and stirred with dry ingredients for seven minutes. The remaining 20% of the water and HRWR admixture were premixed again and added to the mixer. Adding the remaining water with HRWR started the transition from powder to paste. Visual assessment of the mixture's flowability was needed to determine the right time for fiber addition, as by then the mixture should be flowable. Once a viscous, smooth mixture was obtained, the fibers were added and mixed for one minute, then mixed for another three minutes. The final thixotropic UHPC was used to evaluate the properties of the mixture in both its fresh and hardened states.

Figure 3.2 illustrates the appearance of the mixtures at different stages of the mixing process, as previously described. In Figure 3.2, photograph (1) shows the mixture immediately after sand and silica fume are combined. Photograph (2) displays the mixture after adding cement and slag. Photograph (3) captures the mixture following the addition of the first portion of the premixed liquid (80% water + 100% WRT). Photograph (4) demonstrates the mixture after the second portion of the premixed liquid (20% water + 100% HRWR) is added. Finally, photograph (5) presents the final product after the fibers have been incorporated.

Figure 3.2 Appearance of the mixtures at various stages of the mixing process

3.4 Test Methods

3.4.1 Fresh and Early-Age Properties Testing

3.4.1.1 Practical Applications of Test Methods in the Field

There are several fresh state property test methods that must be performed to verify a good UHPC Overlay mixture. However, it is important to assess the practical uses of these test methods to understand how they are actually applied in the field and the reason for their development at the laboratory level. As shown in Figure 3.3, each test method is responsible for specific applications.

Static flow refers to the ability of the UHPC overlay to spread and self-level under its own weight without external vibration. This property ensures that the overlay material is stable and spreadable enough for the paver to begin placement. On the other hand, dynamic flow describes the behavior of the UHPC overlay when subjected to external forces or vibration. In

the context of UHPC overlay placement, dynamic flow facilitates proper compaction and fills voids in the roughed concrete substrate (for overlay applications) and around reinforcement (for structural repairs). It is important to note that insufficient static and dynamic flows can lead to poor consolidation, resulting in weak bonding and delamination. Meanwhile, excessive fluid UHPC can cause uneven thickness and runoff issues, especially on steeper slopes. Therefore, ensuring the proper flow of UHPC overlay mixtures is essential for successful field applications.

In addition to standard flow evaluation tests, Patting Response (PR) and Vibration Slope Stability (VSS) tests were developed to assess how UHPC overlay material behaves on inclined surfaces. PR measures the material's response to vibration (paver), aiming for a smooth and well-consolidated surface. In other words, it gauges how flexible and easy the material is to work with under vibration to achieve a smooth surface without roughness. Meanwhile, the practical use of the VSS test is clear. It evaluates the constructability of UHPC on inclined surfaces, ensuring that the material spreads evenly under the paver without sliding down the sloped bridge surface. This test confirms that the material reaches a smooth, well-consolidated finish.

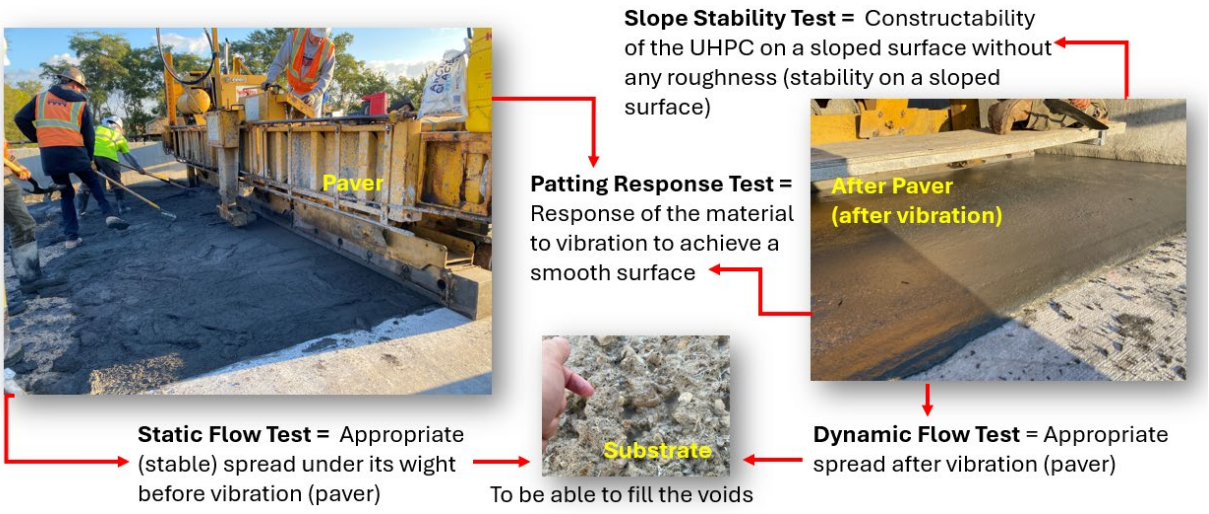

Figure 3.3 Practical applications of fresh properties tests.

3.4.1.2 Flow Test

The flowability of each UHPC overlay mixture was measured to determine adequate thixotropic properties and overall workability. The standard flow table used has a 10-inch diameter and is equipped with flow cone with a four-inch diameter at the bottom and a 2.5-inch diameter at the top, as specified in ASTM C230. Static flow testing followed ASTM C1856, while dynamic flow testing was performed in accordance with ASTM C1437. After measuring the average static flow diameter at two minutes, the table was dropped 25 times, and the average dynamic flow diameter was recorded. The conventional UHPC at static flow and the thixotropic overlay UHPC after static and dynamic flow tests are illustrated in Figure 3.4.

(a) Static flow of conventional UHPC

(b) Static flow of overlay UHPC

(c) Dynamic flow of overlay UHPC)

Figure 3.4 Examples of UHPC mixtures after flow test.

The static and dynamic flows were measured at 0 and 30 minutes after mixing. The material was kept inside a container and covered with a plate between tests. Before conducting the test at 30 minutes, the material was agitated for 30 seconds. For the overlay UHPC, the material is expected to maintain its flowability for at least 30 minutes to ensure proper placement. The acceptance criteria for evaluating flow results are based on an extensive review

of relevant literature and established specifications from authoritative agencies (IADOT (2022), NJDOT, FHWA (2022)). The acceptance criteria for static flowability are defined as less than six inches, while for dynamic flow, the criteria are set at more than six inches. Failure to meet the specified flow results at the designated times in either of the flow tests indicates that the mixture has not met the acceptance test criteria. Table 3.2 shows sample photographs of passed and failed mixtures.

Table 3.2 Recommended criteria for flow test.

Pass		**Fail**	
Static<6”	Dynamic>6”	Static>6”	Dynamic <6”
			

3.4.1.3 Patting Response (PR) Test

Since the UHPC overlay material will be subjected to a paver (an external energy source) for compaction, the performance of the fresh mixtures under external energy was evaluated using a newly developed Patting Response (PR) test. Because thixotropic UHPC must respond well to vibration for proper compaction and placement, a PR was created to assess the developed UHPC mixtures. The test measures how easily the material responds to vibration, ensuring it creates a smooth surface and maintains optimal viscosity, meaning it is neither too fluid nor too stiff.

Once the dynamic flow test was completed, the agitated UHPC overlay mixtures were patted 10 to 15 times to evaluate their response to external energy (Figure 3.5). The PR was determined based on the appearance of the UHPC mixture after patting.

(a) Mixture appearance after dynamic flow test (prior to patting)

(b) Patting

(c) Mixture appearance after patting

(d) Flowable UHPC (F1)

(e) Stiff overlay UHPC (F2)

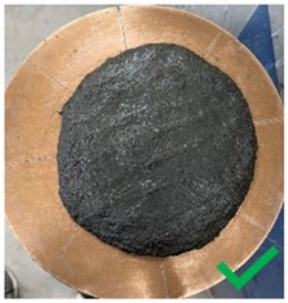

(f) thixotropic UHPC (P1)

(g) Semi-Thixotropic UHPC (P2)

Figure 3.5 Test process and results from PR test.

As shown in Figure 3.5, if the material is too flowable, the handprints left after patting will not stay, which is considered failure mode 1 (F1). Conversely, if the material is not flowable enough, the handprints will not be imprinted at all due to the stiff surface, classified as failure mode 2 (F2). On the other hand, if the handprints remain after patting and the surface of the UHPC has a uniform texture without any irregularities, the mixture passes the test, known as passing mode 1 (P1). However, there are cases where the mixture responds well to external

energy by visibly imprinting handprints, but the imprint surface is not perfectly smooth; this is considered a pass with the condition that the mixture passes the constructability test, referred to as passing mode 2 (P2). In this study, the PR test was performed whenever a flow test was conducted, meaning that failure at either 0 or 30 minutes indicated the mixture failed the test.

3.4.1.4 Vibration-Slope Stability (VSS) Test

To validate the mixtures' ability to maintain the desired slope before and during vibration, a Vibration-Slope Stability (VSS) test was conducted. The test setup included a 12" x 12" x 4" steel frame positioned at a 5° slope (8.75% grade) and securely attached to a vibrating table, as shown in Figure 3.4. To simulate the surface of a roughened bridge deck, a 12" x 12" x 2" masonry block with a slightly rough surface was placed inside the testing setup. The fresh UHPC overlay, with a one-inch thickness, was manually spread on top of the masonry block and finished to a smooth surface for better assessment. The installed material was vibrated at a laboratory vibrating table control level 5 and 6500 rpm vibration frequency for one minute to evaluate the UHPC overlay mixture's performance under vibration at this specific slope. Figure 3.6 illustrates the testing process of the developed UHPC overlay mixtures for slope stability under vibration.

If the difference between the preset slope angle of the test frame and the surface angle of the UHPC after placement before vibration was less than or equal to 1.0 degrees ($\Delta\ Angle_{ap} \leq 1.0°$), it indicated that the material was sufficiently stable for the intended slope, thus partially passing the test. If the angle remained stable after vibration, showing a change of less than 0.5 degrees ($\Delta\ Angle_{av} \leq 0.5°$), it demonstrated that the material maintained consistent flow under vibration, ensuring uniform thickness and adherence to the intended slope, and thus fully passing the test. Conversely, if the angle either before vibration (after placement) exceeded 1.0 degrees ($\Delta\ Angle_{ap} > 1.0°$) or after vibration exceeded 0.5 degrees ($\Delta\ Angle_{av} > 0.5°$), it suggested that

the material might be too fluid for the intended slope, leading to test failure.

Here, ΔAngle_{ap} and ΔAngle_{av} represent the absolute differences between the preset frame slope and the measured UHPC surface angles before and after vibration, respectively. A mixture passed the VSS test only when $\Delta\text{Angle}_{ap} \leq 1.0^{\circ}$ and $\Delta\text{Angle}_{av} \leq 0.5^{\circ}$; these limits are not additive. It is important to note that failure in either Angle_{ap} (angle after placing) or Angle_{av} (angle after vibration) indicates that the mixture failed the test in this study. Table 3.3 displays the recommended criteria and sample photographs of UHPC overlay with Pass/Fail results.

Figure 3.6 Vibration-Slope Stability (VSS) test setup and process.

Table 3.3 Recommended criteria for Vibration-Slope Stability (VSS) test.

	Initial condition	**Pass**		**Fail**	
	Before placing UHPC	Δ $Angle_{ap}$<=1.0º	Δ $Angle_{av}$<=0.5º	Δ $Angle_{ap}$=>1.0º	Δ $Angle_{av}$=>0.5º
		After placing/Before vibration UHPC	After vibration UHPC	After placing/Before vibration UHPC	After vibration UHPC
Sample		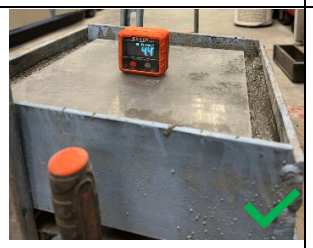			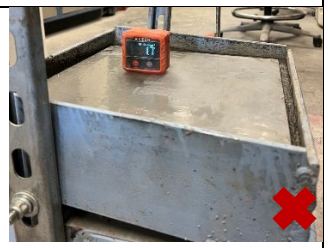
Description	NA	The angle after placement remained within the specified range, indicating that the material is sufficiently stable for the identified slope.	The angle after vibration remained stable, indicating that the material possesses sufficient resistance to flowability under vibration and maintains the intended slope.	The angle after placing UHPC decreased considerably which implies that the material exhibits excessive flowability even without external vibration.	The angle after vibration substantially decreased/increased which implies the material may be excessively fluid for the intended slope.

3.4.1.5 Heat of Hydration

The assessment of hydration heat is a useful tool for understanding the cement hydration process, especially in its early stages. An isothermal calorimeter, following ASTM C1702 standards, was used to measure the initial and final setting times as well as the UHPC's heat of hydration under constant conditions (23°C) within the first 72 hours. Figure 3.7 shows an isothermal calorimeter made up of eight individual units, each designated for holding separate samples during testing. After mixing, a specimen weighing 110±10 g of UHPC was quickly placed into a small plastic cup. The cup containing the specimen was then inserted into the calorimeter to start the test. Using a computer program, data were collected at 60-second intervals over 72 hours to create a curve of heat generation rate versus hydration time. The initial and final setting times were determined by analyzing the first derivative of the heat evolution curve. According to Hu et al. (2014), the initial setting time occurs when the first derivative reaches its maximum value, while the final setting time is when the first derivative drops to zero. Figure 3.5 shows the heat of hydration test setup and an example of the results.

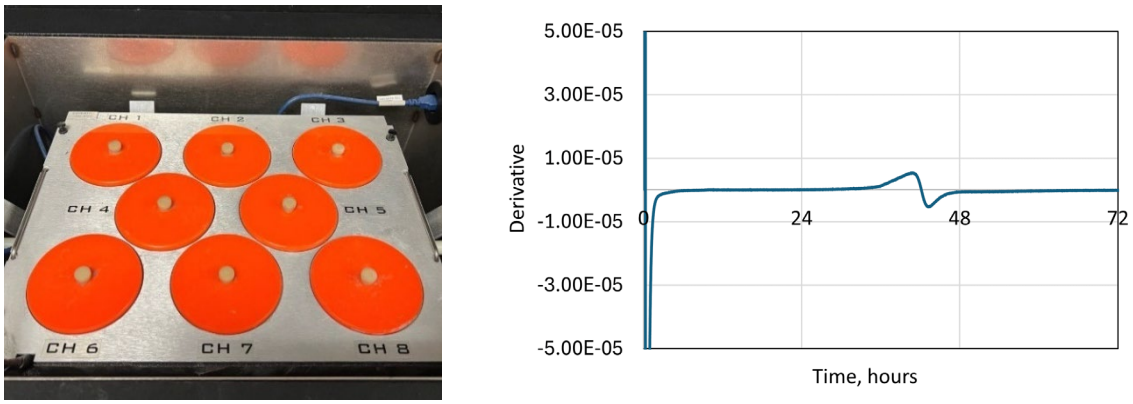

(a) Isothermal calorimeter test units (b) An example of results

Figure 3.7 Heat of hydration test.

3.4.2 Mechanical Properties Testing

3.4.2.1 Compressive Strength Test

The developed UHPC overlay mixtures should also meet performance requirements in the hardened state. The compressive strength test was performed on each UHPC mixture following ASTM C1856. After curing for 7, 14, 28, and 56 days in a water tank with lime, the cast 3” x 6” cylinders were ground at both ends before testing. Three specimens were tested for each case, and an average value was reported.

3.4.2.2 Static Modulus of Elasticity

The static modulus of elasticity (MOE) of UHPC mixes was determined following ASTM C469. Three 4” × 8” cylindrical specimens for each mix were tested after 28 days of curing in water tank with lime, and the average MOE value was reported. Deformation measurements were obtained using a gauge attached to the test setup shown in Figure 3.8.

Figure 3.8 Static modulus of elasticity test setup.

3.4.2.3 Flexural Strength Test

According to ASTM C1856, the flexural strength test of UHPC follows the guidelines of ASTM C1609/C1609M for evaluating the flexural performance of fiber-reinforced concrete. The specimen size varies depending on fiber length. The steel fibers used had a length of 0.5 inches, which allows for a minimum cross-section of three inches by three inches. According to ASTM C1609, the minimum effective length (L) of the flexural specimen should be three times its depth and no less than 12 inches. Three specimens measuring 3 x 3 x 16 inches from each mix were tested for flexural strength using four-point loading, as shown in Figure 3.9. A Tinius Olson testing machine was employed to apply compressive load until failure. The load was applied at a displacement rate starting at up to 0.003 in./min until a mid-span deflection of L/900, then gradually increased to 0.008 in./min until reaching a mid-span deflection of L/150. Mid-span deflection of the specimens was recorded with two LVDTs attached to the steel base and directed towards a steel frame mounted on the top middle section of each specimen. As shown in Figure 3.10, results are considered valid when cracks appear in the middle third of the beam. Figure 3.11 presents an idealized load-deflection curve from the flexural test. The actual width and depth of each specimen were measured to ensure accurate calculation of flexural strength. The strength was determined using bending theory for linear elastic materials and gross (uncracked) section properties in accordance with ASTM C1609.

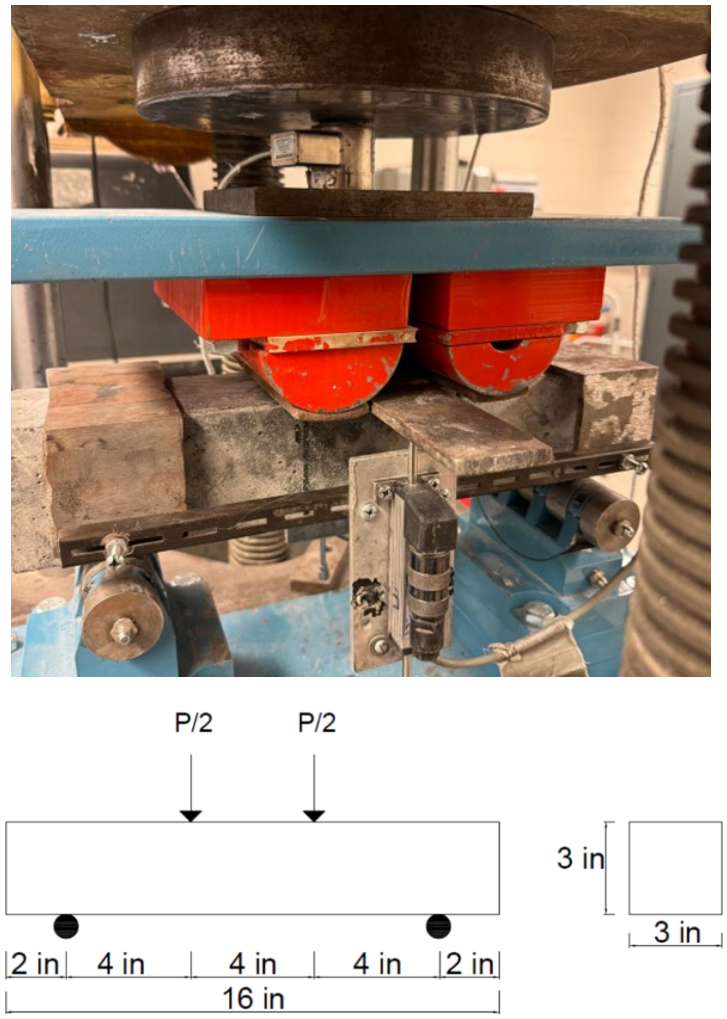

Figure 3.9 Flexure Strength Test Setup.

Figure 3.10 Accepted failure.

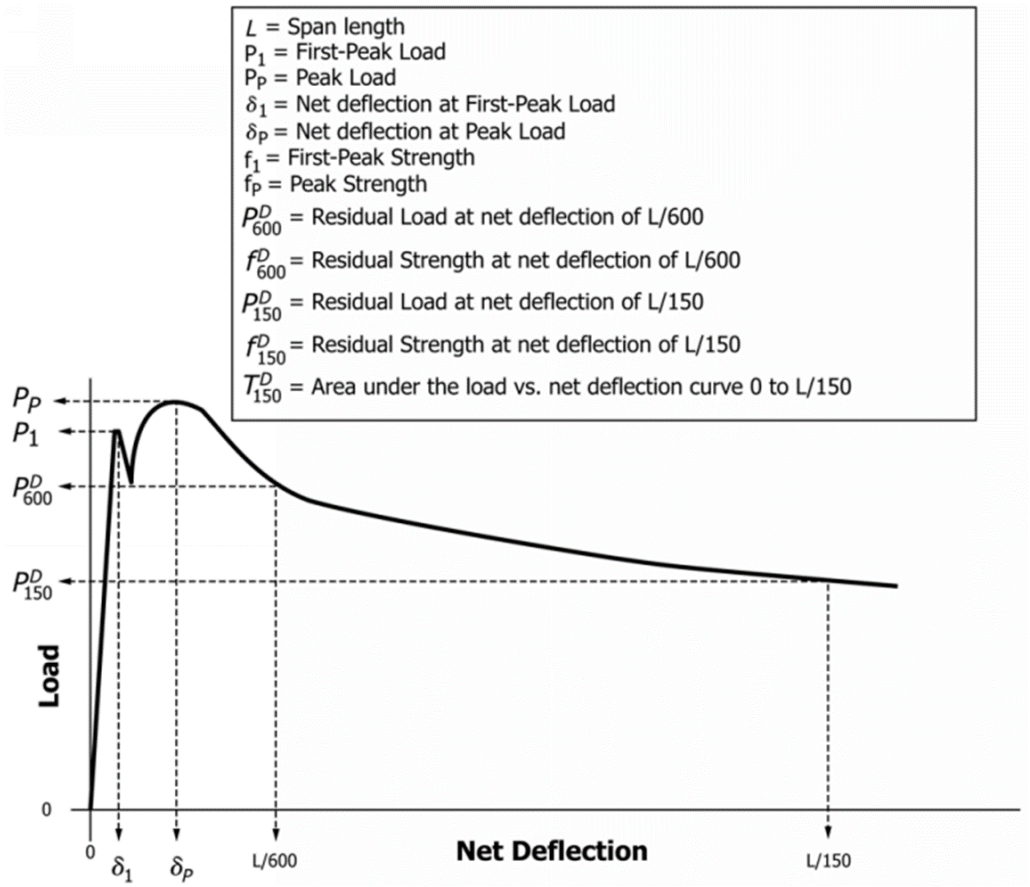

Figure 3.11 Idealized load-deflection curve for flexure test.

3.4.2.4 Uniaxial Tensile Strength Test

The uniaxial tensile response of UHPC mixes was tested in accordance with AASHTO T 397. The used steel fibers had a length of 0.5 in., which allows a cross-section for a tension specimen of 2 in. x 2 in. The length of the test specimens with transfer plates shall be sufficient to allow for the gripping of each end plus the gauge length: thus, 17 in., 6 in., and 5 in. were used for total length, transfer plate length, and gauge length respectively, as clarified in Figure 3.12. Four 2 in. x 2 in. x 17 in. prisms were tested for each mix. An aluminum plate with 0.125 in. thickness was used as a transfer plate and it had dimensions of 2 in. x 6 in., as shown in Figure 3.12. Before installing the aluminum transfer plate, the specimens' surfaces were roughened with sandpaper. The transfer plate was affixed to the specimen using high-stiffness structural epoxy,

per AASHTO T 397. Then, the specimens were clamped with six C-clamps, as shown in Figure 3.13. The deformation of the specimens was measured using a set of LVDTs that collectively monitored the movement of one cross-sectional plane of the test specimen relative to another. These planes are at the right angles to the applied force as well as the longitudinal centroidal axis of the specimen. A parallel ring extensometer apparatus was used for these measurements. Four LVDTs are affixed to the lower ring, and the bearing points for these transducers are located on the upper ring, as shown in Figure 3.12. The distance between the upper and lower rings was 4 in. The average transducer reading represented the axial deformation over the gauge length. An MTS machine was used to conduct the tensile test. The grip pressure on the upper and lower grips should be sufficient to hold the test specimen without slippage during the test. A tensile load was applied to the specimen via a constant crosshead displacement rate of 0.006 in./minute. The test specimen was only considered successful when the crack localization happened in the gauge length. The tensile strength and strain were calculated using the theory for linear elastic material and cross-sectional (uncracked) properties. Figure 3.14 shows the idealized typical tensile stress–strain response of a UHPC Specimen.

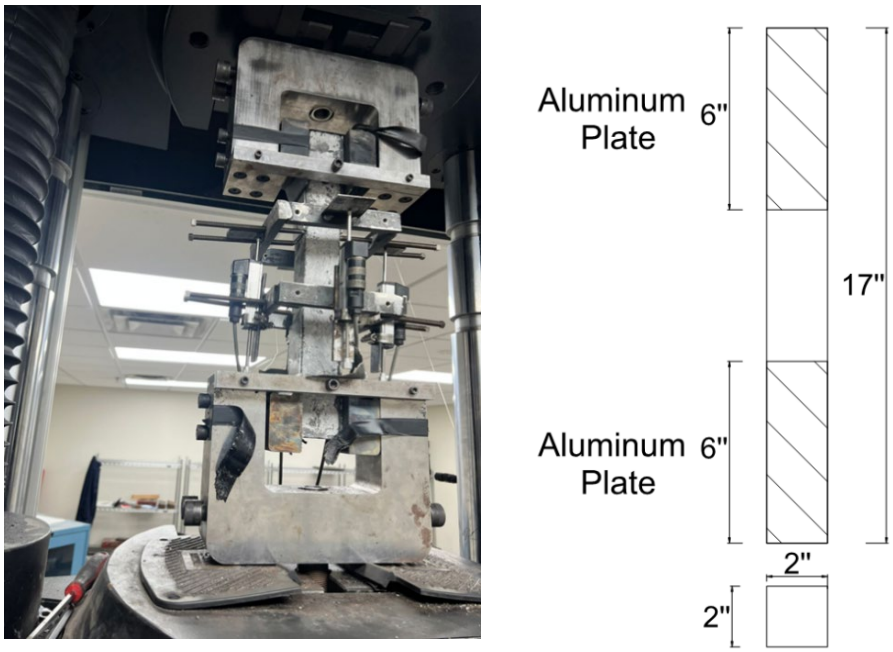

Figure 3.12 Uniaxial tensile strength test setup.

Figure 3.13 Clamping of Specimens.

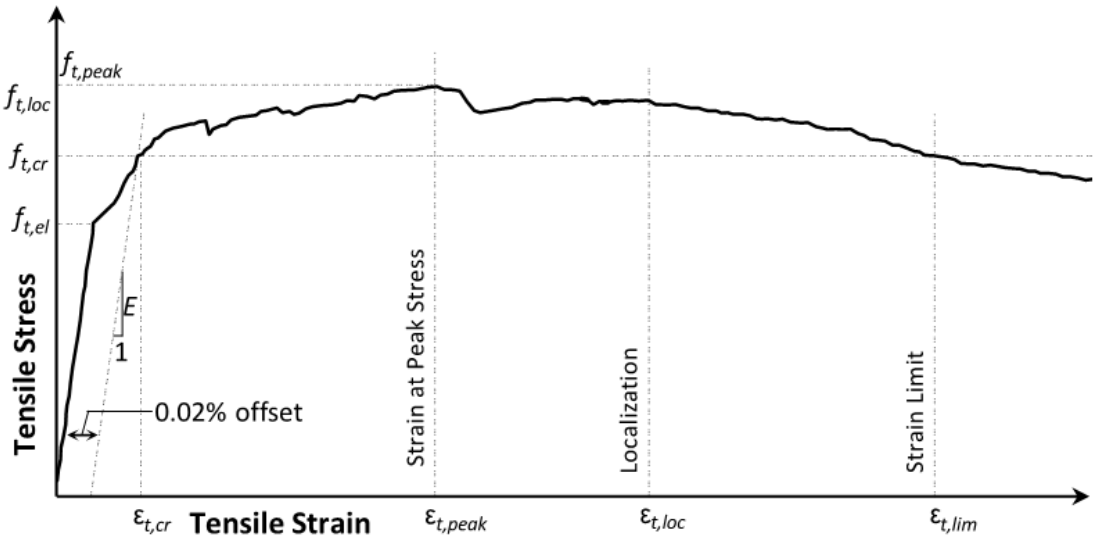

Figure 3.14 Idealized typical tensile stress-strain response of UHPC specimen.

where,

$f_{t,cr}$	=	effective cracking strength
$f_{t,el}$	=	elastic tensile strength
$f_{t,peak}$	=	peak tensile strength
$f_{t,loc}$	=	localization stress
$\varepsilon_{t,cr}$	=	strain at effective cracking strength
$\varepsilon_{t,lim}$	=	tensile strain limit
$\varepsilon_{t,loc}$	=	localization strain
$\varepsilon_{t,peak}$	=	strain at peak strength

3.4.2.5 Bond Strength Test

The bond between the UHPC overlay and the NC slab was assessed following ASTM C1583. A two-inch diameter circular cut, perpendicular to the surface, was drilled into the composite section using coring equipment. The drilling extended at least 0.5 inches below the interface between the UHPC overlay and the NC slab. After drilling, the surface was cleaned of debris and allowed to dry. Next, a fast-curing epoxy adhesive was applied to bond the steel disk to the test specimen. Once the adhesive cured, the tensile loading device was attached to the steel disk using a coupling device. A tensile load was then applied at a steady rate of 5 ± 2 psi/sec. As shown in Figure 3.15, the tension force was aligned parallel to the test specimen and along its

axis. Figure 3.16 depicts possible failure modes, which can occur within the substrate, at the concrete-overlay interface, within the overlay, or at the epoxy-overlay interface.

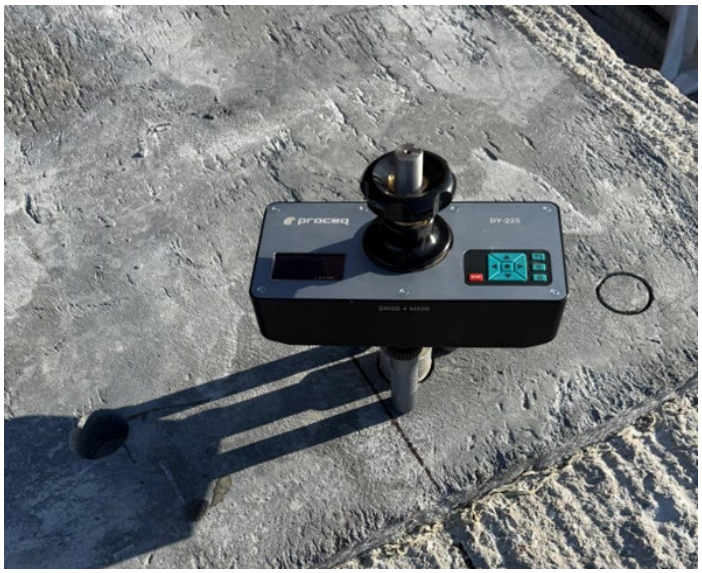

Figure 3.15 Bond strength test setup.

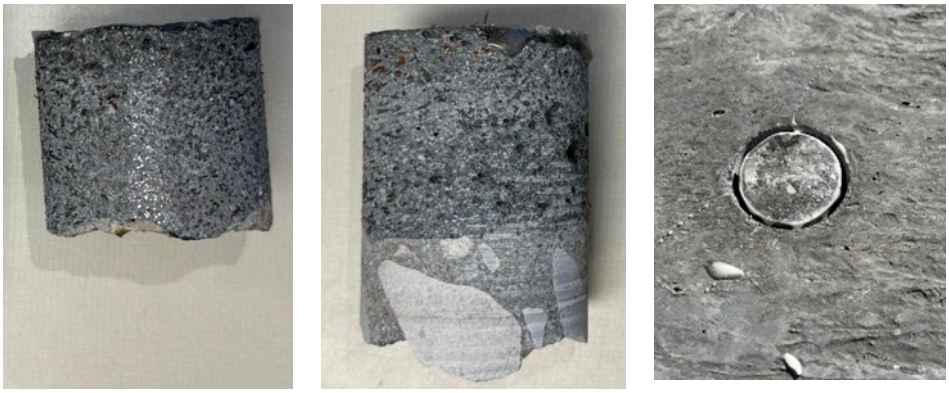

(a) At NC-UHPC interface (b) In NC substrate (c) In glue between UHPC and steel disc

Figure 3.16 Failure locations of pull-off test.

3.4.3 Durability Properties Testing

3.4.3.1 Freeze-thaw Cycling

The freeze-thaw resistance of the developed UHPC mixes was tested according to ASTM C666 using three standard prism specimens per mix, each measuring 3 in. × 4 in. × 16 in. The specimens were cured for 14 days in a lime-water tank before undergoing rapid freezing and thawing cycles in water. The Humboldt freeze-thaw cabinet with multiple channels (including one controlled) is shown in Figure 3.17. Durability was evaluated for each specimen at regular intervals, usually every 30 cycles, by measuring the relative dynamic modulus of elasticity (RDME) using a Sonometer (Resonance Frequency Test Apparatus), as shown Figure 3.18. The percentage of mass loss was also recorded to present the degradation of UHPC mixes with respect to time (Freeze-thaw cycle). The degradation of UHPC found in visual inspection during the test is also presented with a photo.

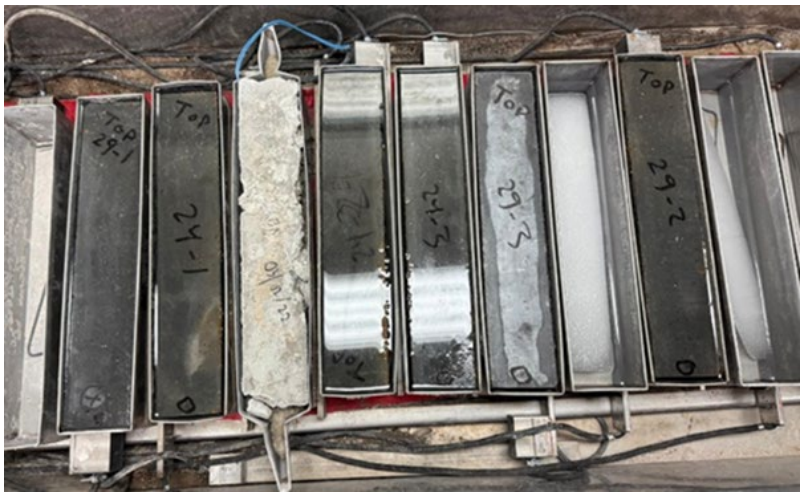

Figure 3.17 UHPC specimens in the freeze-thaw chamber.

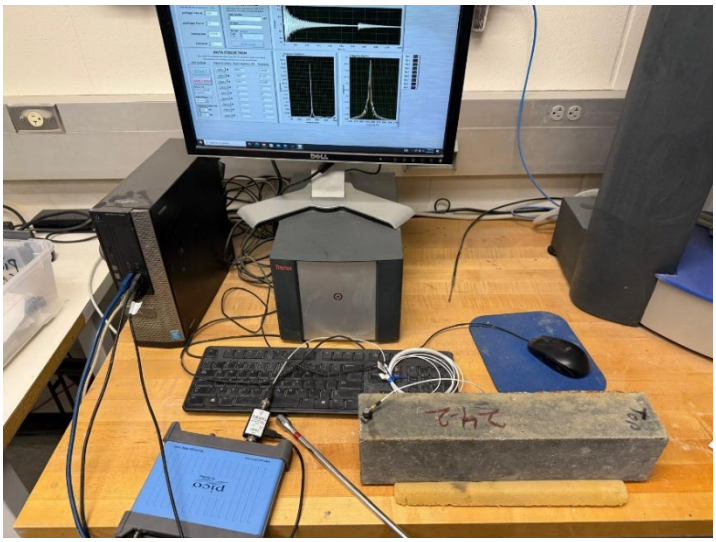

Figure 3.18 Freeze-thaw resistance test setup with sonometer.

3.4.3.2 Rapid Chloride Penetration Test (RCPT)

The Rapid chloride penetration test (RCPT) was performed following AASHTO T 277/ASTM C1202 to evaluate chloride ion permeability in UHPC mixes. Three samples per mix were tested at 28 days, consistent with ASTM C1202, and again at 56 days due to the slow hydration associated with concrete containing supplementary cementitious materials (SCM), which enhances chloride resistance over time. A cylindrical core sample measuring 2±0.12 inches thick was saw-cut from the top of a 4" × 8" cylinder, as shown in Figure 3.19(a). The specimen's circular perimeter was sealed with an epoxy coating and then vacuum-saturated for four hours, as shown in Figure 3.19(b). After a 16- to 20-hour rest period, it was placed in the Applied Voltage Cell, as shown in Figure 3.19(c), where a 60V DC voltage was applied for six hours. The charge passed (coulombs) was recorded and compared to Table X1.1 in ASTM C1202, categorizing the concrete's chloride penetrability.

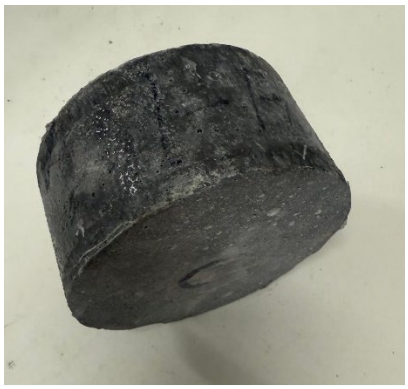

(a) Saw-cut UHPC specimen for rapid chloride penetration test

(b) Sample preparation in vacuum saturation chamber

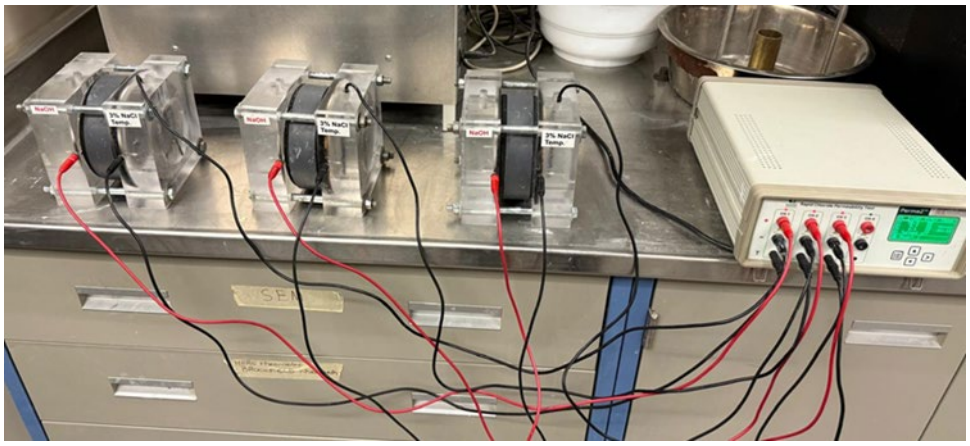

(c) RCPT test in applied voltage cell

Figure 3.19 Rapid chloride penetration test (RCPT) setup.

3.4.3.3 Surface Resistivity

The surface resistivity test was performed on 4” × 8” cylindrical concrete specimens according to the AASHTO TP 95 guideline, which assesses concrete’s resistance to chloride ion penetration. Three specimens were tested in a saturated surface dry (SSD) condition, and the average resistivity value along with the standard deviation was reported. Measurements were taken on the peripheral surfaces of the cylinders, as shown in Figure 3.20, using a four-probe

Wenner array device, ensuring consistent readings. The recorded surface resistivity values were then compared with Table 1 in AASHTO TP 95 to categorize the chloride-ion penetrability of the mix.

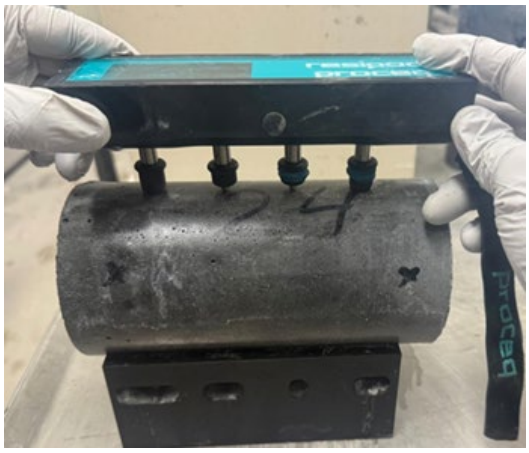

Figure 3.20 Surface resistivity test of concrete.

3.4.3.4 Drying Shrinkage

The drying shrinkage of the developed UHPC mixtures was measured following AASHTO T160/ASTM C157, using standard prism specimens with dimensions of 3” × 3” × 11.25”, as shown in Figure 3.21. Immediately after mixing, the fresh UHPC was poured into prism molds with an effective gauge length of 10 inches, ensuring uniform placement in a single layer. The specimen surface was then smoothed using multiple strokes of a trowel. To prevent moisture loss, the samples were covered with a plastic sheet. After this initial hardening period, the specimens were demolded and stored under environmental conditions of 22±3°C temperature and 25±5% relative humidity. Two specimens were cast for each UHPC mix. Shrinkage measurements were conducted using a length comparator at specific time intervals: 1, 3, 7, 14, 28, 56, 90, 120, 150, and 180 days.

Figure 3.21 Drying shrinkage test setup.

3.5 Summary

This chapter offered a comprehensive overview of the UHPC overlay experimental program, highlighting key aspects such as mixture design, mixing procedures, and testing methods for both fresh and hardened properties, including durability.

The mixture design section explored various binder contents, water-to-binder ratios, fiber contents, and different proportions of HRWR and WRT to achieve optimal performance. Multiple mix groups were evaluated to capture a range of workability and mechanical behaviors suitable for field applications. The mixing process was carefully detailed to ensure uniformity and consistency across all batches.

The chapter also explored the practical applications of fresh-state tests in the field, highlighting their importance. Acceptance criteria for fresh-state tests were recommended to

effectively evaluate performance and identify the best mixtures for UHPC overlay and structural repair. Additionally, the chapter presented the experimental matrix and testing procedures used to assess mechanical properties such as compressive, tensile, and flexural strength, along with durability indicators including RCPT, shrinkage, and freeze-thaw resistance. These tests serve as a foundation for selecting high-performing UHPC mixes suitable for both repair and new construction projects.

Chapter 4 Mixture Development and Evaluation

4.1 Introduction

Chapter 4 focuses on the process of selecting and assessing the promising UHPC overlay mixture. As explained in the previous chapter, the approach for material proportioning was based on an experimental study that investigated how different parameters affect key UHPC properties, including fresh-state properties and compressive strength. In this study, the development and evaluation of the UHPC overlay mixture design followed a systematic two-phase plan.

In Phase I, the research examined the effects of binder content, water-to-binder ratio, fiber content, and the amounts of HRWR and WRT on the performance of the UHPC overlay. The optimal mixture was determined based on acceptable flow, PR, and VSS. Then, Phase II evaluated the performance of the selected mixtures. Since the promising mixtures were chosen based on flow, PR, and VSS test results, other test methods were applied only to the selected mixtures in Phase II. Table 4.1 demonstrates a summary of test methods in accordance with their application across different phases.

Table 4.1 Summary of test methods based on phases.

Test methods		**Phase I**	**Phase II**
Fresh and Early Age Properties	Flow	Yes	Yes
	VSS	Yes	Yes
	PR	Yes	Yes
	Heat of Hydration	No	Yes
Mechanical Properties	Compressive Strength	Yes	Yes
	Modulus of Elasticity	No	Yes
	Flexural Strength	No	Yes
	Bond Strength	No	Yes
	Direct Tension	No	Yes
Durability Properties	RCPT	No	Yes
	Freeze/Thaw Resistance	No	Yes
	Electric Resistivity	No	Yes
	Shrinkage	No	Yes
Constructability	Constructability	No	Yes

In Phase II, four UHPC overlay mixtures from Groups B, C, E, and F were selected for further performance assessment. Although several mixtures in each group were successful, the only difference among them was the amount of incorporated admixture, which can be adjusted within recommended flow ranges. For the performance testing, mixtures with a dynamic flow greater than seven inches from each group were chosen to ensure adequate workability. This phase thoroughly assesses the fresh and early-age properties as well as the mechanical characteristics of the four selected UHPC overlay mixtures. The mixtures were prepared in large laboratory quantities, approximately 1 ft^3, to replicate field batching conditions.

4.2 Phase I: Mixture Development

In this study, various UHPC overlay mixtures were prepared with different binder contents, w/b, fiber contents, and varying dosages of WRT and HRWR admixtures, as illustrated in Table 4.2. The mixtures were divided into seven groups, each distinguished by the specific amount of incorporated materials. There are two combinations of binder content (1900 pcy and 1450 pcy) and w/b (0.180 and 0.196). According to special provisions from DOTs such as IADOT (2022), NYSDOT (2022), and NJDOT (2025), a minimum fiber content of 3% is required to achieve the strain-hardening properties essential for UHPC overlay applications. Therefore, 3% fiber incorporation was chosen as one of the mixture development options, along with cases using 2% fiber content. The range of incorporated admixtures is also provided in Table 4.2. The identification of each mixture is based on the following parameters: the percentage of fibers from the total volume, binder content, w/b, and the amounts of HRWR and WRT admixtures in pcy as exhibited later in Table 4.3. For each mixture ID, shortened mixture IDs were adhered to in order of mixing for further use in the paper.

Table 4.2 Descriptions of each group based on mixture parameters.

Groups	Binder Content (pcy)	w/b	Fiber Content (%)	HRWR (pcy)	WRT (pcy)
Group A	1900	0.180	2	51	21
Group B	1900	0.180	2	0-21	44-65
Group C	1450	0.196	2	0-3	47-54
Group D	1450	0.180	2	4-8	54-73
Group E	1450	0.196	3	3-4	47-59
Group F	1900	0.180	3	3-5	47-62
Group G	1450	0.180	3	10	62

The reference mixture was categorized as conventional Cast-in-Place (CIP) UHPC from Group A, which is a non-proprietary, self-consolidating UHPC developed by the research team through a recently completed Nebraska DOT (NDOT) project (SPR-P1(18) M072) titled "Feasibility Study of Development of Ultra-High-Performance Concrete (UHPC) for Highway Bridge Applications in Nebraska" (Mendonca et al., 2020). Therefore, Group A includes only one control conventional UHPC with high flowability (9.3 inches of static flow) and self-consolidating properties, as detailed in Tables 4.2 and 4.3. However, because of the thixotropic nature of the UHPC overlay material, the quantities of admixtures were adjusted accordingly in each group while keeping all other parameters constant. Group B and F (which is the 3% fiber content case of group B) mixtures were derived from the conventional UHPC base with significantly reduced amounts of HRWR and WRT. These adjustments aimed to modify the mixture to a more thixotropic nature while maintaining the desired consistency. As depicted in Table 4.3, several successful Groups B and F mixtures passed all the tests mentioned earlier. Group D mixtures had a lower binder content of 1450 pcy compared to Group B mixtures, which contained 1900 pcy. Despite this reduction, the w/b) remained constant at 0.180. The binder content was proportionally decreased, keeping the silica (8%) and slag (30%) percentages the same as in the Group B mixture designs (Mendonca et al., 2018). The main reason for testing a mixture with reduced binder content was the relatively low need for high compressive strength in

deck overlay applications. Deck overlays usually function as protective layers rather than significantly enhancing structural strength (Wibowo and Sritharan, 2018). However, adjustments in admixture quantities did not produce successful overlay mixtures for either Group D or Group G, which is the 3% case of Group D. The main problem appeared to be the limited amount of water added (Mendonca et al., 2020), causing surface roughness during patting and ultimately leading to failure of the PR test, even though the flow and VSS tests were passed. As a result, for Groups C and E (with 3% fiber content), the w/b was increased to 0.196 while keeping the low binder content of 1450 pcy. Similar to Groups B and D, the amounts of HRWR and WRT in Groups C and E were adjusted to achieve the desired flowability, which was successful.

The key to changing self-compacting behavior to a thixotropic one lies in the use of admixtures. Unlike self-consolidating UHPC, the thixotropic overlay UHPC requires a higher amount of WRT than HRWR to keep flowability for a longer time. Therefore, within each of the six developed groups, only the admixture amounts were adjusted to achieve proper ranges, while other parameters stayed the same. Table 4.3 summarizes the results of flows at 0 and 30 minutes, PR at 0 and 30 minutes, VSS at 0 minutes post-mixing, and 28-day compressive strength for all mixtures. A comparison of the results shows that applying WRT alone without HRWR increases flowability over time. An appropriate amount of HRWR balances the effect of WRT, helping to maintain stable flowability. The ideal HRWR amount was found to be around 3-5 pcy, as too much HRWR disrupts this balance and causes a notable decrease in flow over time. The suitable WRT range is between 47-54 pcy. However, because the mixture's consistency can vary depending on batch size, mixing energy, temperature, and mixing time, adjustments in HRWR and WRT amounts may be necessary in the field to achieve the desired consistency. The flow results for the mixtures in Groups B and C (and respectively, Groups F and E) generally

increased within a certain range during testing. In contrast, Group D mixtures showed reduced flowability, sometimes failing to maintain proper dynamic flow for up to 30 minutes.

Generally, increased fiber content is believed to reduce flowability (Abbas et al., 2015; Meng and Khayat, 2018; Wu et al., 2016). This effect may be due to the larger specific surface area caused by higher fiber content and the randomly dispersed steel fibers within the matrix, which act as a structural framework, hindering the flow of fresh concrete (Abbas et al., 2015; Meng and Khayat, 2018; Wu et al., 2016). This study observed that raising fiber content from 2% to 3% has little impact on the flowability of all groups, as long as the WRT amount is not too large. The trend was clear in Groups C and E, where static flow results were higher for Group C mixtures compared to Group E, although dynamic flow results were fairly similar. However, within the scope of this paper, increasing the fiber content required a corresponding reduction in sand content, which might explain the stable flowability despite the change in fiber amount. It has also been observed that, at the same fiber content and w/b ratio, higher binder content results in better flowability, as seen in Groups B and D. The increased flowability in Group B can be attributed to the higher paste content, which decreases viscosity and enhances the mixture's flowability (Mendonca et al. 2020). Additionally, the higher paste content improves cohesion by reducing segregation (Mendonca et al. 2020). On the other hand, the difference in binder content does not significantly impact static flow results within Groups B and C or Groups E and F, except for slightly higher results in Group B for the same reason. It is also important to note that a higher w/b in Group C mixtures did not necessarily lead to higher flow values.

As exhibited in Table 4.3, all test methods provided an overall assessment of the developed thixotropic UHPC overlay mixtures. Results showed that the newly developed PR and VSS results closely align with the static and dynamic flow test results, while offering a more

comprehensive evaluation of the workability of the UHPC mixtures. This includes assessing flowability (with and without vibration), slope stability (with and without vibration), and surface smoothness in response to vibration. Results indicated that, except for Groups A and D, most groups produced successful mixtures for overlay UHPC after necessary adjustments. As expected, the Group A mixture did not meet the criteria due to its self-consolidating nature. According to PR, Group D mixtures may face issues responding to vibration based on the acceptance criteria provided.

Table 4.3 Flow, PR, VSS, compressive strength, and unit weight results of UHPC overlay.

Groups	Mixture No.	Mixture ID	Flow (0') (in.)		Flow (30') (in.)		PR (0')	PR (30')	VSS	f'_c 28d	Unit weight (pcf)
			Static	Dynamic	Static	Dynamic			Angle		
A	CIP	CIP-1900-0.180-H51-W21	9.3	N/A	N/A	N/A	N/A	N/A	N/A	N/A	N/A
B	Mix 3	F2%-1900-0.180-H21-W44	10.5	N/A	9.5	N/A	N/A	N/A	N/A	12.3±2.1	155
	Mix 4	F2%-1900-0.180-H10-W44	4.0	6.8	4.0	5.9	P1	P1	N/A	13.4±2.9	155
	Mix 5	F2%-1900-0.180-H0-W56	4.0	5.8	4.0	5.6	F2	F2	P	11.8±2.4	155
	Mix 6	F2%-1900-0.180-H0-W69	5.1	7.8	7.1	8.4	P1	F1	F	13.7±0.3	155
	Mix 12	F2%-1900-0.180-H4-W65	4.1	7.0	6.8	7.6	P1	P1	P	12.5±1.1	155
	Mix 13	F2%-1900-0.180-H4-W61	4.1	7.0	5.5	7.3	P1	P1	P	12.0±1.5	155
	Mix 16	F2%-1900-0.180-H4-W56	6.2	7.8	5.6	7.5	P1	P1	F	14.6±0.9	155
	Mix 18	F2%-1900-0.180-H0-W61	4.0	6.3	4.0	6.7	P1	P1	P	14.5±1.1	155
	Mix 28	F2%-1900-0.180-H3-W52	5.1	7.8	5.1	7.5	P1	P1	P	14.0±0.6	156
	Mix 29	F2%-1900-0.180-H3-W47	4.1	7.3	4.1	7.0	P1	P1	P	13.9±0.1	154
C	Mix 7	F2%-1450-0.196-H0-W52	4.0	6.3	5.0	7.0	P1	P1	P	13.3±0.2	157
	Mix 8	F2%-1450-0.196-H3-W54	5.3	7.0	5.5	7.1	P1	P1	P	14.8±0.6	157
	Mix 14	F2%-1450-0.196-H3-W52	4.3	6.9	6.0	7.3	P1	P1	P	11.9±1.7	157
	Mix 15	F2%-1450-0.196-H3-W47	4.0	6.3	4.1	6.0	P1	P1	P	13.9±0.1	157
	Mix 19	F2%-1450-0.196-H0-W49	4.0	6.1	4.0	6.0	P1	P1	P	12.9±0.8	157
D	Mix 9	F2%-1450-0.180-H8-W54	5.3	7.2	4.5	6.0	P1	F2	P	14.5±1.0	159
	Mix 11	F2%-1450-0.180-H8-W73	6.5	7.7	4.0	5.0	P1	F2	F	N/A	158
	Mix 17	F2%-1450-0.180-H4-W54	5.6	7.4	5.5	6.9	P1	F2	P	15.0±0.7	159
E	Mix 20	F3%-1450-0.196-H4-W59	6.8	8.4	6.3	7.8	P2	P2	F	14.8±0.7	162
	Mix 24	F3%-1450-0.196-H3-W54	4.8	7.4	5.5	7.3	P1	P2	P	13.7±1.0	161
	Mix 26	F3%-1450-0.196-H3-W47	4.1	6.6	4.1	6.6	P1	P1	P	13.1±0.3	158
F	Mix 21	F3%-1900-0.180-H5-W62	7.0	8.5	7.5	8.9	P1	P1	F	14.6±0.5	160
	Mix 22	F3%-1900-0.180-H4-W58	6.6	8.4	7.0	8.3	P1	P1	F	14.8±0.1	158
	Mix 23	F3%-1900-0.180-H4-W56	5.7	7.7	6.2	7.8	P1	P1	P	13.8±0.3	158
	Mix 25	F3%-1900-0.180-H3-W54	4.0	7.0	4.3	7.0	P1	P1	P	16.1±0.7	158
	Mix 27	F3%-1900-0.180-H3-W47	4.0	6.6	4.0	5.9	P1	P1	P	14.3±0.2	159
G	Mix 10	F3%-1450-0.180-H10-W62	4.8	6.8	4.0	5.0	P1	F2	P	14.4±1.9	157

Figure 4.1 illustrates the relationship between flow and the angle of VSS results. Mixtures labeled as "Pass" passed the VSS test, maintaining their angle after placement and vibration, whereas mixtures labeled as "Fail" failed the test. Results show that static and dynamic flow results correlate well with VSS test results. The dynamic flow graph indicates that mixtures with a flow value exceeding eight inches are generally considered to have failed the VSS, with some exceptions that fell within the acceptable range but failed the static flow by exceeding six inches.

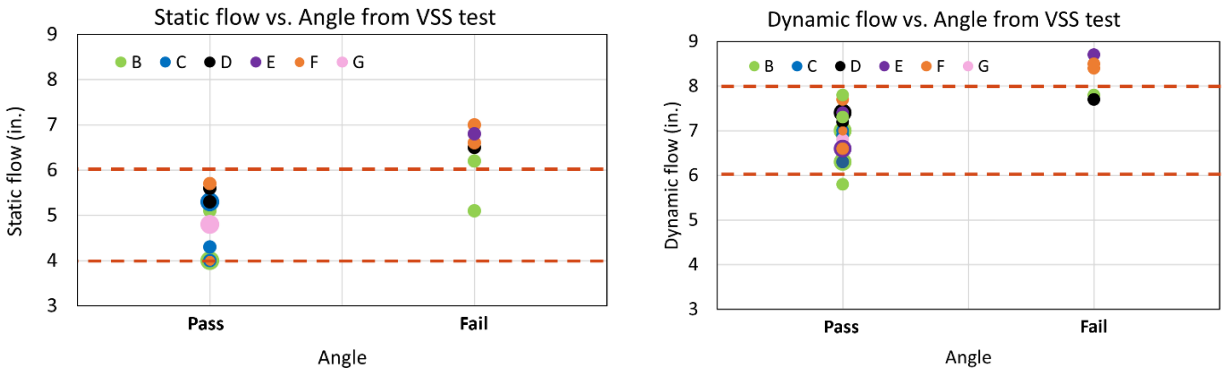

Figure 4.1 Correlation between flow values and VSS angle of overlay UHPC mixtures.

In this study, the evaluation of the developed mixture's flow results was based on the most commonly accepted criteria, which define less than six inches for static flow and more than six inches for dynamic flow. However, after analyzing the VSS results, the criteria remained the same for the static case but were adjusted to a range of 6-8 inches for dynamic flow. It is important to note that these criteria are based on tests conducted on a five-degree slope. With smaller slope angles, there might be no flow off the crowned bridge due to vibration. Since VSS provides a more direct assessment of slope stability under vibration, it is advisable to perform this test during the mixture development stage to confirm the suitability of the mixtures.

However, because the VSS test is complex, in field conditions, the research team recommends static and dynamic flow ranges that correlate with slope stability under vibration.

4.3 Phase II: Mixture Evaluation

4.3.1 Fresh and Early-Age Properties Testing

Based on the performance evaluation results, four UHPC overlay mixtures from Groups B, C, E, and F were selected for further constructability assessment. Although several mixtures in each group were successful, the only difference among them was the amount of incorporated admixture, which can be adjusted within acceptable flow ranges. A wooden test frame measuring 41 inches by 9 inches by 1 inch was built to simulate a mock-up slab construction. The setup was positioned at a two-degree angle (3.5% grade) to assess the performance of UHPC under sloped conditions. A one-inch thick UHPC overlay was then applied to the wooden surface using surface vibration, as shown in Figure 4.2, to mimic the consolidation process of a paver in the field, the test was conducted 15-30 minutes after the mixing was completed. The material was placed from the top to the bottom of the slope. After confirming that the material did not flow out under its own weight (without vibration), surface vibration was applied to distribute the material from top to bottom of the slope. The material began to respond and spread evenly as the surface vibration moved toward the sloped side. Figure 4.2 demonstrates the UHPC overlay placing process for four selected groups.

(a) Group B (b) Group C (c) Group E (d) Group F

Figure 4.2 Placing of overlay UHPC slabs.

The acceptance criteria for this test were as follows: if the material spread freely with the surface vibration but stopped flowing without the application of surface vibration, it passed the test. However, the mixture did not pass the test if the material required external assistance beyond surface vibration to flow. Constructability results for all mixtures met the acceptable requirements, except for Group F, which exhibited a more viscous mixture than the other groups. Figure 4.2 illustrates that external force, such as using a trowel, was necessary to spread the UHPC overlay, indicating that surface vibration alone was insufficient for material spread and consolidation. This indicates a stiffer, more viscous material. Additionally, visual observations during the placement of the UHPC overlay suggested that the material might not adequately fill the voids on the roughened surface of the bridge deck substrate, which is required for strong bonding. In contrast, the other overlay mixtures spread continuously on a sloped surface with surface vibration, requiring no external assistance and providing a smooth surface.

The evaluation of constructability included examining the surface condition of the hardened slabs on both top and bottom surfaces. The final placed UHPC overlay must be free of

large air voids and honeycombs to ensure the integrity and durability of the structure. Figure 2.3 presents UHPC overlay slabs at the hardened stage. Measurements show that the proportion of surface air voids larger than 0.09 in² comprises 0.29% for Group B, 0.16% for Group C, 0.17% for Group E, and 0.37% for Group F, respectively. These results indicate that the mixtures performed well in minimizing large air voids, demonstrating good consolidation and a smooth surface. Even Group F demonstrated good results, thanks to external assistance beyond surface vibration for consolidation.

(a) Group B (b) Group C (c) Group E (d) Group F

Figure 4.3 Bottom surfaces of overlay UHPC slabs.

The results of the flow, PR, and constructability of the four developed overlay mixtures are presented in Table 4.4. Constructability results confirm the performance of the selected mixtures by correlating well with flow and PR results, thereby proving the relevance of the

developed test methods. By showing marginal dynamic flow (6") results at 30 minutes, the Group F mixture failed the constructability test, which might indicate that more vibration power (or more time of vibration) is required for a stiffer material. On the other hand, the research team recommends a dynamic flow value of seven inches or higher at 25 drops to ensure proper constructability and strong bonding. However, additional data is required to validate this recommendation further.

Table 4.4 Flow, PR, and constructability results of UHPC overlay.

Group	Mixture No.	Mixture ID	Workability Test Results				
			Time	Static Flow	Dynamic Flow	PR	Constructability
B	Mix 29	F2%-1900-0.180-H3-W47	0'	4.1"	7.6"	P1	P
			30'	4.1"	6.8"	P1	
C	Mix 8	F2%-1450-0.196-H3-W54	0'	6.0"	7.6"	P1	P
			30'	5.8"	7.0"	P1	
E	Mix 24	F3%-1450-0.196-H3-W54	0'	5.4"	8.0"	P2	P
			30'	6.3"	7.8"	P1	
F	Mix 25	F3%-1900-0.180-H3-W54	0'	4.0"	6.6"	P1	F
			30'	4.0"	6.0"	P1	

Figure 4.4 illustrates the results of the heat of hydration tests for a reference UHPC and three groups; the data for group F are not available. The figure shows that low binder content and increased WRT dosage lead to a reduction in peak heat release. Moreover, as the binder content decreases, the peak shifts to the right, indicating delayed hydration.

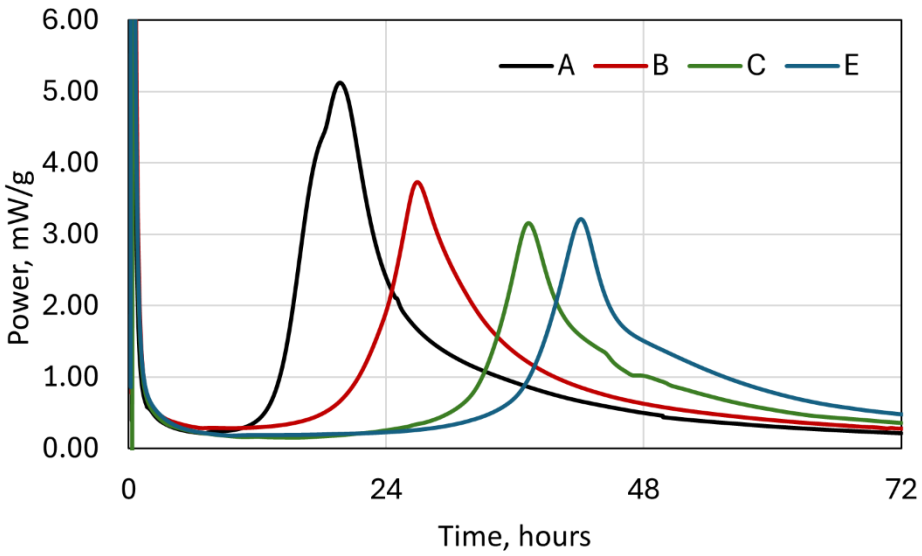

(a) Heat of hydration

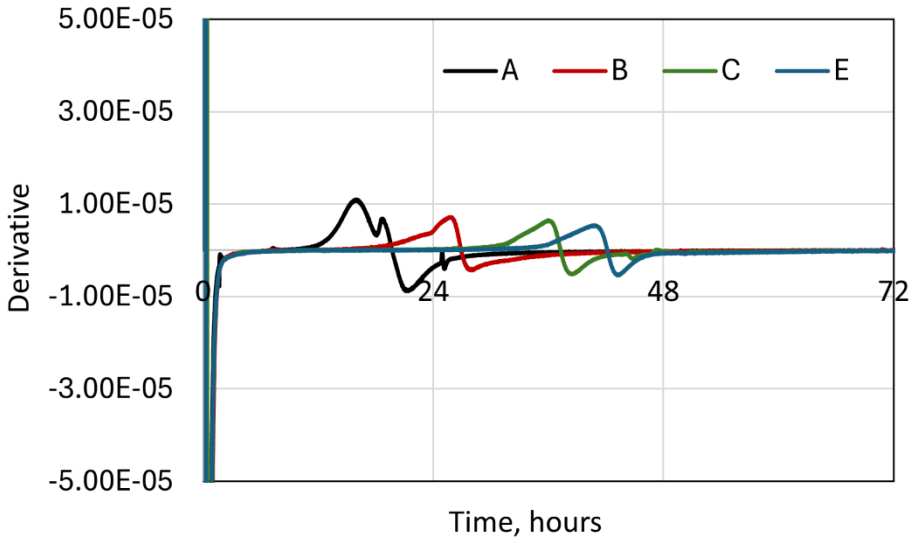

(b) First derivative of heat generation rate

Figure 4.4 Heat of hydration test results.

Table 4.5 presents the initial and final set times as determined by analyzing the derivative of heat generation during the hydration process. It should be noted that the results of calorimeter test set times are usually well correlated with the set times measured according to ASTM C403.

Notably, the inclusion of WRT significantly prolongs both the initial and final setting times and reduces the rate of heat generation at a constant temperature, as observed in the results for the reference UHPC and group B mixture. The delayed initial and final setting times for overlay UHPC mixtures were also observed in the casted specimens, which remained soft after 24 hours of demolding.

Table 4.5 Heat of hydration test results.

Group	Mixture No.	Mixture ID	Peak Power (mW/g)	Initial Setting Time (hrs)	Final Setting Time (hrs)
A	Ref	F2%-1900-0.18-H51-W21	5.1	16.0	19.7
B	Mix 29	F2%-1900-0.18-H3-W47	3.7	25.7	26.9
C	Mix 8	F2%-1450-0.20-H3-W54	3.1	36.0	37.3
E	Mix 24	F3%-1450-0.20-H3-W54	3.2	40.9	42.1

4.3.2 Mechanical Properties Testing

Compressive Strength

Figure 4.5 presents the average compressive strength versus the age of the four developed UHPC overlay mixtures. The results indicate that while the compressive strengths of all four UHPC overlay mixtures exceeded the 14 ksi requirement at 28 days as specified by IADOT (2022), they did not meet the 18 ksi requirement set by NJDOT (2025), and NYSDOT (2022). It is worth noting that this 18 ksi requirement aligns with the standards for CIP UHPC, as ASTM 1856 mandates a 28-day compressive strength of 17 ksi for CIP UHPC. However, UHPC overlays serve a different purpose compared to CIP UHPC. According to Wibowo and Sritharan (2018), UHPC overlays are primarily designed for protection rather than to enhance structural

strength. Thus, properties such as tensile strength, durability, and bonding ability are more crucial for overlay applications. Consequently, the 14 ksi 28-day strength is deemed acceptable, and all four mixtures meet this criterion. Furthermore, the increase in strength over time ensures the long-term load-bearing capacity, longevity, and structural integration of the UHPC overlay. It is significant to note that the mixtures with lower binder contents (Groups C and E) presented almost the same 28-day compressive strength results as the mixtures of Groups B and F.

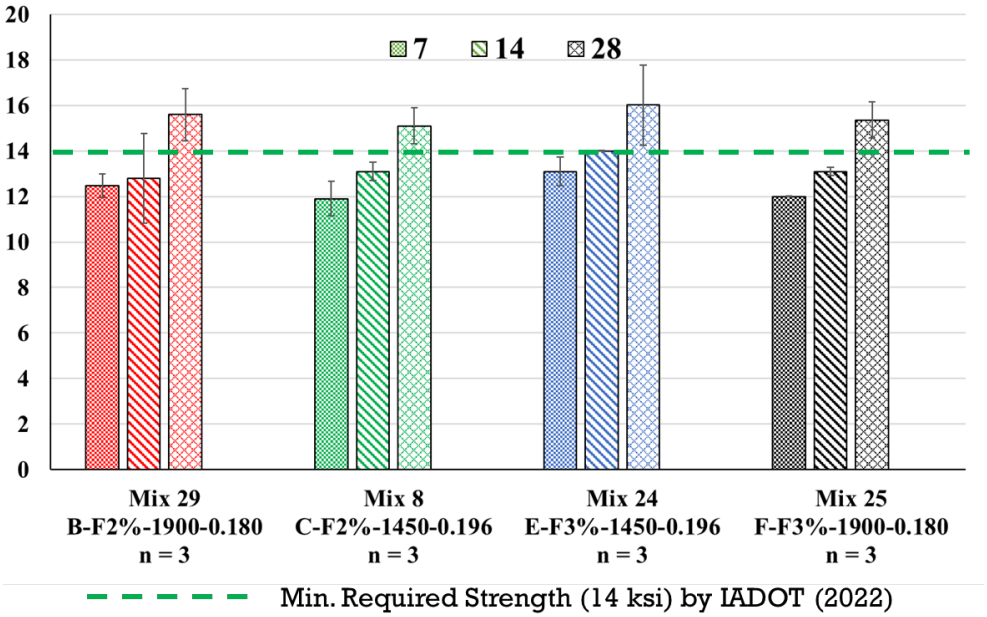

Figure 4.5 Compressive strength of developed UHPC overlay mixtures at different ages.

Flexural Strength

Figure 4.6 presents the calculated flexural strength versus the average midspan deflection for the four developed UHPC mixes. Mixes 29 and 24 showed strong performance and were therefore repeated twice, cast and tested in duplicate, to ensure consistency and verify their high flexural strength.

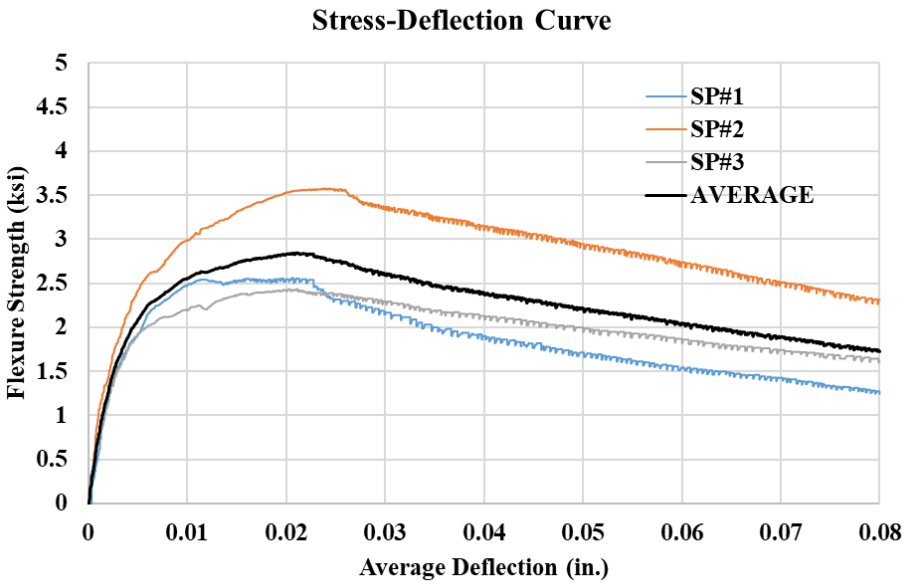

(a) Mix 8

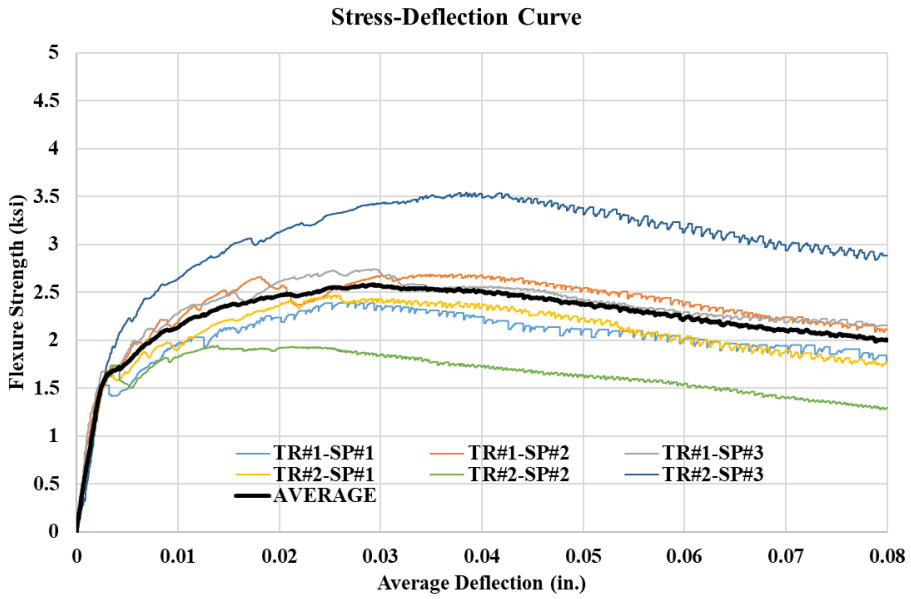

(b) Mix 29

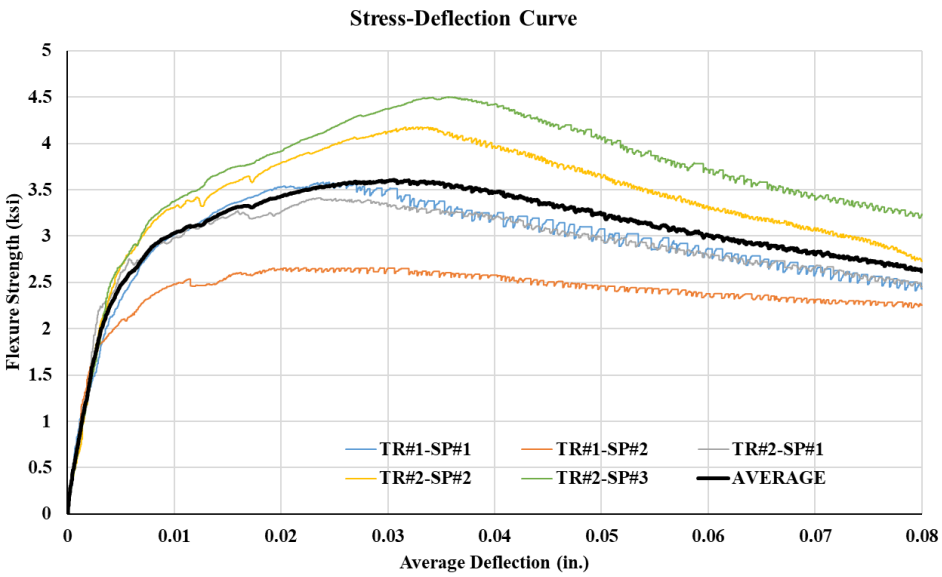

(c) Mix 24

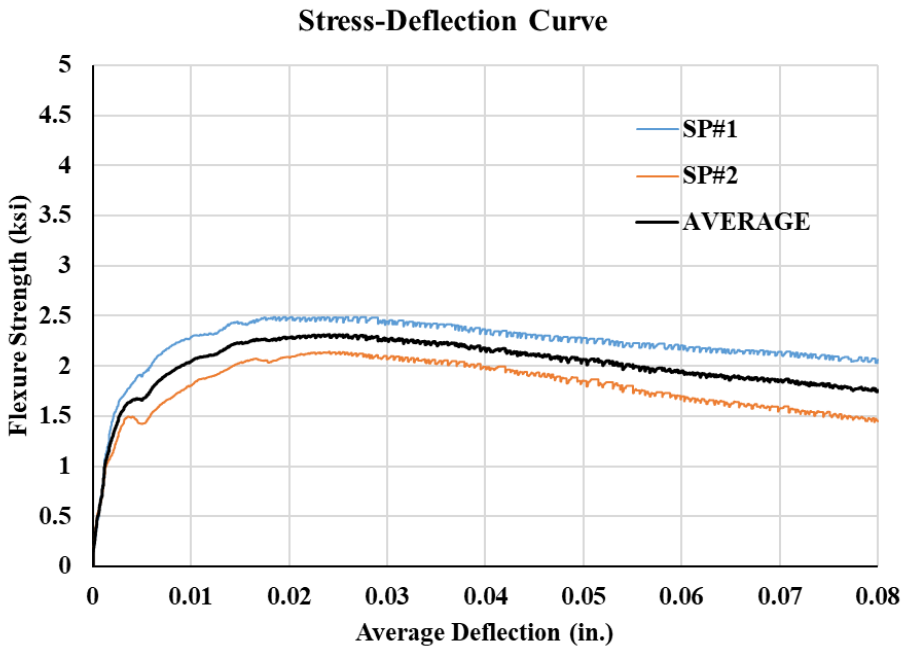

(d) Mix 25

Figure 4.6 Flexure test results of UHPC mixes.

All the average curves for all mixes were combined together for comparison, as shown in Figure 4.7. The average first cracking and peak strengths for each mix were calculated and

compared to the minimum limits recommended by PCI TR-9-22 for flexural strength: 1.5 ksi and 2 ksi, respectively, as shown in Figure 4.8. The average residual strength relative to the first cracking strength for each mix was calculated and compared with 0.75, as recommended by PCI. TR-9-22, as shown in Figure 4.9. It can be seen that all mixes achieved the minimum limits recommended by PCI. TR-9-22.

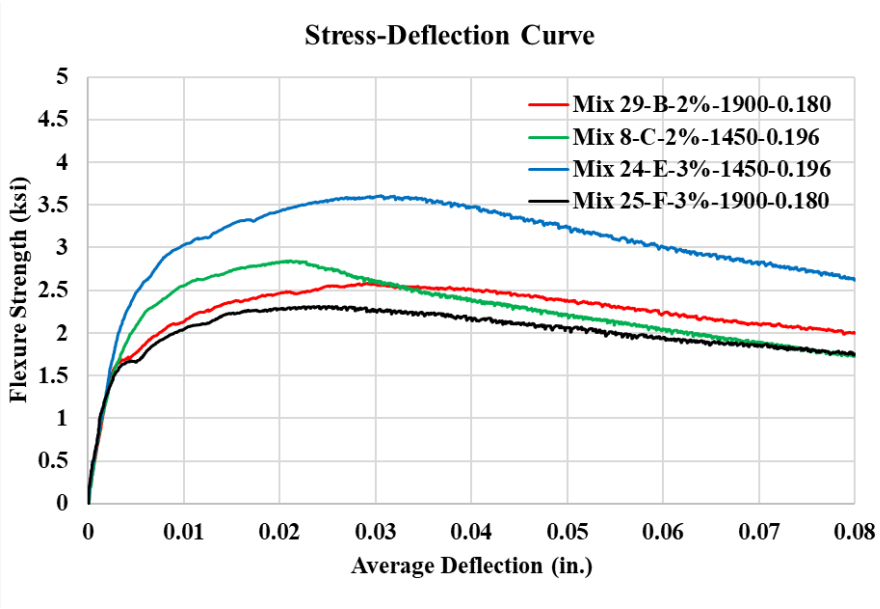

Figure 4.7 The average flexure test curves for each mix.

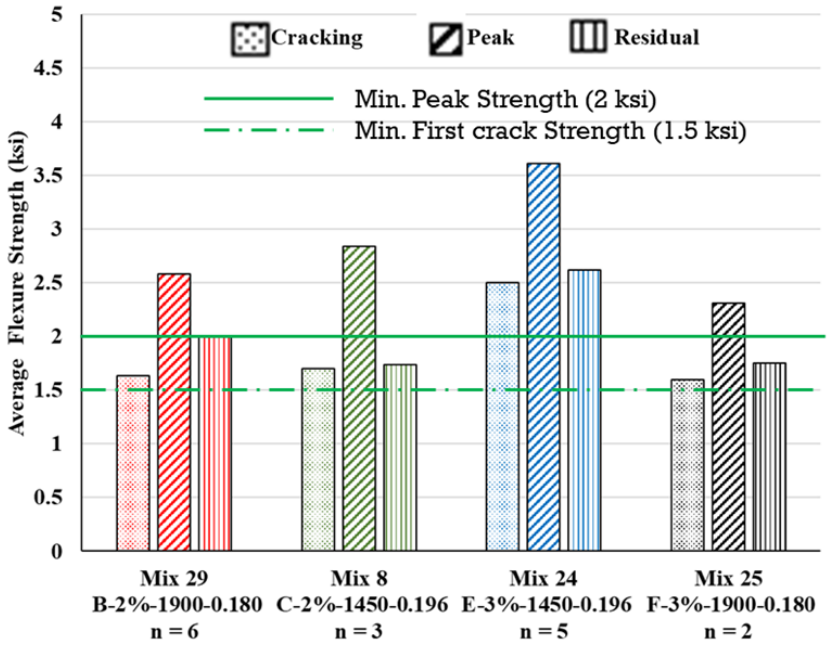

Figure 4.8 Average flexural cracking, peak, and residual strengths compared to PCI. TR-9-22 minimum limits.

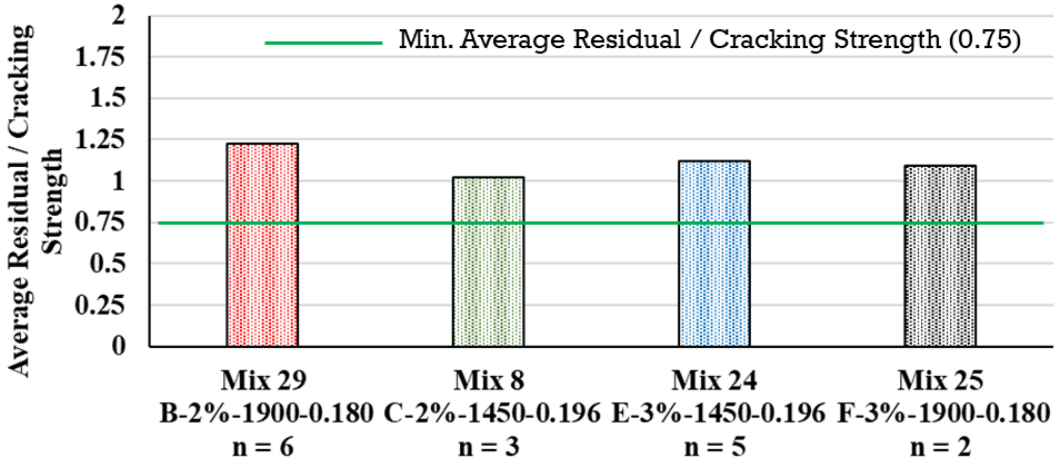

Figure 4.9 Average flexural residual strength over cracking strength compared to PCI. TR-9-22 minimum limits.

Uniaxial Tensile Strength

The tensile test results for the four groups are presented in Figure 4.10 through Figure 4.13. Multiple trials were performed for each mix because crack localization occurred outside the

gauge length in approximately 50% of the specimens. As a result, the strain values of these failed specimens were not representative. Therefore, the average stress-strain curve for each group was calculated using only the specimens that passed. The four groups were compared based on their average stress-strain curves, as shown in Figure 4.14.

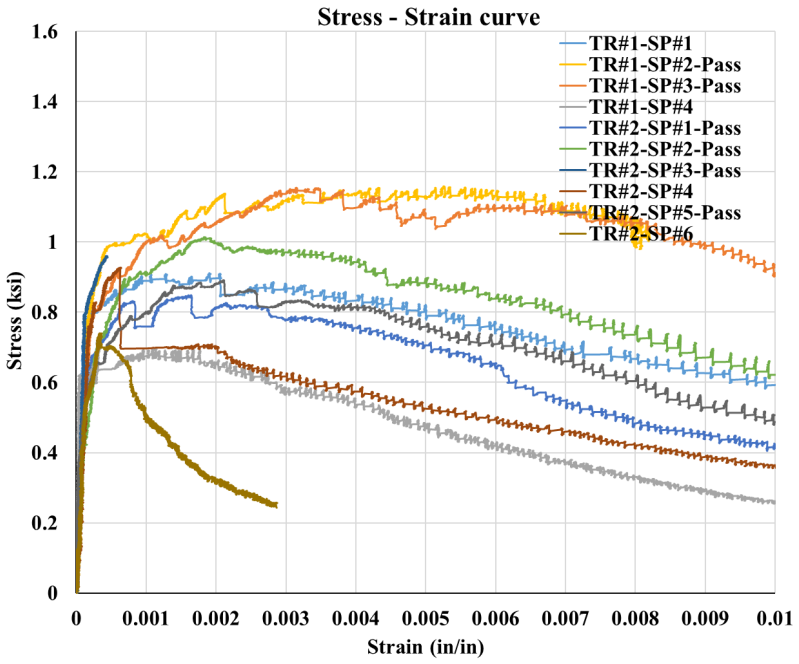

(a) Stress-strain curves for all specimens

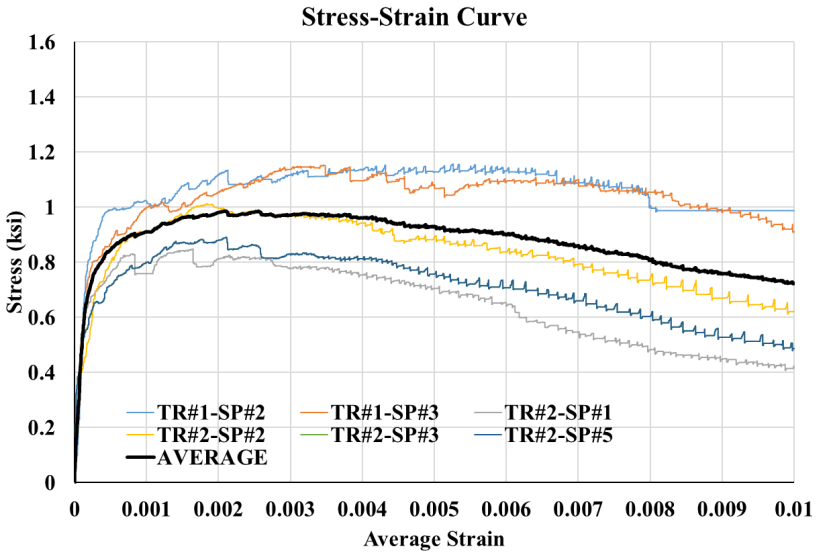

(b) Stress-strain curves for passing specimens and the average

Figure 4.10 Uniaxial tensile test results for Mix 29.

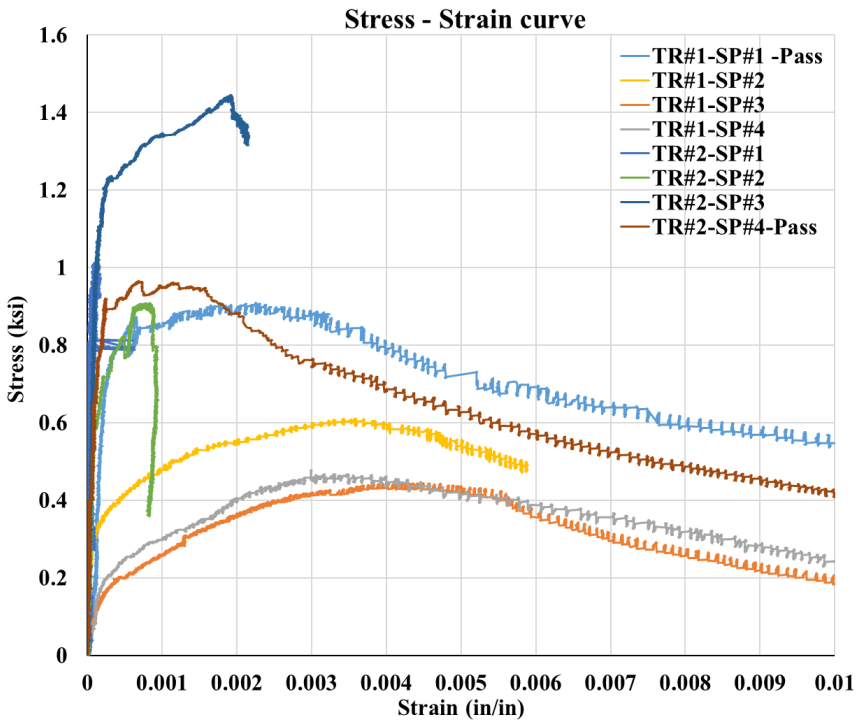

(a) Stress-strain curves for all specimens

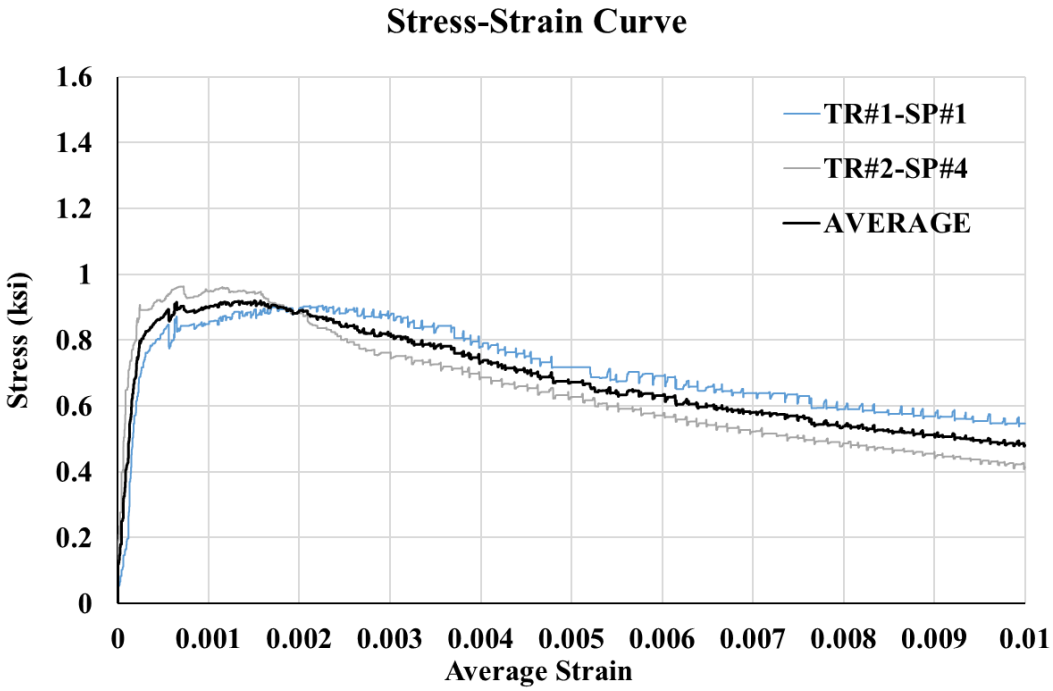

(b) Stress-strain curves for passing specimens and the average

Figure 4.11 Uniaxial tensile test results for Mix 8.

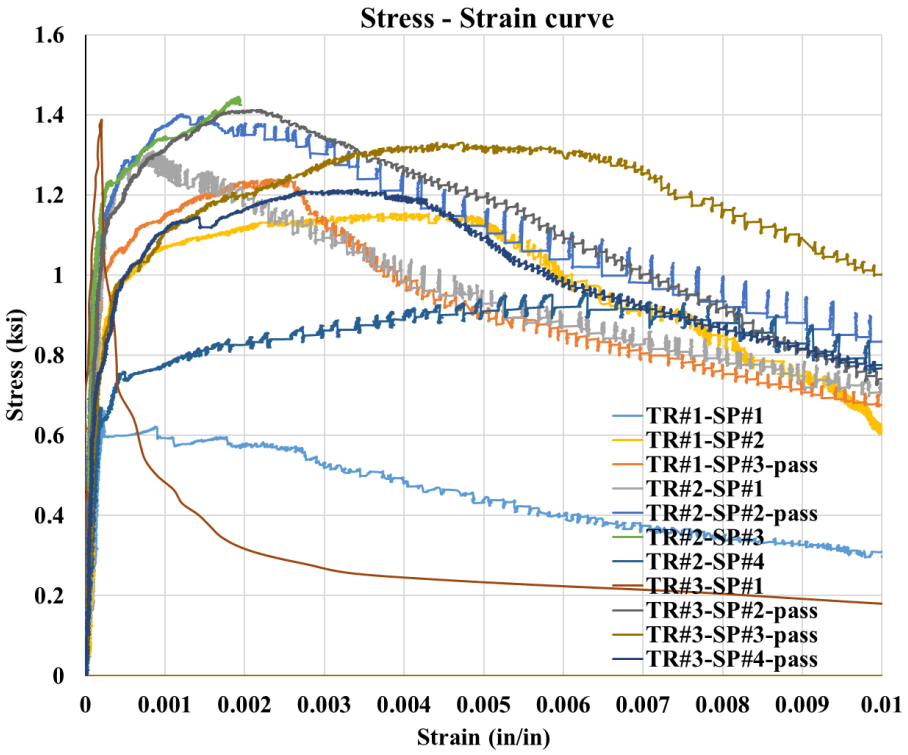

(a) Stress-strain curves for all specimens

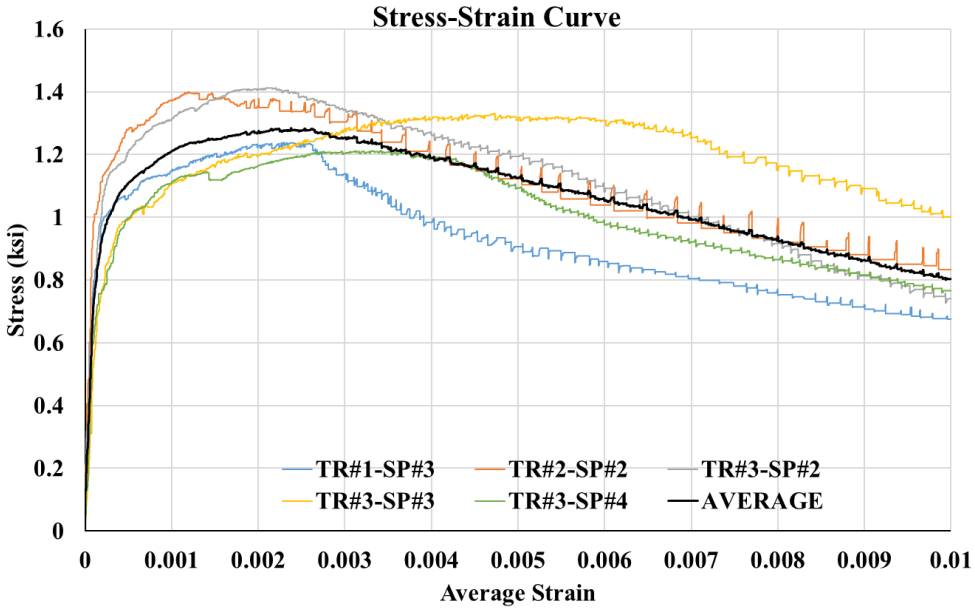

(b) Stress-strain curves for passing specimens and the average

Figure 4.12 Uniaxial tensile test results for Mix 24.

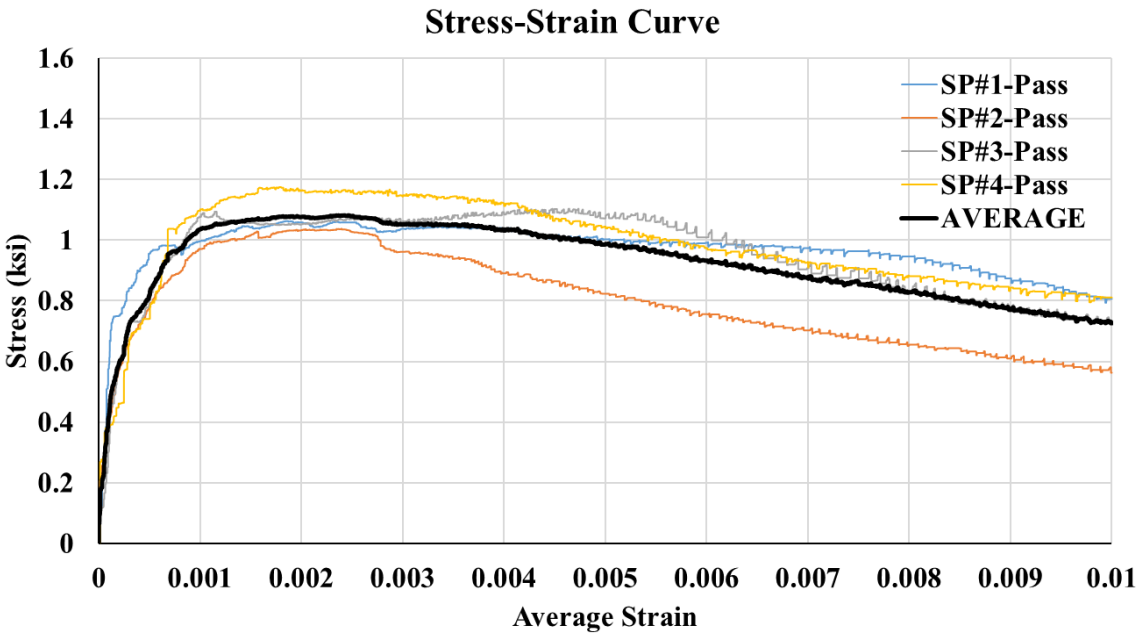

Figure 4.13 Uniaxial tensile test results for Mix 25.

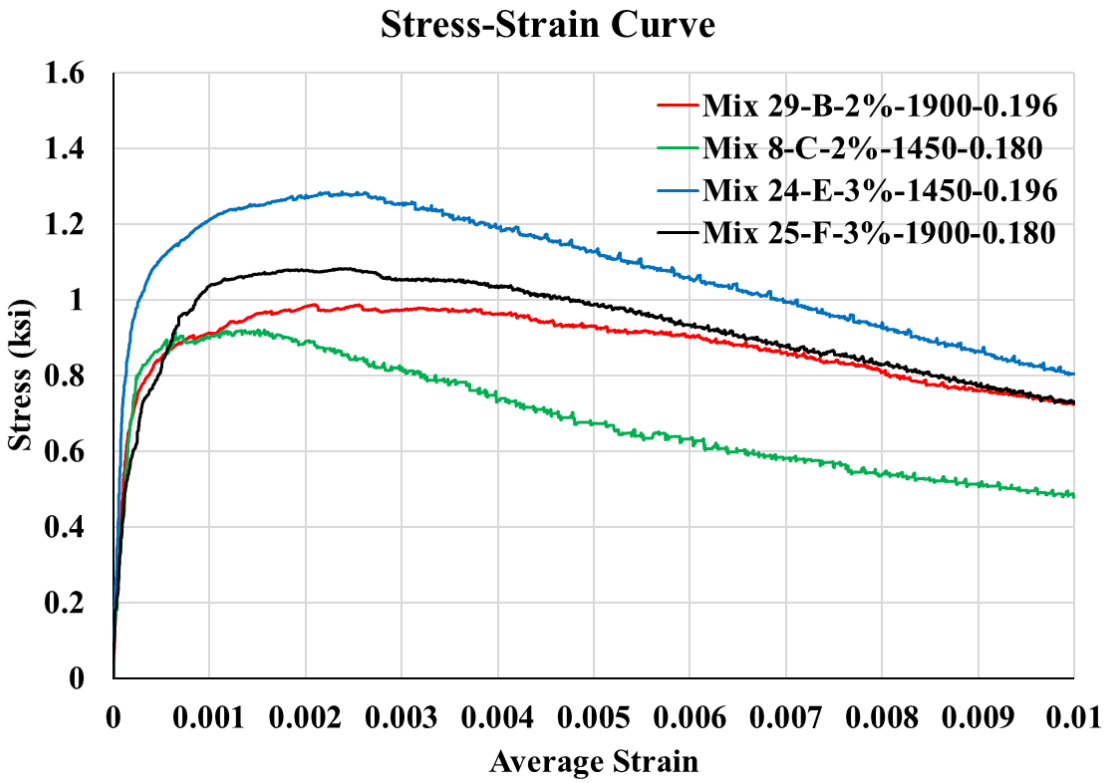

Figure 4.14 The average uniaxial tensile test curves for the four groups.

The average cracking strength and crack localization strength for each mix were calculated and compared to the AASHTO T 397-22 minimum cracking strength requirement of 0.75 ksi, as shown in Figure 4.15. Additionally, the average crack localization strain was evaluated against the AASHTO minimum limit of 0.0025, as illustrated in Figure 4.16.

Mix 8 showed the lowest tensile cracking strength, crack localization strength, and strain, mainly because of its low binder and fiber content. It did not meet the minimum crack localization strain requirement and was therefore excluded. Mixes 29, 24, and 25 met the AASHTO T 397-22 criteria. Among these, Mix 24 demonstrated the highest strength, while Mix 29 achieved the highest crack localization strain. Their results also closely approached the NJDOT minimum cracking strength requirement of 1 ksi and the peak-to-cracking strength ratio of 1.25.

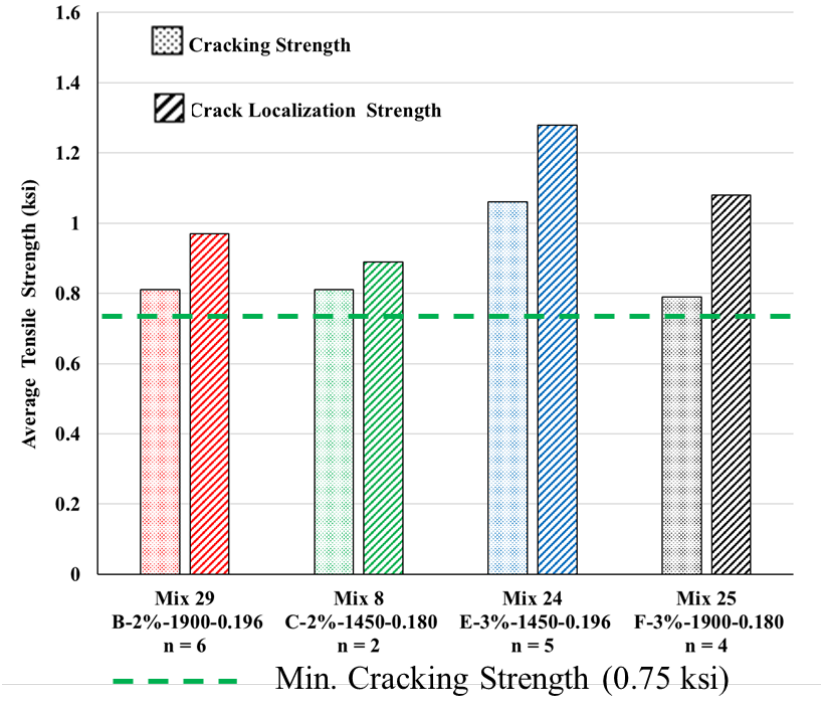

Figure 4.15 The uniaxial tensile strength test results with AASHTO T 397-22 limits.

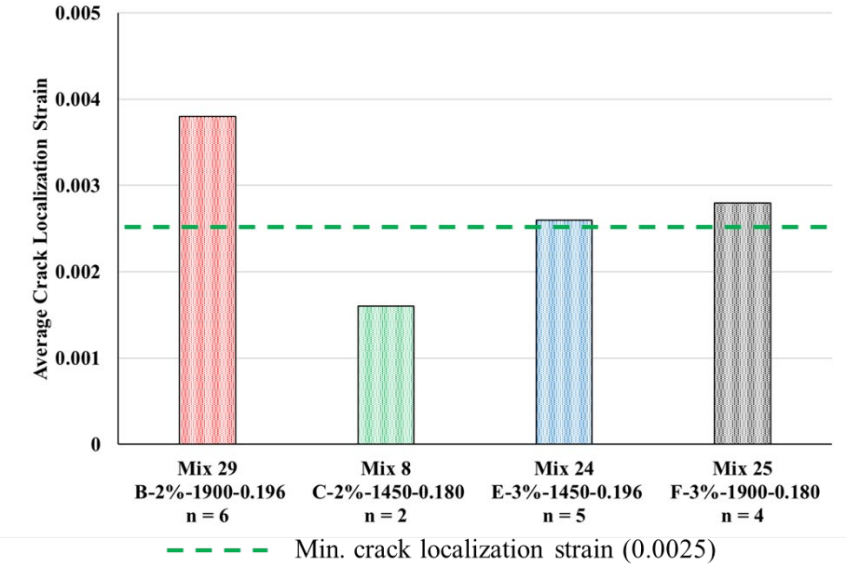

Figure 4.16 The tensile strain test results with AASHTO T 397-22 limits.

Bond Strength

Due to the good mechanical properties of mixes 29 and 24, they were selected for the bond strength test. Two NC slabs were cast with dimensions of 8.5 inches in width, 48 inches in length, and 3.5 inches in thickness, as shown in Figure 4.17.

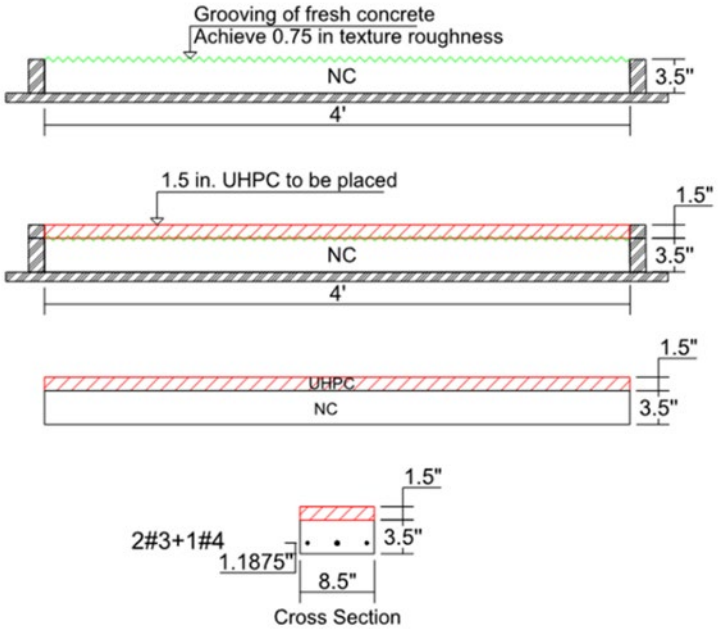

Figure 4.17 Schematic drawing of the small-scale slabs with UHPC overlay.

The fresh concrete surface was manually grooved to achieve a roughness of 0.75 inches at 2.5-inch spacing. Additionally, the NC slabs were sloped by 2% to evaluate the stability of the UHPC mixes. A 1.5-inch-thick layer of each mix was then cast on the slabs. Both mixes demonstrated good workability with no signs of overflow or instability, as shown in Figure 4.18. The pull-off test was then conducted to evaluate the bond strength between the NC and Mixes 29 and 24. The bond strength values, and corresponding failure locations are presented in Table 4.6.

Figure 4.18 Casting the small-scale slabs with UHPC overlay.

Table 4.6 Pull-off test for small scale specimens.

Sample	Mix 29		Mix 24	
	Bond Strength (ksi)	Failure	Bond Strength (ksi)	Failure
1	0.14	NC substrate	0.21	NC substrate
2	0.32	Adhesive material	0.24	Adhesive material
3	0.29	NC substrate	0.14	NC substrate
4	0.15	Interface	0.27	NC substrate
5	0.17	NC substrate	0.28	NC substrate
6	0.21	NC substrate	0.21	NC substrate
Average	0.21		0.23	
Std. Dev.	0.07		0.05	
COV (%)	32%		22%	

4.4 Analysis of Cost-Effectiveness

Given the high costs associated with proprietary UHPC overlay products, which significantly restrict their widespread use, this study aims to develop non-proprietary UHPC overlay mixtures that demonstrate strong performance using locally sourced materials in Nebraska. After identifying suitable raw material sources and designing the UHPC overlay mixtures, a cost analysis was performed for the four selected groups in Phase II based on the expenses of these raw materials. Table 4.7 provides a summary of the sources, locations, and unit costs ($/per ton) of the various raw materials used in the UHPC overlay mixtures. It should be noted that the unit costs were determined based on information provided by local producers and may fluctuate depending on material availability.

Table 4.7 Unit cost of materials.

Material	Type	Source and location	Unit cost	Unit
Cement	Type I/L	Ash Grove Cement Company Louisville, NE	$105	Ton
Silica fume	Force 10,000 densified silica	GCP Grace Construction Products	$1080	Ton
Slag	Grade 100	Central Plains Cement Company Omaha, NE (terminal)	$123	Ton
Sand	No.10	Lyman-Richey Corporation Omaha, NE	$10	Ton
Straight steel fiber	Dramix OL 13/.20 micro steel fiber	Bekaert	$2,600	Ton
HRWR	Premia 150	Chryso	$18.50	Gallon
WRT	Optima 100	Chryso	$18.50	Gallon

Table 4.8 Base costs of successful mixtures.

Group	Mixture No.	Mixture ID	Cost/yd^3
B	Mix 29	F2%-1900-0.180-H3-W47	$643
C	Mix 8	F2%-1450-0.196-H3-W54	$611
E	Mix 24	F3%-1450-0.196-H3-W54	$783
F	Mix 25	F3%-1900-0.180-H3-W54	$828

The base cost of the four successful mixtures was calculated based on the unit cost of materials, as illustrated in Table 4.8. The cost of these developed UHPC mixtures varies according to binder content and the amount of fiber incorporated. As expected, the mixture from Group F, which has a high binder content (1900 pcy) and 3% fiber content, was the most expensive option at approximately $828 per yd^3. In contrast, the Group E mixture, with a lower binder content, was about $45 less expensive. It is important to note that fiber cost has the most significant impact on overall cost, while the difference in binder content only accounts for a $45 variation. However, the cost analysis was conducted based on the mixtures shown in Table 4.8, and any changes in admixture amounts due to factors such as mixing energy, temperature, and batch size will consequently affect the cost per yd^3. Additionally, material unit costs are subject

to change, so the actual cost will depend on the location and availability of raw materials at the time of construction.

4.5 Summary

This chapter presented two phases of development and evaluation for UHPC mixes. Phase I examined the effects of different total binder quantities, w/b ratios, varying amounts of HRWR and WRT admixtures, and different fiber contents on the performance of UHPC overlays. Detailed results and discussions are available in Appendix A and Appendix B. This chapter included the results of flow, PR, VSS, compressive strength, and unit weight of UHPC overlay mixtures over time, along with the final criteria for flow selection. New acceptable flow criteria were recommended based on the PR and VSS results. Successful thixotropic UHPC overlay mixtures were achieved by adjusting HRWR and WRT in all groups except Groups D and G. Based on these test results, four mixtures were selected for further performance evaluation, which was presented in Phase II.

Phase II offered a detailed assessment of the four chosen mixtures from Groups B, C, E, and F, focusing on their constructability, fresh and early-age properties, compressive strength, flexural strength, tensile strength, and bond strength. The constructability test confirmed that the selected mixtures were stable and spread evenly under vibration, although one mixture from Group F needed extra help. All four mixtures successfully passed the fresh property tests, matching results from small batch trials. However, new flow criteria were introduced because Group F failed the constructability test, setting a static flow range of four to six inches and a dynamic flow range of seven to eight inches. The analysis of early-age properties showed that lower binder content and higher WRT dosages caused delays in setting time. Despite these differences, all mixtures met the requirements for compressive and flexural strength. Mixes 29, 24, and 25 also met the tensile strength standards, while Mix 8 did not due to its low binder and

fiber content and was therefore excluded. Although Mix 25 met all performance criteria, it was not selected for economic reasons because of its high binder and fiber content, which required more energy to consolidate. Consequently, Mixes 29 and 24 were chosen for the full-scale mockup specimens. The tests conducted in this chapter, along with the durability tests, were repeated for Mixes 29 and 24 during the mockup construction, as detailed in Chapter 6.

Chapter 5 Flexural Capacity Prediction

5.1 Introduction

This chapter presents an analytical approach for predicting the service and ultimate flexural capacity of composite reinforced concrete bridge decks with UHPC overlays, following the latest AASHTO LRFD guide specifications for structural design using UHPC. The AASHTO-UHPC (2024) material models for tension and compression, along with the strain compatibility approach, are employed to predict the flexural capacity under both positive and negative moment loading conditions. The interface shear between the deck concrete and UHPC is checked according to AASHTO guide specifications. The chapter also provides a design example applying the proposed equations to determine the ultimate flexural capacities for positive and negative bending moments. Furthermore, a parametric study investigates the impacts of varying UHPC thickness, compressive strength, crack localization strength, and crack localization strain on the flexural capacity of the composite section.

5.2 Material Models

To predict the flexural capacity of the composite section, the constitutive models for UHPC, NC, and steel should be determined. The behavior of UHPC under compression and tension can be assumed according to AASHTO-UHPC (2024). For more simplification, the post peak behavior of UHPC under compression and tension is ignored after reaching the maximum compressive and crack localization strength, respectively. The behavior of UHPC can be assumed to be elastic perfectly plastic under compression, as shown in Figure 5.1 (a). For the behavior of UHPC under tension, it can be assumed to be a bilinear relationship, as shown in Figure 5.1 (b).

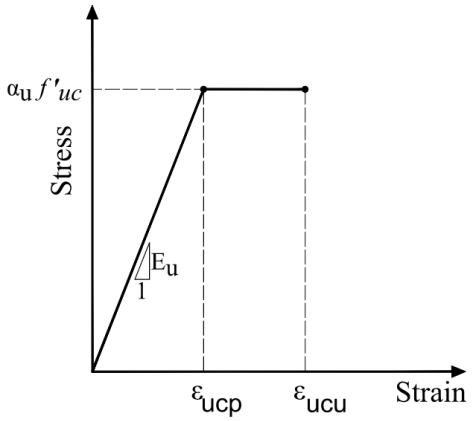

(a) Compression

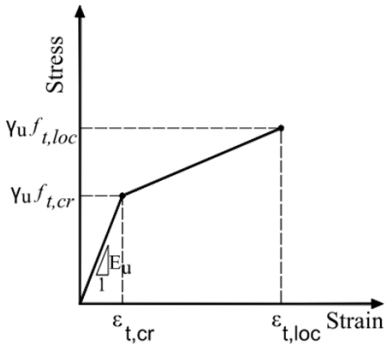

(b) Strain-hardening tension model

Figure 5.1 Idealized tensile stress-strain model for UHPC (AASHTO-UHPC).

f'_{uc} = compressive strength of UHPC

ε_{ucu} = ultimate compressive strain, assumed to be 0.0035

ε_{ucp} = elastic compressive strain

α_u = reduction factor to account for the nonlinearity of the compressive stress-strain response; it shall not be greater than 0.85 (AASHTO-UHPC).

$f_{t,cr}$ = effective cracking strength of UHPC

$\varepsilon_{t,cr}$ elastic tensile strain limit of UHPC corresponding to a cracking strength ($\gamma_u f_{t,cr}$)

$f_{t,loc}$ = crack localization strength of UHPC

$\varepsilon_{t,loc}$ = crack localization strain of UHPC

γ_u = reduction factor to account for undesirable fiber orientation or other effects, assumed to be 1.0 in absence of physical testing (AASHTO-UHPC).

E_u = modulus of elasticity for UHPC, as defined in (5.1.

$$E_u = 2{,}500 K_{1u} f'^{\,0.33}_{uc} \quad (5.1)$$

where K_{1u} is a correction factor which shall be taken as 1.0 in absence of physical testing, and f'_{uc} in ksi.

The elastic compressive strain of UHPC, ε_{ucp}, is calculated as follows:

$$\varepsilon_{ucp} = \frac{\alpha_u f'_{uc}}{E_u} \quad (5.2)$$

For NC, the tensile strength is neglected in calculating the ultimate flexural strength. Since in most cases the compressive strain in NC does not reach the ultimate compressive strain of 0.003, the use of stress block approximation is inappropriate. The compression model proposed by Thorenfeldt et al. (1987) and Collins and Mitchell (1991) is used in this study. The stress-strain relationship can be determined, as defined in (5.3.

$$f_c(\varepsilon_c) = \left(\frac{n\left(\frac{\varepsilon_c}{\varepsilon'_c}\right)}{n - 1 + \left(\frac{\varepsilon_c}{\varepsilon'_c}\right)^{nk}}\right) f'_c \quad (5.3)$$

where,

f'_c = compressive strength of normal concrete

f_c = stress at any strain ε_c

ε'_c = strain when f_c reaches to f'_c

n = a curve-fitting factor equal to $0.8 + \left(\frac{f'_c}{2500}\right)$ where f'_c is in psi

k = a factor to control the slope of the ascending and descending branches of stress-strain curve, taken equal to 1.0 for $\frac{\varepsilon_c}{\varepsilon'_c}$ less than 1.0 and taken $0.67 + \left(\frac{f'_c(psi)}{2500}\right)$ for $\frac{\varepsilon_c}{\varepsilon'_c}$ grater than 1.0

E_c = modulus of elasticity for normal concrete is determined as follows:

$$E_c = 120{,}000\ K_{1c}\gamma_c^2 f_c'^{0.33} \tag{5.4}$$

where γ_c represents the unit weight of normal concrete in kcf, K_{1c} is a correction factor set to one in absence of physical testing, and f_c' in ksi.

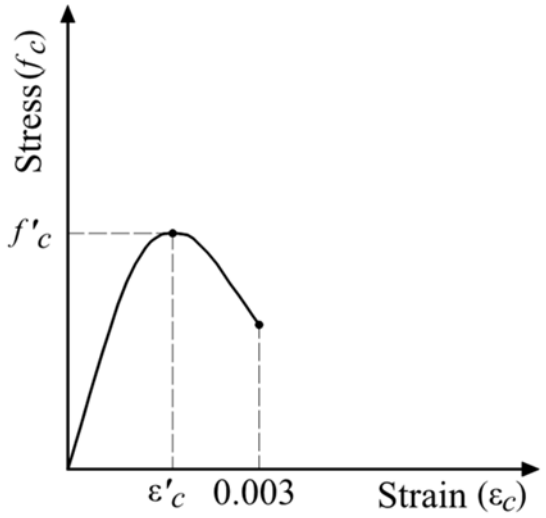

Figure 5.2 Material model of normal concrete (NC) in compression (Thorenfeldt et al., 1987) and (Collins and Mitchell, 1991).

Traditional rebar steel is used in this study. The steel is assumed to be elastic perfectly plastic, as clarified in Figure 5.3.

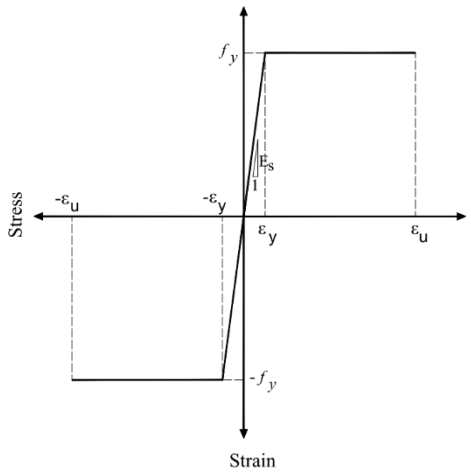

Figure 5.3 Material model for steel (AASHTO LRFD, 2020)

where,

f_y = yield stress of reinforcement steel.

ε_y = yield strain of reinforcement steel.

ε_u = ultimate strain of reinforcement steel depends on the grade and diameter of the reinforcing steel

ε_s = strain at different loading assumed (0 to ε_u)

E_s = reinforcement modulus of elasticity, equal to 29000 ksi

5.3 Methodology

To calculate the flexural capacity of a normal concrete (NC) bridge deck with a reinforced or unreinforced UHPC overlay, this approach is proposed based on strain compatibility, formulating all key parameters as functions of the neutral axis depth from the compression side. A perfect bond is assumed between the normal concrete slab and the UHPC overlay; thus, interface shear is checked to confirm there is no slippage between the two materials.

In normal concrete slabs with UHPC overlay composite sections, failure may occur through several mechanisms depending on the neutral axis location. These include the crushing of the UHPC, crushing of the NC in compression, localization of cracks in the UHPC under

tension, or tension failure of the reinforcement, whichever happens first. These failure modes are identified by assessing the computed values of the minimum sectional curvature when:

1. The compressive strain at the extreme compression fiber of UHPC reaches the compression strain limit, ε_{ucu},
2. The compressive strain at the extreme compression fiber of the normal concrete reaches the compression strain limit, ε_{cu},
3. The net tensile strain at the extreme tension fiber of the UHPC reaches the UHPC tensile strain limit, $\varepsilon_{t,loc}$, and
4. The strain in the extreme tension steel reaches the minimum total elongation strain of reinforcing steel, ε_u.

A perfect bond between steel and concrete is assumed. The assumptions of plane sections and no slippage at the interface between the NC bridge deck and UHPC overlay were applied. Figure 5.4 shows a typical section of a normal concrete bridge deck slab with UHPC overlay with a total height of h and a width of b.

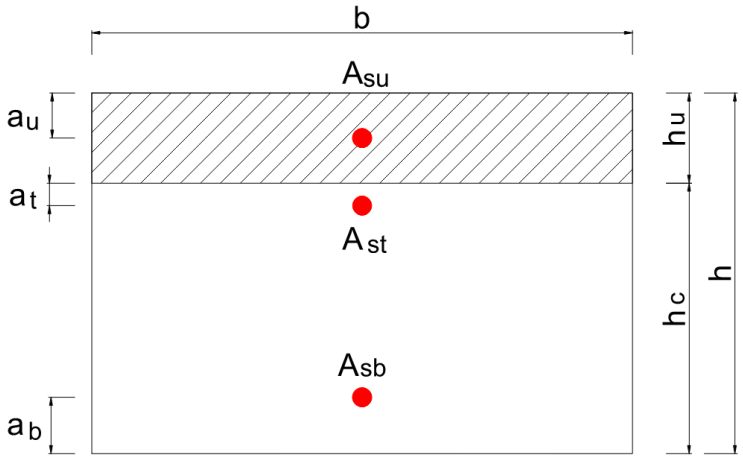

Figure 5.4 Typical section of normal concrete bridge deck slab with UHPC overlay.

where,

B = width of composite section

h = total height of the composite section

h_u = height of UHPC overlay

h_c = height of the NC bridge deck

A_{su} = area of reinforcement in UHPC overlay

A_{st} = area of top reinforcement in the NC bridge deck

A_{sb} = area of bottom reinforcement in the NC bridge deck

a_u = distance between the center of reinforcement in the UHPC layer and the top fiber of the UHPC layer

a_t = distance between the center of the top reinforcement and the top fiber of the NC bridge deck

a_b = distance between the center of the bottom reinforcement and the bottom fiber of the NC bridge deck

The composite section experiences two different loading directions based on its location on the transverse direction of the bridge. At mid-span, the composite section is subjected to a positive bending moment (UHPC in compression zone). Above girder lines, the composite section is subjected to a negative bending moment (UHPC in tension zone). The calculation of the ultimate capacity of the composite section is presented in the following subsections.

5.4 Flexure Capacity of NC Slab with UHPC Overlay

5.4.1 Under Positive Moment

For the composite section under positive bending moment at the ultimate state, the entire section of normal concrete slab, and the bottom and top reinforcement are in the tension zone, as it is most likely for the neutral axis to be in the UHPC layer. Figure 5.5 shows the analytical model of the composite section subjected to a positive ultimate moment based on the simple plastic theory of composite sections. The section capacity is controlled by either UHPC's

ultimate compressive strain (ε_{ucu}) or the rupture strain of the bottom reinforcement. The contribution of the UHPC tension force below the neutral axis is neglected for simplification, as it has a small moment arm and does not significantly affect the calculated flexural capacity. The value of compression UHPC depth (c) is obtained by the equilibrium of axial forces, as clarified in (5.5.

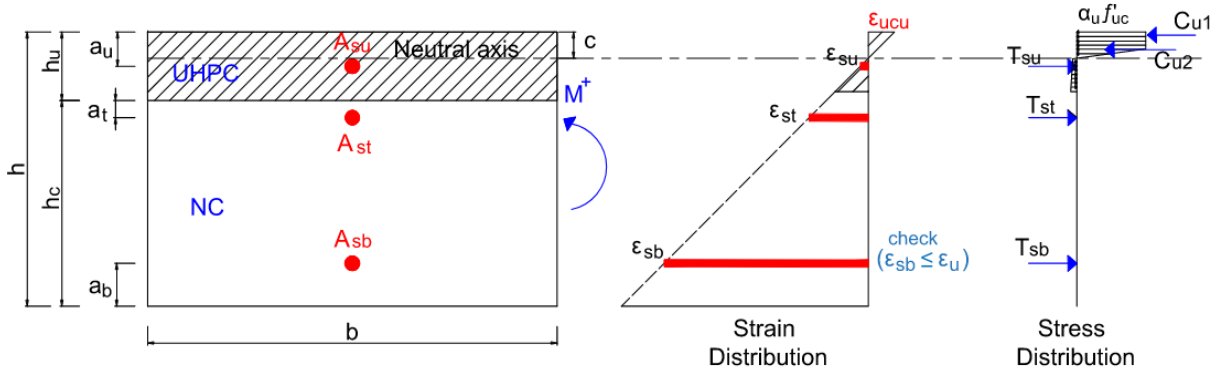

Figure 5.5 Analytical model of the composite section under a positive ultimate moment.

$$T_{su}(c) + T_{st}(c) + T_{sb}(c) = C_u(c) \tag{5.5}$$

where,

$T_{su}(c)$ = the tensile force of the reinforcement steel in the UHPC layer as a function in the neutral axis depth, c, as calculated in (5.6

$T_{st}(c)$ = the tensile force of the top reinforcement steel as a function in the neutral axis depth, c, as calculated in (5.7

$T_{sb}(c)$ = the tensile force of the bottom reinforcement steel as a function in the neutral axis depth, c, as calculated in (5.8

$C_u(c)$ = the resultant compressive force in the UHPC layer as a function in the neutral axis depth, c, as, as calculated in (5.9 and (5.10

$$\mathrm{T}_{su}(c) = A_{su}\, E_s \text{ min of } \begin{cases} \varepsilon_y \\ \dfrac{a_u - c}{c}\, \varepsilon_{ucu} \end{cases} \tag{5.6}$$

$$\mathrm{T}_{st}(c) = A_{st}\, E_s \text{ min of } \begin{cases} \varepsilon_y \\ \dfrac{h_u + a_t - c}{c}\, \varepsilon_{ucu} \end{cases} \tag{5.7}$$

$$\mathrm{T}_{sb}(c) = A_{sb}\, E_s \text{ min of } \begin{cases} \varepsilon_y \\ \dfrac{h - a_b - c}{c}\, \varepsilon_{ucu} \end{cases} \tag{5.8}$$

$$\mathrm{C}_{u1}(c) = 0.85\, f'_{uc}\, b\, (1 - \frac{\varepsilon_{ucp}}{\varepsilon_{ucu}})c \tag{5.9}$$

$$\mathrm{C}_{u2}(c) = 0.85\, f'_{uc}\, b\, \frac{\varepsilon_{ucp}}{\varepsilon_{ucu}}\, c \tag{5.10}$$

The positive nominal moment capacity of the section (Mn.p) is determined by the addition of the moments of each force around the section's centerline. (5.11 shows the calculation of the composite section's positive nominal moment capacity in terms of the neutral axis depth, c.

$$\begin{aligned} \mathrm{M}_{n.p} = {} & \mathrm{T}_{su}(c).(a_u - c) + \mathrm{T}_{st}(c).(h_u + a_t - c) + \mathrm{T}_{sb}(c).(h - a_b - c) \\ & + \mathrm{C}_{u1}(c).(1 + \frac{\varepsilon_{ucp}}{\varepsilon_{ucu}}).\frac{c}{2} + C_{u2}(c).\frac{\varepsilon_{ucp}}{\varepsilon_{ucu}}.\frac{2c}{3} \end{aligned} \tag{5.11}$$

Likewise, in the case of UHPC in the tension zone, the ultimate moment is determined by multiplying the nominal moment by the resistance factor (ϕ), as illustrated in (5.22. However, the determination of the resistance factor (ϕ) itself should be according to AASHTO LRFD 2020. The two design specifications have the same values for (ϕ) that is 0.9, and 0.75 for tension-controlled, and compression-controlled sections, respectively. Nonetheless, the ductility here is dependent on the tensile strain in the extreme tension steel, as depicted in Equation 5.12. The tensile strain of the bottom reinforcement is calculated by Equation 5.13.

$$\phi = \begin{cases} 0.75, & \varepsilon_{s.b} < 0.002 \\ 0.75 + 0.15\dfrac{(\varepsilon_{s.b} - 0.002)}{(0.005 - 0.002)}, & 0.002 \le \varepsilon_{s.b} \le 0.005 \\ 0.9, & \varepsilon_{s.b} > 0.005 \end{cases}$$ Equation 5.12

$$\varepsilon_{s.b} = \frac{h - a_b - c}{c}\,\varepsilon_{ucu}$$ Equation 5.13

5.4.2 Under Negative Moment

For the composite section under negative bending moment at the ultimate state, the normal concrete slab is in the compression zone, while the UHPC layer, top reinforcement, and reinforcement in the UHPC layer are in the tension zone. The bottom reinforcement strain may be either in tension or in compression, depending on the location of the neutral axis. Figure 5.6 illustrates the analytical model of the composite section subjected to a negative ultimate moment, based on the simple plastic theory of composite sections for calculation. The strain in the composite section is assumed to be controlled by the UHPC crack localization strain, $\varepsilon_{t,loc}$. However, the compression strain in the bottom fiber of NC should be checked to be less than the ultimate compression strain (0.003). Then, the strain in the reinforcement is determined based on the geometrical relationships of similar triangles. The stress distribution is calculated based on the strain distribution and the provided material models.

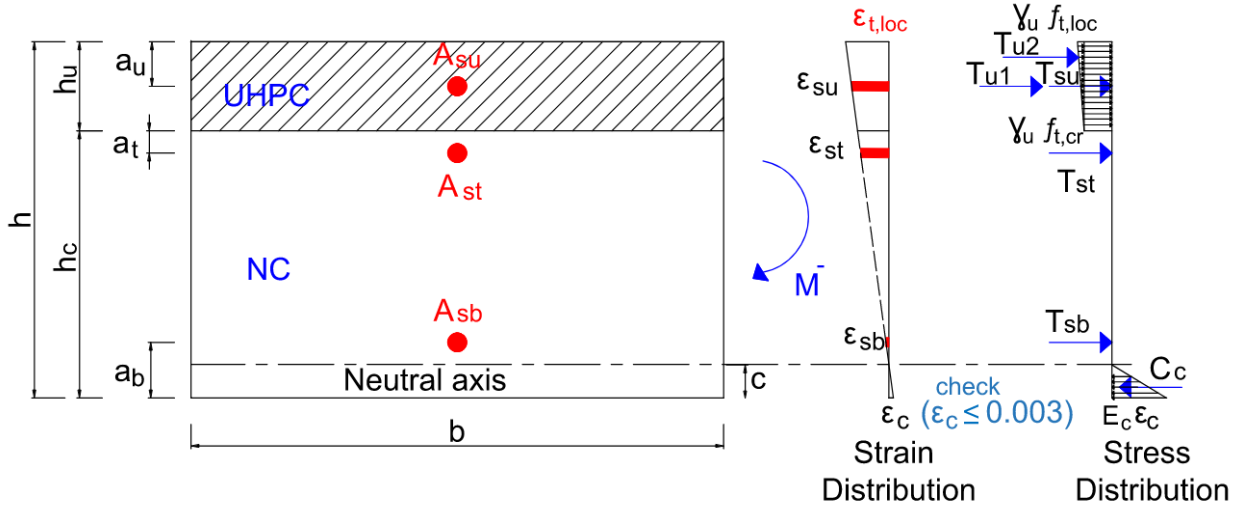

Figure 5.6 Analytical model of the composite section under a negative ultimate moment.

The value of compression concrete depth c at the NC section is obtained by the equilibrium of axial forces, as depicted in (5.14.

$$T_u + T_{su}(c) + T_{st}(c) + T_{sb} = C_c(c) \tag{5.14}$$

where,

T_{u1} = rectangular resultant tensile force in the UHPC layer, as calculated in (5.15

T_{u2} = triangle resultant tensile force in the UHPC layer, as calculated in (5.16

$T_{su}(c)$ = the tensile force of the reinforcement steel in the UHPC layer as a function in the neutral axis depth, c, as calculated in (5.17

$T_{st}(c)$ = the tensile force of the top reinforcement steel as a function in the neutral axis depth, c, as calculated in (5.18

$T_{sb}(c)$ = the tensile force of the bottom reinforcement steel as a function in the neutral axis depth, c, as calculated in (5.19

$C_c(c)$ = resultant compressive force in the NC as a function in the neutral axis depth, c, as calculated in (5.20

$$T_{u1} = f_{t,cr}\, b\, h_u \tag{5.15}$$

$$T_{u2} = 0.5\,(f_{t,loc} - f_{t,cr})\, b\, h_u \tag{5.16}$$

$$T_{su}(c) = A_{su}\, E_s\, min\, of \begin{cases} \varepsilon_y \\ \dfrac{h - c - a_u}{h - c}\, \varepsilon_{t,loc} \end{cases} \quad (5.17)$$

$$T_{st}(c) = A_{st}\, E_s\, min\, of \begin{cases} \varepsilon_y \\ \dfrac{h_c - c - a_u}{h - c}\, \varepsilon_{t,loc} \end{cases} \quad (5.18)$$

$$T_{sb}(c) = A_{sb}\, E_s\, min\, of \begin{cases} \varepsilon_y \\ \dfrac{a_b - c}{h - c}\, \varepsilon_{t,loc} \end{cases} \quad (5.19)$$

$$C_c(c) = 0.5.E_c.\frac{c}{h - c}\,.\varepsilon_{t,loc}\,.c.b \quad (5.20)$$

The negative nominal moment capacity of the section (Mn.n) is determined by the summation of the moments of each force around the section's centerline. Equation 5.21 presents the calculation of the composite section negative nominal moment capacity in terms of the neutral axis depth, c.

$$M_{n.n} = T_{u1}.\left(h - c - \frac{h_u}{2}\right) + T_{u2}.\left(h - c - \frac{h_u}{3}\right) + T_{su}(c).(h - c - a_u) + T_{st}(c).(h_c - c - a_t) + T_{sb}(c).(a_b - c) + C_{c.c}(c).\left(\frac{2c}{3}\right) \quad \text{Equation 5.21}$$

Then, the design negative moment capacity is determined by multiplying the nominal capacity with the resistance factor (ϕ), as depicted in (5.22. According to AASHTO-UHPC (2024), the resistance factor (ϕ) should be set to 0.9 for sections with a curvature ductility ratio (μ) greater than the curvature ductility ratio limit (μl), which is 3.0. For sections with a curvature ductility ratio (μ) less than 1.0 or unreinforced UHPC sections, the value of ϕ is 0.75. For sections where the curvature ductility ratio, μ, ranges between the curvature ductility ratio limit, 1.0 and 3.0, the value of ϕ can be determined through linear interpolation from 0.75 to 0.90, as

illustrated in (5.23 and shown in Figure 5.7. This reflects the improved reliability of ductile sections, allowing for higher resistance factors in design.

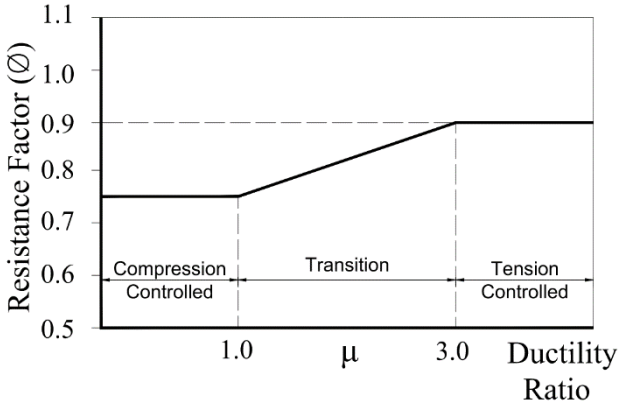

Figure 5.7 Variation of the flexural resistance factor (ϕ) with the curvature ductility ratio (μ) for reinforced UHPC sections (AASHTO-UHPC).

$$M_r = \phi . M_n \tag{5.22}$$

$$\phi = \begin{cases} 0.75, & \mu < 1.0 \\ 0.75 + 0.15\dfrac{(\mu - 1.0)}{(\mu_\ell - 1.0)}, & 1.0 \le \mu \le 3.0 \\ 0.9, & \mu > 3.0 \end{cases} \tag{5.23}$$

The curvature ductility ratio, μ, which is defined as the ratio of the sectional curvature at the nominal moment resistance (ψ_n) to the baseline sectional curvature ($\psi_{s\ell}$), should be calculated as follows:

$$\mu = \frac{\psi_n}{\psi_{s\ell}} \tag{5.24}$$

$$\psi_n = \frac{\varepsilon_{t,loc}}{h - c} \tag{5.25}$$

$$\psi_{s\ell} = \frac{\varepsilon_{s\ell}}{h - c - a_u} \tag{5.26}$$

where,

ψ_n = sectional curvature at nominal flexural strength

$\psi_{s\ell}$ = sectional curvature when the stress in the extreme tension steel in the UHPC layer is equal to the steel service stress limit, as computed in (5.26 (1/in.)

$\varepsilon_{s\ell}$ = service strain in the extreme tension steel in the UHPC layer when the steel stress is equal to 80 % of the yielding stress of the reinforcement, (in./in.)

5.5 Interface Shear

The presented equations for the flexural capacity predictions assumed a perfect bond between the UHPC layer and the NC slab. Thus, the ultimate interface shear stress (v_u) should be checked to be less than the interface shear resistance (ϕv_{ni}). Assuming the bridge deck is continuous over multiple girder lines, the ultimate interface shear stress (v_u) is calculated using (5.27 assuming the distance between inflection points is 0.6S.

$$v_u = max\ of \begin{cases} \dfrac{H_p}{b\ .\ 0.3S} \\ \dfrac{H_n}{b\ .\ 0.2S} \end{cases} \tag{5.27}$$

where,

H_p = horizontal shear force acting on the interface plane under a positive moment

H_n = horizontal shear force acting on the interface plane under a negative moment

b = width of composite section

S = Spacing between supporting girders

Although AASHTO-UHPC (2024) provides guidance for calculating the interface shear resistance in Section 1.7.4.3 based on various surface preparation scenarios that yield different cohesion values between NC and UHPC, these cohesion values are not updated to reflect the specific case of a UHPC overlay. Therefore, it is recommended to determine the actual cohesion value through pull-off testing in accordance with ASTM C1583/C1583M-20. For design and

quality assurance purposes, the cohesion value should be established by ASTM C1583 pull-off testing for each project and should be re-evaluated whenever the surface preparation method, substrate condition, or UHPC overlay mixture changes significantly. Equation (5.28) presents the calculation of interface shear resistance (ϕv_{ni}).

$$\phi v_{ni} = \phi . C \tag{5.28}$$

where,

ϕ = shear resistance factor equal to 0.9

C = cohesion Factor from Pull-off test

5.6 Design Example

The FHWA design example (FHWA, 2024) is selected in this study to illustrate the proposed approach presented earlier. The example presents the design of an NC bridge deck according to AASHTO-LRFD specifications. The top 1.5 in. from the NC cover is replaced with an unreinforced UHPC overlay, ensuring no additional weight due to the replacement. The bridge deck has a total width of 55.375 ft and a constant thickness of 8 in. A 1 ft wide strip is designed using the equivalent strip method as a continuous slab with a span of 9 ft–8 in. (i.e., girder spacing) and 3 ft–6.25 in. overhang. Transverse deck reinforcement is #5-grade-60 A615 reinforcing steel at 7 in. spacing for the bottom layer and 9 in. spacing for the top layer. The bottom and top clear covers are 1 in. and 2.5 in., respectively, as shown in Figure 5.8. The calculated factored positive and negative bending moments are 13.38 kip.ft/ft and 8.95 kip.ft/ft, respectively. The capacity of the designed section under positive and negative moments is calculated according to AASHTO-LRFD and found to be 17.17 kip.ft/ft and 9.13 kip.ft/ft, respectively. Table 5.1 shows the properties of NC, UHPC, and reinforcement used in this example.

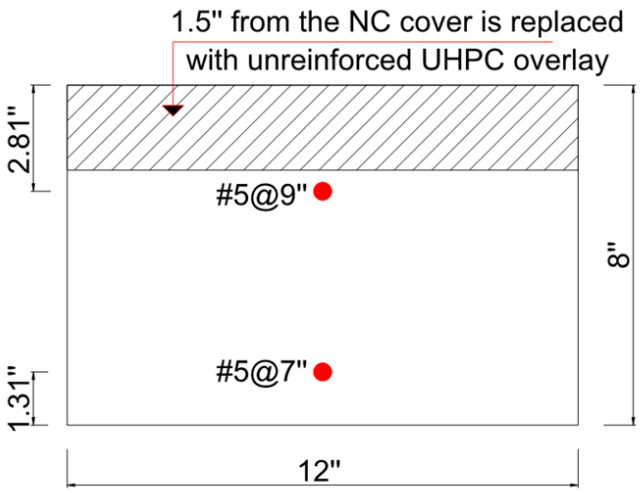

Figure 5.8 The design of NC bridge deck section (FHWA, 2024).

Table 5.1 NC and UHPC properties.

Material Properties	**NC**	**UHPC**
Compressive strength, ksi	4	14
Modulus of elasticity, ksi	4285	6025
Cracking strength, ksi	neglected	0.75
Crack localization strength, ksi	N/A	0.9
Ultimate compressive strain	0.003	0.0035
Crack localization strain	N/A	0.0025
Reinforcing Steel (A615) properties		
Yield strength, ksi	60	
Modulus of elasticity, ksi	29000	
Yield strain	0.002	
Rupture strain	0.09	

Ultimate Flexure Capacity of the Composite Section Under Positive Bending Moment

Using (5.5 to (5.10, the neutral axis depth (c) is 0.42 in. Table 5.2 shows the forces and strains in UHPC, NC, and reinforcement, and the corresponding moment arms for the calculated c = 0.4 in. The nominal positive moment capacity, $M_{n.p}$, in (5.11, is equal to 22.8 kip.ft/ft. The flexural resistance factor (ϕ) is 0.9 as the tensile strain in the bottom reinforcement $\varepsilon_{s.b}$ is 0.05,

which is less than the rupture strain of 0.09. The design flexural capacity of the composite section under positive moment is 20.5 kip.ft/ft.

Table 5.2 Forces, strains, and moment arms for UHPC, NC, and reinforcement under positive nominal moment

Item	Force (kip)	Strain in bars (ε_{si})	Distance from CG to the neutral axis (in.)
$T_{st}(c)$	24.8	0.0213	2.4
$T_{sb}(c)$	32	$0.0555 \leq 0.09$	6.3
$C_{u1}(c)$	24.7	N/A	0.31
$C_{u2}(c)$	32.1	N/A	0.15

Ultimate Flexure Capacity of the Composite Section Under Negative Bending Moment

Using (5.14 to (5.20, the neutral axis depth (c) is found to be 1.8 in. and the corresponding forces and strains in UHPC, NC, and reinforcement are listed in Table 5.3. The nominal negative moment capacity, $M_{n.n}$, in Equation 5.21, is equal to 14.4 kip.ft/ft. According to AASHTO-UHPC (2024), the flexural resistance factor (ϕ) should be 0.75 when there is no reinforcement in the UHPC layer. Therefore, the design flexural capacity of the composite section under negative moment is 10.8 kip.ft/ft. The strain at the bottom fiber of the NC section is 0.0007, which is less than the NC compressive strain limit of 0.003.

Table 5.3 Forces, strains, and moment arms for UHPC, NC, and reinforcement under negative nominal moment.

Item	Force (kip)	Strain in bars (ε_{si})	Distance from CG to the neutral axis (in.)
T_{u1}	13.5	N/A	5.5
T_{u2}	1.4	N/A	5.7
$T_{st}(c)$	16.4	0.0014	3.4
$T_{sb}(c)$	-2.8	-0.0002	-0.5
$C_c(c)$	28.4	N/A	1.2

Note: The negative sign means that the bar is in compression

Interface Shear Check

For the same design example, the interface shear strength (v_h) is found to be 0.11 ksi, using (5.27. To ensure adequate bond performance, the interface shear demand must be less than the interface shear resistance, which was determined from the pull-off test, as defined in (5.28. Appendix D presents detailed calculations in PTC Mathcad, demonstrating how each equation is substituted and solved to obtain the final results presented in this example. To conclude, in addition to the good mechanical properties of UHPC such as high density, low permeability, and high abrasion resistance which are good for increasing the life cycle of the bridge deck, using UHPC, with low mechanical properties compared to literature, as an overlay material increases the positive and negative nominal flexural capacity by 12% and 35%, respectively, as shown in Figure 5.9.

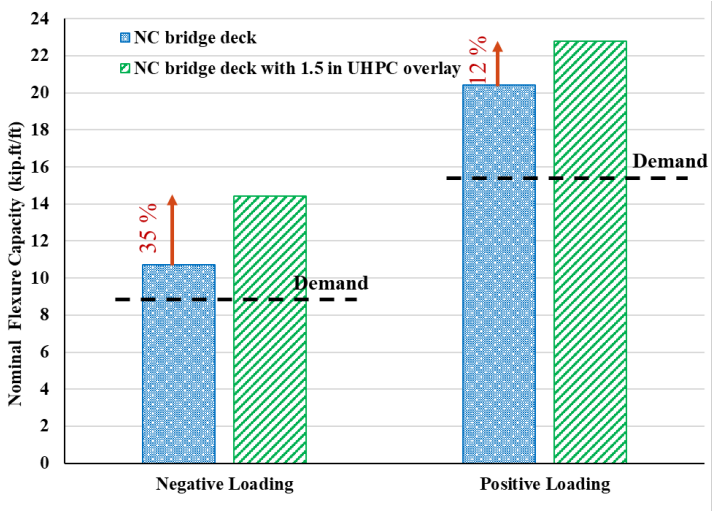

Figure 5.9 The demand vs calculated ultimate flexural capacity.

5.7 Parametric Study

In this section, the influence of UHPC thickness, compressive strength, crack localization strength, and crack localization strain on the flexural capacity of the composite section is presented. This study provides insights into the significance of each parameter in optimizing the bridge deck flexural capacity.

Effect of UHPC Thickness

For the same NC bridge deck with UHPC overlay used in the design example, the UHPC thickness is varied from 1 in. to 3 in. The proposed approach is used to calculate the positive and negative ultimate flexural capacity for each thickness. Figure 5.10 shows the calculated ultimate negative and positive flexural capacity for each UHPC thickness. It is evident that increasing UHPC thickness enhances the negative flexural capacity, as UHPC will be in the tension zone and contribute to the tension force on the section. Changing UHPC thickness has no effect on the positive flexural capacity.

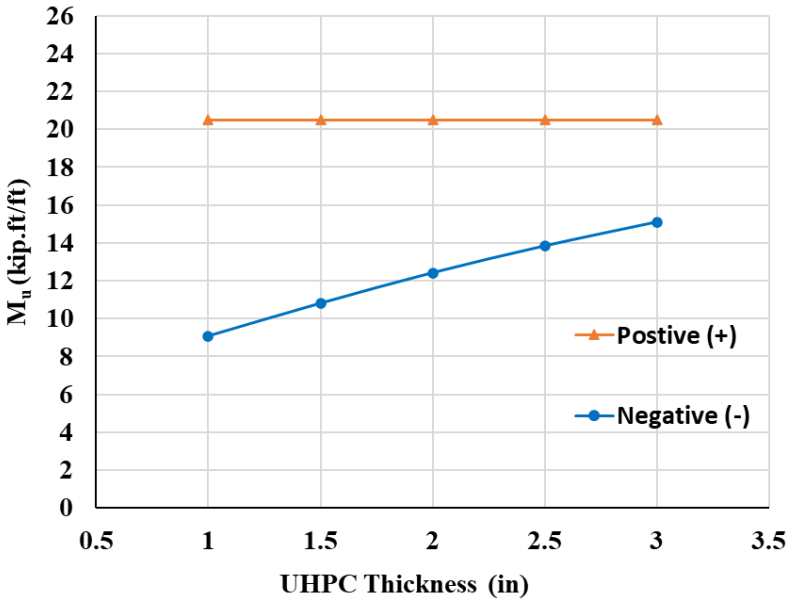

Figure 5.10 Effect of UHPC thickness on ultimate flexural capacity.

Effect of UHPC Compressive Strength

The compressive strength of UHPC varied from 12 ksi to 18 ksi. Figure 5.11 shows the calculated ultimate negative and positive flexural capacity for each UHPC compressive strength. It can be observed that increasing UHPC compressive strength has no effect on the negative flexural capacity as the behavior is related to the tensile strength of UHPC. Likewise, increasing UHPC compressive strength has no significant impact on the positive flexural capacity, as the behavior is related to the compressive strength of UHPC.

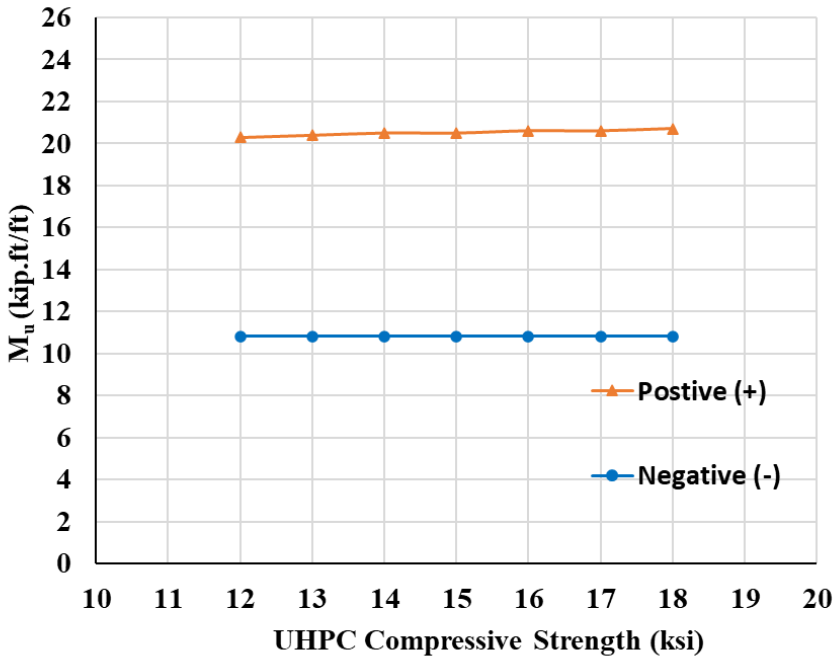

Figure 5.11 Effect of UHPC compressive strength on the ultimate flexural capacity.

Effect of UHPC Crack Localization Strength

The crack localization strength of UHPC is varied from 0.9 ksi to 1.5 ksi. Figure 5.12 shows the calculated ultimate positive and negative flexural capacities for each UHPC crack localization strength. It can be seen that increasing UHPC crack localization strength results in

an increased negative flexural capacity. However, it has little effect on the positive flexural capacity because the moment arm of the UHPC layer just below the neutral axis is small.

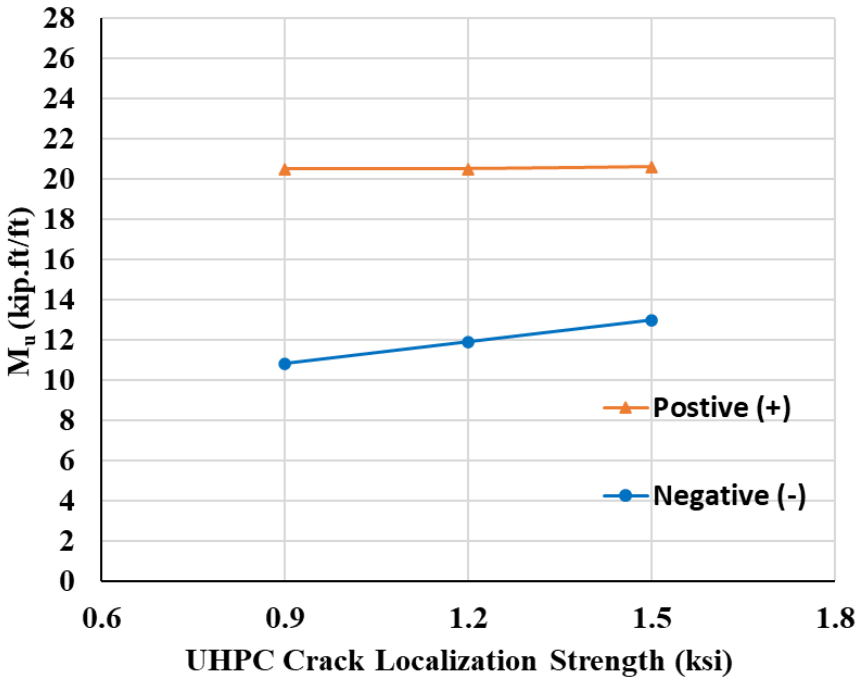

Figure 5.12 Effect of UHPC crack localization strength on the ultimate flexural capacity

Effect of UHPC Crack Localization Strain

The crack localization strain of UHPC is varied from 0.0025 to 0.0075. Figure 5.13 shows the calculated ultimate positive and negative flexural capacities for each UHPC crack localization strain. It can be observed that increasing UHPC crack localization strain results in a slight increase in the negative flexural capacity. At the same time, there is no effect on the positive flexural capacity.

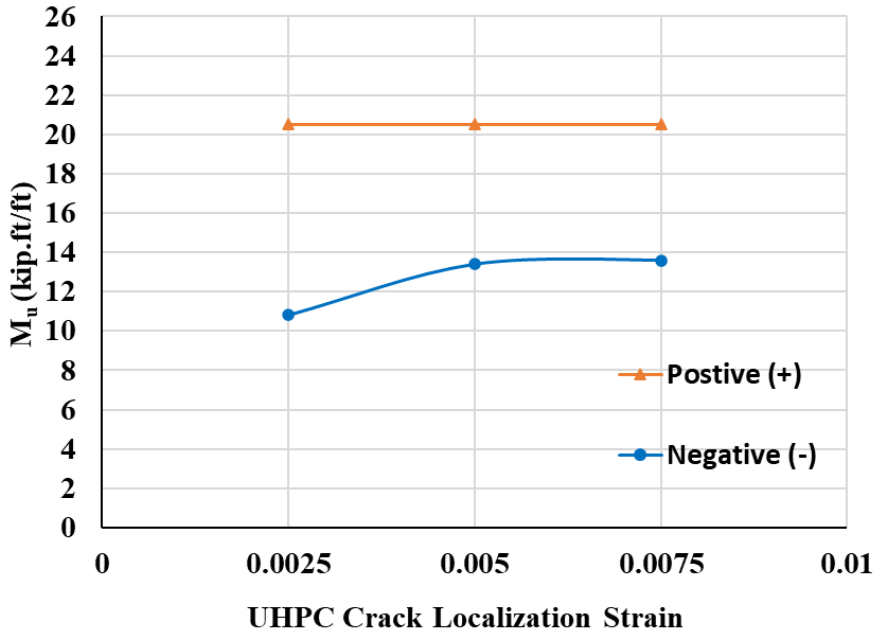

Figure 5.13 Effect of UHPC crack localization strain on the ultimate flexural capacity.

5.8 Summary

This chapter presented an analytical method for predicting the flexural capacity of composite reinforced concrete bridge decks overlaid with UHPC, in accordance with the AASHTO-UHPC (2024) guide specifications. A strain compatibility approach was used to evaluate the ultimate moment capacities under positive and negative bending conditions. Idealized constitutive models were applied for UHPC, normal concrete (NC), and reinforcing steel. UHPC was modeled as elastic perfect plastic in compression and bilinear strain-hardening in tension, while NC and steel were modeled based on established codes and literature. The analysis considered multiple failure mechanisms, including crushing of UHPC or NC, crack localization in UHPC in tension, and rupture of steel reinforcement, depending on the neutral axis location and curvature thresholds. Flexural moment capacities were calculated through axial force equilibrium and curvature analysis, with ductility assessments used to select appropriate

resistance factors. The chapter also addressed interface shear resistance to validate the assumption of a perfect bond between the UHPC overlay and NC deck. In UHPC overlay applications where guideline values are not directly applicable, the use of pull-off testing was recommended to determine cohesion parameters.

The proposed analytical framework provided a reliable method for predicting the structural capacity of NC slabs with a UHPC overlay. The chapter also included a design example demonstrating the effective use of the proposed equations to determine the additional flexural capacity gained by replacing 1.5 inches of the concrete cover with a UHPC overlay. The results indicated that the nominal flexural capacity increased by approximately 12% under positive bending moments and 35% under negative bending moments, even when using a UHPC overlay with lower mechanical properties than structural-grade UHPC. For ease of application, Appendix D offers detailed calculations using PTC Mathcad, showing how to substitute and solve the proposed equations to replicate the results of the design example.

A parametric study was also included in this chapter to investigate the effects of varying the UHPC thickness, compressive strength, crack localization strength, and crack localization strain on the flexural capacity of the composite section. This analysis offers useful insights into which parameters should be improved to enhance the flexural performance of composite bridge decks. In Chapter 6, this method will be validated by comparing the predicted flexural capacities with experimental results from full-scale mockup slab tests.

Chapter 6 Mockup Construction and Testing

6.1 Introduction

This chapter describes the experimental program conducted to evaluate the constructability of newly developed UHPC overlay mixes by casting them on full-scale sloped slabs. The fresh, mechanical, and durability properties were also assessed. Six full-scale NC slabs were cast and prepared using three common surface preparation methods: surface retarder (SR), fine milling (FM), and regular milling (TM) to simulate field conditions for UHPC overlay applications. The aim was to examine their impact on the bond strength between the NC substrate and the UHPC overlay, as well as on the flexural performance. The mechanical properties of the UHPC mixes obtained from testing were used in the analytical models introduced in Chapter 5 to predict the flexural capacity of the composite slabs and to verify the models against experimental results.

6.2 Mockup Construction and Material Testing

6.2.1 NC Specimens: Design and Fabrication

The six full-scale slabs were designed following the Nebraska DOT Bridge Office Policies and Procedures (BOPP) manual, with overall dimensions of 4 ft in width, 10 ft in length, and 7.2 in. in thickness. The slabs were reinforced with #5-grade-60 A615 bars spaced 12 in. apart on the bottom and #4-grade-60 A615 bars spaced 12 in. apart on the top. Figure 6.1 presents the schematic drawing of the slab dimensions and reinforcement details. Mix 47BD was used for the NC, with a specified 28-day compressive strength of 4 ksi. The mix design is provided in Table 6.1. Limestone aggregate with a nominal maximum size of one inch was included in the mix.

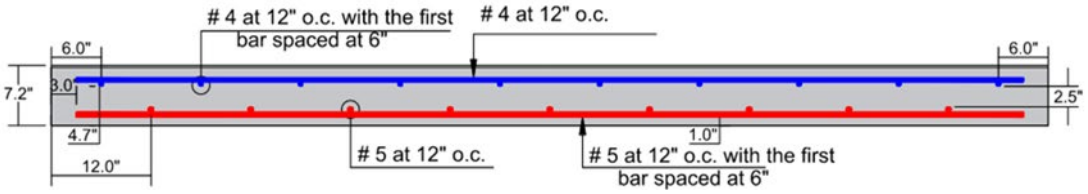

(a) Section view

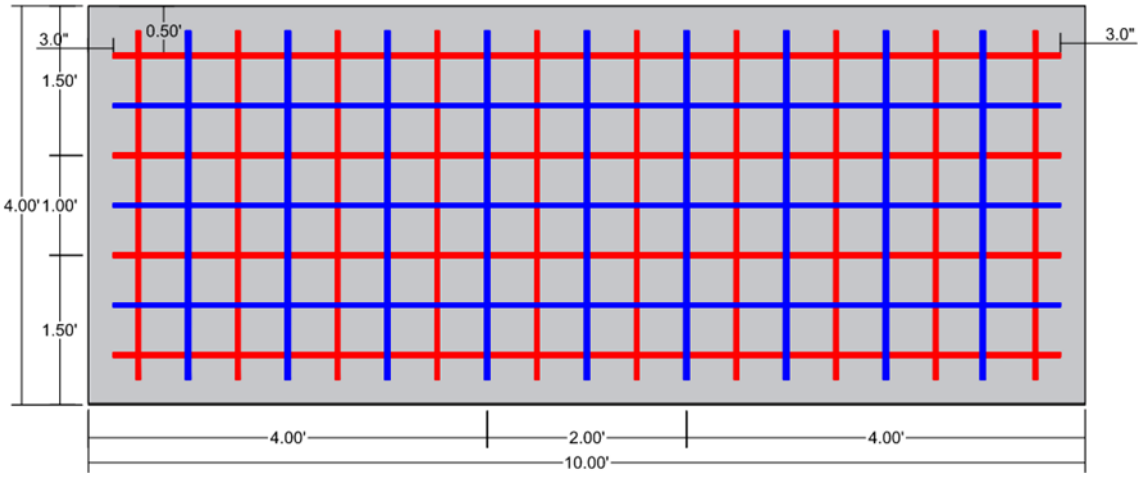

(b) Plan view

Figure 6.1 Schematic drawing of slab dimensions and reinforcement details.

Table 6.1 Preliminary Mix Proportions for Mix 47BD.

Mix ID	Proportion
Cementitious Materials (lb/cy)	658
Water (lb/cy)	263
Limestone (lb/cy)	862
Sand & Gravel (lb/cy)	1965
WR (fl oz/cwt)	8.0
AEA (fl oz/cwt)	1.5

N.B.: w/cm ratio was maintained at 0.41
WR: Water Reducer
AEA: Air-Entraining Agent

Figure 6.2 illustrates the construction process of the NC slabs. All NC slabs were covered with plastic sheeting after casting to ensure proper curing.

(a) Rebar Placement and Formwork Setup

(b) Concrete Pouring and Placement

(c) Freshly Finished Concrete Surface

(d) Plastic Sheet Covering for Curing

Figure 6.2 Construction Process of NC Slabs: Reinforcement, Casting, and Curing.

6.2.2 Surface Preparation

This study employed various commercially available surface preparation methods to roughen the NC slab before casting the UHPC overlay. A surface retarder was applied to the fresh NC of two slabs to expose the aggregates, while two levels of milling were performed on the remaining four slabs, with each level applied to two slabs. It is important to note that surface retarders can only be used on fresh concrete and are therefore limited to newly constructed bridge decks. In contrast, milling is used on hardened concrete of both newly constructed and existing bridge decks, making it more suitable for rehabilitation.

For the two slabs treated with a surface retarder, two commercially available products were used, with each retarder applied to one slab. Figure 6.3 shows the NC slab treated with Top-Cast surface retarder (Blue) from Dayton Superior, which was applied at a rate of 200–300 ft^2/gallon. The used retarder was designed to achieve a roughness of 1/8 to 3/8 in.

Figure 6.3 Application of Top-Cast surface retarder (Blue) from Dayton Superior on fresh concrete.

Figure 6.4 presents the NC slab treated with Master-Finish XR surface retarder (Pink) from Master Builders. This retarder was applied at a rate of 150–200 ft²/gallon, with targeted surface roughness between 3/8 and 1/2 inches.

Figure 6.4 Application of Master-Finish XR surface retarder (Pink) from Master Builders on fresh concrete.

Both surface retarders were applied immediately after placing and screeding the fresh NC. They were removed 12 to 16 hours after application using high-pressure water, as shown in Figure 6.5. A pressure washer delivering a maximum pressure of 3300 psi and a flow rate of 2.3 gallons per minute was used.

Figure 6.5 Removal of surface retarder using high-pressure water.

The two surface retarders demonstrated similar efficiency in exposing the aggregate. Figure 6.6 provides an image of the prepared surface after removing the surface paste.

(a) Slab prepared with Master-Finish XR surface retarder (Pink) from Master Builders

(b) Slab prepared with Top-Cast surface retarder (Blue) from Dayton Superior

Figure 6.6 Prepared surface after surface retarder removal.

The average surface roughness was measured using a caliper following ASTM D8271-21, as shown in Figure 6.7. Surface roughness is defined as the peak-to-valley distance. For each slab, 15 readings were taken at five locations, each measuring 6 × 6 inches. The average surface roughness was found to be (0.2 ± 0.04) inches. Additionally, surface roughness was evaluated using ICRI-CSP comparator chips and was found to correspond to CSP-9.

Figure 6.7 Measuring surface roughness using a caliper.

For the four slabs prepared by milling, a local contractor used the same equipment typically employed in milling applications in bridge decks to mill the slabs at their yard. To facilitate the milling process, the slabs were buried in the ground so that their top surfaces were leveled with the surrounding ground, as shown in Figure 6.8.

Figure 6.8 Milling process of concrete slabs using concrete deck milling equipment.

Two levels of milling were applied, with each level used on two slabs. The fine-texture milling had a 5/8 in. spacing between teeth with 0.1 in. texture roughness, as shown in Figure 6.9 (a). The other level of milling is the typical one used in construction, which had a few worn teeth causing some high areas in the pattern (around 0.25 in. texture roughness in addition to the regular 5/8 in. spacing between teeth with 0.1 in. texture roughness, as shown in Figure 6.9 (b). The surface roughness of fine and typical milling corresponded to CSP-7 and CSP-9, respectively.

(a) Fine milling (b) Typical milling

Figure 6.9 Two levels of milling.

6.2.3 Casting UHPC Overlay

Due to the good workability and mechanical properties of Mix 24 and 29, they were chosen for the mockup application. Mix proportions are shown in Table 6.2.

Table 6.2 Proportions for Mix 29 and Mix 24

Ingredient	Type	SSD Quantity lb/cy	
		Mix 29	Mix 24
Cement	Type 1L	1206	895
Silica Fume	Force 10,000 D	161	120
Slag	GGBFS	585	435
Fine Sand	No.10	1610	2186
Water	Including Ice	316	244
Workability Retaining Admixture (WRA)	Chryso Optima 100	47.2	53.6
High Range Water Reducer (HRWR)	Chryso Premia 150	2.8	2.6
Steel Fibers	**Micro Straight**	**264 (2%)**	**396 (3%)**
Total Binder Content	**-**	**1950**	**1450**
Water/Binder Ratio	**-**	**0.196**	**0.180**

To evaluate the workability and stability of the two mixes, all slabs were raised on one side to create a 2% slope. A 2×4 piece of lumber was placed around the perimeter to achieve a thickness of 1.5 inches, while the UHPC slab had overall dimensions of 3 × 8.5 ft. Before casting the UHPC overlay, the slabs were thoroughly cleaned using high-pressure water to remove debris and dirt. Additionally, they were wetted to attain a saturated surface dry condition as shown in Figure 6.10.

Figure 6.10 Preparation and slope adjustment of slabs for UHPC overlay application.

The UHPC was mixed in 4.3 ft^3 batches using a high-shear Imer 750 mixer. The UHPC was manually placed and consolidated using a vibratory leveling screed with a speed range of 4,000 to 7,000 rpm. Figure 6.11 illustrates the application of mixes 29 and 24 on the 2% sloped slab. Both mixes initially exhibited low flowability across all surface preparation techniques; however, once agitated, they demonstrated sufficient workability to achieve consolidation and fill corners without any signs of overflow or instability. All the UHPC layers were immediately covered with plastic sheeting after casting to ensure proper curing.

(a) During placement (b) Finished surface

Figure 6.11 NC slab with UHPC overlay.

Figure 6.12 and Table 6.3 display the as-built dimensions and reinforcement details, accounting for dimensional changes resulting from construction and the different surface preparation techniques. The actual dimensions were used in analytical calculations to predict the flexure capacity.

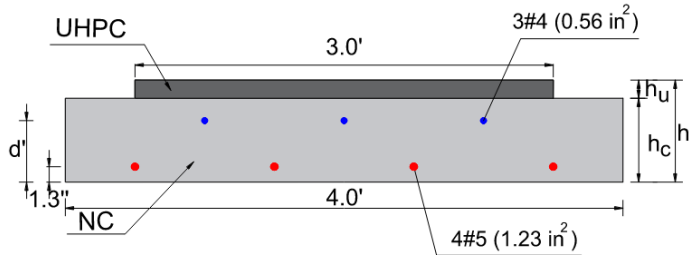

(a) Section view

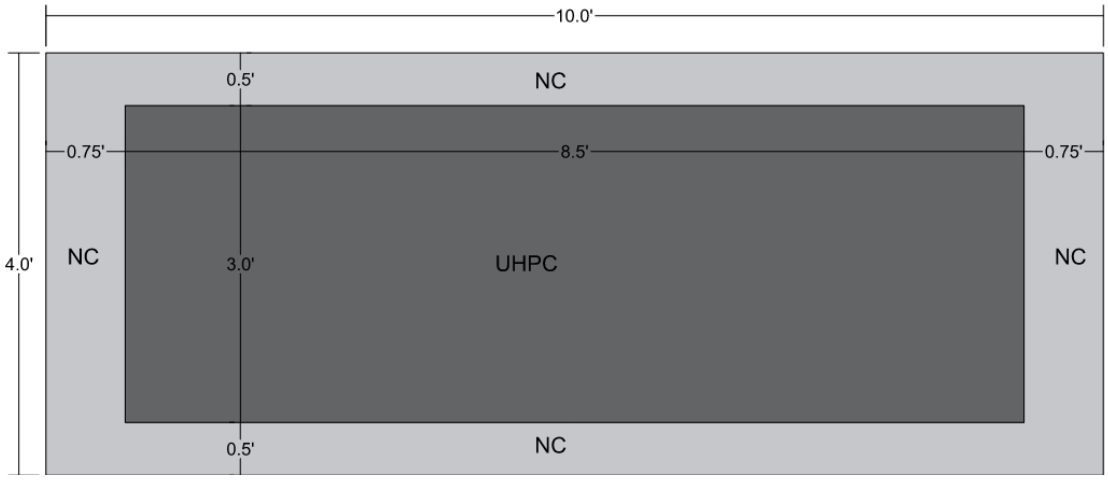

(b) Plan view

Figure 6.12 As-built dimensions and reinforcement details of composite slabs

Table 6.3 Specimens identification and as-built dimensions.

Loading Direction	Mix	Surface Preparation Technique	Dimension (in.)			
			h_c	h_u	h	d'
Positive (P)	29	SR	6.81	1.50	8.31	5.50
		FM	7.80	1.65	9.45	4.50
		TM	7.00	1.65	8.65	5.50
	24	SR	7.25	1.65	8.90	5.50
		FM	6.90	1.65	8.55	4.50
		TM	7.13	1.50	8.63	5.50
Negative (N)	29	SR	6.81	1.60	8.41	5.50
		FM	7.65	1.50	9.15	4.50
		TM	7.00	1.65	8.65	5.50
	24	SR	6.66	1.56	8.22	5.50
		FM	6.63	1.60	8.23	4.50
		TM	7.13	1.65	8.78	5.50
Ave.			**7.06**	**1.60**	**8.66**	**5.17**
Std. Dev.			**0.36**	**0.07**	**0.37**	**0.49**
COV			**5%**	**4%**	**4%**	**10%**

6.2.4 Material Properties

6.2.4.1 Fresh and Early-Age Properties

The static and dynamic flow tests were conducted on Mixes 29 and 24, from Groups B and E respectively, and the results are shown in Figure 6.13. The measured values fall within the ranges commonly reported in the literature, 4.0 to 6.0 in. for static flow and 6.0 to 8.0 in. for dynamic flow. Both mixes also passed the Patting Response (PR) test.

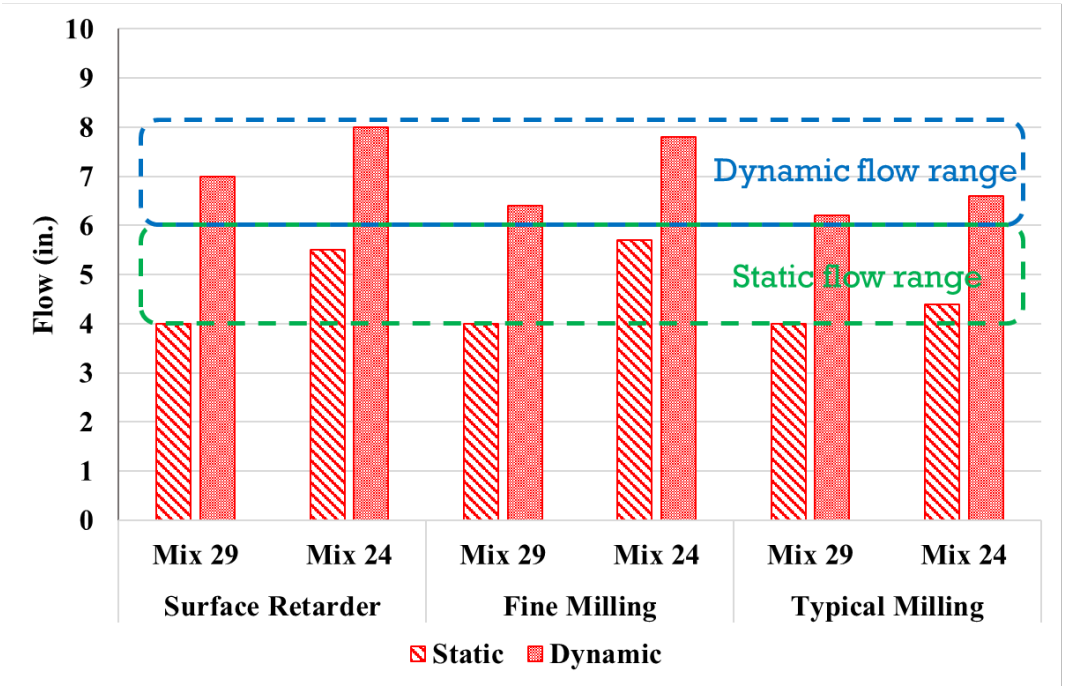

Figure 6.13 Static and dynamic flow test results.

6.2.4.2 Mechanical Properties

Compressive Strength

The compressive strength of the NC slabs and the UHPC overlay tested at 28 days are shown in Figure 6.14. Both mixes met the minimum recommended compressive strength of 14 ksi specified by IADOT, as presented in Table 2.8.

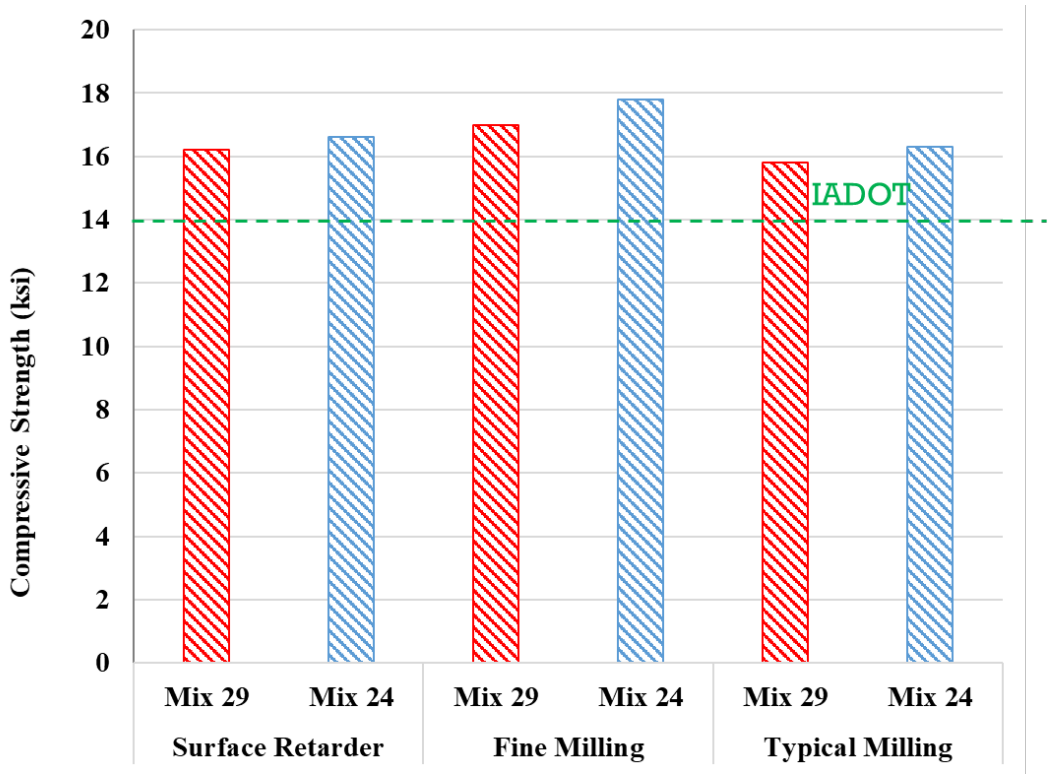

Figure 6.14 28-day compressive strength test results.

Modulus of Elasticity

The modulus of elasticity (MOE) was measured for Mix 29 and Mix 24, and compared to AASHTO-UHPC, as presented in Figure 6.15. Both mixes showed close results to the MOE calculated based on AASHTO-UHPC and met the minimum requirement of 6500 ksi specified by NJDOT.

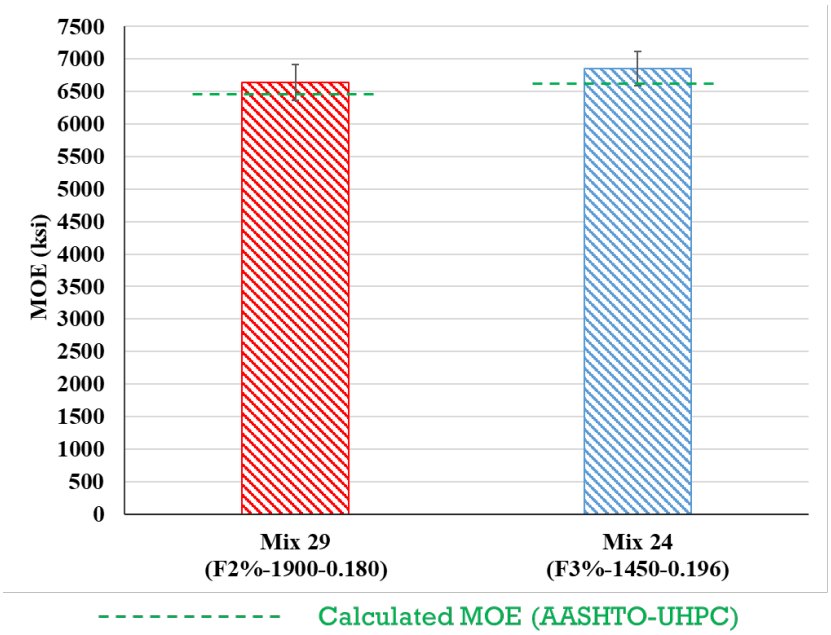

Figure 6.15 MOE test results compared with AASHTO-UHPC.

Flexural Strength

Similar to the previous trials in Chapter 4, both mixes showed comparable results, as shown in Figure 6.16. They met the PCI TR-9-22 minimum requirements for first cracking strength (1.5 ksi) and peak strength (2 ksi). Additionally, the average ratio of residual strength to first cracking strength for both mixes exceeded the recommended value of 0.75. Mix 24 exhibited a 60% increase in flexural capacity compared to Mix 29 attributed to the higher fiber content. Nevertheless, both mixes demonstrated adequate flexural strength with excellent post-cracking behavior and toughness.

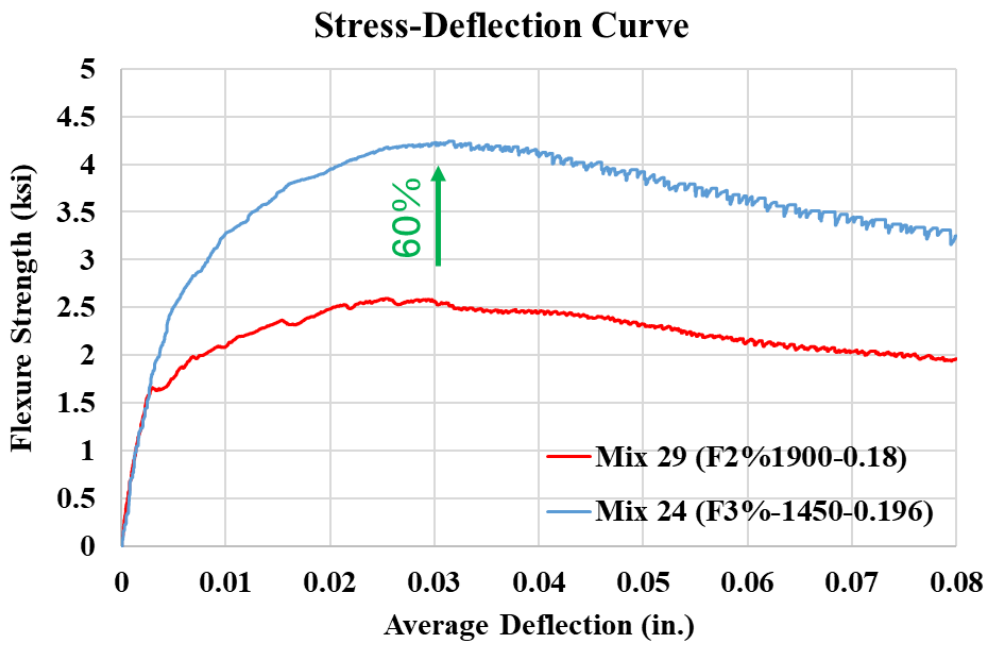

Figure 6.16 Flexure test results

Uniaxial Tensile Strength

Similar to the previous trials presented in Chapter 4, both mixes showed comparable results, as illustrated in Figure 6.17. They met the AASHTO-UHPC minimum cracking strength requirement of 0.75 ksi and achieved an average crack localization strain of 0.0025. Additionally, their results closely approached the NJDOT criteria of a 1 ksi minimum cracking strength and a peak-to-cracking strength ratio of 1.25 presented in Table 2.9. Mix 24 exhibited a 22% increase in crack localization strength compared to Mix 29, but a 30% reduction in crack localization strain, which allows the material to sustain additional loading prior to the onset of crack localization.

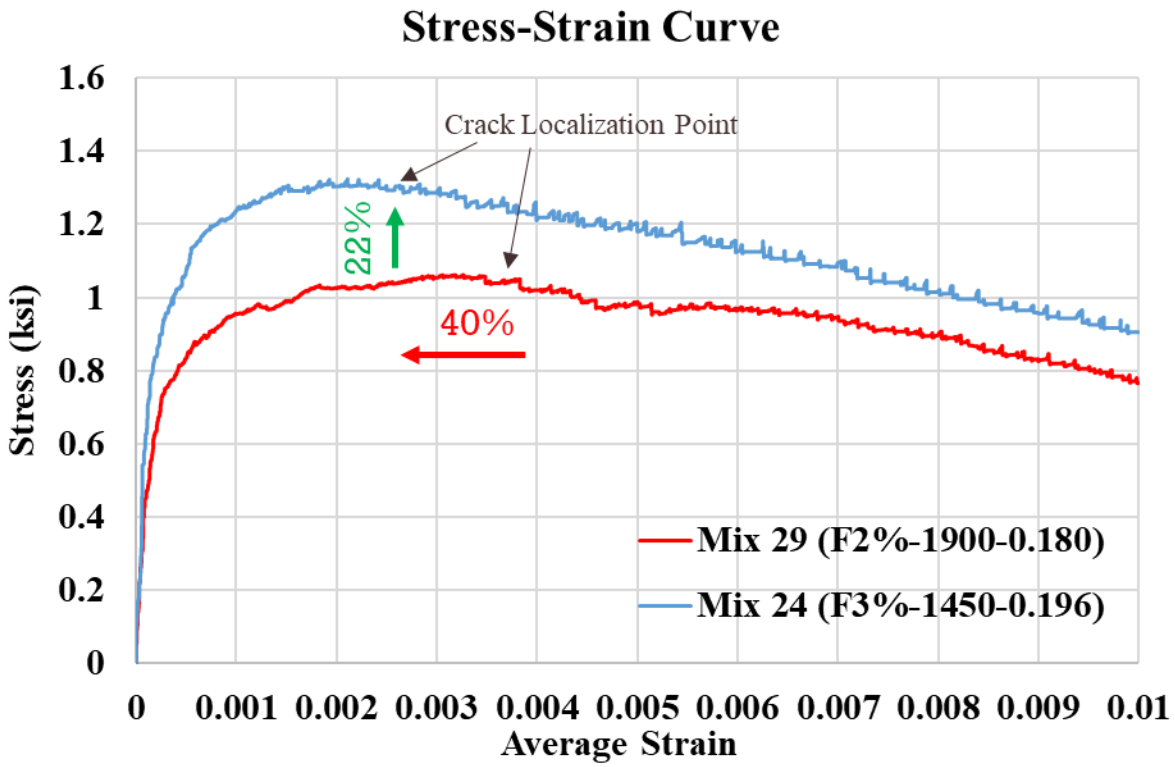

Figure 6.17 Uniaxial tensile test results

Bond Strength

The pull-off test, conducted according to ASTM C1583, was used to evaluate the bond strength between Mix 29 and Mix 24 and NC slabs prepared using surface retarder (SR), fine milling (FM), and typical milling (TM). Six core samples were extracted from each slab at various locations to represent the full surface area. The pull-off test results are summarized in Table 6.4. Failure generally occurs at the interface between the NC and the UHPC overlay, except for the samples marked with a single asterisk (*) or those with values shown in red, which indicate failure at the NC substrate or at the glue layer, respectively. Test results were excluded from the analysis when failure occurred at the glue layer. Figure 3.16 illustrates the typical failure modes observed in pull-off tests. To statistically analyze the pull-off results, a one-way

analysis of variance (ANOVA) was performed to assess the effect of surface preparation (SR, FM, TM) on bond strength for both mixes. "Significant" refers to statistical significance at $\alpha = 0.05$, indicating that the likelihood of the observed differences occurring by random chance is less than 5%. The analysis revealed a significant effect of surface preparation on bond strength for both Mix 29 ($p = 0.0015$) and Mix 24 ($p < 0.0001$). Thus, post-hoc pairwise comparisons using Tukey's Honestly Significant Difference (HSD) were conducted to evaluate differences between each pair of surface preparation techniques. The Tukey HSD results showed that SR resulted in significantly higher bond strength compared to FM and TM in both mixes, while no significant difference was observed between FM and TM in both mixes.

Table 6.4 Pull-off test results.

Sample No.		**Bond Strength (ksi)**					
		Mix 29 (F2%-1900-0.180)			**Mix 24 (F3%-1450-0.196)**		
		SR	**FM**	**TM**	**SR**	**FM**	**TM**
1		0.34*	0.18	0.11	[0.26]	0.22	0.16
2		0.21	0.15	0.15	[0.38]	0.19	0.20
3		0.27	[0.21]	0.20	0.4*	0.21	0.20
4		0.26	0.21	0.21	0.29	0.16	0.17
5		0.34*	0.15	0.10	0.34	0.20	0.12
6		0.20	0.21	0.13	0.37*	0.22	0.13
Average		**0.27**	**0.18**	**0.15**	**0.35**	**0.20**	**0.16**
Std. Dev.		**0.06**	**0.03**	**0.05**	**0.06**	**0.02**	**0.03**
COV (%)		**22%**	**17%**	**31%**	**13%**	**11%**	**21%**
ANOVA		**Significant (p = 0.0013)**			**Significant (p = 0.00013)**		
Tukey HSD	**SR vs FM**	**Significant**			**Significant**		
	SR vs TM	**Significant**			**Significant**		
	FM vs TM	**Not significant**			**Not significant**		

*Failure happened at substrate NC
[Values in red and bracketed are excluded as failure happened at the glue.]

Overall, the pull-off test results demonstrated that slabs prepared with surface retarder achieved higher bond strength than those prepared by milling. This is attributed to the enhanced interlock between the NC and UHPC layers and the potential introduction of microcracks by the

milling process, as described in ICRI guidelines. Additionally, slabs prepared by fine milling (FM) and typical milling (TM) showed no significant difference in bond strength, although lower values were observed in tests conducted along the worn-tooth lines of TM slabs, shown in Figure 6.9 (b), compared to the fine-milled areas. As shown in Figure 6.18, the pull-off test results for the milled slabs were consistent with FHWA-HRT-17-097 (12), which was previously discussed in the literature. To further investigate the adequacy of the bond achieved through different surface preparation techniques, full-scale slabs were tested under flexural loading to assess bond behavior at peak load. Detailed results and analysis are presented in the flexural testing section.

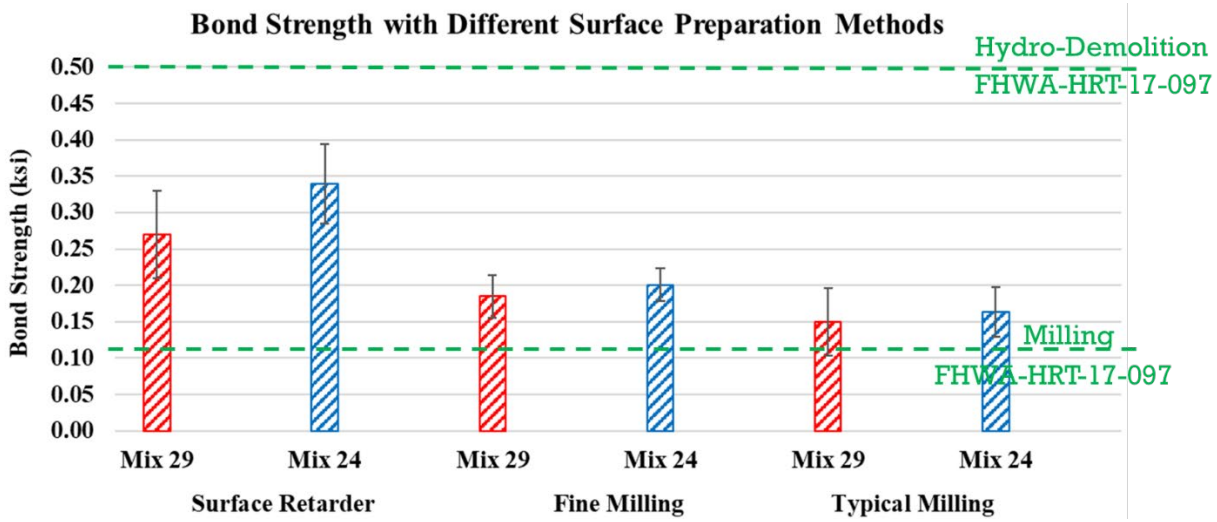

Figure 6.18 Pull-off test results compared with FHWA-HRT-17-097

To visually inspect the interface between the UHPC layer and the NC slab, Core samples with 4-in. diameters were extracted through the full thickness of the composite slabs. The visual inspection revealed good consolidation between the two developed UHPC mixes, and the NC slabs were prepared using SR, FM, and TM surface preparation techniques, as shown in Figure 6.19. A uniform distribution of steel fibers was observed in both UHPC mixes, with only minor,

isolated voids and no signs of segregation, indicating stable, well-consolidated material behavior under vibration and placement conditions.

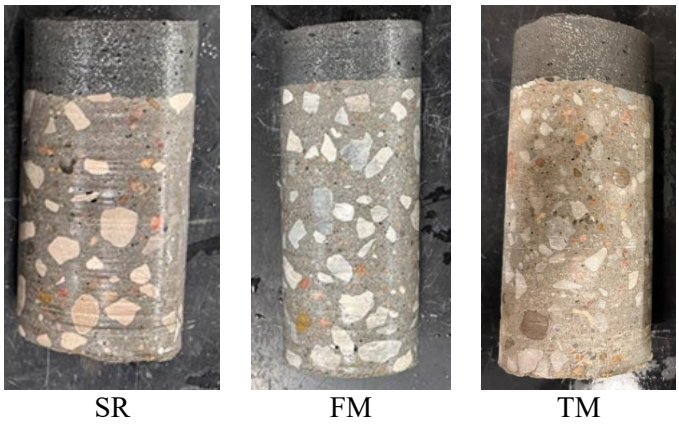

SR FM TM

(a) Mix 29 (F2%-1900-0.180)

SR FM TM

(b) Mix 24 (F3%-1450-0.196)

Figure 6.19 NC-UHPC interface with three surface preparation

6.2.4.3 Durability Properties

Freeze-Thaw Cycling

The freeze-thaw resistance results confirm that both Mix 29 and Mix 24 demonstrate outstanding durability. As shown in Figure 6.20, mass loss remained negligible (≈0%) after 300 cycles, well within the NDOT acceptance limit of -5%.

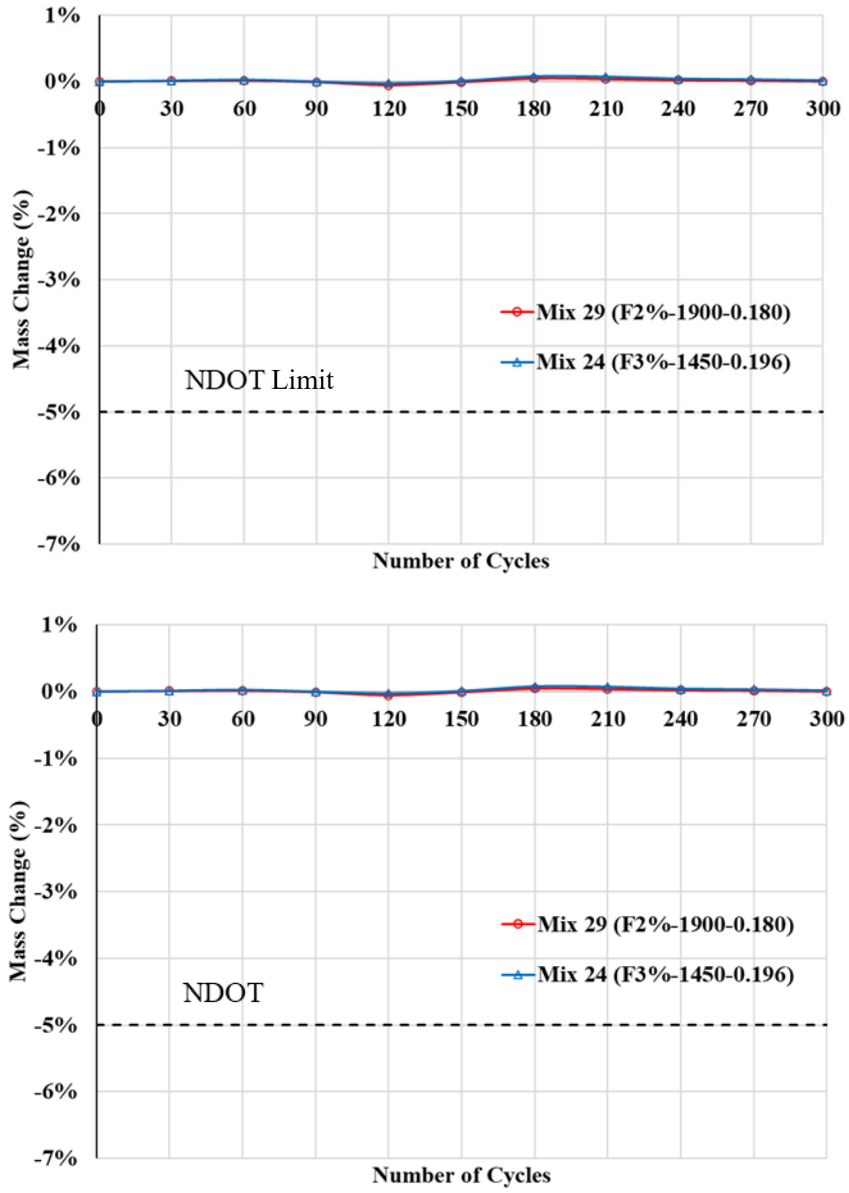

Figure 6.20 Mass change in F-T resistance test

The mass loss results were further validated by the visual inspection of the specimens before and after the 300 cycles of freezing-thawing, as shown in Figure 6.21, which confirmed that no scaling, spalling, or surface deterioration occurred during the F-T testing.

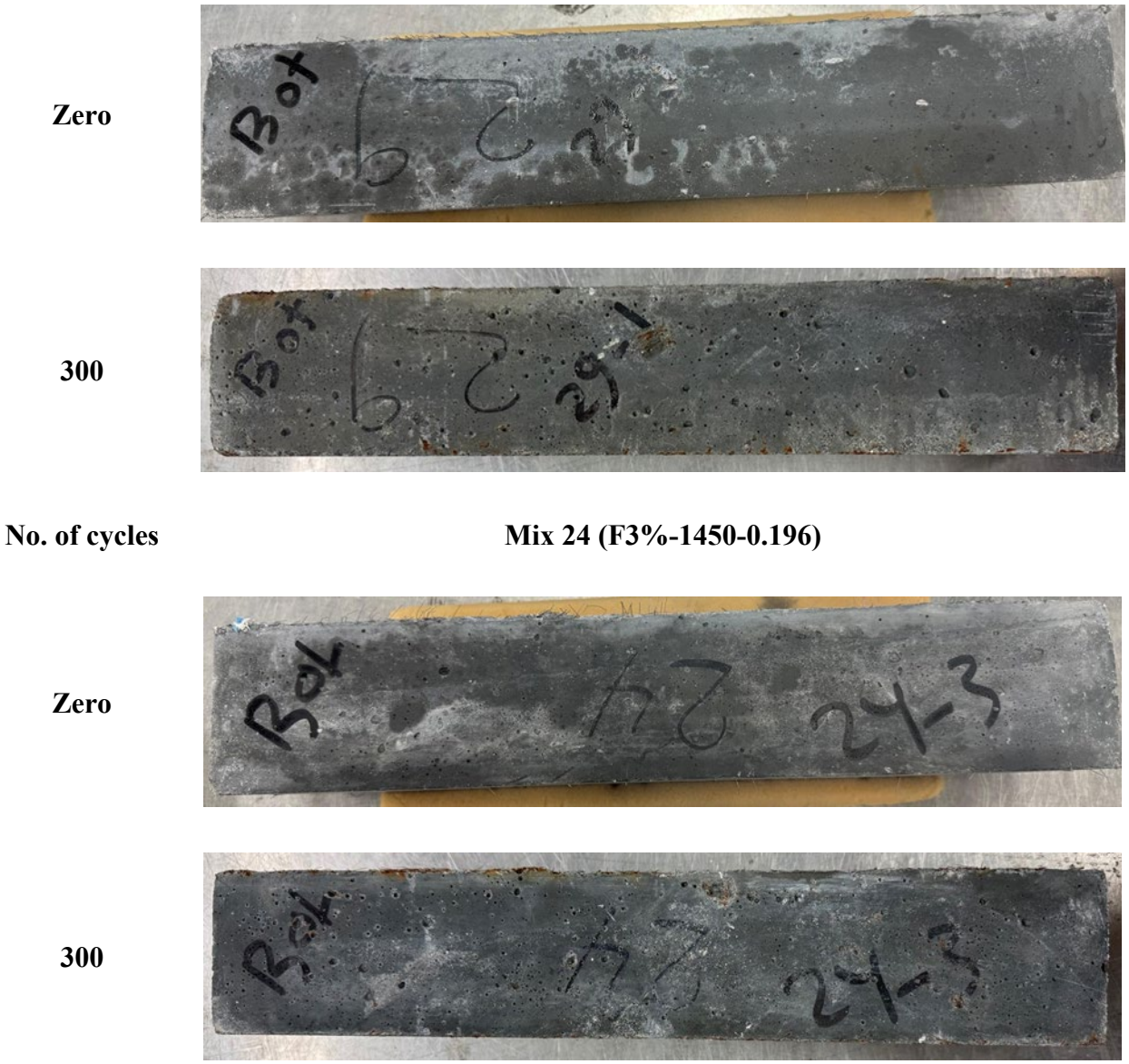

Figure 6.21 Representative specimens after 300 cycles of freezing-thawing test.

Similarly, Figure 6.22 shows that both mixes maintained the relative dynamic modulus of elasticity after 300 cycles, and in fact, slightly increased. This increase can be attributed to continued hydration and matrix densification during wet-dry cycling. Importantly, the relative dynamic modulus values remained far above the NDOT threshold of 70%, confirming

outstanding durability. Overall, the results confirm that both Mix 29 and Mix 24 possess exceptional freeze-thaw resistance, making them suitable candidates for bridge deck overlays in cold-climate regions. Moreover, both mixes met the acceptance criteria of IADOT, NYSDOT, NJDOT, and the commercial Ductal® overlay presented in Table 2.8.

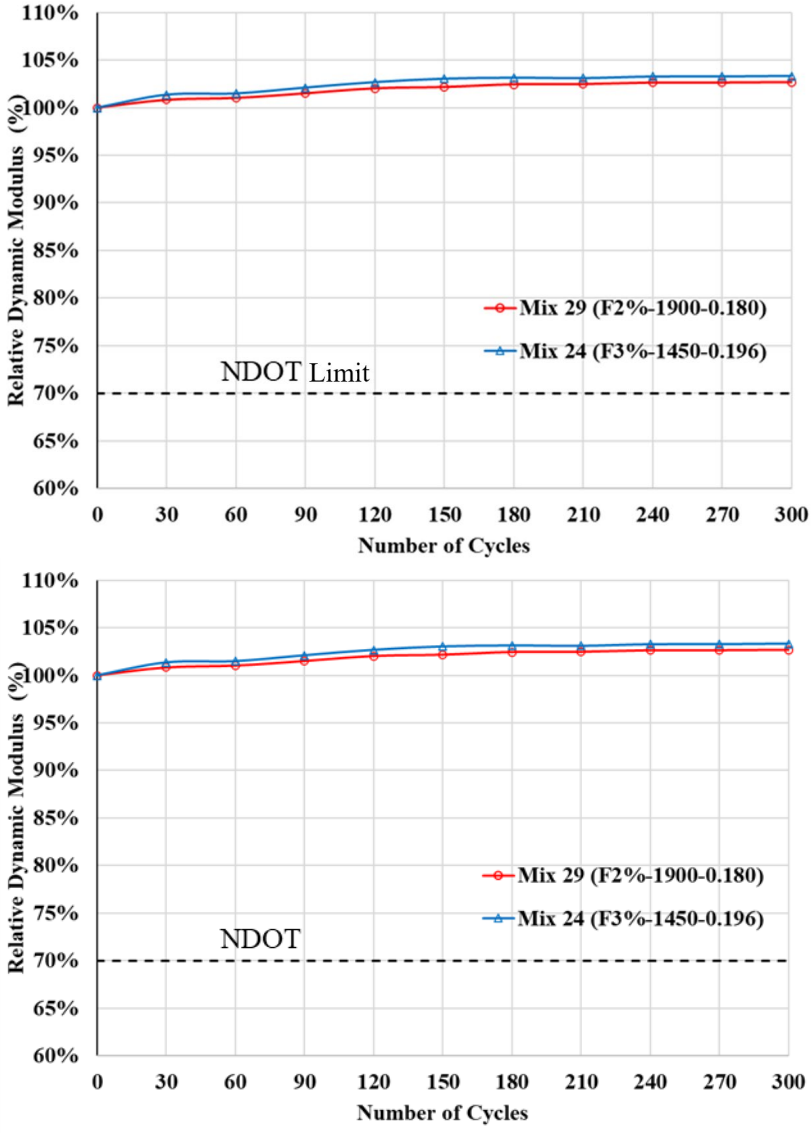

Figure 6.22 Relative dynamic modulus of elasticity results.

RCPT

Figure 6.23 presents the rapid chloride penetration test (RCPT) results alongside the chloride permeability classifications defined in AASHTO T277/ASTM C1202. The tested specimens did not have steel fibers due to their high conductivity as steel fibers may influence the charge passed if they form conductive pathways within the concrete matrix. The test results indicated negligible charge passed, which was classified as “negligible rapid chloride permeability”. Moreover, both mixes met the acceptance criteria of IADOT, NYSDOT, and NJDOT for UHPC overlay. This demonstrates the excellent durability and dense microstructure of both UHPC mixtures, confirming their strong resistance to chloride ion ingress and suitability for bridge deck overlay applications.

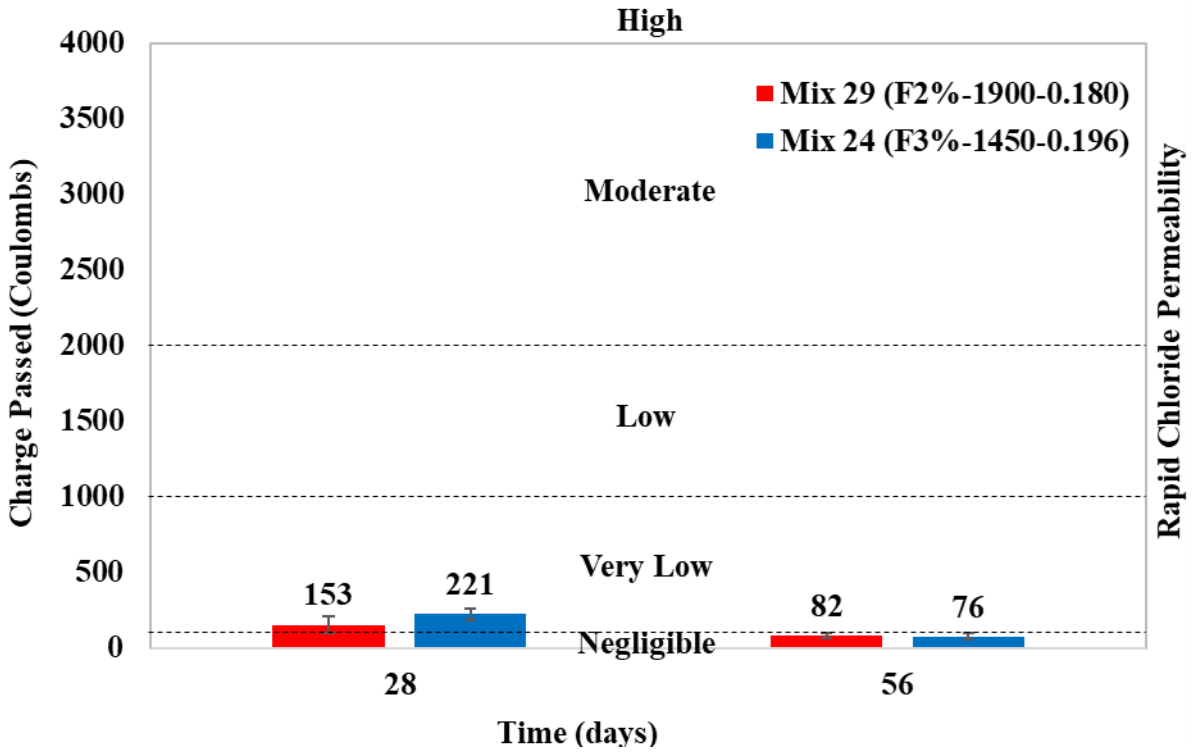

Figure 6.23 RCPT results compared with ASTM C1202 outlines.

Surface Resistivity

The surface resistivity test further supports the findings from the RCPT test. The surface resistivity test was conducted according to AASHTO TP95 (2014) on Mixes 24 and 29 using specimens prepared without steel fibers due to their high conductivity, steel fibers may influence surface resistivity measurements if they form conductive pathways within the concrete matrix. As shown in Figure 6.24, the results indicate that both mixes exhibited high surface resistivity. At 28 and 56 days, the chloride ion penetration for both mixes were classified as "very low."

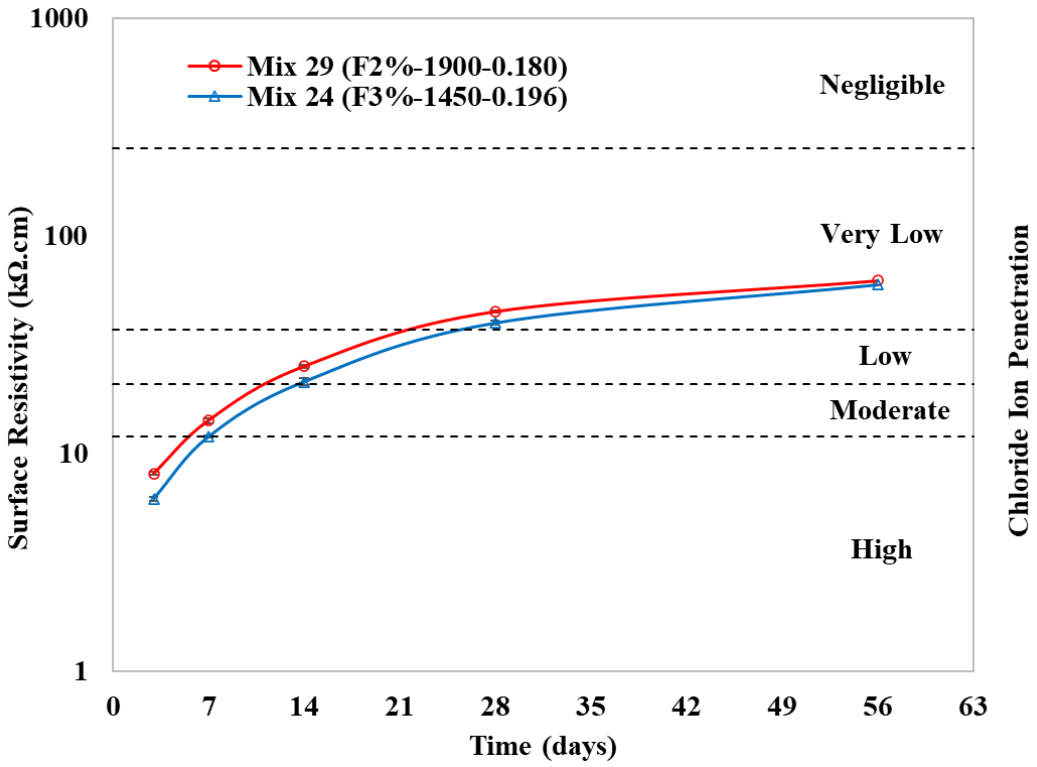

Figure 6.24 Surface resistivity test results.

Drying Shrinkage

Figure 6.25 presents the drying shrinkage results of UHPC mixes over a 180-day period. Mix 29 shows significantly higher shrinkage than Mix 24 which is attributed to the higher binder

content but it still met the acceptance criteria of IADOT, NYSDOT, NJDOT, and the commercial Ductal® overlay presented in Table 2.8. The relatively low shrinkage observed for both mixes reduces the risk of delamination between the NC slabs and the UHPC layer due to early-age cracking, a finding that was further confirmed in the full-scale slab tests.

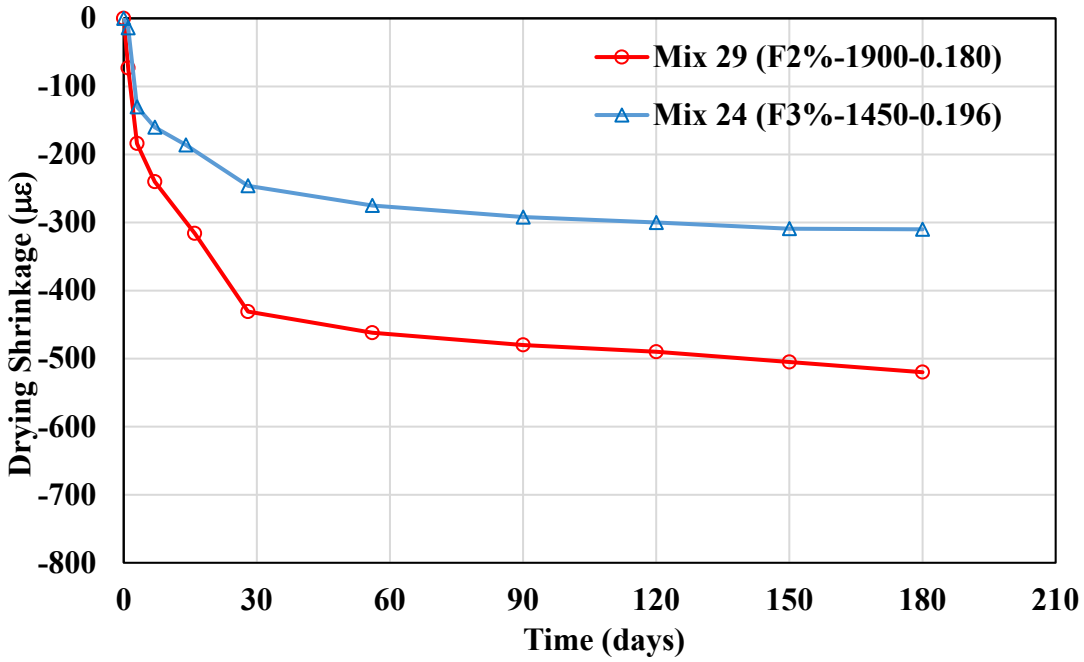

Figure 6.25 Drying shrinkage test results.

6.3 Mockup Flexural Testing

All slabs were tested 28 days after casting. Each slab was tested twice: first under a positive bending moment, with the UHPC layer in the compression zone, as shown in Figure 6.26 (a). After the test underpositive bending moment, the test slab was flipped upside down, and the second test was conducted under negative bending moment, where the UHPC layer was in the tension zone, as shown in Figure 6.26 (b). A load cell was used to measure the applied load on the specimens, while a string potentiometer was positioned at mid span to measure vertical

deflection. The linear variable differential transformers (LVDTs) were used to detect any slippage between the UHPC layer and the NC slab. Additionally, strain gauges were installed at the tested sections to monitor strain behavior.

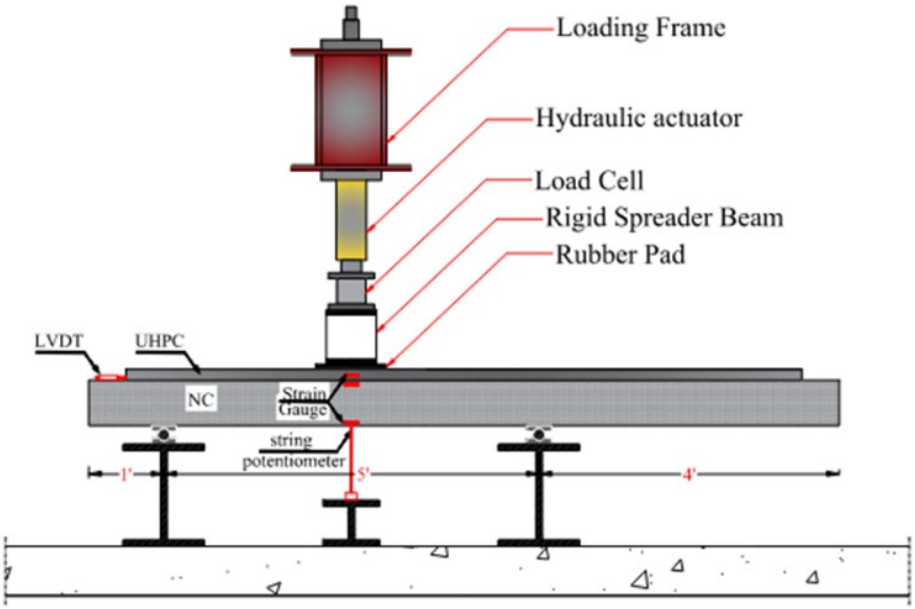

(a) Under positive moment (UHPC layer in compression zone)

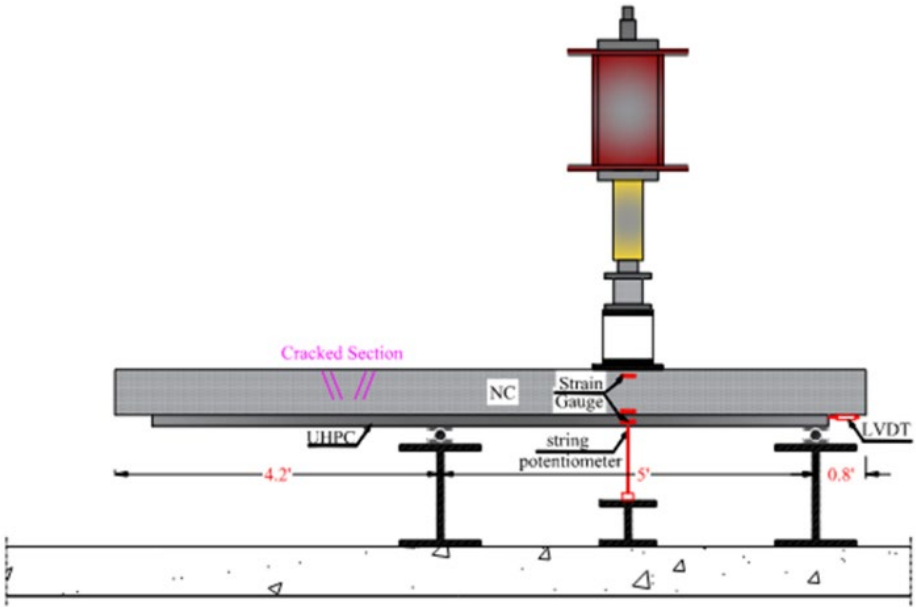

(b) Under negative moment (UHPC layer in tension zone)

Figure 6.26 Test Setup and instrumentation.

The measured flexural capacity of the composite slabs was compared with their calculated nominal flexural capacity, as well as with the nominal capacity of the original NC slabs prior to replacing the NC clear cover with the UHPC overlay, to show how the flexural capacity changes with different mixtures and surface preparation techniques. This difference was caused by changes in the slab's as-built dimensions due to construction and surface preparation methods. The experimentally determined mechanical properties of both NC and UHPC materials were used to predict the flexural capacity.

6.3.1 Under Positive Moment

The six slabs were tested under positive bending moment, as shown in Figure 6.27.

SR 29

SR 24

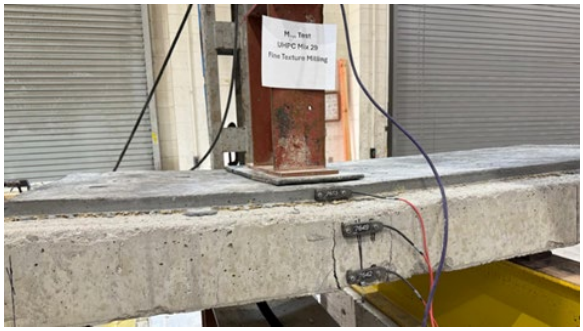

FM 29

FM 24

TM 29

TM 24

Figure 6.27 Test Setup of the six slabs under positive moment.

The flexural capacity versus mid-span deflection curves for the slabs are shown in Figure 6.28. All the slabs exhibited similar behavior regardless of UHPC mix or surface preparation technique. Dashed lines represent the calculated nominal flexural capacity for the composite slab

and the calculated nominal flexural capacity for the NC slab prior to replacing the NC clear cover with the UHPC.

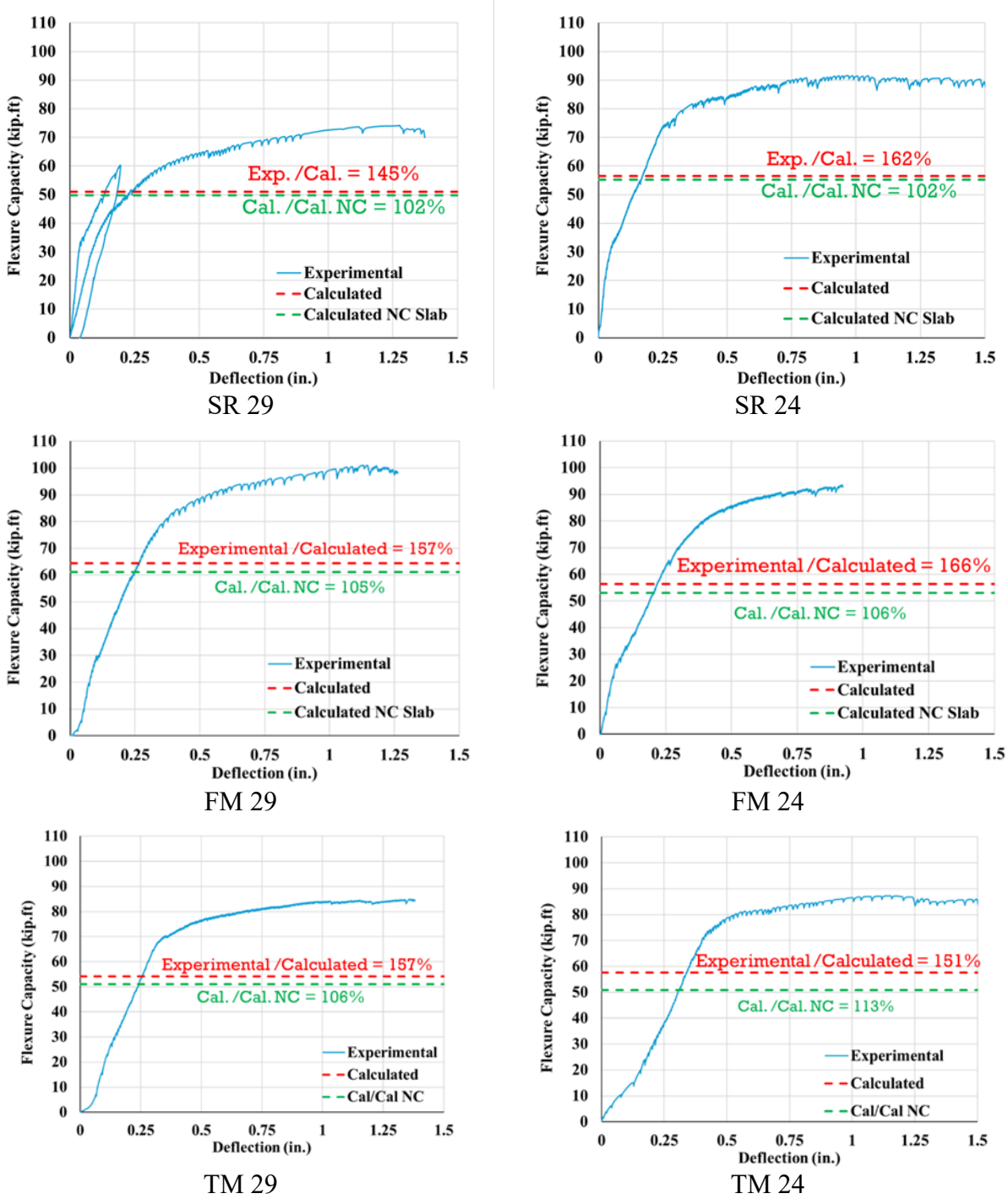

Figure 6.28 Flexural capacity versus mid-span deflection of the six slabs under positive moment

No LVDT readings indicated any slippage between the NC slabs and the UHPC layers, as shown in Figure 6.29.

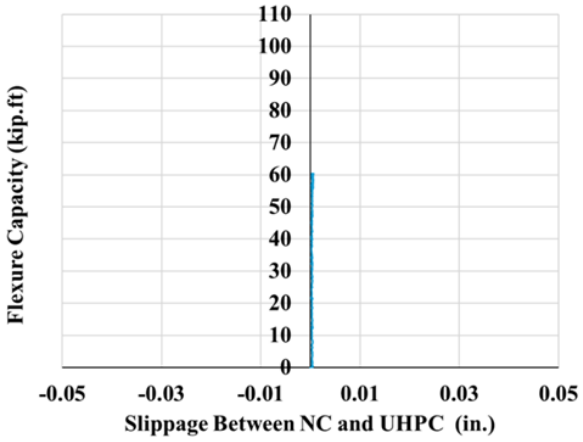

SR 29

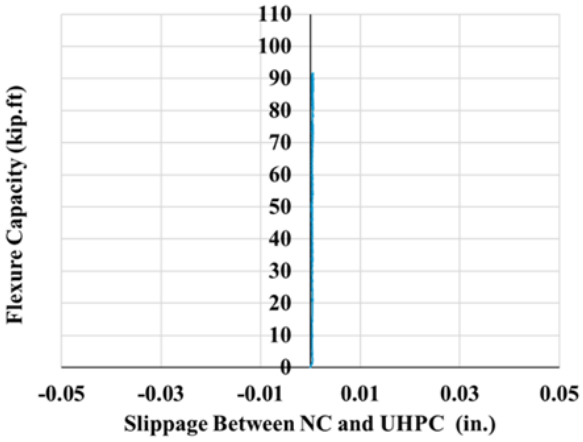

SR 24

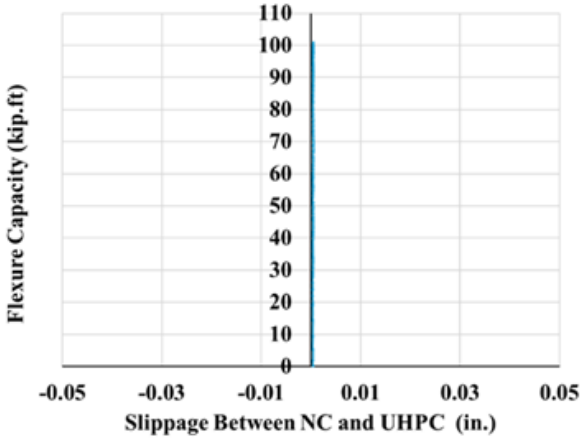

FM 29

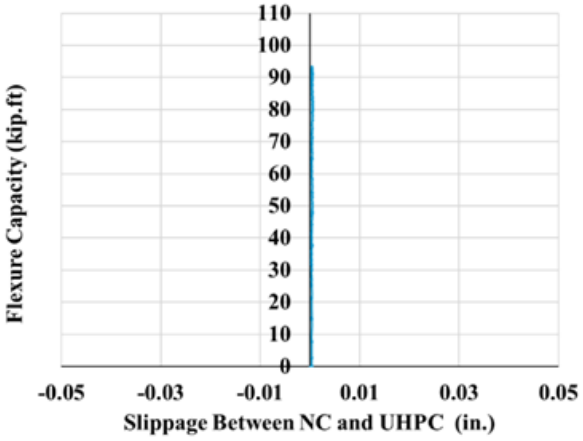

FM 24

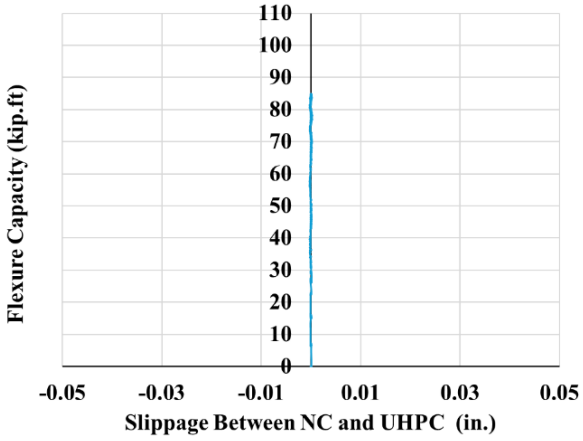

TM 29

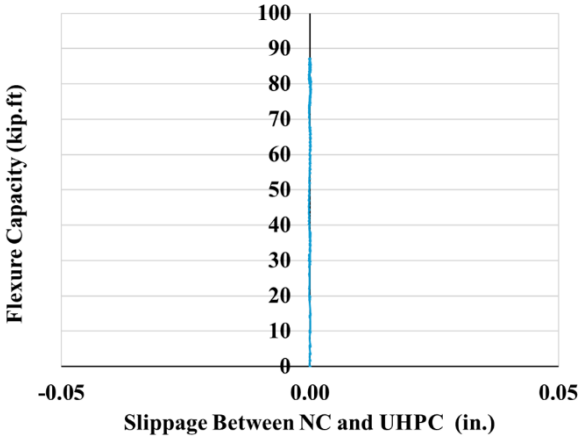

TM 24

Figure 6.29 LVDT readings of the six slabs under positive moment

No cracks were observed at the interface between the NC slab and the UHPC layer, as shown in Figure 6.30, whereas many cracks were observed on the tension side. All the slabs exhibited yielding of the tensile reinforcement and displayed signs of crushing in the UHPC overlay under the point load.

Top view (Crushing of UHPC)

Side view (Cracks in tension side)

(a) SR 29 (b) SR 24

Figure 6.30 Failure mode under positive moment.

The flexural capacity versus mid-span deflection curves for all slabs under both positive loadings are combined and presented in Figure 6.31. The experimental flexural capacities, along with the calculated capacities for the composite section and the original NC slab (prior to replacing the concrete cover with the UHPC overlay), are summarized in Table 6.5.

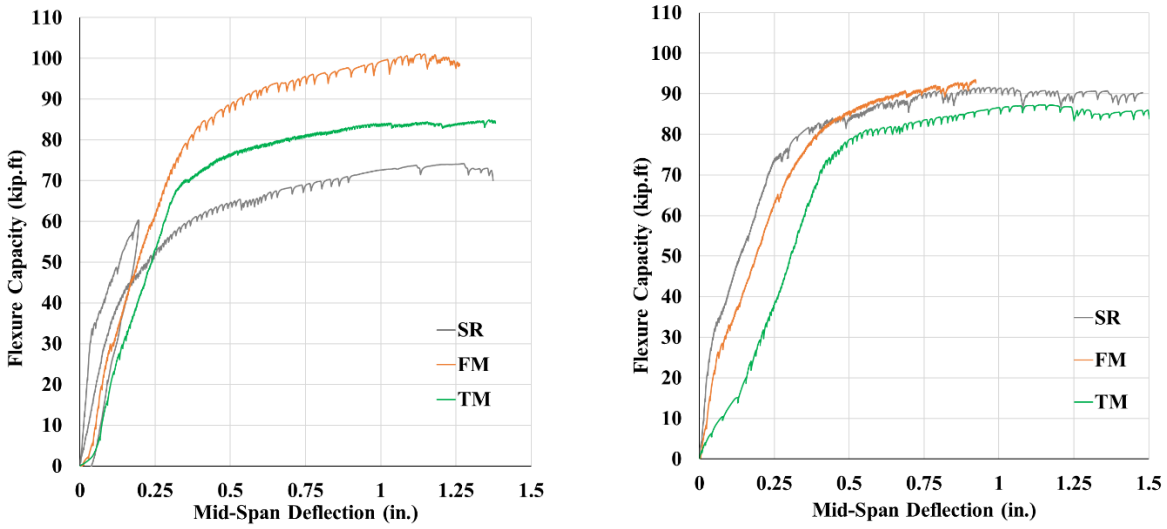

(A) Mix 29 (b) Mix 24

Figure 6.31 Flexural capacity versus mid-span deflection for positive moment testing of composite slabs.

Table 6.5 Experimental and calculated flexural capacity under positive moment.

Mix	Surface Preparation Technique	Flexure Capacity (kip.ft)			Exp./Cal. Composite	Cal. Composite/Cal. NC
		Exp. Composite	Cal. Composite	Cal. NC		
29	SR	74.2	51.0	49.8	145.4%	102.5%
	FM	101.0	64.4	61.2	156.8%	105.2%
	TM	84.9	54.1	51.0	156.9%	106.1%
24	SR	91.6	56.5	55.3	162.1%	102.2%
	FM	93.2	56.3	53.0	165.5%	106.2%
	TM	87.2	57.6	50.8	151.4%	113.4%

Average	-	-	-	156.4%	105.9%
Std. Dev.	-	-	-	7.2%	4.1%
COV	-	-	-	4.6%	3.8%

The composite slabs showed an average experimental-to-calculated flexural capacity ratio of 156.4%, indicating a sufficient bond between the NC and UHPC layers, even at peak load, which surpassed the ultimate interface shear stress. This high ratio could result from the actual yield strength of the tension reinforcement being higher than the specified values used in the predictions. The low coefficient of variation (4.6%) of the ratio of experimental to calculated flexural capacity suggests that the UHPC mix and surface preparation method have little effect on the flexural performance of the composite slab. The significant differences in flexural capacity among individual slabs are primarily due to differences in the thickness of NC and UHPC, as well as the depth of reinforcement in the as-built slabs, as shown in Table 6.3.
The ratio of the calculated composite to the NC slab's flexural capacity averaged 105.9%, showing that the added UHPC layer offered only a modest increase in theoretical capacity under compression. The prediction models also verified that the interface shear stress caused by loading was less than the measured bond strength. This supports the presence of a strong bond between the NC and UHPC layers, even at peak load.

6.3.2 Under Negative Moment

The same six slabs that were tested under positive bending moment were rotated and flipped to be tested under negative bending moment at the location undamaged by the first test, as shown in Figure 6.32.

SR 29

SR 24

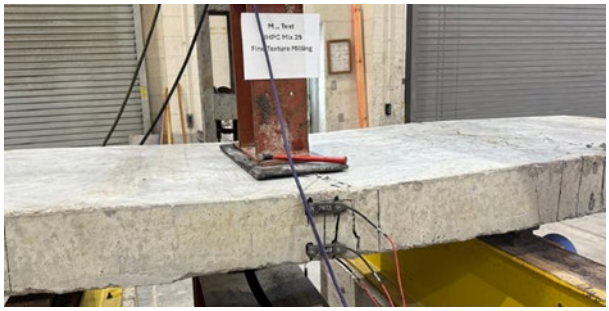

FM 29

FM 24

TM 29

TM 24

Figure 6.32 Test setup of the six slabs under negative moment.

The flexural capacity versus mid-span deflection curves for the six slabs are shown in Figure 6.33. Dashed lines show the calculated nominal flexural capacity for the composite slab and the calculated nominal flexural capacity for the NC slab prior to replacing the NC clear cover with the UHPC. All six slabs exhibited similar behavior regardless of the UHPC mix and surface preparation techniques.

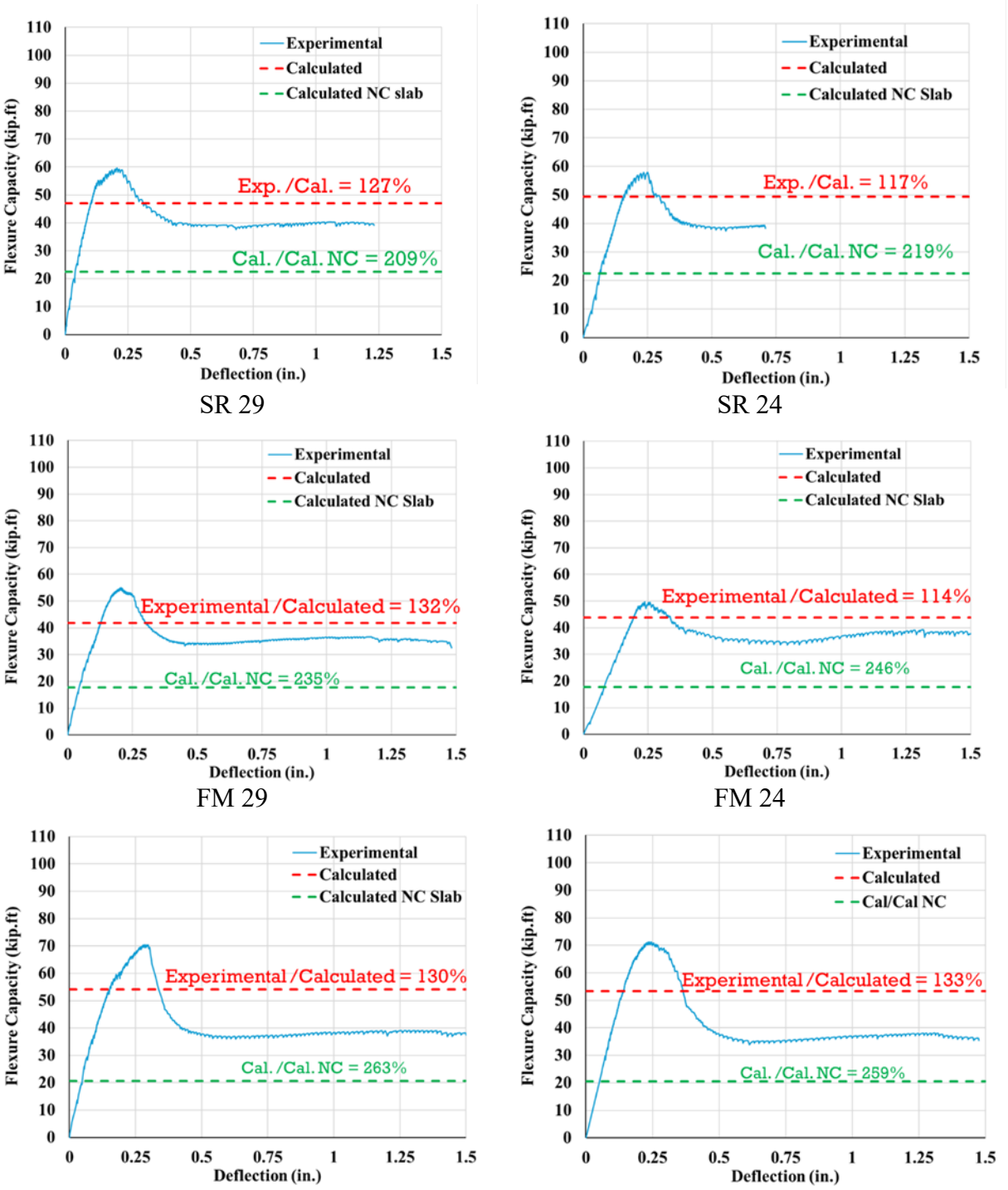

Figure 6.33 Flexural capacity versus mid-span deflection under negative moment.

No LVDT readings indicated any slippage between the NC slabs and the UHPC layers, as shown in Figure 6.34.

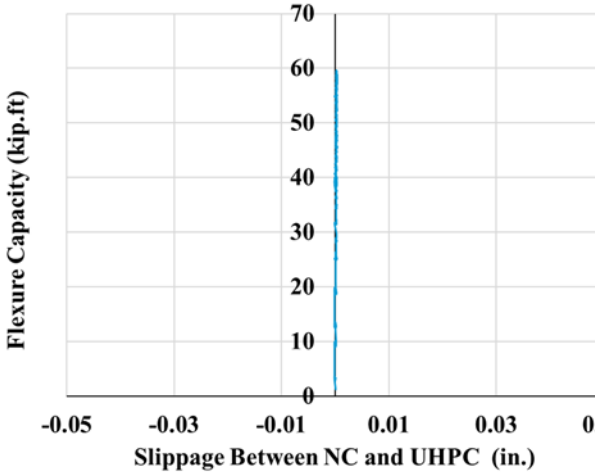

SR 29 N

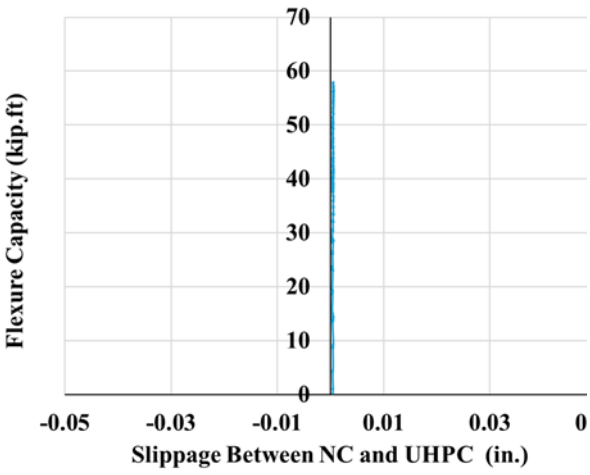

SR 24 N

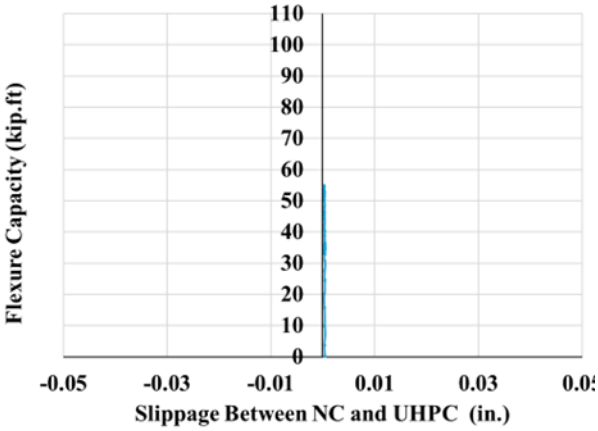

FM 29

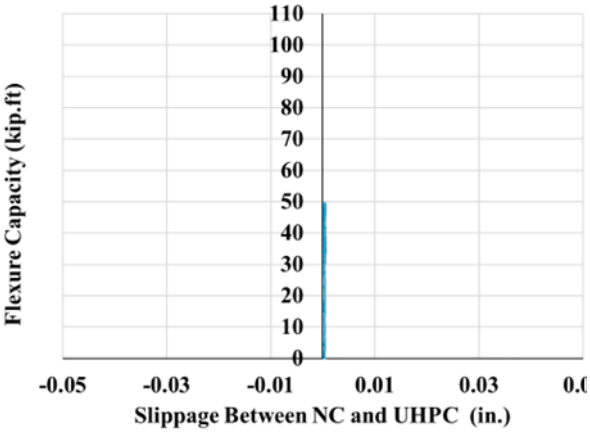

FM 24

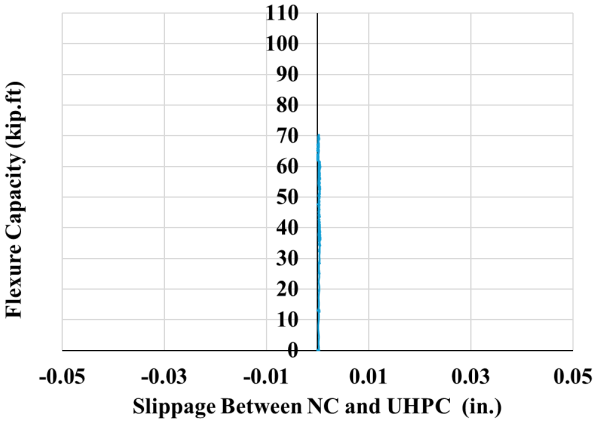

TM 29

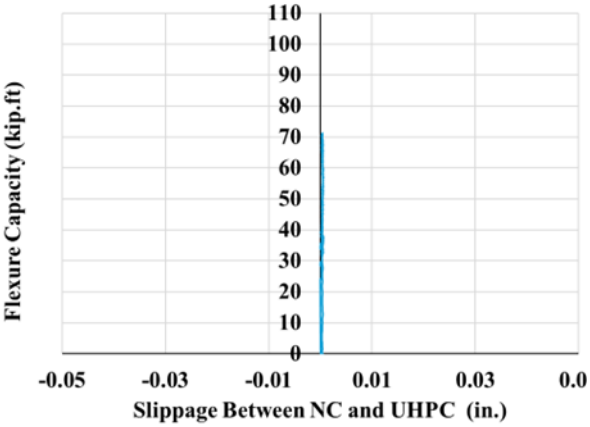

TM 24

Figure 6.34 LVDT readings of the six slabs prepared under negative moment.

No cracks were observed at the interface between the NC slab and the UHPC layer. The slabs exhibited high flexural capacity until crack localization occurred in the UHPC layer. After the UHPC layer ruptured, the flexural capacity declined, and the slab behaved like a standard NC slab. Ultimately, the NC slab failed due to yielding of the tension reinforcement followed by crushing of the NC in compression as shown in Figure 6.35.

Bottom view (rupture of the UHPC layer)

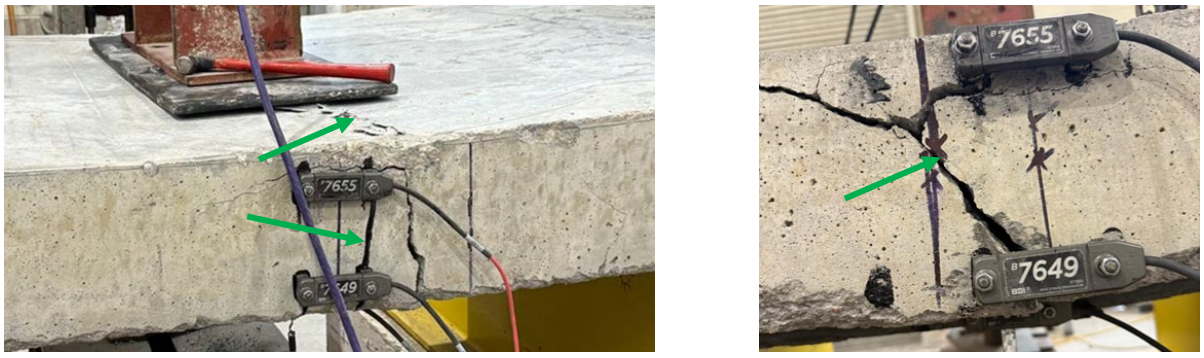

Side view (cracks in tension side and crushing of NC after the rupture of the UHPC layer)

(a) SR 29 (b) SR 24

Figure 6.35 Failure mode under negative moment.

The flexural capacity versus mid-span deflection curves for all six slabs under negative moment loading are combined in Figure 6.36. The experimental flexural capacities, along with the calculated capacities for the composite section and the original NC slab (prior to replacing the concrete cover with the UHPC overlay), are also summarized Table 6.6.

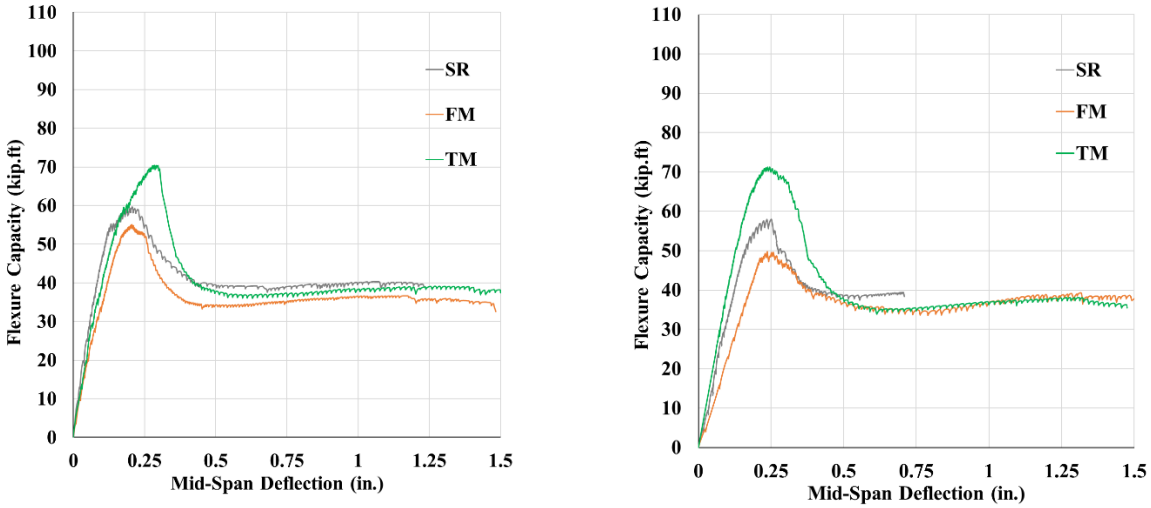

(A) Mix 29 (b) Mix 24

Figure 6.36 Flexural capacity versus mid-span deflection for negative moment testing of composite slabs.

Table 6.6 Experimental and calculated flexural capacity under negative moment.

Mix	Surface Preparation Technique	Flexure Capacity (kip.ft)			Exp./Cal. Composite	Cal. Composite/Cal. NC
		Exp. Composite	Cal. Composite	Cal. NC		
29	SR	59.7	47.0	22.5	127.0%	208.9%
	FM	55.1	41.8	17.8	131.8%	234.8%
	TM	70.5	54.1	20.6	130.2%	262.6%
24	SR	58.0	49.4	22.5	117.4%	219.4%
	FM	49.8	43.8	17.8	113.8%	245.9%
	TM	71.2	53.4	20.6	133.4%	259.3%
Average		-	-	-	125.6%	238.5%
Std. Dev.		-	-	-	8.1%	21.6%
COV		-	-	-	6.5%	9.0%

The composite slabs exhibited an average experimental-to-calculated flexural capacity ratio of 125.6%, which indicates adequate bond between the NC and UHPC layers, even at peak load, exceeding the ultimate interface shear stress. The low coefficient of variation (6.5%) of the ratio of experimental-to-calculated flexural capacity indicates that the UHPC mix and the surface

preparation technique do not have a significant effect on the flexural performance of the composite slab. The significant differences in the flexural capacity among individual slabs are primarily due to differences in thickness of NC and UHPC, and depth of reinforcement in the as-built slabs as shown in Table 6.3. A significant increase in the flexural capacity happened after replacing the NC cover with the UHPC overlay since the average calculated composite-to-NC slab capacity ratio reached 238.5%, confirming the UHPC layer nearly doubled the flexural capacity when placed in the tension zone.

6.4 Summary

This chapter aimed to evaluate the constructability, fresh properties, mechanical performance, and durability of the developed UHPC overlays (Mix 24 and Mix 29). It also documented the construction and testing of six normal concrete (NC) slabs overlaid with these mixes. Three surface preparation techniques: surface retarder, fine milling, and typical milling were used to assess their effect on the bond between the UHPC overlay and the NC substrate.

The fresh, mechanical, and durability properties of both UHPC mixes met or exceeded values reported in the literature, confirming their suitability for overlay applications. Surface preparation using a surface retarder on fresh normal concrete achieved a higher bond strength with UHPC overlay than that of using fine and typical milling techniques. This enhanced bond strength is attributed to the superior exposed aggregate interlock achieved with a surface retarder, which outperforms the surface roughening produced by milling. Core inspections demonstrated good consolidation between the UHPC overlays and NC slabs. Durability evaluations: including freeze-thaw resistance, electrical resistivity, RCPT, and shrinkage validated the long-term performance of the UHPC overlays.

Flexural testing demonstrated that all three surface preparation techniques using field equipment applied in this study provided sufficient bond between the NC slabs and the non-

proprietary UHPC mixes, even beyond peak load. Additionally, the results indicated a slight improvement in the composite slab's capacity under positive moment and a significant increase under negative moment (almost doubling the strength). The measured flexural capacity of the composite slabs exceeded the predicted nominal capacities in both positive and negative moments, with average ratios of experimental-to-calculated capacities at 156.4% and 125.6%, respectively. Low coefficients of variation suggested that the behavior of the composite slabs was consistent regardless of the surface preparation technique or UHPC mix used. Lastly, the experimental results closely matched the analytical models, confirming the predictive accuracy of the proposed method.

Chapter 7 Summary, Conclusions and Recommendations

7.1 Summary

This study investigated the feasibility of developing an economical, non-proprietary UHPC overlay mixture using locally available materials for bridge deck overlay applications in Nebraska. A series of non-proprietary thixotropic UHPC overlay mixtures with varying binder content, w/b, fiber content, and admixture dosages were prepared and evaluated. These mixtures were assessed using static and dynamic flow tests, as well as the newly developed Patting Response (PR) and Vibration-Slope Stability (VSS) tests.

The mechanical properties were assessed for the mixtures that satisfied the workability requirements to identify those suitable for further evaluation using mockup specimens. Full-scale slabs were then built using surface retarder, fine milling, and typical milling surface preparation techniques to simulate field conditions. These mockups were utilized to evaluate constructability and structural performance. The mechanical properties of the selected two mixes were re-evaluated for quality assurance (QA) and durability properties were tested to ensure acceptable long-term performance. Full-scale slabs were subsequently subjected to both positive and negative moment loadings to determine their flexural capacity and assess the bond performance between the UHPC overlay and the prepared surfaces using different surface preparation methods. Flexure test results were compared to the predicted capacities according to AASHTO UHPC Design Specifications. A parametric study was conducted to analyze the effects of varying UHPC thickness, compressive strength, crack localization strength, and crack localization strain on the flexural capacity of the composite section.

7.2 Conclusions

Based on the results of the laboratory material testing and constructability evaluation, the following conclusions can be made:

1. The static and dynamic flow, PR, and VSS tests can effectively assess different aspects of thixotropic UHPC overlay and provide comprehensive information on workability features, such as having proper spread, good vibration response, and slope stability during vibration for overlay construction.
2. In addition to static and dynamic flow tests for the UHPC overlay mixture, the PR test can be easily performed on-site as a quality control measure, especially to assess the mixture's ability to achieve surface smoothness after vibration.
3. When comparing results from different test methods, static and dynamic flow results align well with the VSS results. However, because the VSS test is complex, it may be more suitable to use it during the mixture development stage in the lab.
4. High-thixotropic UHPC overlay mixtures can be achieved with a high dosage of workability-retaining admixtures (WRT), using both 1900 and 1450 pcy binder contents and w/b ratios of 0.180 and 0.196, respectively. Of the seven groups evaluated, Group A is a conventional (self-consolidating) UHPC that was deemed not suitable for overlay; Groups D and G did not yield flow due to limited water content, while Groups B, C, E, and F demonstrated excellent workability for overlay construction.
5. Mixtures with fiber contents of 2% and 3% showed satisfactory workability results. However, more research is needed on the mechanical and durability properties to identify the optimal fiber content for UHPC overlay mixtures.
6. Unlike conventional UHPC, which typically contains a high dosage of high-range water reducer (HRWR), overlay UHPC requires a different approach because of its thixotropy needs and longer construction time. Specifically, overlay UHPC needs a large amount of workability-retaining admixture (WRT) and a smaller amount of HRWR. Research

shows that an optimal balance of HRWR improves WRT effectiveness, leading to stable flowability. The recommended range for WRT in the developed overlay UHPC mixes is 47-54 pcy, with HRWR much lower at 3-5 pcy.

7. Since the mixture's consistency can vary depending on batch size, mixing energy, temperature, and mixing time, adjustments to the amounts of HRWR and WRT may be necessary to achieve the recommended consistency in the field.
8. Constructability evaluation confirmed the effectiveness of the developed test methods. When assessing the constructability of promising mixtures from four different groups, it is recommended that the static flow be less than six inches and the dynamic flow between seven and eight inches at 25 drops to ensure successful UHPC overlay construction.

Based on the results of the mechanical and durability testing of the UHPC mixtures, and the structural testing of the mockup slabs, the following conclusions can be made:

1. Mixes 29 and 24 met all fresh, mechanical, and durability criteria set by most state DOTs standards. These mixes demonstrated excellent freeze-thaw durability with minimal mass loss, had negligible chloride permeability after 56 days, and maintained shrinkage below approximately 500 micro-strains after 180 days.
2. Surface preparation using a surface retarder on fresh normal concrete resulted in a higher bond strength with the UHPC overlay compared to using fine and typical milling techniques. This increased bond strength is due to exposed aggregate interlock achieved with the surface retarder, which outperforms the surface roughening produced by milling.
3. Flexural testing showed that all three surface preparation methods using field equipment used in this study produced sufficient bond between the NC slabs and the non-proprietary UHPC mixes, even beyond peak load.

4. The measured flexural capacity of composite slabs surpassed the predicted nominal capacities in both positive and negative moments, with average ratios of experimental to calculated capacities at 156.4% and 125.6%, respectively. Low coefficients of variation showed that the composite slabs behaved similarly regardless of the surface preparation technique or UHPC mix used.
5. Replacing 1.5 inches of the NC cover with a UHPC overlay significantly enhanced flexural capacity under negative moments, essentially doubling the capacity. However, there was no significant improvement under positive moments.
6. The AASHTO-UHPC Design Specifications Section 1.7.4.3 cohesion values do not apply to UHPC overlay applications. More accurate values should be obtained from pull-off tests per ASTM C1583/C1583M-20, as confirmed by experimental validation.
7. The parametric study showed that increasing the UHPC thickness, crack localization strength, and crack localization strain improve the flexural capacity under negative moment only, that is, when the UHPC layer is in the tension zone. In contrast, increasing the UHPC compressive strength does not significantly affect the flexural capacity under either positive or negative moments.

7.3 Recommendations for Implementation

UHPC overlay presents a promising long-term solution for the problem of deteriorating bridge decks in Nebraska. Laboratory testing and mockup work conducted in this study have demonstrated the viability of Nebraska's non-proprietary UHPC mixtures and confirmed their excellent mechanical and durability performance. However, successful transition from research to field application requires a structured implementation plan that addresses construction logistics, quality control, and field readiness. This section outlines the essential steps for NDOT to adopt UHPC overlays as a standard method for bridge deck overlay and structural repair.

7.3.1 Importance of Implementation

As demonstrated in national deployments, successful construction depends on reliably producing UHPC at the field scale, preparing the deck surface to ensure proper bonding, sequencing the placement to avoid cold joints, and applying curing and grinding procedures suitable for the local climate. These activities must be tested and refined through real-world field trials. A demonstration project will give NDOT engineers, inspectors, and contractors the chance to gain hands-on experience with these procedures, identify logistical or operational issues, and adapt construction practices to Nebraska's materials, climate, and contractor capabilities. This step is essential for developing future specifications, establishing acceptance criteria, and ensuring UHPC overlays can be implemented consistently statewide.

7.3.2 Key Steps for Implementation

7.3.2.1 Synthesis of State and National UHPC Overlay Experience

The first step in the implementation process is to gather relevant information from FHWA, AASHTO, and other state departments of transportation that have used UHPC overlays. This involves reviewing surface preparation methods such as milling, milling combined with hydro-demolition, or full hydro-demolition; assessing mixing and batching techniques ranging from on-site pan mixers to ready-mix trucks or mobile high-shear mixers; and analyzing placement strategies employed by other states. Additionally, understanding curing practices is crucial, including whether a curing compound alone suffices or if extra plastic sheeting is necessary in windy or cold conditions. It is also important to review national QA/QC procedures related to flow, temperature, density, air content, and early-age strength testing to ensure they align with Nebraska's practices. The information collected from reports, specifications, and interviews with engineers and contractors will provide the basis for developing Nebraska-specific practices and procedures.

7.3.2.2 Field-Ready Logistics for Production, Placement, and Quality Control

After reviewing national practices, NDOT can create a set of field procedures that align with Nebraska's laboratory findings and construction environment. These procedures should clearly define the preferred methods for surface preparation, including the desired profile and bond expectations. They should also specify the most appropriate mixing strategy, covering batching order, mixer capacity, crew size, and allowable time limits for mixing and placement. Production planning must consider the expected placement rate, lane width, vibration method, and screed movement to ensure a continuous, uniform overlay without cold joints. Curing and finishing procedures must be detailed, including application methods, curing times, grinding tolerances, and the sequence of grinding and grooving. Quality-control and acceptance procedures should outline how to document fresh UHPC properties, monitor environmental conditions during placement, verify compressive strength, and perform bond assessments needed for project approval. To complement the description of these construction activities, Figure 7.1 illustrates typical field steps in UHPC overlay production, placement, and curing as documented in the 2024 IADOT Cass County Bridge Overlay Project.

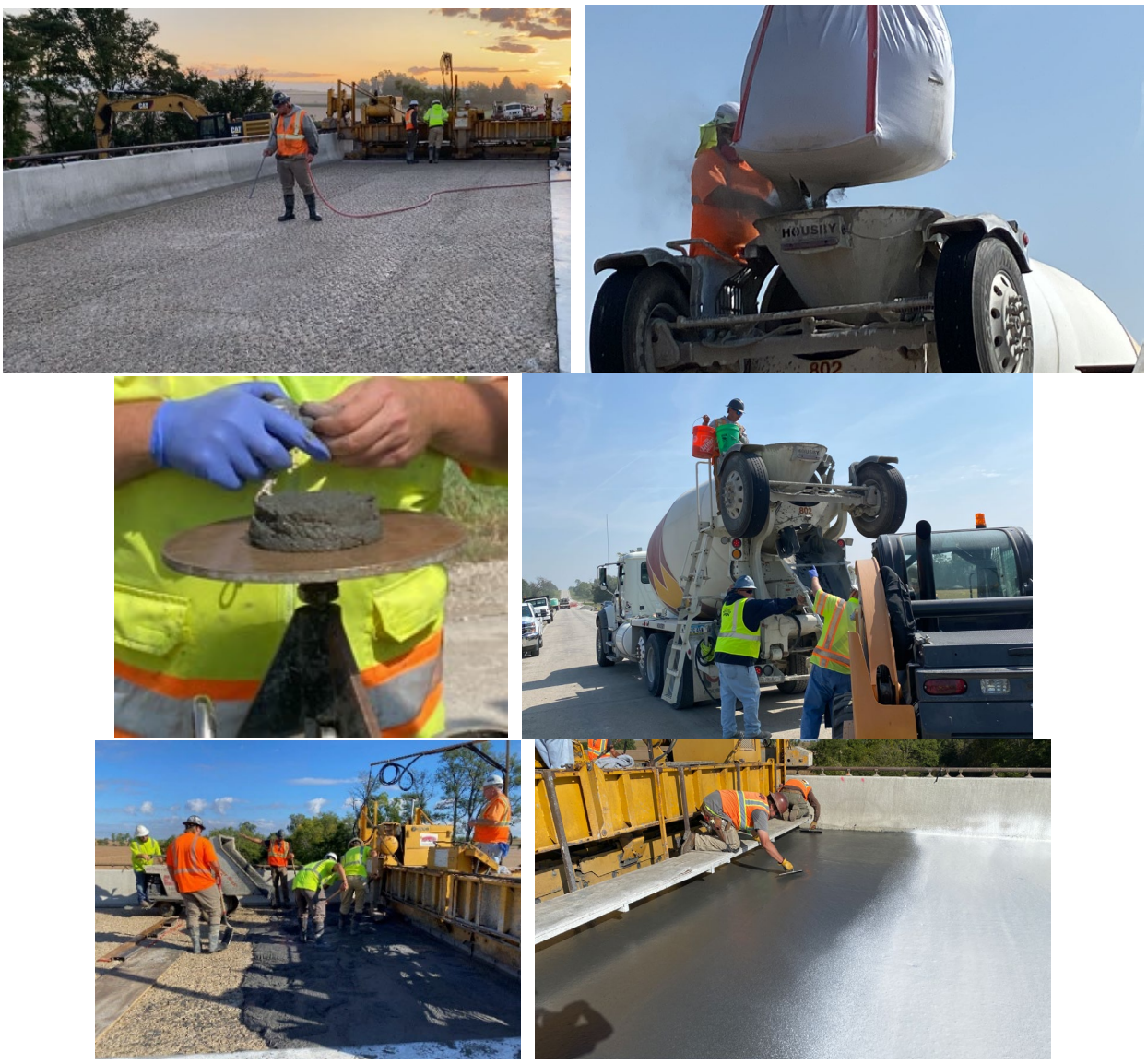

Figure 7.1 UHPC overlay construction, including substrate preparation, batching, QA/QC, placement, and curing (2024 IADOT Cass County Bridge Overlay Project).

To support the development of Nebraska-specific field procedures, Table 7.1 summarizes the principal construction and quality-control decision points for UHPC overlays, compiled primarily from FHWA TechNote FHWA-RC-24-0008 (2024) and related national experience.

Table 7.1 Key Decision Factors for UHPC Overlay Implementation.

Category	Options / Considerations
Surface Preparation	Hydro-demolition; Milling + Hydro-demolition; Milling only
Overlay Thickness	Typically, 1.0–2.0 in. (≥1.5 × fiber length + allowance for grinding)
Mixing Method	On-site pan or high-shear mixer; ready-mix truck with extended mixing; mobile mixer
Placement Method	Continuous placement using buggies, conveyors, vibrating screed, or UHPC paver
Curing	Spray-applied curing compound; compound + plastic sheeting in adverse weather
Finishing / Grinding	Overfill 0.25–0.5 in.; grind and groove after curing
QC/QA Testing	Flow, density, temperature, air content, compressive strength, bond testing as needed
Repair / Maintenance	UHPC slurry for small voids; grinding and recasting for larger areas

7.3.2.3 Full-Scale Mockup and Training

Before starting a field demonstration project, a full-scale mockup should be built to mimic actual placement conditions. The mockup enables NDOT and contractor personnel to work with the designated UHPC mixture, mixing equipment, and placement tools in a controlled setting. This process helps verify that the chosen equipment performs as expected, records batching cycle times, and evaluates the workability retention of the UHPC mixture under real-world conditions. It also gives field crews the chance to practice vibration, finishing, and curing techniques while becoming familiar with the surface-thickness control needed for later grinding. Constructability issues identified during the mockup can be addressed proactively before fieldwork begins. Additionally, the mockup acts as a training platform for NDOT inspectors, helping them become familiar with the quality-control procedures required during placement and early-age curing.

Figure 7.2 Examples of UHPC Overlay Mockups (Left: from 2023 UHPC Symposium; Right: from 2024 IADOT Cass County Bridge Overlay Project)

7.3.2.4 Pilot Bridge Demonstration Project

Once the mockup is successfully completed, NDOT should move forward with a pilot bridge overlay to test UHPC performance in real-world conditions. The bridge selected should be based on factors such as traffic volume, deck condition, geometry, staging constraints, and compatibility with UHPC overlay thickness requirements. The demonstration project will thoroughly evaluate substrate preparation methods, batching logistics, placement sequences, environmental impacts, and early-age strength development. Detailed records of placement conditions, curing performance, finishing quality, and any constructability issues will assist NDOT in enhancing construction procedures and adjusting acceptance criteria as needed. The findings from the demonstration will establish a foundation for incorporating UHPC overlays into NDOT's rehabilitation practices and contractual requirements.

7.3.3 Development of NDOT Guidelines and Specifications

The final step in the implementation plan is to develop NDOT-specific guidelines, specifications, and training materials that incorporate lessons learned from the mockup and pilot bridge project. These documents should include detailed instructions on surface preparation, mixing and batching procedures, placement and curing practices, as well as field acceptance criteria. The guidelines should also feature checklists for inspectors, suggested documentation forms, and troubleshooting tips for common construction issues. A concise implementation guide summarizing best practices, key decision points, and recommended field procedures will help ensure consistent statewide adoption.

Implementing UHPC overlays will significantly improve the durability and service life of Nebraska bridge decks. UHPC's dense matrix and excellent mechanical properties reduce chloride penetration, decrease freeze–thaw damage, and boost overall structural performance. Nebraska's non-proprietary UHPC mixes provide a cost-effective and locally accessible alternative to commercial materials. Field applications will improve contractor readiness and NDOT expertise, simplifying the integration of UHPC overlays into routine maintenance and rehabilitation projects. Ultimately, using UHPC overlays will extend the lifespan of critical infrastructure and reduce long-term maintenance costs.

7.4 Recommendations for Future Work

While this study offered valuable analytical and experimental insights into the behavior of NC bridge decks with UHPC overlays, it had some limitations. The assessment mainly focused on static loading conditions, without examining long-term fatigue performance. Additionally, the study did not explore the performance of construction joints between adjacent UHPC overlay sections, nor did it consider site-specific factors such as variability in surface

preparation or field application conditions. Therefore, the following are recommendations for future work:

1. Develop design provisions specific to the cohesion of UHPC overlays with applied using different surface preparation techniques.
2. Examine the fatigue behavior of UHPC overlays under repeated traffic loading, emphasizing both material performance and bond strength.
3. Examine the performance of construction joints between adjacent UHPC overlay sections under static and fatigue loading to ensure structural integrity.

References

Aaleti, S., Petersen, B., & Sritharan, S. (2013). Design guide for precast UHPC waffle deck panel system, including connections (No. FHWA-HIF-13-032). United States. Federal Highway Administration. https://rosap.ntl.bts.gov/view/dot/26129

Aaleti, S., & Sritharan, S. (2017). Investigation of a suitable shear friction interface between UHPC and normal strength concrete for bridge deck applications (No. InTrans Project 10-379). https://trid.trb.org/View/1470040

AASHTO. (2024). Guide Specifications for Structural Design with Ultra-High Performance Concrete, 1st edition. Washington, DC: American Association of State Highway and Transportation Officials.

AASHTO LRFD. (2020). Bridge Design Specifications. Washington, DC: American Association of State Highway and Transportation Officials, Ninth edition.

AASHTO T 160. (2017). Standard Method of Test for Length Change of Hardened Hydraulic-Cement Mortar and Concrete. Washington, DC: American Association of State Highway and Transportation Officials.

AASHTO T 277. (2007). Standard Method of Test for Rapid Determination of the Chloride Permeability of Concrete. Washington, DC: American Association of State Highway and Transportation Officials.

AASHTO T 397. (2022). Standard Method of Test for Uniaxial Tensile Response of Ultra-High Performance Concrete. Washington, DC: American Association of State Highway and Transportation Officials, First edition.

AASHTO TP 95. (2014). Standard Method of Test for Surface Resistivity Indication of Concrete's Ability to Resist Chloride Ion Penetration. Washington, DC: American Association of State Highway and Transportation Officials.

Abbas, S., Soliman, A. M., & Nehdi, M. L. (2015). Exploring mechanical and durability properties of Ultra-High Performance Concrete incorporating various steel fiber lengths and dosages. Construction and Building Materials, 75, 429–441. https://doi.org/10.1016/j.conbuildmat.2014.11.017

ASTM C1202 – 19. (2019). Standard Test Method for Electrical Indication of Concrete's Ability to Resist Chloride Ion Penetration. ASTM International, West Conshohocken, PA. https://doi.org/10.1520/C1202-19

ASTM C1437 – 20. (2020). Standard Test Method for Flow of Hydraulic Cement Mortar. ASTM International, West Conshohocken, PA. https://doi.org/10.1520/C1437-20

ASTM C150 / C150M – 20. (2020). Standard Specification for Portland Cement. ASTM International, West Conshohocken, PA. https://doi.org/10.1520/C0150_C0150M-20

ASTM C157 / C157M – 17. (2017). Standard Test Method for Length Change of Hardened Hydraulic-Cement Mortar and Concrete. ASTM International, West Conshohocken, PA. https://doi.org/10.1520/C0157_C0157M-17

ASTM C1583 / C1583M – 20. (2020). Standard Test Method for Tensile Strength of Concrete Surfaces and the Bond Strength or Tensile Strength of Overlay Materials by Direct Tension (Pull-off Method). ASTM International, West Conshohocken, PA. https://doi.org/10.1520/C1583_C1583M-20

ASTM C1609 / C1609M – 19. (2019). Standard Test Method for Flexural Performance of Fiber-Reinforced Concrete (Using Beam With Third-Point Loading). ASTM International, West Conshohocken, PA. https://doi.org/10.1520/C1609_C1609M-19

ASTM C1702 – 17. (2017). Standard Test Method for Measurement of Heat of Hydration of Hydraulic Cementitious Materials Using Isothermal Conduction Calorimetry. ASTM International, West Conshohocken, PA. https://doi.org/10.1520/C1702-17

ASTM C1856 / C1856M – 17. (2017). Standard Practice for Fabricating and Testing Specimens of Ultra-High Performance Concrete. ASTM International, West Conshohocken, PA. https://doi.org/10.1520/C1856_C1856M-17

ASTM C230 / C230M – 14. (2014). Standard Specification for Flow Table for Use in Tests of Hydraulic Cement. ASTM International, West Conshohocken, PA. https://doi.org/10.1520/C0230_C0230M-14\

ASTM C39/C39M – 21. (2021). Standard Test Method for Compressive Strength of Cylindrical Concrete Specimens. ASTM International, West Conshohocken, PA. https://doi.org/10.1520/C0039_C0039M-21

ASTM C403 / C403M – 16. (2016). Standard Test Method for Time of Setting of Concrete Mixtures by Penetration Resistance. ASTM International, West Conshohocken, PA. https://doi.org/10.1520/C0403_C0403M-16

ASTM C469 / C469M – 14. (2014). Standard Test Method for Static Modulus of Elasticity and Poisson's Ratio of Concrete in Compression. ASTM International, West Conshohocken, PA. https://doi.org/10.1520/C0469_C0469M-14

ASTM C494 / C494M – 19. (2019). Standard Specification for Chemical Admixtures for Concrete. ASTM International, West Conshohocken, PA. https://doi.org/10.1520/C0494_C0494M-19

ASTM C666 / C666M – 15. (2015). Standard Test Method for Resistance of Concrete to Rapid Freezing and Thawing. ASTM International, West Conshohocken, PA. https://doi.org/10.1520/C0666_C0666M-15

ASTM C989 / C989M – 18. (2018). Standard Specification for Slag Cement for Use in Concrete and Mortars. ASTM International, West Conshohocken, PA. https://doi.org/10.1520/C0989_C0989M-18

ASTM D8271 – 21. (2021). Standard Test Method for Measurement of Surface Profile of Prepared Concrete Surfaces Using a Laser Profilometer. ASTM International, West Conshohocken, PA. https://doi.org/10.1520/D8271-21

Bodenlos, K. D., & Fowler, D. W. (2003). Qualification of concrete workability by means of the vibrating slope apparatus (Research Report ICAR 105-2). Aggregates Foundation for Technology, Research, and Education.

Brühwiler, E. (2012). Rehabilitation and strengthening of concrete structures using ultra-high performance fiber reinforced concrete. In M. G. Alexander, H.-D. Beushausen, F. Dehn, & P. Moyo (Eds.), Concrete repair, rehabilitation and retrofitting III (pp. 72–79). Taylor & Francis Group.

Brühwiler, E. (2018). "Structural UHPFRC" to enhance bridges. Structural Engineering International, 129, 140–158. https://infoscience.epfl.ch/record/260450

Collins, M. P., & Mitchell, D. (1991). Prestressed Concrete Structures (Vol. 9). Prentice Hall, Englewood Cliffs, NJ.

Crop, L. (2018). Project case study: Replacement of Bridge 1-438 on Blackbird Station Road connections and deck overlay.

Delaware River and Bay Authority (DRBA). (n.d.). Delaware Memorial Bridge deck overlay project on the New Jersey bound span.

E. Brühwiler, Swiss Standard SIA 2052 UHPFRC: Materials, Design and Application. Swiss Society of Engineers and Architects, Lausanne, Switzerland, 2016.

Engineering Center at Iowa State University. (2017). Investigation of a suitable shear friction interface between UHPC and normal strength concrete for bridge deck applications: Final report. https://www.intrans.iastate.edu

FHWA. (n.d.). Design example: Precast/Prestressed concrete. U.S. Department of Transportation. Retrieved June 13, 2025, from https://www.fhwa.dot.gov/bridge/lrfd/pscus04.cfm

FHWA. (2022). Design and construction of UHPC-based bridge preservation and repair solutions (FHWA-HRT-22-065). https://doi.org/10.21949/1521867

FHWA. (2018). Project case study: Replacement of Bridge 1-438 on Blackbird Station Road—Ultra-high performance concrete connections and deck overlay. Federal Highway Administration. https://www.fhwa.dot.gov/bridge/abc/docs/Blackbird-Station-Road_casestudy.pdf

FHWA. (2017). Field testing of an Ultra-High Performance Concrete overlay (FHWA-HRT-17-096). https://doi.org/10.21949/1521867

FHWA. (2024). TechNote: Construction Joints for Ultra-High Performance Concrete (UHPC) Overlays. Publication No. FHWA-RC-24-0008.

FHWA. (2018). Ultra-High Performance Concrete for bridge deck overlays (FHWA-HRT-17-097).

FHWA. (2025). UHPC overlays expand use of contractor crews and ready-mix trucks. Every Day Counts News, Federal Highway Administration. Retrieved from https://www.fhwa.dot.gov/innovation/everydaycounts/edcnews/20250220.cfm

Graybeal, B. A., & Haber, Z. B. (2021). Ultra-High Performance Concrete (UHPC) overlays: An example of lifecycle cost analysis (FHWA-HRT-23-012). https://highways.dot.gov/research

Haber, Z. B., Foden, A., McDonagh, M., Ocel, J. M., Zmetra, K., & Graybeal, B. A. (2022a). Design and Construction of UHPC-Based Bridge Preservation and Repair Solutions (FHWA-HRT-22-065). United States. Federal Highway Administration, Office of Infrastructure Research and Development. https://rosap.ntl.bts.gov/view/dot/62435

Haber, Z. B., McDonagh, M., Foden, A., & Sadasivam, S. (2022b). Ultra-High Performance Concrete (UHPC) Overlays: An Example of Lifecycle Cost Analysis (FHWA-HRT-23-012). https://rosap.ntl.bts.gov/view/dot/64952

Haber, Z. B., Munoz, J. F., De la Varga, I., & Graybeal, B. A. (2018). Bond characterization of UHPC overlays for concrete bridge decks: Laboratory and field testing. Construction and Building Materials, 190, 1056–1068. https://doi.org/10.1016/j.conbuildmat.2018.09.167

Harris, D. K., Carbonell Muñoz, M. A., Gheitasi, A., Ahlborn, T. M., & Rush, S. V. (2015). The challenges related to interface bond characterization of ultra-high-performance concrete with implications for bridge rehabilitation practices. Advances in Civil Engineering Materials, 4(2), 75–101. https://doi.org/10.1520/ACEM20140034

Holcim. (2023). Ductal® overlay product sheet. https://www.holcim.us/sites/us/files/2023-05/ductal_overlay_product_sheet_v2.pdf

IADOT. (2022). Special provisions for Ultra High Performance Concrete overlay. Iowa Department of Transportation, SP-150886.

ICRI Committee 310. (2013). Selecting and Specifying Concrete Surface Preparation for Sealers, Coatings, Polymer Overlays, and Concrete Repair. International Concrete Repair Institute, Rosemont, IL.

Mendonca, F., Abo El-Khier, M., Morcous, G., & Hu, J. (2020). Feasibility study of development of Ultra-High Performance Concrete (UHPC) for highway bridge applications in Nebraska (Report No. SPR-P1(18) M072). Nebraska Department of Transportation.

Meng, W., & Khayat, K. H. (2018). Effect of hybrid fibers on fresh properties, mechanical properties, and autogenous shrinkage of cost-effective UHPC. Journal of Materials in Civil Engineering, 30(4). https://doi.org/10.1061/(asce)mt.1943-5533.0002212

Nebraska Department of Transportation (NDOT). (2025). Bridge Design Manual. Nebraska Department of Transportation, Bridge Division, Lincoln, NE.

NJDOT. (2025). Sample draft special provisions for UHPC overlay. New Jersey Department of Transportation.

NYSDOT. (2022). Special provisions for Ultra High Performance Concrete overlay. New York State Department of Transportation, 584.21010001.

Ocel, J., Foden, A., & Gentz, C. (2022). Ultra-High Performance Concrete (UHPC) for Bridge Preservation and Repair: An EDC-6 Workshop developed for the Montana Department of Transportation, August 16, 2022. Federal Highway Administration, Helena, MT.

Precast/Prestressed Concrete Institute (PCI) Concrete Materials Technology Committee. (2022). Guidelines for the Use of Ultra-High-Performance Concrete (UHPC) in Precast and Prestressed Concrete (PCI TR-9-22). Chicago, IL: Precast/Prestressed Concrete Institute. https://doi.org/10.15554/TR-9-22

Sritharan, S., Doiron, G., Bierwagen, D., Keierleber, B., & Abu-Hawash, A. (2018). First application of UHPC bridge deck overlay in North America. Transportation Research Record, 2672(26), 40–47. https://doi.org/10.1177/0361198118755665

Steelike. (n.d.). Claiborne Pell Newport Bridge. Retrieved June 13, 2025, from https://steelike.com/projects/claiborne-pell-newport-bridge/

Swiss Society of Engineers and Architects. (n.d.). SIA 2052: Guidelines for Ultra-High-Performance Fiber-Reinforced Concrete (UHPFRC). https://www.sia.ch

Swiss Society of Engineers and Architects, Ultra-Hochleistungs-Faserbeton (UHFB) – Baustoffe, Bemessung und Ausführung (German Draft – SIA 2025). Swiss Society of Engineers and Architects, Zurich, Switzerland, 2023.

Tahat, M. F. (2023). Performance Evaluation and Design Considerations for Reinforced Ultra-High Performance Concrete (UHPC) Bridge Decks and Connections (Doctoral dissertation, The University of Nebraska-Lincoln).

Thorenfeldt, E., Tomaszewicz, A., & Jensen, J. J. (1987). Mechanical Properties of High-Strength Concrete and Applications in Design. In Proc., Symposium Proceedings, Utilization of High-Strength Concrete, Stavanger, Norway.

Toledo, W. (n.d.). Field implementation and monitoring of an Ultra-High Performance Concrete bridge deck overlay. https://orcid.org/0000-0002-3436-5118

UHPC Solutions. (n.d.). Bridge Rehabilitation Case Studies. UHPC Solutions North America. https://www.uhpcsolutions.com/case-studies

UHPC Solutions. (2018). Little Heaven case study. https://www.uhpcsolutions.com/little-heaven-case-study

Use of Ultra-High-Performance Concrete for Bridge Deck Overlays Final Report. (2018). Iowa Department of Transportation (InTrans Projects 16-573 and 16-574), Federal Highway Administration. https://www.intrans.iastate.edu

Wibowo, H., & Sritharan, S. (2018). Use of ultra-high-performance concrete for bridge deck overlays (No. IHRB Project TR-683). Iowa Highway Research Board, Iowa Department of Transportation, & Federal Highway Administration. https://trid.trb.org/View/1506096

Wu, Z., Shi, C., He, W., & Wu, L. (2016). Effects of steel fiber content and shape on mechanical properties of Ultra High Performance Concrete. Construction and Building Materials, 103, 8–14. https://doi.org/10.1016/j.conbuildmat.2015.11.028

Ye, H., Huang, A., Jiang, C., & Wang, W. (2023). Experimental Investigation on Fatigue Improvement of Orthotropic Steel Bridge Deck Using Steel Fiber Reinforced Concrete. International Journal of Concrete Structures and Materials, 17(5), 935–948. https://doi.org/10.1186/s40069-023-00607-2

Zhang, Y., Zhu, Y., Yeseta, M., Meng, D., Shao, X., Dang, Q., & Chen, G. (2019). Flexural behaviors and capacity prediction on damaged reinforced concrete (RC) bridge deck strengthened by ultra-high performance concrete (UHPC) layer. Construction and Building Materials, 215, 347–359. https://doi.org/10.1016/j.conbuildmat.2019.04.229

Appendix A Results of Flow and PR Tests

A.1 Flow results

Table A.1 presents the flow results of UHPC overlay mixtures measured at 30-minute intervals, extending up to 90 minutes. The 0-minute mark represents the flow immediately after mixing. The evaluation criteria are based on PR and slope results, with the target ranges being 4.1-6.0 inches for static flow and 6.5-8 inches for dynamic flow. Mixtures highlighted in green indicate those that maintained acceptable flow properties, meeting the criteria throughout the 90-minute period.

Table A.1 Flow results of UHPC overlay mixtures over time.

Groups	Mixture ID	Mixture ID	Flow (0") (in.)		Flow (30') (in.)		Flow (60') (in.)		Flow (90') (in.)	
			Static	Dynamic	Static	Dynamic	Static	Dynamic	Static	Dynamic
CIP	**CIP**	CIP-1900-0.180-H51-W21	9.3	N/A	N/A	N/A	N/A	N/A	N/A	N/A
B	**Mix 3**	F2%-1900-0.180-H21-W44	10.5	N/A	9.5	N/A	8.3	N/A	7.0	N/A
	Mix 4	F2%-1900-0.180-H10-W44	4.0	6.8	4.0	5.9	4.0	5.3	N/A	N/A
	Mix 5	F2%-1900-0.180-H0-W56	4.0	5.8	4.0	5.6	4.0	6.3	4.0	5.9
	Mix 6	F2%-1900-0.180-H0-W69	5.1	7.8	7.1	8.4	8.1	8.9	9.0	N/A
	Mix 12	F2%-1900-0.180-H4-W65	4.1	7.0	6.8	7.6	7.3	8.0	7.3	8.0
	Mix 13	F2%-1900-0.180-H4-W61	4.1	7.0	5.5	7.3	6.0	7.4	6.5	7.5
	Mix 16	F2%-1900-0.180-H4-W56	6.2	7.8	5.6	7.5	5.8	7.3	6.2	7.5
	Mix 18	F2%-1900-0.180-H0-W61	4.0	6.3	4.0	6.7	5.1	7.4	6.1	7.3
	Mix 28	F2%-1900-0.180-H3-W52	5.1	7.8	5.1	7.5	5.5	7.6	5.9	8.2
	Mix 29	F2%-1900-0.180-H3-W47	4.1	7.3	4.1	7.0	4.3	7.1	4.4	7.3
C	**Mix 7**	F2%-1450-0.196-H0-W52	4.0	6.3	5.0	7.0	6.0	7.0	6.6	7.4
	Mix 8	F2%-1450-0.196-H3-W54	5.3	7.0	5.5	7.1	6.0	7.3	6.0	7.3
	Mix 14	F2%-1450-0.196-H3-W52	4.3	6.9	6.0	7.3	6.0	7.0	5.3	6.8
	Mix 15	F2%-1450-0.196-H3-W47	4.0	6.3	4.0	6.0	4.3	6.2	4.8	6.7
	Mix 19	F2%-1450-0.196-H0-W49	4.0	6.1	4.0	6.0	4.3	6.6	5.6	7.2
D	**Mix 9**	F2%-1450-0.180-H8-W54	5.3	7.2	4.5	6.0	4.0	5.0	N/A	N/A
	Mix 11	F2%-1450-0.180-H8-W73	6.5	7.7	4.0	5.0	N/A	N/A	N/A	N/A
	Mix 17	F2%-1450-0.180-H4-W54	5.6	7.4	5.5	6.9	5.4	6.9	5.1	6.4
E	**Mix 20**	F3%-1450-0.196-H4-W59	6.8	8.4	6.3	7.8	5.8	7.5	5.4	7.0
	Mix 24	F3%-1450-0.196-H3-W54	4.8	7.4	5.5	7.3	5.4	7.1	5.1	7.0
	Mix 26	F3%-1450-0.196-H3-W47	4.1	6.6	4.1	6.6	4.8	6.6	4.6	6.6
F	**Mix 21**	F3%-1900-0.180-H5-W62	7.0	8.5	7.5	8.9	7.7	8.5	7.6	8.6
	Mix 22	F3%-1900-0.180-H4-W58	6.6	8.4	7.0	8.3	7.1	8.4	6.4	8.0
	Mix 23	F3%-1900-0.180-H4-W56	5.7	7.7	6.2	7.8	7.0	8.2	6.9	8.0
	Mix 25	F3%-1900-0.180-H3-W54	4.0	7.0	4.3	7.0	5.1	7.3	5.9	7.5
	Mix 27	F3%-1900-0.180-H3-W47	4.0	6.6	4.0	5.9	4.0	6.6	4.0	6.7
G	**Mix 10**	F3%-1450-0.180-H10-W62	4.8	6.8	4.0	5.0	4.0	4.8	N/A	N/A

A.2 PR results

Table A.2 presents the PR results measured at 30-minute intervals, extending up to 90 minutes. The majority of the mixtures successfully passed the PR test, with only a few severe cases failing, where the flow results were entirely outside the acceptable range. The fact that some mixtures failed the flow tests but still passed the PR test suggests that their flow results were only marginally higher or lower than the designated criteria.

Table A.2 PR results of UHPC overlay mixtures over time.

Groups	Mixture ID	Mixture ID	PR (0")	PR (30")	PR (60")	PR (90")
B	Mix 4	F2%-1900-0.180-H10-W44	P1	P1	F2	F2
	Mix 5	F2%-1900-0.180-H0-W56	F2	F2	F2	F2
	Mix 6	F2%-1900-0.180-H0-W69	P1	F1	F1	F1
	Mix 12	F2%-1900-0.180-H4-W65	P1	P1	F1	F1
	Mix 13	F2%-1900-0.180-H4-W61	P1	P1	P1	P1
	Mix 16	F2%-1900-0.180-H4-W56	P1	P1	P1	P1
	Mix 18	F2%-1900-0.180-H0-W61	P1	P1	P1	P1
	Mix 28	F2%-1900-0.180-H3-W52	P1	P1	P1	P1
	Mix 29	F2%-1900-0.180-H3-W47	P1	P1	P1	P1
C	Mix 7	F2%-1450-0.196-H0-W52	P1	P1	P1	P1
	Mix 8	F2%-1450-0.196-H3-W54	P1	P1	P1	P1
	Mix 14	F2%-1450-0.196-H3-W52	P1	P1	P1	P1
	Mix 15	F2%-1450-0.196-H3-W47	P1	P1	P1	P1
	Mix 19	F2%-1450-0.196-H0-W49	P1	P1	P1	P1
D	Mix 9	F2%-1450-0.180-H8-W54	P1	F2	F2	F2
	Mix 11	F2%-1450-0.180-H8-W73	P1	F2	F2	F2
	Mix 17	F2%-1450-0.180-H4-W54	P1	P1	P2	F2
E	Mix 20	F3%-1450-0.196-H4-W59	P2	P2	F1	F1
	Mix 24	F3%-1450-0.196-H3-W54	P1	P2	F1	F1
	Mix 26	F3%-1450-0.196-H3-W47	P1	P1	P1	P2
F	Mix 21	F3%-1900-0.180-H5-W62	P1	P1	P2	F1
	Mix 22	F3%-1900-0.180-H4-W58	P1	P1	P1	F1
	Mix 23	F3%-1900-0.180-H4-W56	P1	P1	P2	F1
	Mix 25	F3%-1900-0.180-H3-W54	P1	P1	P1	P1
	Mix 27	F3%-1900-0.180-H3-W47	P1	P1	P1	P1
G	Mix 10	F3%-1450-0.180-H10-W62	P1	F2	F2	F2

Appendix B Analysis of the Impact of Different Design Parameters

B.1 Effect of Binder Content on Flow

Figure B.1Figure B.2illustrate the impact of different groups with 2% and 3% fibers on flow values over time, respectively. It should be noted that the amount of incorporated HRWR varies between three, four, and five throughout the mixtures, as indicated on the graphs. Static flow results at the same amount of incorporated admixtures were fairly consistent across all groups with different binder content and w/b ratios for both cases (2% and 3% fibers). This consistency implies that binder content does not significantly affect static flow results. However, dynamic flow results varied; Group B mixtures exhibited increased flow compared to Groups C and D mixtures at the same dosage of HRWR and WRT (Figure B.1). This increase in flow for Group B can be attributed to the higher paste content, which reduces viscosity and consequently enhances the mixture's flowability. Additionally, the higher paste content improves cohesion by reducing segregation. It is important to note that a higher w/b ratio in Group C mixtures does not necessarily result in higher flow values. This is because the increased w/b ratio compensates for the reduced binder content to maintain consistency.

Additionally, the flow results for Group B and C mixtures generally increased over time within a certain range. In contrast, Group D mixtures showed a decrease in flowability over time, failing to maintain proper dynamic flow for up to 30 minutes (Figure B.1). The primary reason for the reduced flowability in Group D mixtures is the limited water content. With a reduced binder content, the sand amount increased significantly. Unlike Group C mixtures, the water content in Group D mixtures was kept low (w/b = 0.180), resulting in poor flowability. Due to the failure of the mixture with 2% incorporated fibers, there are no mixtures from Group D that include 3% fibers (Figure B.2).

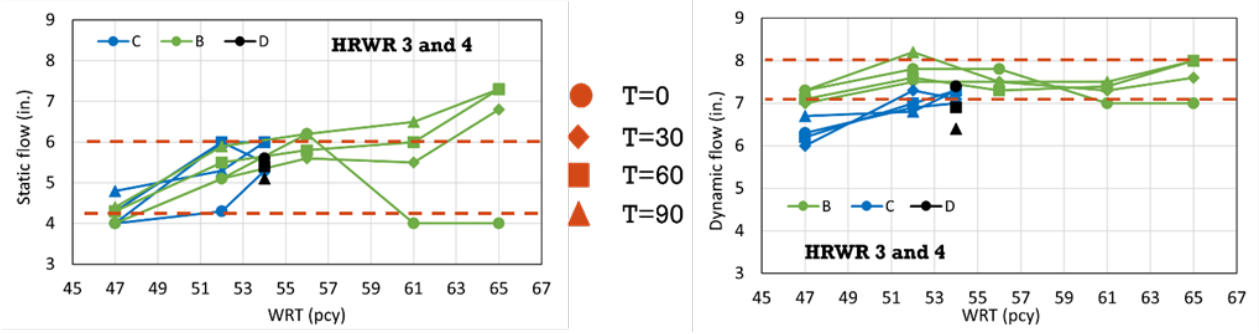

Figure B.1 Impact of different groups with 2% fibers on flow over time.

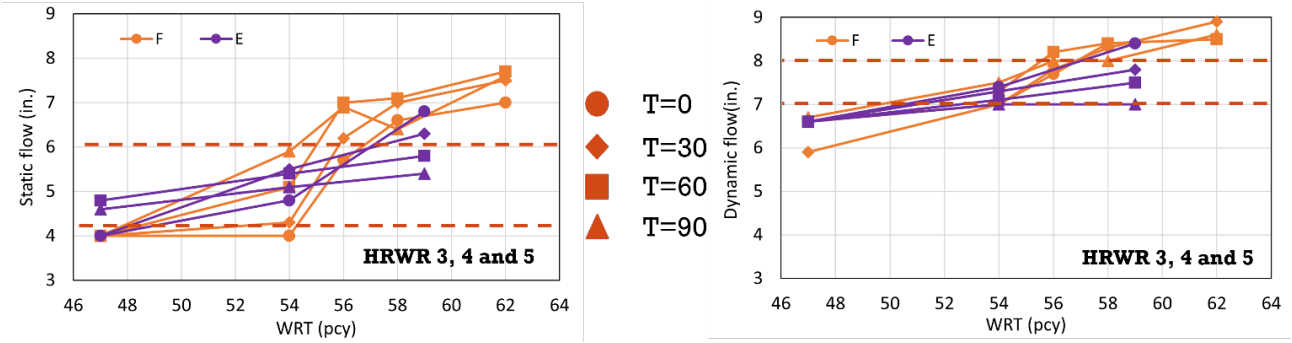

Figure B.2 Impact of different groups with 3% fibers on flow over time.

B.2 Effect of Different Fiber Amounts on Flow

Since Group F and E mixtures are the same as Group B and C, respectively, but with 3% fiber content, the impact of fibers on flow over time can be observed in Figure B.3 and Figure B.4. For Groups B and F, higher flow values were observed for mixtures with 3% fibers when the amount of WRT exceeded 56 pcy. Generally, increased fiber content is believed to decrease flowability (Abbas et al., 2015; Meng and Khayat, 2018; Wu et al., 2016). This phenomenon may be attributed to the increased specific surface area resulting from the higher fiber content. Additionally, the randomly distributed steel fibers within the matrix acted as a structural framework, ultimately impeding the flow of fresh concrete. This was the case for Groups C and E, where static flow results were higher for Group C mixtures compared to Group E, although

dynamic flow results were relatively similar. It should be noted that increasing the fiber content results in a corresponding reduction in sand content, which helps offset the potential reduction in workability due to higher fiber content. The differences in the effects of fiber content between the groups can be explained by variations in paste content and w/b ratio, which also affect flowability. In conclusion, there is a minimal impact of increased fiber content from 2% to 3% on workability if the WRT amount is not excessively large.

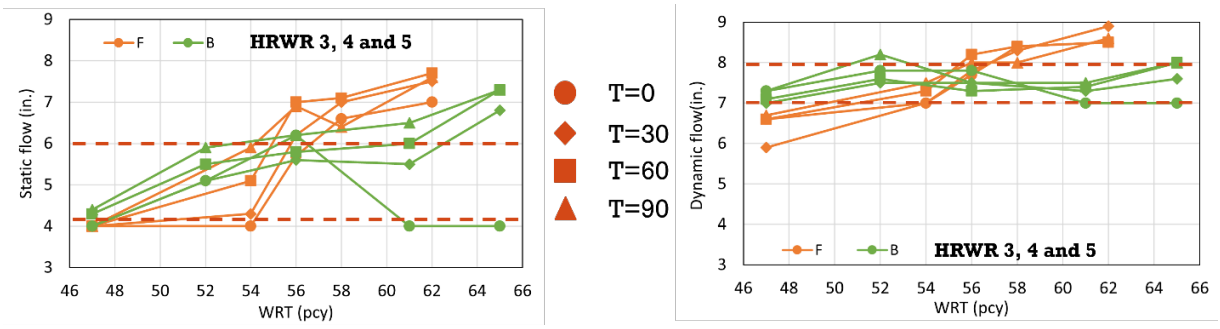

Figure B.3 Impact of fiber amount within groups B and F on flow over time.

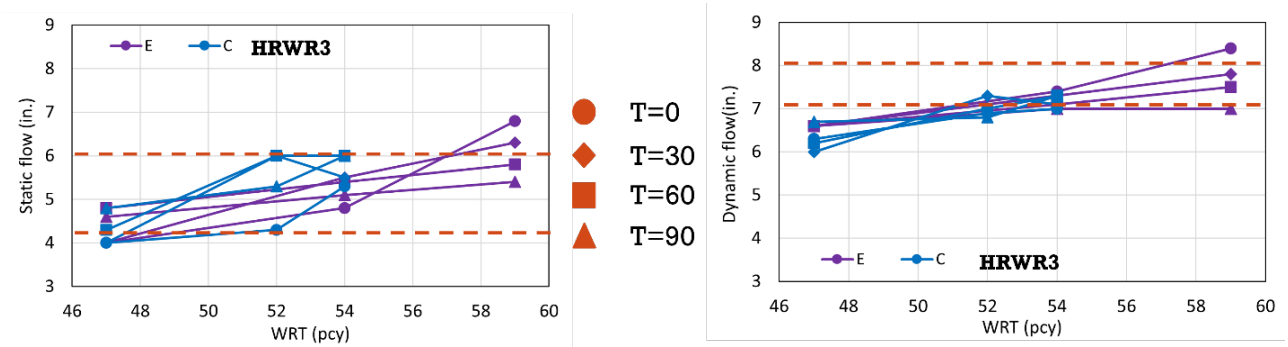

Figure B.4 Impact of fiber amount within groups C and E on flow over time.

B.3 Effect of HRWR and WRT on Flow

Figure B.5 Figure B.6 illustrate the impact of varying amounts of HRWR on flow over time within Groups B and C, respectively. From Figure B.5, it is evident that incorporating

HRWR positively affects flowability by allowing a reduced dosage of WRT. At 56 pcy of WRT, the dynamic flow results are very small and fall out of range for cases with 0 HRWR but are significantly higher with 4 pcy of HRWR. Furthermore, the variation in flow over time without HRWR is greater than with HRWR, and the flow results increase significantly over time. This indicates that while HRWR contributes to increased initial workability, a reduction in flowability over time can also be observed.

Similar conclusions can be drawn from Figure B.6. Initial flow results are lower without the incorporation of HRWR, but over time, the flow results increase considerably. This reinforces the observation that HRWR does not aid in maintaining flow over time, as its absence results in greater variation and less stability in the flowability of the mixtures. However, an appropriate amount of HRWR balances the effect of WRT, facilitating stability of flowability over time and maintaining good initial flowability without high variation. The optimal amount was identified as approximately 3-5 pcy, as an excessive amount of HRWR can disrupt the balance between WRT and HRWR, leading to a drastic drop in flow over time. This can be observed in Figure B.6, where the amount of HRWR was 8 pcy, resulting in a sudden drop in flow even at 30 minutes, despite the initial high flowability for both static and dynamic flows.

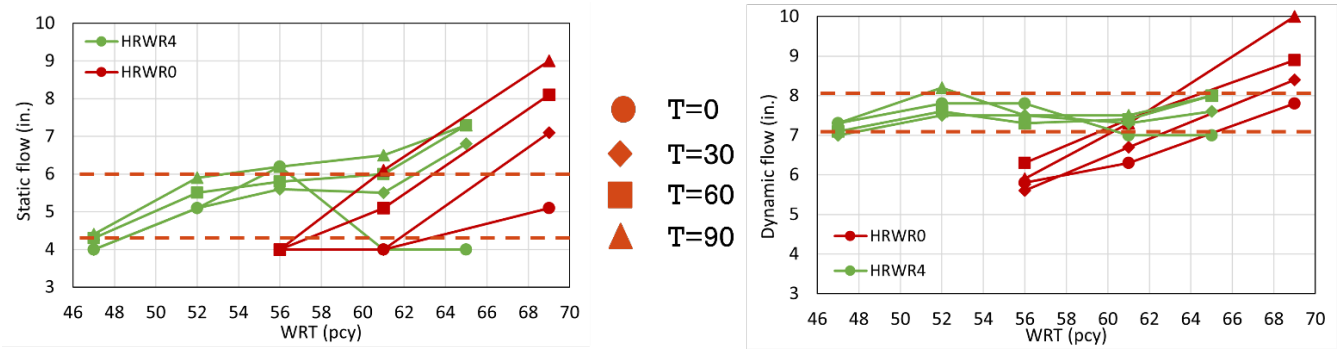

Figure B.5 Impact of HRWR within group B on flow over time.

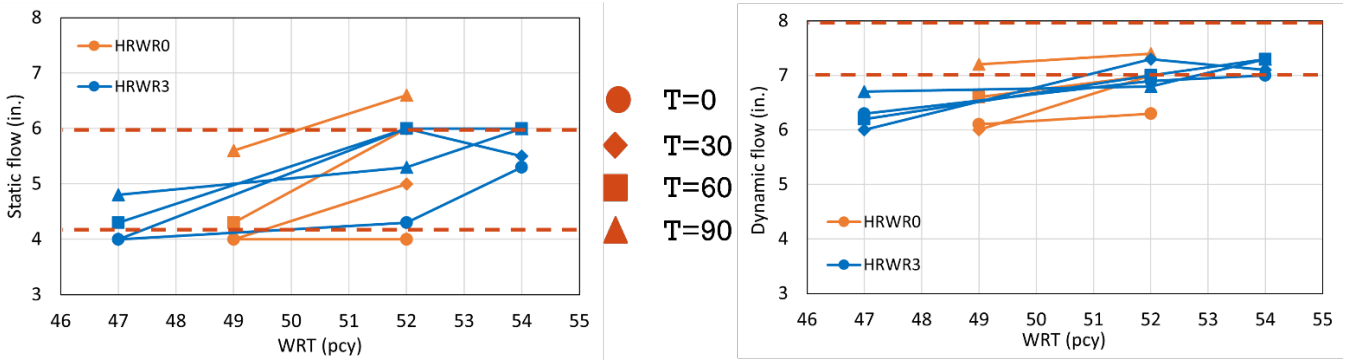

Figure B.6 Impact of HRWR within group C on flow over time.

Appendix C Case Study IADOT Cass County Bridge Overlay Project

C.1 Introduction

The UHPC Overlay project on the Cass County Bridge in Iowa aimed to enhance the durability and performance of the bridge using UHPC overlay. The project began with a mock-up on September 18, 2023, to evaluate the UHPC mixture and its application process. The mock-up, with a size of two cubic yards, served as a preliminary test to ensure the mixture's suitability and the effectiveness of the application techniques.

Following the successful mock-up, the UHPC overlay was applied to the bridge in two separate phases. The first lane was paved on one designated day, followed by the second lane on another day. This phased approach ensured proper application and curing of the UHPC overlay, contributing to the overall quality and longevity of the bridge surface.

C.2 Surface Preparation

The UHPC overlay project was implemented on a new bridge deck, which underwent fairly aggressive hydro-demolishment prior to the application of the overlay (Figure C.1). This process raised concerns about achieving full consolidation of the UHPC material. The bridge deck has a slope ranging from 2% to 5%, which required careful consideration during the overlay application to ensure uniform coverage and proper adhesion. The overlay with a thickness of 1.25 inches was placed.

To prepare for the first phase of casting, the surface was wetted on Tuesday, the day before casting commenced (Figure C.2). Just before applying the UHPC overlay, excess water was removed by air-blowing, as shown in Figure C.2, bringing the surface to an SSD condition. This preparation step was crucial to promote optimal bonding between the existing concrete surface and the new UHPC overlay.

Figure C.1 Surface of bridge deck after hydro-demolition.

Figure C.2 From left to right: wet surface; removing excess water by air-blowing before the UHPC placement (SSD condition).

C.3 Materials and Mixing

Ready-mix trucks, with 5-6 cubic yards of UHPC being mixed per truck, were used for the project. Each mixing session lasted 45-60 minutes. It should be noted that the typical mixing time for UHPC using a shear mixer is 20-30 minutes. Controlling the mixing temperature was crucial; if necessary, cold water was sprayed on the outside of the mixer to maintain the desired temperature. Each batch of UHPC was prepared using 3,500 pounds of premix per bag. Once the desired consistency was achieved, 44 pounds (20 kilograms) of fiber per bag were added to the mixture. Figure C.3 exhibits an overview of materials utilized at the job site.

Following the overlay application the truck was pressure washed for up to 1.5 hours. This process involved thorough watering down, which potentially left the truck cleaner than it was before the project. UHPC is generally difficult to clean; however, the inclusion of fibers in the mixture helped to scratch out residuals, contributing to a more effective cleaning process.

Figure C.3 UHPC materials at the job site.

C.4 Mockup Batch on 9/18/23

On September 18th, a mockup batch was prepared using two bags of premix and 20 bags of fiber. The following sequence of events occurred:

- **11:39 AM:** Loading of water and chemicals commenced. The initial mix included 48 pounds of Optima 100 (without Premia 150) and 654 pounds of water.
- **11:52 AM:** The mixer drum temperature was recorded at 82°F.
- **11:55 AM:** Fiber loading began with a conveyor belt.

- **12:33 PM:** The temperature reached 87°F, with static flow measured at four inches and dynamic flow at seven inches.
- **12:36 PM:** An additional pound of Premia 150 and eight pounds of water were added to the mix.
- **12:48 PM:** The temperature was 89°F, with static flow measured at 4.25 inches and dynamic flow at 7.5 inches, at which point the placement process started.

This mockup batch demonstrated the importance of closely monitoring and adjusting mix components to achieve the desired flow properties and temperature conditions necessary for optimal UHPC overlay performance. Figure C.4 depicts the batching process of the UHPC overlay mix.

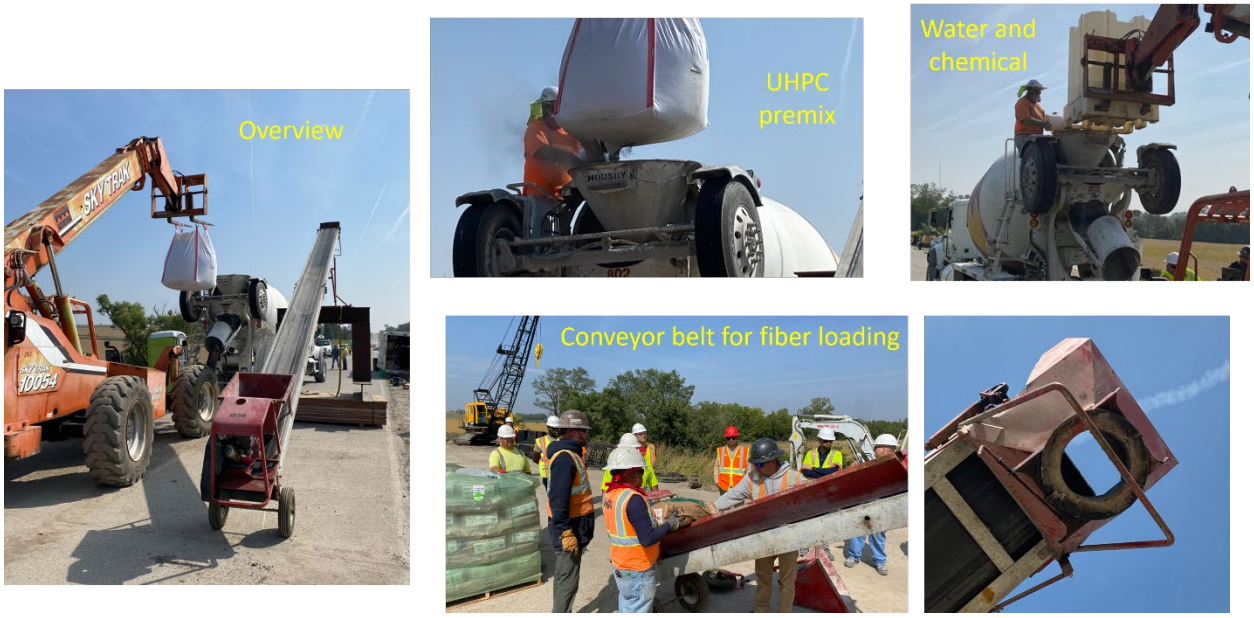

Figure C.4 IADOT Cass County Bridge Overlay Project – Batching.

C.5 Workability

The target for the static flow was 4-4.5 inches, while the dynamic flow target was 7.5-8 inches. During the initial flow test in the mock-up, the static flow reached 4 in. and the dynamic flow reached 7 in. Adjustments were made by adding Premia-150 and water. This adjustment process was also applied in actual UHPC overlay placements to ensure proper workability for consolidation and strong bonding. Figure C.5 illustrates the excellent static and dynamic flows of the UHPC overlay. Additionally, the response of the overlay mixture to external energy, such as the paver in this context, was assessed by patting the material after the dynamic flow test, as shown in Figure C.6. The main purpose of this was to apply external force and observe the material's reaction. The clear handprint left after patting demonstrates how well the material responded to vibration.

Figure C.5 Flow after adjustment (4.25” static, 7.5” dynamic).

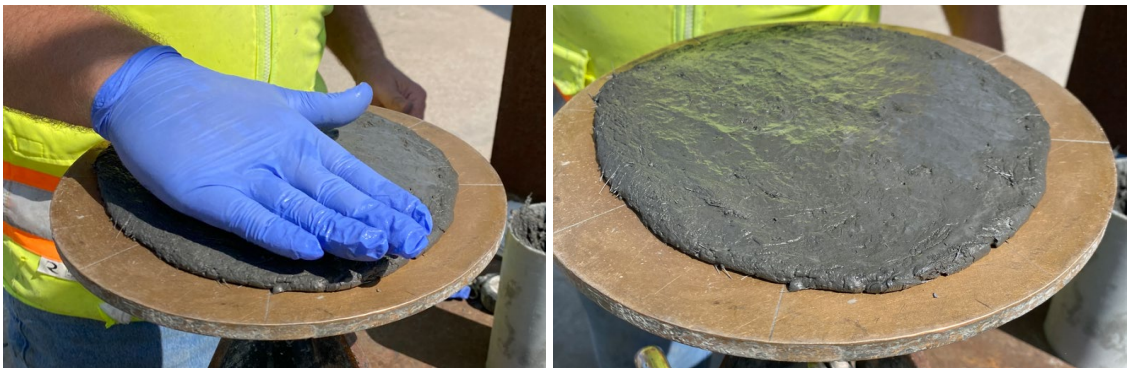

Figure C.6 Material reacts well under external energy (vibration).

C.6 Placement and Consolidation

A Thin Lift UHPC Overlay Paver (Low slump paver) was employed for the placement and consolidation of the material. The material was conveyed and deposited using a motorized buggy. Figure C.7 shows the placement and consolidation process of the UHPC overlay and the spread of the material before paving is applied.

Figure C.7 From left to right: UHPC overlay installation and consolidation with a paver; Spread of material before consolidation.

C.7 Finishing and Curing

After the material was freshly placed, a white curing compound was sprayed on it and covered with plastic to prevent dehydration. Any spots that were not properly consolidated by

the paver were subsequently hand-finished to ensure uniformity and quality. Figure C.8 presents the process of hand-finishing and implementation of a white compound.

Figure C.8 From left to right: Hand-finishing after paving; Application of white curing compound.

Appendix D Detailed Calculations of the Design Example (Section 5.7)

Input Parameter

Output

Geometry

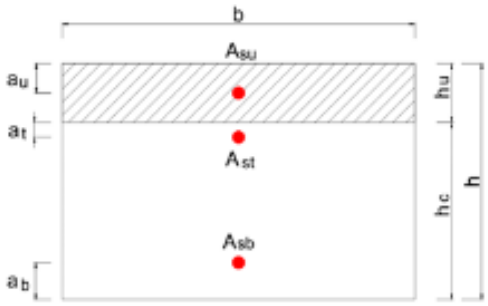

Section Width $b := 12\ in$

Span Length $L := 116\ in$

UHPC Thickness $h_u := 1.5\ in$

Normal Concrete Thickness $h_c := 6.5\ in$

$a_u := 0.75\ in$

$a_t := 2.81\ in - h_u = 1.31\ in$

$a_b := 1.31\ in$

Total Section Depth $h := h_u + h_c = 8\ in$

Area of UHPC $A_u := b \cdot h_u = 18\ in^2$

Area of Normal Concrete $A_c := b \cdot h_c = 78\ in^2$

Material Properties

Normal Concrete (NC)

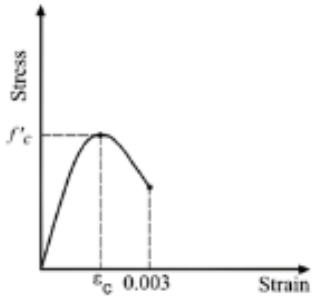

Compressive Strength $f_c' := 4000\ psi$

Density $\gamma_{nc} := 0.15$ kcf

MOE $E_c := 120000 \cdot (\gamma_{nc})^2 \left(f_c' \cdot ksi^2\right)^{\frac{1}{3}} = 4285.983\ ksi$

Curve fitting factor $n := 0.8 + \frac{f_c'}{2500\ psi} = 2.4$

controlling factor $k := 0.67 + \frac{f_c'}{9000\ psi} = 1.114$

Strain when f_c reaches f_c' $\varepsilon_c' := \frac{f_c'}{E_c} \cdot \left(\frac{n}{n-1}\right) = 0.0016$

Ultra High Performance Concrete (UHPC)

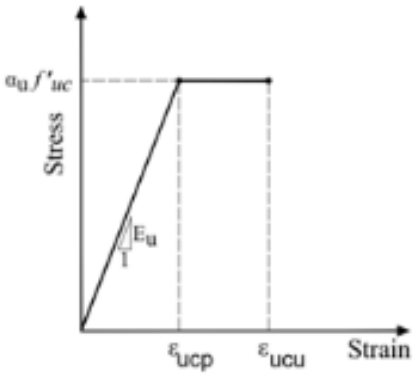

UHPC in Compression

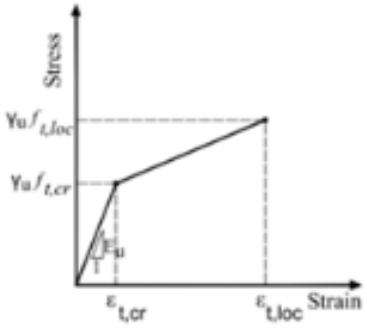

UHPC in Tension

Compressive Strength $f_{uc}' := 14000\ psi$

MOE $E_u := 2500 \cdot \left(f_{uc}' \cdot ksi^2\right)^{\frac{1}{3}} = 6025.356\ ksi$

Elastic Compressive Strain $\varepsilon_{ucp} := \frac{0.85 \cdot f_{uc}'}{E_u} = 0.002$

Ultimate Compressive Strain $\varepsilon_{ucu} := \max\left(0.0035, \varepsilon_{ucp}\right) = 0.0035$

Cracking strength $f_{t.cr} := 0.75\ ksi$

Cracking Strain $\varepsilon_{t.cr} := \frac{f_{t.cr}}{E_u} = 0.00012$

Crack Localization Strength $f_{t.loc} := 0.9\ ksi$

Crack Localization Strain $\varepsilon_{t.loc} := 0.005$

Reinforcement (A615)

Yield Strength	$f_y := 60\ ksi$
MOE	$E_s := 29000\ ksi$
Yield Strain	$\varepsilon_y := \frac{f_y}{E_s} = 0.002$
Rupture Strain	$\varepsilon_u := 0.09$
Area of bottom Reinforcement	$A_{sb} := 0.532\ in^2$
Area of Top Reinforcement	$A_{st} := 0.413\ in^2$
Area of Reinforcement in the UHPC Layer	$A_{su} := 0 \cdot 0.31 \cdot in^2 = 0\ in^2$

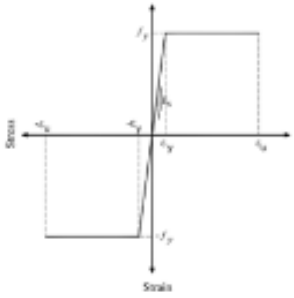

Ultimate Moment Capacity of the Composite Section under Positive Bending Moment

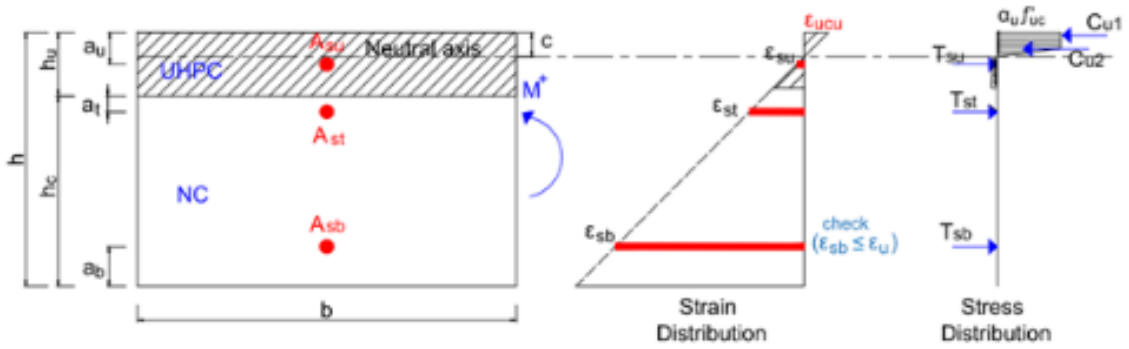

Forces

UHPC Comp. Force (rect.) $C_{c.uhpc1}(c) := 0.85\ f_{uc}' \cdot b \cdot \left(1 - \frac{\varepsilon_{ucp}}{\varepsilon_{ucu}}\right) \cdot c$

UHPC Comp. Centroid (rect.) $Z_{c.uhpc1}(c) := \frac{c}{2} \cdot \left(1 + \frac{\varepsilon_{ucp}}{\varepsilon_{ucu}}\right)$

UHPC Comp. Force (tri.) $C_{c.uhpc2}(c) := 0.85\ f_{uc}' \cdot b \cdot \frac{\varepsilon_{ucp}}{\varepsilon_{ucu}} \cdot c$

UHPC Comp. Centroid (tri.) $Z_{c.uhpc2}(c) := \frac{2 \cdot c}{3} \cdot \frac{\varepsilon_{ucp}}{\varepsilon_{ucu}}$

Force in bottom Reinforcement $T_{sb}(c) := A_{sb} \cdot E_s \cdot min\left(\varepsilon_y, \frac{h - a_b - c}{c} \cdot \varepsilon_{ucu}\right)$

Force in Top Reinforcement $T_{st}(c) := A_{st} \cdot E_s \cdot min\left(\varepsilon_y, \frac{h_u + a_t - c}{c} \cdot \varepsilon_{ucu}\right)$

Force in Reinforcement in the UHPC Layer $T_{su}(c) := A_{su} \cdot E_s \cdot min\left(\varepsilon_y, \frac{a_u - c}{c} \cdot \varepsilon_{ucu}\right)$

Analysis

Depth of Neutral Axis

$$c_{eq} := \text{root}\left(C_{c.uhpc1}(c) + C_{c.uhpc2}(c) - T_{sb}(c) - T_{st}(c) - T_{su}(c), c, 0.001\ in, h\right) = 0.4\ in$$

	Force	Moment arm
UHPC (Compression rect.)	$C_{c.uhpc1}(c_{eq}) = 24.7\ kip$	$Z_{c.uhpc1}(c_{eq}) = 0.311\ in$
UHPC (Compression tri.)	$C_{c.uhpc2}(c_{eq}) = 32\ kip$	$Z_{c.uhpc2}(c_{eq}) = 0.149\ in$

Bottom Reinforcement $T_{sb}(c_{eq}) = 31.92\ kip$ $(h - a_b - c_{eq}) = 6.293\ in$

Top Reinforcement $T_{st}(c_{eq}) = 24.8\ kip$ $(h_u + a_t - c_{eq}) = 2.413\ in$

Reinforcement in UHPC layer $T_{su}(c_{eq}) = 0\ kip$ $(a_u - c_{eq}) = 0.353\ in$

Strain

Bottom Reinforcement $\varepsilon_{sb} := \varepsilon_{ucu} \cdot \frac{h - a_b - c_{eq}}{c_{eq}} = 0.0555$

$Check := \text{if}(\varepsilon_{sb} \le \varepsilon_u, \text{“OK”}, \text{“Rupture Strain Controls”}) = \text{“OK”}$

Top Reinforcement $\varepsilon_{st} := \varepsilon_{ucu} \cdot \frac{h_u + a_t - c_{eq}}{c_{eq}} = 0.0213$

Reinforcement in UHPC layer $\varepsilon_{su} := \varepsilon_{ucu} \cdot \frac{a_u - c_{eq}}{c_{eq}} = 0.0031$

Nominal Moment Capacity Under Positive Loading

$$M_{n.p} := C_{c.uhpc1}(c_{eq}) \cdot Z_{c.uhpc1}(c_{eq}) + C_{c.uhpc2}(c_{eq}) \cdot Z_{c.uhpc2}(c_{eq}) + T_{sb}(c_{eq}) \cdot (h - a_b - c_{eq}) + T_{st}(c_{eq}) \cdot (h_u + a_t - c_{eq}) + T_{su}(c_{eq}) \cdot (a_u - c_{eq}) = 22.76\ kip \cdot ft$$

Strain in Extreme Tension Reinforcement $\varepsilon_t := \varepsilon_{ucu} \cdot \frac{h - a_b - c_{eq}}{c_{eq}} = 0.055$

Strength Reduction Factor $\phi := min\left(0.9, \max\left(0.75, 0.75 + 0.15 \cdot \frac{\varepsilon_t - \varepsilon_y}{0.003}\right)\right) = 0.9$

Design Flexural Strength Under Positive Loading

$M_{u.p} := \phi \cdot M_{n.p} = 20.48\ kip \cdot ft$

Ultimate Moment Capacity of the Composite Section under Negative Bending Moment

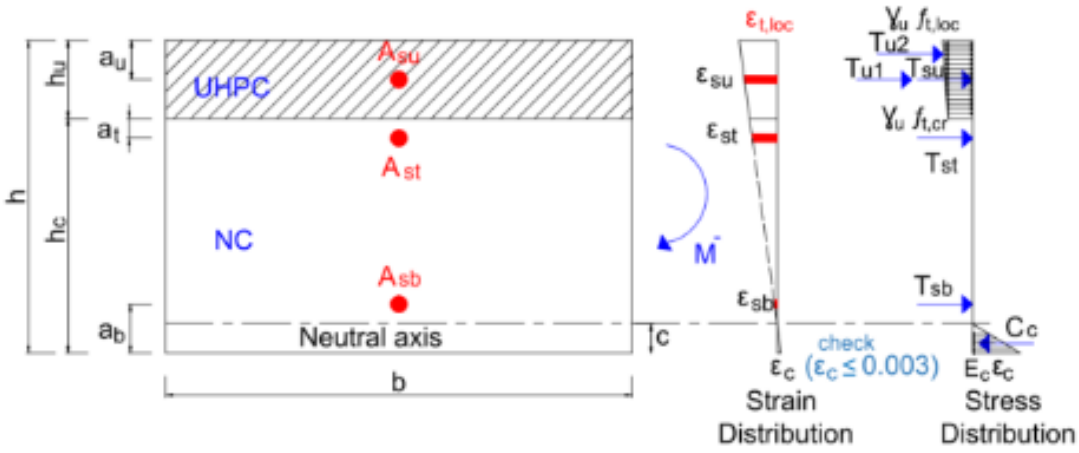

Forces

NC Strength at strain ε_c $\quad \varepsilon_c(c) := \frac{c}{h-c} \cdot \varepsilon_{t.loc}$

$$f_c(c) := \text{if}\left(\frac{c}{h-c}\cdot\frac{\varepsilon_{t.loc}}{\varepsilon_c'} \le 1,\ \frac{n\cdot\frac{\frac{c}{h-c}\cdot\varepsilon_{t.loc}}{\varepsilon_c'}}{n-1+\left(\frac{\frac{c}{h-c}\cdot\varepsilon_{t.loc}}{\varepsilon_c'}\right)^n}\cdot f_c',\ \frac{n\cdot\frac{\frac{c}{h-c}\cdot\varepsilon_{t.loc}}{\varepsilon_c'}}{n-1+\left(\frac{\frac{c}{h-c}\cdot\varepsilon_{t.loc}}{\varepsilon_c'}\right)^{n\cdot k}}\cdot f_c'\right)$$

NC Force $\quad C_{c.nc}(c) := \int_0^c \left(f_c(c)\cdot b\right) \mathrm{d}c \ \text{in}$

NC Centroid $\quad Z_{c.nc}(c) := \dfrac{\int_0^c c\cdot f_c(c)\,\mathrm{d}c \ \text{in}}{\int_0^c f_c(c)\,\mathrm{d}c \ \text{in}}$

UHPC Tensile Force (rect.) $\quad T_{t.uhpc1} := f_{t.cr}\cdot b\cdot h_u = 13.5\ \textit{kip}$

UHPC Tensile Centroid (rect.) $\quad Z_{t.uhpc1}(c) := h - c - \frac{h_u}{2}$

UHPC Tensile Force (Tri.) $\quad T_{t.uhpc2} := 0.5\ \left(f_{t.loc} - f_{t.cr}\right)\cdot b\cdot h_u = 1.4\ \textit{kip}$

UHPC Tensile Centroid (Tri.) $\quad Z_{t.uhpc2}(c) := h - c - \frac{h_u}{3}$

Force in bottom Reinforcement $T_{sb}(c) := A_{sb} \cdot E_s \cdot min\left(\varepsilon_y, \frac{a_b - c}{h - c} \cdot \varepsilon_{t.loc}\right)$

Force in Top Reinforcement $T_{st}(c) := A_{st} \cdot E_s \cdot min\left(\varepsilon_y, \frac{h_c - c - a_t}{h - c} \cdot \varepsilon_{t.loc}\right)$

Force in Reinforcement in the UHPC layer $T_{su}(c) := A_{su} \cdot E_s \cdot min\left(\varepsilon_y, \frac{h - a_u}{h - c} \cdot \varepsilon_{t.loc}\right)$

Analysis

Depth of Neutral Axis

$$c_{eq} := \text{root}\left(C_{c.nc}(c) - T_{sb}(c) - T_{st}(c) - T_{su}(c) - T_{t.uhpc1} - T_{t.uhpc2}, c, 0.001\ in, 0.99\ h\right) = 1.513\ in$$

	Force	Moment arm
UHPC (rect.) (Tension)	$T_{t.uhpc1} = 13.5\ kip$	$Z_{t.uhpc1}(c_{eq}) = 5.737\ in$
UHPC (Tri.) (Tension)	$T_{t.uhpc2} = 1.4\ kip$	$Z_{t.uhpc2}(c_{eq}) = 5.987\ in$
NC (Compression)	$C_{c.nc}(c_{eq}) = 37.2\ kip$	$Z_{c.nc}(c_{eq}) = 1\ in$
Bottom Reinforcement	$T_{sb}(c_{eq}) = -2.415\ kip$	$(a_b - c_{eq}) = -0.203\ in$
Top Reinforcement	$T_{st}(c_{eq}) = 24.78\ kip$	$(h_c - c_{eq} - a_t) = 3.677\ in$
Reinforcement in UHPC layer	$T_{su}(c_{eq}) = 0\ kip$	$(h - c_{eq} - a_u) = 5.737\ in$

Strain

NC (Compression) $\varepsilon_{c.nc} := \frac{c_{eq}}{h - c_{eq}} \cdot \varepsilon_{t.loc} = 0.0012$

$Check := \text{if}(\varepsilon_{c.nc} \le 0.003, \text{"OK"}, \text{"NC Strain Controls"}) = \text{"OK"}$

Bottom Reinforcement $\varepsilon_{sb} := \varepsilon_{t.loc} \cdot \frac{a_b - c_{eq}}{h - c_{eq}} = -0.00016$

Top Reinforcement $\varepsilon_{st} := \varepsilon_{t.loc} \cdot \frac{h_c - c_{eq} - a_t}{h - c_{eq}} = 0.0028$

Reinforcement in UHPC layer $\varepsilon_{su} := \varepsilon_{t.loc} \cdot \frac{h - a_u}{h - c_{eq}} = 0.0056$

Nominal Moment Capacity

$$M_{n.n} := C_{c.nc}(c_{eq}) \cdot Z_{c.nc}(c_{eq}) + T_{sb}(c_{eq}) \cdot (a_b - c_{eq}) + T_{st}(c_{eq}) \cdot (h_c - c_{eq} - a_t) + T_{su}(c_{eq}) \cdot (h - c_{eq} - a_u) + T_{t.uhpc1}(c_{eq}) \cdot Z_{t.uhpc1}(c_{eq}) + T_{t.uhpc2}(c_{eq}) \cdot Z_{t.uhpc2}(c_{eq}) = 17.85 \ kip \cdot ft$$

Strength Reduction Factor When There is No Tension Reinforcement in the UHPC Layer (AASHTO UHPC, 2024) $\phi := 0.75$

Design Flexural Strength Under Negative Loading

$$M_{u.n} := \phi \cdot M_{n.n} = 13.39 \ kip \cdot ft$$

Interface Shear

Distance between the centroid of Tension Steel and mid-thickness of UHPC overlay

$$d_c := h - \frac{h_u}{2} - a_b = 5.94 \ in$$

Interface Shear Stress

$$v_h := \max\left(\frac{M_{n.p}}{b \cdot 0.3 \cdot L \cdot d_c}, \frac{M_{n.n}}{b \cdot 0.2 \cdot L \cdot d_c}\right) = 0.13 \ ksi$$

Cohesion Factor from Pull-off test $C := 0.24 \ ksi$

Interface Shear Resistance $V_{ni} := 0.9 \ C = 0.216 \ ksi$

Check Interface Shear $\text{check} := \text{if}(V_{ni} > v_h, \text{“OK”}, \text{“NG”}) = \text{“OK”}$